The University Of Sheffield.

Access To Thesis.

- A bound copy of every thesis which is accepted as worthy for a higher degree, must be deposited in the University of Sheffield Library, where it will be made available for borrowing or consultation in accordance with University Regulations.
- All students registering from 2008–09 onwards are also required to submit an electronic copy of their final, approved thesis. Students who registered prior to 2008–09 may also submit electronically, but this is not required.

Author: ..... Dept: .....

Thesis Title: ..... Registration No: .....

For completion by all students:

Submit in print form only (for deposit in the University Library): ☐

Submit in print form and also upload to the *White Rose eTheses Online* server: In full ☐

Edited eThesis ☐

Please indicate if there are any embargo restrictions on this thesis. Please note that if no boxes are ticked, you will have consented to your thesis being made available without any restrictions.

Embargo details: (complete only if requesting an embargo to either your print and/or eThesis)	Embargo required?		Length of embargo (in years)
Print Thesis	Yes ☐	No ☐	_____
eThesis	Yes ☐	No ☐	_____

Supervisor: I, the supervisor, agree to the named thesis being made available under the conditions specified above.

Name: ..... Dept: .....

Signed: ..... Date: .....

Student: I, the author, agree to the named thesis being made available under the conditions specified above.

I give permission to the University of Sheffield to reproduce the print thesis in whole or in part in order to supply single copies for the purpose of research or private study for a non-commercial purpose.

I confirm that this thesis is my own work, and where materials owned by a third party have been used copyright clearance has been obtained. I am aware of the University's *Guidance on the Use of Unfair Means* (www.sheffield.ac.uk/lets/design/unfair)

I confirm that all copies of the thesis submitted to the University (including electronic copies on CD/DVD) are identical in content.

Name: ..... Dept: .....

Signed: ..... Date: .....

For completion by students also submitting an electronic thesis (eThesis):

I, the author, agree that the University of Sheffield's eThesis repository (currently WREO) will make my eThesis available over the internet via an entirely non-exclusive agreement and that, without changing content, WREO may convert my thesis to any medium or format for the purpose of future preservation and accessibility.

I, the author, agree that the metadata relating to the eThesis will normally appear on both the University's eThesis server and the British Library's EThOS service, even if the thesis is subject to an embargo. I agree that a copy of the eThesis may be supplied to the British Library.

I confirm that the upload is identical to the final, examined and awarded version of the thesis as submitted in print to the University for deposit in the Library (unless edited as indicated above).

Name: ..... Dept: .....

Signed: ..... Date: .....

THIS SHEET MUST BE BOUND IN THE FRONT OF THE PRINTED THESIS BEFORE IT IS SUBMITTED

The
University
Of
Sheffield.

POLYMER DIFFUSION ON TOPOGRAPHICALLY PATTERNED SURFACES

Christopher G. Clarkson

Department of Physics and Astronomy

A Thesis Submitted for the Degree of Doctor of Philosophy

March 2015

Abstract

Biological systems are often very efficient and the photosynthetic pathway of *R. Sphaeroides* is a highly efficient example. Controlling the diffusion of biological molecules leads, in part, to the high efficiencies. Using biologically inspired designs may lead to more efficient devices but require control of diffusion. This thesis presents possible mechanisms that can be used to facilitate this by examining diffusion, with fluorescence correlation spectroscopy, of polymeric analogues for parts of the photosynthetic pathway.

Poly(ethylene glycol) (PEG) was diffused on patterned surfaces of poly(oligo[ethylene glycol]methyl ether methacrylate) (POEGMA) brush. Square grids of POEGMA mimic the architecture of the cell membrane and simulate the confinement in the cell membrane. A slow mode of surface diffusion is observed that corresponds to PEG trapped in the grid. The level of confinement is lower than in the cell membrane, (45.6±2.6)% rather than ∼100%, but this is explained by the nature of the systems. Biological molecules are highly interactive while PEG and POEGMA are quite inert. This suggests that while the chemistry of a system is important, structure has a strong impact on diffusion regardless of the materials used.

The responsiveness of the cytosol was modelled by poly(glycerol monomethacrylate)-block-poly(2-hydroxypropylmethacrylate) (PGMA-PHPMA) diblock copolymer nanoparticles in water and the diffusion was examined as a function of temperature and pH. PGMA-PHPMA nanoparticles form cylindrical micelles ($r_H = 58 \pm 18$ nm) at ambient conditions, producing a freestanding gel. Lowering either the solution temperature, or increasing the pH, induces a morphological 'worm'-to-'sphere' transition. The spherical micelles (from $r_H = 16.3 \pm 0.3$ to $r_H = 6 \pm 4$ nm) are accompanied by degelation and an increase in diffusion coefficient of a factor between four (temperature) and eight (pH).

Acknowledgements

There are many people who have contributed to this body of work, in many different ways. Firstly, I would like to thank my supervisor Professor Mark Geoghegan. Mark took a bit of a punt on an undergraduate who'd had a bit of a rubbish penultimate year and I hope that he can look back at this project feeling like it came off! Mark helped me deal with my problems with some tough love at times but I feel the overall result was positive and thank him for that. Aside from the academic considerations, Mark has been fantastic with pointing me in the right direction across a wide range of personal matters. During my time as a Ph.D student I have gotten married, bought a house, decided my future career and most recently found that I will be a father. Mark has been there through it all, offering support throughout.

I want to thank Dr Zhenyu 'Jason' Zhang and Dr Matthew Mears for training me in FCS at the beginning of my studies. Not only that but for their continued support throughout the rest of my time. Matthew in particular was a font of knowledge on all things revolving around FCS and at times about a number of other topics that were either useful or interesting.

As part of a large programme grant such as the Low Dimensional Chemistry (LDC) programme, there are a great number of people that I regularly contact and discuss research with. I appreciate all of them but there are a few specific individuals who have gone above and beyond for me. Professor Graham Leggett was a great help, with his

entire group, in terms of information as to what was and was not possible and pointing fabrication in interesting directions. Dr Robert Ducker and Dr Osama El-Zubir were of great help in the planning stages of my project and assisted in the design of the surfaces I analysed.

From the LDC programme, Mr Alexander 'Ali' Johnson is the candidate for perhaps the most direct help. Ali taught me how to make polymer brushes and how to pattern them for my surfaces, as well as how to characterise them. Although I made some of the larger scale samples myself and characterised them, Ali took over midway through the project and made so many samples that at times I wasn't quite sure what to do with them all! He has also been very supportive during my writing process, proof-reading the sections that directly related to the production of my samples.

Professor Steven Armes and his student Mr Joseph Lovett were instrumental in the responsive polymer work within this thesis. Joe made all of the polymers that were used, while Steve assisted heavily with the explanation of the results. Both are thanked for their discussions which were filled not only with great science but also good humour.

Thanks also go to my Sixth Form Physics teacher for setting me on the path that has ended with this thesis. Until I reached the age of 17 I had the idea of being a medic in my head. Dr Peter Conway showed me physics and I haven't looked back.

All of this would not have been possible without the support of my family. My Dad and my Wife in particular have read this transcript numerous times, dealing with all sorts of outrageous typos! My Dad slaved away for hours trying to teach me enough biology, and his pet topic in evolution, to formulate my arguments without making them sound like intelligent design!

My Mother and Father have been fantastic throughout the whole process. Neither have the faintest clue about physics, but have continuously listened to me whittle on about it for the past 8 years. They were the very first sounding board for my ideas until I met my Wife, and now have only been demoted to second fiddle. I have not forgotten all of your help and support.

Rather strangely, I must also thank my cat. My wife adopted this cat to save it from being put down. Suteneko (came with the name, apparently means 'Orphan Cat' in Japanese) is the original scaredy cat and doesn't go outside. During the writing process, while at home, she has come to check on me every few hours and proceeds to chastise me if I'm not taking sufficient breaks from the computer screen. Hopefully she'll now stop yowling at me!

Finally, thanks go to my Wife. Catherine has kept me sane throughout the process, she has made sure that I eat, exercise and sleep. She has forced me to stop when I've fitted data for sixteen hours straight and equally given me a kick when I've been a bit lazy. Without her I would not be in the position I am now, so I want to show my great appreciation now and forever.

Contributions to Work

Christopher Clarkson produced early patterned surfaces, involving both the interferometric lithographic techniques as well as the growth of polymer brushes. He was also involved in early characterisation experiments (AFM, Water contact angle and XPS) of these samples. All FCS was completed by Christopher Clarkson and all confocal microscopy presented were also obtained by Christopher Clarkson. Unless otherwise stated all figures were drawn by Christopher Clarkson.

Alexander Johnson was responsible for all further production of patterned surfaces and particularly those used for the diffusion studies. Alexander also characterised all of these surfaces.

Joseph Lovett produced and characterised all of the diblock copolymer gel samples used in this thesis.

List of Abbreviations

ADP - Adenosine Diphosphate

APTES - (3-Aminopropyl)triethoxysilane

ATP - Adenosine Triphosphate

ATRP - Atom Transfer Radical Polymerisation

D - Diffusion Coefficient

d - dimensionality

DLS - Dynamic Light Scattering

DOPE - l-α-dioleoylphosphatidylethanolamine

FCS - Fluorescence Correlation Spectroscopy

FRAP - Fluorescence Recovery After Photobleaching

GFP - Green Fluorescent Protein

HOMO - Highest Occupied Molecular Orbital

IL - Interferometric Lithography

J - Mass Flux

LH1 - Light Harvesting Complex 1

LH2 - Light Harvesting Complex 2

LUMO - Lowest Unoccupied Molecular Orbital

M - Molar Mass

MSK - Membrane Skeleton

N - Degree of Polymerisation

NPPOC - nitrophenylpropyloxycarbonyl

NRK Epithelial Cells - Normal Rat Kidney Epithelial Cells

OID - Oligomerisation-Induced Trapping

PEG - Poly(ethylene glycol)

PGMA - poly(glycerol monomethacrylate)

PHPMA - poly (hydroxypropyl methacrylate)

POEGMA - Poly(oligo[ethylene glycol] methyl ether methacrylate)

Q - Ubiquinone

QH_2 - Ubiquinol

R - Resolution

R_g - Radius of Gyration

RC - Reaction Centre Protein Complex

RhB - Rhodamine B

SAM - Self-Assembled Monolayer

Si-ATRP - Surface Initiated Atom Transfer Radical Polymerisation

SNOM - Scanning Near-field Optical Microscopy

SNP - Scanning Near-field Photolithography

SD - Saffman-Delbrück

SPT - Single Particle Tracking

T - Temperature

TEM - Transmission Electron Microscopy

X_c^2 - Confinement Parameter

XPS - X-ray Photoelectron Spectroscopy

η - Viscosity

λ - Wavelength of Light

μ - Mobility

ρ - Concentration

Unless otherwise stated, all errors are standard deviations from the mean.

Contents

Chapter 1

Introduction

This thesis will examine portions of the photosynthetic pathway of *Rhodobacter sphaeroides*, and in particular the diffusion of charge carriers through the pathway. By recognising the similarities between the goals of the photosynthetic pathway and those of humans, some of design principles that make photosynthesis so effective will be examined.

To allow the examination of diffusion within the photosynthetic pathway a set of analogous polymeric systems will be produced and observed using fluorescence correlation spectroscopy (FCS). A set of patterned polymer brush surfaces will be produced to examine the portion of the photosynthetic pathway that occurs inside the cell membrane of the bacteria, while a block copolymer gel will be used as an analogue for the cytosol of the bacteria. This chapter will justify the use of these polymeric systems in the context of the bacterium. There will also be a discussion concetning why it is desirable to examine the photosynthetic pathway of *R. Sphaeroides*, as well as the basic theory for in the design of the analogous systems and understanding of results.

This thesis will demonstrate how suitable surfaces can be designed and manufactured, as well as how these surfaces can be used to control the diffusion of a polymer. This control can be compared favourably with the behaviour commonly observed in eukaryotic

cells, and demonstrates how the structure of a surface can have a significant impact on the diffusion of a polymer by confining the polymer to a specific region of the surface. The action of a polymer gel, with regard to temperature and pH changes, will be used to suggest a possible mechanism for the control of diffusion within the cytosol of the cell. A significant change in diffusion is observed with changes in either parameter, and this could be used to add directionality to the random motion, usually observed in diffusion, so as to guide molecules of interest to a specific area.

Finally, the results of the two studies will be used to discuss the photosynthetic pathway as well as to suggest possible designs for devices using the results. Future work to extend this thesis will be suggested and discussed.

1.1 Photosynthesis in *Rhodobacter sphaeroides*

The bacteria *Rhodobacter sphaeroides* obtains energy via photosynthesis. *R. Sphaeroides* uses an array of just five proteins within the cell membrane to do this, illustrated in the simple flow chart depicted in figure 1.1(a) [1]. The protein Light-Harvesting Complex 2 (LH2) enters an excited state when photons are incident upon it. This excited state is an exciton, which hops between neighbouring LH2 proteins until it reaches the Light-Harvesting Complex 1 (LH1) [1, 2]. Once the exciton reaches LH1, the energy is funnelled into the photosynthetic reaction centre protein complex (RC). The LH1 proteins cluster tightly around the RC complex allowing this energy to be transferred very quickly. This joint LH1-RC complex acts to generate ubiquinol (QH_2) by pumping protons from the extracellular side of the membrane into the complex (figure 1.1(b)). These protons are then bound to ubiquinone (Q) to produce the QH_2. QH_2 travels through the membrane itself, between the aliphatic tails of the phospholipids, to another protein complex, cytochrome bc_1 [1, 2]. Cytochrome bc_1 oxidisies QH_2 back into Q, while concurrently pumping the protons into the cytosol of the cell (figure 1.1(b)) [2]. The redox cycle of QH_2 to Q

acts to provide a pathway for electron transfer between the LH1-RC complex and the cytochrome bc_1 complex. This, in conjunction with the proton pumping, serves to form a trans-membrane proton gradient which is utilised by the ATP synthase protein to convert Adenosine Diphosphate (ADP) to Adenosine Triphosphate (ATP) (the currency of energy within the cell).

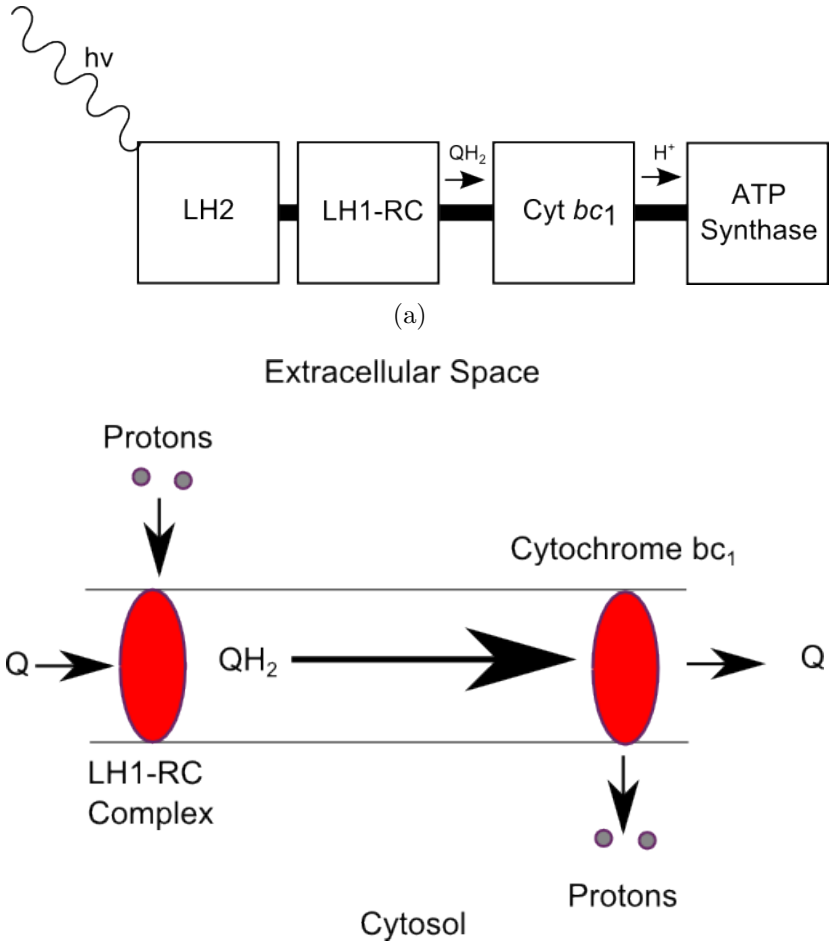

Figure 1.1: A set of figures illustrating the photosyntheric pathway of *Rhodobacter sphaeroides*. Figure 1.1(a) is a simple flow chart depicting the photosynthetic pathway of *Rhodobacter sphaeroides*. Figure 1.1(b) illustrates how the protons are pumped across the cell membrane by way of the ubiquinone (Q) to ubiquinol (QH_2) cycle.

It is noteworthy that the entire photosynthetic pathway is contained in a vesicle on the membrane, known as the chromatophore vesicle. The chromatophore vesicle is a spherical

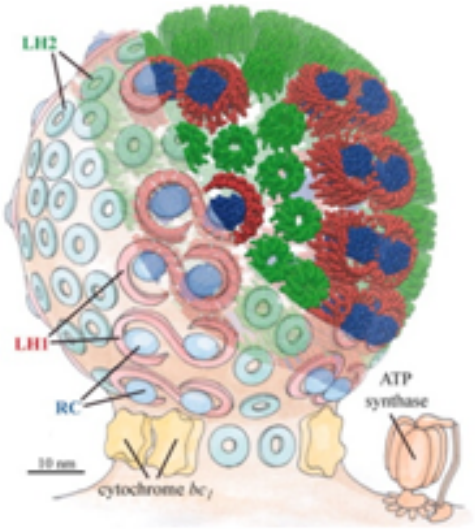

Figure 1.2: The chromatophore vesicle is where the photosynthetic pathway of *R. Sphaeroides* is located. The vesicle is a spherical envagination into the cytoplasm of the cell. The figure shows the internal side of the vesicle. Green units are LH1 proteins, red units are LH2 proteins, and blue units are RC protein complexes. The cytochrome bc_1 and ATP synthase are also shown. Reproduced from [4] with permission.

pocket that points into the cell (figure 1.2) with a diameter of around 50 nm, making it roughly the same dimensions as the channel length within a commercial transistor [1, 2]. The photosynthetic pathway is also incredibly efficient. It converts photons to ATP at about 3% power efficiency, while the portion of the pathway that leads to a proton being pumped into the internal side of the cell membrane (the pathway up until cytochrome bc_1) is in the region of 90% power efficient [3].

The efficiency of the photosynthetic pathway of *R. Sphaeroides* is incredibly high in comparison to artificial devices (the comparison will be addressed more fully in section 1.3). What is most interesting about the efficiency is the nature of the process that is occuring. *R. Sphaeroides* uses proteins to complete the photosynthetic pathway, yet these proteins are capable of diffusing independently of one another. To add to this the molecules the proteins require to function are also diffusing independently. The idea that such a process can lead to high efficiencies seems counter-intuitive. It seems clear that

the bacteria must have some mechanisms to control diffusion, to reduce the inherent randomness of the motion so that these efficiencies can be achieved.

This thesis will address the idea that the cell has strategies to control the diffusion of molecules. Membrane mobility will be considered, particularly with regards to the motion of proteins and charge carriers. The response of the cytosol, and by extension the cytoplasm, will also be discussed with regards to the diffusion of molecules of importance to the photosynthetic pathway. It is strongly emphasised that these topics are not only applicable to the photosynthetic pathway of *R. Sphaeroides*, but also to any process that takes place within the membrane or cytosol of any cell.

1.1.1 Membrane Mobility

Cell membranes are made up of phospholipids and proteins (for an in depth discussion of membrane structure see section 1.5) [5]. Lipid mobilities are known to be faster in artificial membranes than in cell membranes, and similarly protein diffusion is known to vary in the same way (see table 1.1 found in section 1.5). The slowing is seen as a short term confinement of diffusing species to regions of the membrane [6]. In this way, the parts of the photosynthetic pathway (or any other process) can be kept in close proximity so as to increase efficiencies.

The action of the LH2 complex to collect a range of wavelengths of light is clearly an important factor in the efficiency of the photosynthetic process. However, once the photon of light is absorbed the proteins responsible (a variant of chlorophyll) must transfer the energy between themselves until the excited state can be passed to the LH1-RC complex. There can be no energy conversion if the excited state is simply allowed to dissipate, and certainly the vast majority of photons absorbed must be transferred to the LH1-RC complex for the startling level of efficiency to be possible. It could be argued that the cell just needs to have a suitably large number of complexes, both LH2 and

LH1-RC, to ensure this is the case. The LH2 complexes must be kept close enough to each other to facilitate transport of the excited state and must be close enough to the destination of the transfer, the reaction centre. We know the photosynthetic pathway is only used within the chromatophore vesicle. The proteins responsible are packed into the membrane such that they are only found in the vesicle. This packing can be taken as the biological system controlling the diffusion to ensure the complexes stay close to one another.

The ability of *R. sphaeroides* to control the diffusion of membrane molecules is perhaps most clearly exemplified by the transport of ubiquinol from the LH1-RC complex to the cytochrome bc_1. This raises several questions pertaining to how this control is determined and it is therefore pertinent to discuss the membrane structure in greater detail.

There are many other examples of cell membrane based processes and many of these processes demonstrate the ability of the cell membrane to regulate the position of proteins both spatially and temporally. An example of this is oligomerisation-induced trapping (OID), where the process of proteins forming dimers and oligomers, reduce their apparent diffusion coefficient and become traped within a certain region of the membrane [7, 8]. This is of particular use in sensing, as this process makes it explicit where the a signal was incident upon the cell [9]. The mechanism behind this process is believed to be the involvement of the membrane skeleton (MSK) which is present in all cells.

Section 1.5 discusses the idea that the MSK acts as barriers that are used by cell membranes to prevent proteins from moving away from their required regions of the membrane. Two specific examples are provided (the polarisation of the neuron cell and the sensing of stimuli) that demonstrate the ability of the cell membrane to control diffusion so that processes can be completed efficiently.

1.1.2 Cytoplasmic Response

The Cytoplasm is the region of the cell that is bounded by the cell membrane, compromising the cytosol and the cells organelles. The cytosol is the gel-like substance that can be viewed as the matrix that the organelles are suspended in. The cytosol contributes up to 55% of the cell volume [5]. A gel is a very fitting description of the cytosol as it consists of roughly 20% (by weight) protein, which is a similar proportion of macromolecules in polymer gels.

The proteins of the cytosol perform a wide range of tasks, but are predominantly treated as being responsible for intermediary metabolism (for instance liberating energy from sugars and ATP) [5]. The cytosol is also often the location of proteins that are required for forming complexes at the cell membrane. The signalling mechanisms involving the CD59 protein demonstrate the idea that membrane mobility is controlled by the cell. The signalling mechanism also requires the protein Gαi from the cytoplasm to activate the complex and the PLCγ protein to release the signal into the cell as IP3 molecules [9]. This suggests that there is some way to effectively get proteins to the regions of the cytosol where the proteins are required to do their intended purpose. The alternative is that cytosol is saturated with every macromolecule, such that any process will have a large number of the required molecules in close proximity. The idea that the cytosol contains only 20% macromolecules (by weight) suggests this is not the case.

It seems desirable to have some control over diffusion in the bulk in response to stimuli bought about by the photosynthetic pathway (such as local pH) of *R. Sphaeroides*. By having some method of control, the cell would be able to maximise the number of protons that reach the ATP synthase protein and subsequently opimize the energy conversion that is possible.

The decrease in power efficiency from 90% (to the point in the pathway where cy-

tochrome bc_1 oxidises ubiquinol) to 3% (the end of the pathway where ATP is produced) is obviously very large, and in a device this loss would need to be minimised. Some of this decrease is unavoidable, as previously described the pathway allows for two protons to be pumped across the cell membrane, one at the LH1-RC complex and a second at the cytochrome bc_1. In the simplest description possible, ATP synthase is a rotating generator that produces ATP as it turns [10]. To allow it to turn it requires protons, which it pumps across the cell membrane in opposition to those pumped over during the rest of the pathway. The number of protons required for the rotational motion varies with the ATP synthase itself, each species has a slightly different sequence of amino acids and as such, there can be differences in how the ATP synthase rotates. In the case of *R. Sphaeroides*, the protein rotates in 120^o angles (90^o as each proton is used followed by a further 30^o turn as the ATP synthase orientates itself) as it pumps protons, meaning that three protons are required for a full revolution [11]. In addition to this, a fourth proton is required to bond the phosphate group to the ADP molecule so as to produce ATP.

The cytosol, the fluid that makes up the cytoplasm, consists of three main components; water, ions and macromolecules. While it is possible for the cell to use the ions within the cytoplasm to allow for this process, it should be noted that the concentration of ions remains quite stable [12]. Using this as a starting point, it can be summised that the four protons required come from the photosynthetic pathway itself.

Four protons requires two photons to be absorbed by the light-harvesting proteins. This means that as an upper limit, the power conversion efficiency would be bounded to 45% for the entire pathway. This works on the basis that every proton was used. Clearly this is not the case as the true efficiency is 15 times smaller than this 'perfect' value. Therefore protons must 'escape' the system somehow.

The first candidate to explain the reduction is the number of ATP synthase proteins

present. There is a single ATP synthase for each vesicle [2], meaning that each protein must collect pumped protons from roughly 8000 $n\text{m}^2$ of membrane. Considering that the ATP synthase itself is a roughly cylindrical protein, with a radius of roughly 5 nm, it seems impressive that the protein can manage to collect one proton in every fifteen produced. In terms of device design, the introduction of more proton collecters would conceivably rectify the majority of the reduction. It could be postulated that *R. Sphaeroides* simply does not require more ATP synthase proteins as the amount of ATP produced is sufficient for its needs. The cell would therefore not produce any more ATP synthase proteins. This logic will be discussed in section 1.2.

The diffusion of protons in three dimensions will be occur very quickly, with no constraints the protons will diffuse randomly. While possible, it intuitively feels unlikely that even as many as one proton in fifteen will make it to the ATP synthase without some form of help. Simple order of magnitude calculations suggest that the ATP synthase protein takes up only 1% of the area of the chromatophore vesicle, while collecting 7% of all protons. This argument of scale, in conjunction with the idea that the protons will diffuse randomly, is enough to suggest that there is some additional method for controlling motion.

In terms of diffusion, it is plausable that gradients (be that chemical, charge or some other type of gradient) might be used to direct motion within the cytosol. Gradients have been used with polymers to direct diffusion [13, 14, 15]. These ideas will be developed fully in section 1.4 & 1.6.

1.2 Biological Processes and Evolution

It is well known that biological systems are exceptionally well adapted for their purposes. Due to natural selection over four billion years, nature has produced techniques to deal with most desirable processes and these techniques are as efficient as required. Nature

has not wasted time and energy making them more elaborate or complicated than is necessary; crucially if there is a threshold that needs to be met, nature will meet it rather than waste energy exceeding it. Examples such as the appendix could be used to counter this point, but it should be noted that at some point the appendix was required and that now it is surplus to requirement it is being lost in many races due to natural selection. If a process is only required to be 50% efficient a biological system will deem this sufficient and not aim for any higher. This is not supposed to suggest that biological systems are ill-designed but simply that there is generally a reason for a certain design. Although there are usually built in redundancies (like the appendix), in most cases these are evolved out if they place unnecessary energy strain on the system.

In general, biological processes are incredibly efficient. Some of these processes have analogues as artificial processes; for example in terms of sensing, energy collection and processing of materials and photosynthesis is one example of a complete process humans would be interested in. It seems sensible to compare how we as humans use artificial means to reach the same end product as nature and to see what it is possible to learn from these systems.

Evolution is constrained by physical laws and as such biological processes cannot perform 'magical' processes (for example, Maxwell's Demon) that we as human beings cannot replicate. Biological systems must still follow the laws of thermodynamics and as a consequence these systems can theoretically be replicated outside of the biological environment. Evolution by natural selection is change due to environmental factors, be that disease, climate, or competition; spontaneous mutation is a further method of change.

The key point to remember about evolution is that any successful traits or systems come about due to competition. Processes advance only enough so as to give an edge over others, whether that be across different species or within a species. Humans however are

somewhat different in this respect as, for all intents and purposes, we have no competition through which to advance in the strictest sense of evolution. Rather it could now be argued that humans change their environments to suit themselves rather than adapting to it. It could be further argued that humans are actually in competition with their environment and this can be taken even further to suggest that humans compete with the universe itself. It is therefore critical for processes to maximise their efficiency, since for a species for survive in the long term it needs to be as efficient as physical laws allow.

Bacteria have the means to complete thousands of processes under a variety of conditions. Typically these cells are smaller than those of eukaryotic cells, such as those within our own bodies, being typically between 0.5 μm and 5.0 μm [5]. Often it is desirable for these cells to complete processes that produce outputs that we, as humans, might need. These biological processes are inherently stoicastic being driven by diffusion and controlled by complex inputs such as chemical gradients.

Biological systems are also adept at miniturisation. If the photosynthetic pathway of *R. Sphaeroides* (taking place on a vesicile which is only 50 nm in diameter) were taken in the context of integrated circuits two points can be made. Firstly, while a single transistor is capable of only one 'job', be that amplifying or manipulating signals, the chromatophore vesicle of roughly the same size is capable of an entire photosynthetic pathway. Secondly, this should really only be compared with traditional designs of transistors rather than the more esoteric examples being produced currently. To keep pace with the predictions of Moore's Law, transistors based on single atoms, spintronics and tunnel junctions are being produced in labs, which can be smaller than the length scale of the chromatophore vesicle. This is of course a stunning example of humans sidesteping the problem at hand in terms of miniturisation (such as the physical limits imposed by production methods) to come up with a new approach and render those problems moot. It cannot be said whether biological processes could scale down further, there is simply no evolutionary advantage

to being smaller.

The message that this should convey is that while a biological process is efficient, because of the way biological processes develop there is often room for improvement. *R. Sphaeroides* collects light from a specific region of the electromagnetic spectrum but it would be advantageous in an artificial device to collect from a wider range. To develop improved devices based upon biological processes it is necessary to understand the principles of the biological process so as to produce an artificial equivalent.

1.3 Photovoltaic cells and the photosynthetic pathway

All modern technologies are based upon engineering principles in some form or another. This means that intrinsically, all these systems have binary inputs that are deterministically processed to reach a certain output. If a current A is put into a device B, the output C will occur every time. In doing this, the technologies are as good as our understanding of the procedures that the device B can handle. By understanding the process well, we will know how modifying the input will affect both how the operations of the device and how the output changes. A full understanding of the underlying principle also allows us to know the limits of the device in great detail.

By means of comparison to the photosynthetic pathway of *R. Sphaeroides*, a man-made device using similar principles would be a photovoltaic. A traditional photovoltaic cell is constructed of hard semiconductors such as silicon. In the simplest terms, when light is incident on a photovoltaic cell the photons are absorbed by the semiconducting material. This allows for the liberation of electrons from their atoms allowing the electrons to flow through the material. Due to the construction of the cell the electrons are only able to travel in one direction and therefore electricity is produced and collected (this process is

discussed in more detail in appendix A.1).

A single p-n junction crystalline silicon device is theoretically limited to a power efficiency of 33.7% based on the Shockley-Quiesser limit [16]. The extreme case of a multijunction cell with an infinite number of layers, each layer absorbing a different region of the electromagnetic spectrum, has a corresponding limit of 86% under concentrated light [17]. The most efficient solar cell actually produced at the time of writing (produced in December 2014) is 46% power efficient and was produced at the University of New South Wales [18]. The device has four solar subcells arranged so that three of the cells collect sunlight from a range of wavelengths while a fourth collects excess light that is reflected by mirrors and filters.

An organic solar cell has much more in common with the photosynthetic pathway of the *R. Sphaeroides* bacteria as it is formed from soft matter rather than traditional semiconductors. The most common characteristic of a material used for an organic solar cell, whether it is a small molecule or a polymer, is conjugation (that is a region of alternating double and single covalently bonded carbon atoms). In the simplest terms, a double bond is formed when the electrons in each atom's p_z orbital delocalise to form a bonding orbital between both atoms (π orbital), while also forming another orbital, known as the antibonding orbital (π^* orbital). The electron's most energetically favoured state is to be in the π orbital, while the π^* state acts as an excited state. This makes the π orbital the highest occupied molecular orbital (HOMO) while the π^* is the lowest unoccupied molecular orbital (LUMO). The difference in energy between these two states can then be treated as a classical band gap and generally that band gap is between 1-4 eV.

When light is incident on a suitable organic photovoltaic material, the photon causes an excited state to be formed that is then confined to the molecule if it is small, or to a

region of the polymer chain if it is large. The excited state, with an electron in the LUMO and a hole in the HOMO acts as an electron-hole pair bound together by electrostatic interactions. This is commonly referred to as an exciton. When used in a photovoltaic cell this exciton needs to be separated and the process is much the same as in a tradition semiconductor cell, an effective field is required.

The simplest organic photovoltaic is formed by placing a single layer of an organic electronic material between two metallic conductors (figure 1.3). The metallic conductors are always different materials, selected so that the materials have different work functions. For example, typically Indium Tin Oxide (ITO) is used for one conductor because it has a high work function. In contrast, the second is usually a low work function metal like aluminium. This difference in work functions produces an electric field across the conductive organic layer. This means that when light is incident and an exciton is formed, the difference in potential of the two metal conductors helps to separate the exciton, allowing the electron to go to the positive electrode and the holes to go to the negative. The electrodes are electrical conductors that are in contact with an organic part of the device.

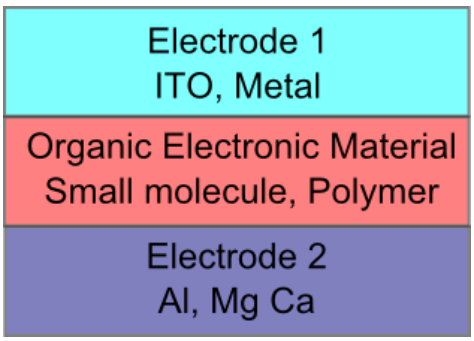

Figure 1.3: A schematic diagram of the design of a single layer organic solar cell

Cells with this type of construction were the earliest to be examined, with Phthalocyanine used as the organic layer. As early as 1958, it was shown that a cell constructed with an

active layer of magnesium phthalocyanine (MgPc) led to a photovoltage of 200 mV [19]. Ghosh *et al.* (1974) recorded a photovoltaic efficiency of 0.01% when a cell with the same active layer was illuminated at 690 nm [20].

Single layer organic cells are not efficient enough to be a suitable design yet problems also exist with simple bilayer polymer cells and as a consequence they also do not work well (figure 1.4). In the simple bilayer design, two polymers with different electron affinities and ionisation energies are placed together between the metal conductors. The idea is that in a similar way to the p-n junction, an electric field will be formed across the interface between the two polymers. In theory, if one layer is an electron donor and the other an electron accepter, the force exerted by the field can be large enough to split the exciton. The major problem with this set up is one of scale. An exciton will typically diffuse 10 nm within an organic electronic material. In order for the exciton to be split, it must reach an interface between the polymer layers. This means the thickness of the layers should ideally match the diffusion length of the exciton, so that all excitons formed can be separated. To capture enough light to actually form excitons the layer thickness needs to be much larger than this, typically 100 nm. Only a small amount of the formed excitons can actually be captured and separated.

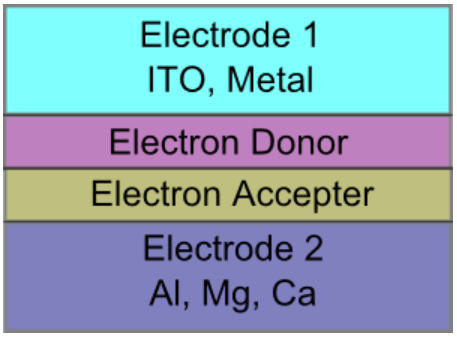

Figure 1.4: A schematic diagram of the design of a bilayer organic solar cell

To remedy the problems associated with being unable to split the excitons, the electron

accepter and donor can be mixed into a blend. If the accepter and donor are selected carefully, the blend will separate to form domains of accepter and donor (Figure 1.5). If the lengthscale of the blend is roughly the same as the lengthscale of the exciton diffusion length then the majority of excitons will be separated at the interface between accepter and donor regions. These types of cell are much more efficient than the other types of organic solar cells and are referred to as organic heterojunction cells. A cell using Buckminsterfullerene (C_{60}) as an accepter and polyphenylene vinylene (PPV) as a donor achieved a power conversion efficiency of 2.9% [21].

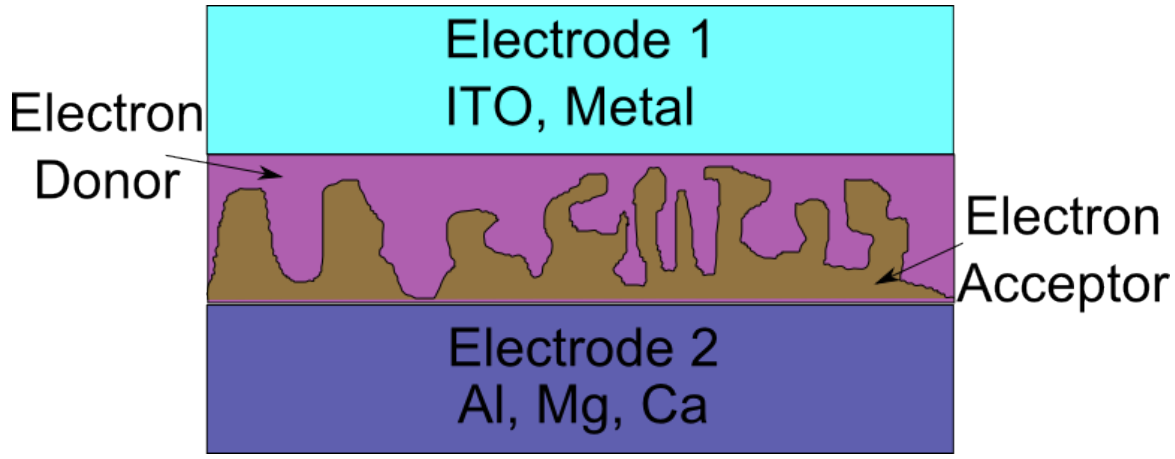

Figure 1.5: A schematic diagram of the design of an organic heterojunction solar cell

With respect to the energy efficiencies seen in *R. Sphaeroides*, the conversion of light to ATP and sugars is in the region of 3% [3]. At first glance this seems on par with the organic solar cells, yet it should be noted that the photosynthetic pathway is more equivalent to a solar cell charging a battery. A more comparable system would be to consider the photosynthetic pathway to the point that ubiquinol is oxidised. As previously stated, this is the equivalent of electron transfer and the diffusion of the ubiquinol is therefore comparable to the flow of current. In this case, the process is much more efficient with the conversion of photons to charged molecules reaching ~90% [3]. This level of efficiency is far superior to even the most advanced semiconductor device.

1.4 Biological Analogues

It has been demonstrated that biological processes are very efficient. The example of photovoltaics and the photosynthetic pathway demonstrate very clearly that biology can often be more efficient than the equivalent artificial process. This observation has led to a whole branch of designs and research that aim to take advantage of the way biological processes work

Biomimetic technologies aim to use the processes observed in nature as some of the operating principles in artifical devices. A crucial factor in bioinspired work is that the material used do not have to be consistent with those seen in the cell. The arguments in section 1.2 illustrate that biological processes are as efficient as the system is required to be for that individual. It is therefore down to humans to take these processes and make them as efficient as we require them to be. One way of achieving this is to understand the biological system, so that the limitations are known and can then be pushed further.

The work in this thesis aims to produce biologically inspired systems that can be used to examine fundamental aspects of the photosynthetic pathway in *R. Sphaeroides*. Section 1.5 describes the structure of the cell membrane as a partitioned fluid. The use of polymers to produce an analogue of the cell membrane structure serves as a method of examing the impact that basic structure has upon diffusion. This makes it possible to remove the complex behaviours seen in biological membranes and to simply observe diffusion on a structure. This analogue would then form the basis of a biomimetic system that would fulfil a job similar to a membrane protein process.

Similar arguments can be made for treating the cytosol of a cell as a polymer gel,

to understand some fundamental behaviour that will be built upon to produce a functioning biomimetic system. A key with the biological analogues used in this thesis are that they are the simplest system that could be used. The desire to then build upon the system, and then integrate these systems will drive future research and development so that not only is an understanding of fundamental diffusion processes increased but that biologically inspired devices and analogues can be produced.

1.5 Membrane Structure

The structure of the cell membrane has been under intense scrutiny for almost 100 years. The first time that the importance of lipids was acknowledged was in 1925 by Gorter and Grendel [22]. It was correctly determined that the membrane is predominantly constructed of lipids and from experiment it was concluded that this membrane was two molecules thick (figure 1.6(a)). Gorter and Grendel also established the orientation of the polar groups, implying that in aqueous conditions the polar head group is in contact with the water molecules while the aliphatic tails are protected inside the bilayer.

This idea of a lipid bilayer was absorbed into the Davson-Danielli model of 1935 [23]. Danielli had made measurements of surface tension on lipid bilayers and believed that the observed surface tension could not arise solely from phospholipid head groups. The solution proposed was to sandwich the lipid bilayer between sheets of globular protein (1.6(b)). However, it is now known that the phospholipids head groups *can* produce the surface tension measurements observed, proving this suggested structure to be incorrect. Despite this the addition of proteins into the model of cell membrane structure was a signifcant step forward.

The Davson-Danielli model remained the accepted way of envisioning the plasma membrane until 1972, when Singer and Nicholson proposed the Fluid Mosaic model [24]. The

flanking membrane layers were abandoned and were therefore replaced with transmembrane proteins (1.6(c)). The model considered the membrane as a two-dimensional liquid through which lipids and proteins could easily diffuse. Singer and Nicholson recognised that on their own, lipids will form these two dimensional liquids, yet they also pointed to the large proportion of proteins within the membrane, suggesting that the proteins act to provide structure to the membrane with the lipids acting as a matrix. The name of the model comes from the idea that the proteins could be treated like the tiles of a complex mosaic. The lipids form the mortar between the tiles. The proteins are capable of forming complexes but once this is the case they become stable and have minimal protein-protein interactions. This leads to the suggestion that there is no long range order in the mosaic pattern, a fact that was borne out with experimental evidence. Singer and Nicholson therefore suggested that non-random distributions of proteins were only formed by some agent extrinsic to the membrane, and that this could be either inside or outside of the cell.

In 1975, Saffman and Delbrück published "Brownian Motion in Biological Membranes" [25]. They described the membrane as a thin layer of viscous fluid that is surrounded by a bulk liquid with very low viscosity. Their model made it possible to use diffusion coefficients to infer the size of nanoscale objects like proteins. The extensions by Hughes, Pailthorpe and White allowed for the description of objects with any size [26]. This allowed for the incorporation of micron-scale objects like domains of lipids.

The Saffman-Delbrück (SD) model, also known as the 2D Continuum Fluid model, and the Fluid Mosaic model are both consistent with treating the cell membrane as roughly homogeneous. While the Fluid Mosaic model explains the gross structure of the membrane, the SD model describe the way molecules should travel through the plane of the membrane.

A typical transmembrane protein is treated as a cylinder in the SD model, with the height of the cylinder (h) being equal to the thickness of the membrane and the radius of

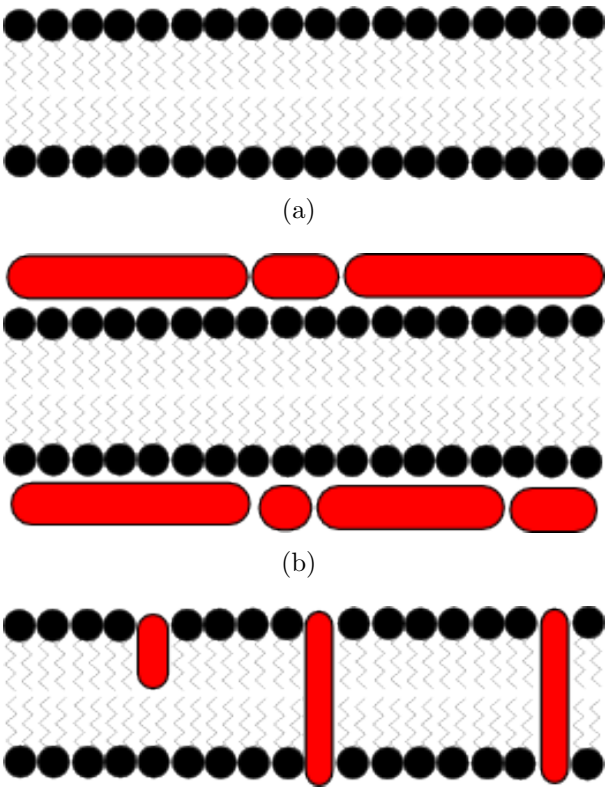

Figure 1.6: The progression of models describing the structure of the cell membrane from the Gorter-Grendel model (a) to the Davson-Danelli model (b) to the Fluid Mosaic model (c). Black circles represent the phospholipid head groups while the black lines represent the phospholipid aliphatic tails. The red blocks represent proteins.

the cylinder is a. The viscosity of the two dimensional fluid (the cell membrane) is given by η, while the viscosity of the surrounding medium is given as η'. The SD model gives the diffusion coefficient of transmembrane proteins as:

$$D_{\mathrm{T}} = \frac{k_B T}{4\pi\eta h}\left(log\left(\frac{\eta h}{\eta' a}\right) - \gamma\right), \tag{1.5.1}$$

$$D_{\mathrm{r}} = \frac{k_B T}{4\pi\eta a^2 h}. \tag{1.5.2}$$

Where D_{T} is the translational diffusion coefficient of the protein, D_{r} is the rotational diffusion coefficient and γ is Euler's Constant.

Over the course of 30 years, these intertwined models were accepted yet there were many observations that could not be reconciled with them. Two critical experimental observations that could not be explained by membrane biologists were:

- The diffusion coefficient of both proteins and lipids was much lower in plasma membranes than in artificially reconstructed membranes (Data demonstrating this is presented in table 1.1). The decrease was different from cell to cell, yet was generally between a factor of 5 and 50.

- When membrane constituents form complexes their diffusion coefficient drops dramatically or the molecules are sometimes immobilised completely [27, 28, 29]. By way of an example, consider the protein E-cadherin which can cluster to form oligomers of various sizes from dimers up to clusters of tens of the protein [7]. Upon oligomerisation the diffusion coefficient decreased by up to a factor of 40 in the case of the largest clusters. Also artificially crosslinked lipids have been observed to exhibit similar behaviour with diffusion coefficients dropping by factors of 5 [8]. This is in disagreement with the SD model, which predicts that the diffusion coefficient is largely unchanged when the size of the diffusant is varied. A typical value for the radius of a transmembrane protein is 0.5 nm. When four such proteins form a tetramer, thereby increasing their radius by a factor of 2, the SD model predicts (through equation (1.5.1)) that there is a decrease in the diffusion rate of only 1.1. Indeed, a decrease in diffusion of only 1.4 is predicted for a complex formed from 100 proteins.

These two problems indicate a need for another model that can explain both situations satisfactorily.

Some further experimental results, using a technique called single particle tracking (SPT), shed some light on possible structures. Single particle tracking makes use of very fast camera technology to follow the motion of a particle. Typically the particle is a colloidal particle

Probe-Protein[1]	Artificial membrane or Cell type[2]	Method	Effective D ($\mu m^2 s^{-1}$)	Time window for D (ms)	Temp (^oC)	Ref
Fl-Integrin αIIbβ3	DMPG:DMPC=1:1	FRAP	0.7 ($\pm$0.06)	$\sim$5000	33	[30]
Fl-Fab-Integrin β1	AG1518	FRAP	0.058 ($\pm$0.002)	3000	37	[31]
Fl-Thy-1	DOPC:SM=1:1	FRAP	0.58 ($\pm$0.04)	1500	24	[32]
Gold-Thy-1	C3H 10T1/2	SPT	0.081 ($\pm$0.007)	<6600	37	[33]
Fl-AchR	DMPC	FRAP	2.4 ($\pm$0.8)	2600	36	[34]
Rh-AchR	Rat Myotube	FRAP	0.016 ($\pm$0.003)	44 000	37	[35]
Fl-Glycophorin[a]	DMPC	FRAP	2	3000	30	[36]
Fl-Glycophorin[a]	DMPC	FRAP	4 ($\pm$2)	1500	30	[37]
Fl-Glycophorin[b]	Erythrocyte (intact)	FRAP	0.0036 ($\pm$0.0017)	10 0000	37	[38]
Fl-Glycophorin[b]	Erythrocyte (ghost)	FRAP	0.047 ($\pm$0.021)	10 0000	37	[38]

[1]Fl-Integrin αIIbβ3, fluorescein-isothiocyanate (FITC)-labeled integrin IIb3; Fl-Fab-Integrin β1, FITC-labeled TS2/16 Fab fragment bound to integrin 1; Fl-Thy-1, FITC-labeled Thy-1; Gold-Thy-1, Colloidal Gold-labeled Thy-1; Fl-AchR, fluorescein-labeled bungarotoxin bound to acetylcholine receptor; Rh-AchR, tetramethylrhodamine-labeled bungarotoxin bound to acetylcholine receptor; Fl-Glycophorin[a], FITC-labeled glycophorin; Fl-Glycophorin[b], fluorescein-thiosemicarbazide-labeled glycophorin.
[2]DMPG, 1,2-dimyristoyl-sn-glycero-3-phosphoglycerol; DMPC, 1,2-dimyristoyl-sn-glycero-3-phosphocholine; AG1518, AG1518 human foreskin fibroblast; DOPC, 1,2-dioleoyl-snglycero-3-phosphocholine; SM, sphingomyelin; C3H 10T1/2, C3H 10T1/2 mouse embryo fibroblast.

Table 1.1: The observed difference in diffusion coefficient of proteins when observed in cell membranes (in red) and artificial membranes. A secondary observation is that the time window used to measure the diffusion coefficient has an impact on the diffusion coefficient that is measured. All uncertainties are standard deviations from the mean.

of gold that is attached to the molecule of interest. In 2002, Fujiwara *et al.* [6], observed that the behaviour of lipids in the membrane could not be caused by simple thermally induced Brownian motion. The lipid, specifically l-α-dioleoylphosphatidylethanolamine (DOPE) tagged with colloidal gold particles of 40 nm diameter, underwent short term confinement followed by hopping between areas of confinement in the long term. This

process was referred to as hop diffusion. It was observed that this was a common occurrence, with more than 85% of collected trajectories demonstrating this behaviour.

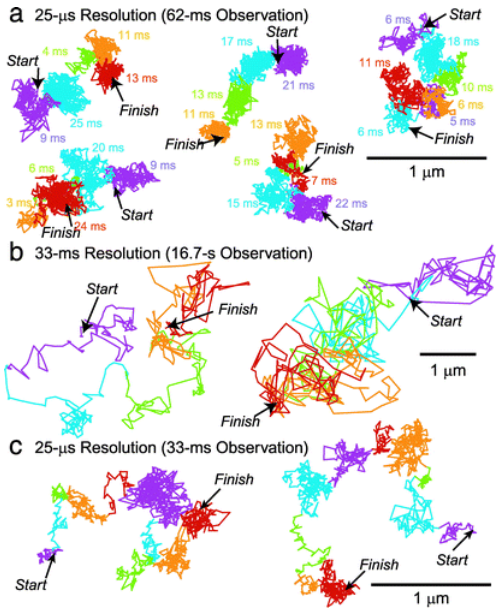

Figure 1.7: Trajectories of lipids in a NRK cell membrane at various framerates as recorded using SPT [39]. Reproduced with permission.

Hop diffusion behaviour was observed at a time resolution of 25 μs (or a frame rate of 40500 s^{-1}) which is over 1000 times faster than standard video rates. When the same experiment is completed at a slower observation rate (33 ms), the behaviour of hopping is not observed but rather the diffusion is seen to proceed as previous experiments have recorded. That is, the diffusion in a cell membrane is slower than that on a reconstructed membrane of liposome.

The experiments of Fujiwara *et al.* used normal rat kidney epithelial (NRK) cells [6], and evaluations of the trajectories with specialised software showed that there were submicron sized compartments that hindered translational diffusion through the membrane. This software was able to extract information concerning the size of the compartment, the diffusion coefficient both within and outside the compartment, as well as the average residency time before a hop to a neighbouring compartment. NRK cells were shown to

have compartments which were around 230 nm across, with an average residency time of 11 ms. This would indicate that the hop diffusion nature would not be observable by standard video rate technologies at 33 ms.

Within the compartment itself, diffusion of DOPE is comparable to that observed in liposomes. This suggests that within a compartment the molecule exhibits normal simple diffusion. It should also be stressed that this behaviour is not limited to this study of NRK cells with SPT. Other groups have observed the same hop diffusion behaviour in subsequent years. The study of Murase *et al.* [8], demonstrated that a wide range of mammalian cells exhibit this behaviour. The study presented data in agreement with Fujiwara *et al.* concerning the size and residency time in NRK cells [6], but also showed that a wide range of compartment sizes (30 nm to 230 nm) and residency times (1 to 17 ms) existed in other cells.

Hop diffusion has not only been observed in lipids but has also been seen in transmembrane proteins. This seems to be consistent throughout all transmembrane proteins, with observation of hop diffusion seen in E-cadherin [40], transferin [41], α2-macroglobulin [41] and the Band 3 protein [42], all of which were observed by just one research group.

The theory proposed to explain hop diffusion in the cell membrane was that the MSK acted in some way to partition the membrane. The MSK has multiple functions, though primarily it acts to give the cell shape and is responsible for resisting mechanical deformation. It is also known that the MSK acts as a scaffold to which proteins attach. The MSK is formed of an array microfilaments of the proteins actin and spectrin, resembling a pearl necklace with no string.

Evidence that the MSK acts to partition the cell membrane came from the study of the Band 3 protein in red blood cells [42]. Firstly it was shown that the Band 3 protein

underwent hop diffusion within red blood cell ghosts. Ghost cells are cells that have had their internal organelles removed and are commonly used in membrane biology. Roughly two thirds of the protein was diffusing via the hop mechanism, with compartments of 110nm diameter and a residency time of 350 ms. The remaining third was shown to be bonded to the spectrin in the MSK.

To show the involvement of the MSK, latex beads were tagged onto an immobile protein while gold colloidal particles were tagged onto the mobile fraction. A laser beam was then focussed on the latex bead to use as optical tweezers. The optical tweezers allow piconewton-scale forces to be exerted on the bead and to move the bead as desired. The bead was moved to deform the MSK as the immobilised protein is dragged with the bead. The result of this was to drag the mobile Band 3 proteins in the direction the bead was dragged. When the bead was returned to its original position, the mobile Band 3 returned to a position close to where it started.

By treating the ghost cells with trypsin, a large portion of the Band 3 protein on the inner leaf of the membrane is removed, while not affecting the actin or spectrin. If the MSK is responsible for the confinement to partitions of the membrane, trypsin treatment should increase the hopping rate. It was observed that the modified Band 3 did indeed hop between partitions more regularly (six times faster), while not changing the size of the corral or the diffusion coefficient within the corral.

The work on the Band 3 protein serves to explain why transmembrane proteins experience this hopping behaviour, in what is now refered to as the Membrane Fence model for the way in which the MSK acts to block diffusion. However, the Membrane Skeleton Fence model does little to explain the behaviour in lipids, particularly those on the outer leaf of the membrane which can not come in to contact with the MSK. The solution to this issue was proposed by Fujiwara *et al.* [6] and Murase *et al.* [8]. Both studies aimed

to elucidate the impact of the MSK on lipids by modulating a number of membrane molecules and structures; such as the membrane skeleton itself, cholesterol (increase in cholesterol produces rafts of lipids), the domain of proteins in the outer leaf, and extracellular matrices. To summerise these studies, it was found that the only parameter which had an effect on the diffusion of lipids was that of the MSK.

To explain the effect of the MSK on lipids in the outer leaf of the membrane, the Transmembrane Protein Picket Model was proposed [39]. Whilst with proteins the MSK acts as a fence, lipids are affected by the proteins that are immobilised on the MSK. The immobile pickets act to increase the viscosity of the membrane for a few nanometres around the protein. This effect is due to steric hindrance and hydrodynamic friction effects.

If immobilised proteins are spread across the MSK at a certain density threshold then it is clear that the protein pickets would act as a diffusion barrier. In fact simulations completed by Fujiwara *et al.*, demonstrated that if the coverage of the compartmental boundary were between only 20% and 30% the observed hop diffusion behaviour could be recovered [6]. It should be stressed that these immobilised proteins do not need to be permanently attached to the MSK. So long as the time the protein is immobilised is longer than the time it takes for the molecule of interest to diffuse across the boundary, the proteins will act as barriers. By way of example the typical time it takes to cross the 10 nm 'barrier' formed by the protein pickets is 10 μs [39], then the protein picket need only be bound to the MSK for a period longer than 10 μs.

The Transmembrane Protein Picket model in conjunction with that of the membrane skeleton fence model shows why transmembrane proteins are affected much more strongly than lipids. They are affected by both the MSK directly as well as by the protein pickets.

With this depth of experimental evidence, it is clear that the cell membrane should

be treated as a two dimensional partitioned fluid rather than as a continuous one. This raises the question: why this might be useful? Previously, the control of diffusion in terms of the photosynthetic pathway of *R. Sphaeroides* was discussed. There are clearly other processes, within any cell, that would benefit from this type of control. The partitioning of neuron cells and the sensing of external stimuli are two examples of the control of diffusion within the cell membrane.

The neuron is split into two distinct parts, the axonal domain where the cell outputs electric signals and the somatodendritic domain which takes the input of signals. These two regions are quite different, with characteristic proteins that are only observed in their own specific domain. These proteins do not mix, yet as the membrane is continuous, there must be some barrier to diffusion that prevents this.

The region between the axonal domain and the somatodendritic domain is referred to as the initial segment, which is an elongated region around 30 nm long. There was some confusion as to the mechanism that could produce the polarisation of proteins, as it appeared that even lipids were blocked into specific domains. SPT experiments in Rat Hippocampal cells confirmed that lipids were confined and that the barrier was located within the initial segment [43]. Studies of diffusion were completed over several days, from newborn cells to cells aged for ten days. The barrier to diffusion formed between days six and ten, and was due to the accumulation of transmembrane pickets into a very dense region of MSK. This very strong barrier acts to prevent the mixing of proteins.

Another process that would benefit from compartmentalisation is the cell sensing external stimuli. Activated receptors are known to join together to form dimers or oligomers [7, 8]. This then causes molecules from the cytoplasm to bind to the dimer/oligomers to form a signalling complex. As shown, the formation of these larger structures severely reduces the rate that the complex can hop between compartments. The complex also is more

likely to anchor to the MSK in a process referred to as oligomerisation-induced trapping. This will often result in the signalling complex becoming trapped in the compartment where the initial signal was first received. In effect, this gives the system memory of the signal origin and acts to give high spatial and temporal resolution for sensing stimuli [9]. Without the partitioning the cell might mistake where, for example, a cache of calcium is located and move it in the wrong direction.

1.6 Aims of this Thesis

It is the main aim of this thesis to examine the diffusion of polymers in a polymeric system analogous to the photosynthetic pathway of *R. Sphaeroides*. Two systems will be examined, firstly a patterned surface designed to mimic the structure of the cell membrane and a second system that aims to mimic a possible cytoplasmic response. Based upon the results of these studies it will be possible to infer certain design principles that might be used to produce biologically inspired devices.

1.6.1 Why Polymers?

The biological systems being examined are incredibly complex, with a vast number of complicated interactions taking place. In order to identify design pricinples that might be of use in devices it is worth simplfying the system. In the case of the diffusion studies provided in this thesis this means moving away from biological molecules and looking at polymers instead. Proteins are notorious for adhering non-specifically to a wide range of materials [44, 45, 46, 47]. To determine the effect that membrane structure and specifically the partitioning of the membrane aids in the control of diffusion, it is worth simplifying the problem somewhat. Similarly to examine how external stimuli cause action in a cytosol analogue, it is necessary to know what impact the stimuli have rather than the complex interaction between proteins.

In addition to proteins there are many other biological molecules present in cells, and it would be equally inappropriate to use these to examine diffusion in biological analogues. Biological molecules interact very strongly with each other and their environment, making it very difficult to isolate features that could be used to design devices or explain certain diffusion behaviours.

Polymers are macromolecules and as such, can have similar molecular weights and conformation to proteins and other biologically relevant molecules. By careful selection of the polymers it is possible to have properties that will aid in the description and functioning of the two studies. In the case of diffusion on surfaces, the diffusing polymers and the polymeric surface can be designed to not only have a similar structure to the partitioning of the cell membrane but to also behave so that only the impact of structure is examined. Similarly the selection of certain polymers can aid the study involving diffusion in the bulk solution by inducing certain changes in the properties of the solution.

The wide range of properties that can be achieved through the use of polymeric systems is very attractive. It is also interesting if similar behaviour can be observed between biological and polymeric systems as this would illustrate the reproducibility of the behaviour without being constrained to biological molecules. In the context of devices this is very important as biological molecules and systems are only optimised to certain conditions, while it is conceivable that the principles that apply to a polymeric system could function across a much wider range of conditions.

1.6.2 Diffusion on Surfaces - Cell membrane analogues

It seems clear that there is a structure to the cell membrane that has a substantial effect on the diffusion of membrane molecules. When considering *R. Sphaeroides*, it is also clear that the chromatophore vesicle itself is not partitioned. By its very nature there is no membrane skeleton directly beneath the vesicle. However, upon considering that

the proteins responsible for the photosynthetic pathway are not found elsewhere in the membrane, it seems reasonable to think that the vesicle is isolated from the rest of the membrane in a similar fashion to how neurons polarise, as described in section 1.5. Could a large array of proteins and membrane skeleton filaments effectively confine the pathway to a vesicle?

To observe the impact of structure in this context a polymeric system has been designed. Specifically, the effect of surface topography on the diffusion of a molecule upon that surface will be examined. The surface in question can be considered analogous to that of the cell membrane, in that it will be partitioned into corrals where diffusion will be unrestricted upon the surface. These corrals will be separated by a barrier that will hinder the diffusion of molecules upon the surface.

An analogue to the membrane molecules is required to diffuse upon this surface. As has been discussed the use of membrane or biological molecules would be inappropriate in this context due to their tendancy to interact very strongly with one another and their environment. Instead, the use of poly(ethylene glycol) (PEG) ($H-(OCH_2CH_2)n-OH$ where n refers to the degree of polymerisation) as an analogue is quite appropriate. PEG is known to be inert in comparison to the biological molecules that are within the cell membrane. In fact, PEG is used as a coating to prevent proteins fouling surfaces and interfaces, or for situations where biocompatibility is a concern, because it does not interact strongly with biological molecules [48, 49].

Due to it's relatively inert nature, PEG has been extensively used for polymer diffusion studies and as a consequence it has well understood behaviours on surfaces [15, 50, 51]. This is ideal for this study as it makes it more obvious when there are deviations from the standard behaviours.

The selection of PEG as the diffusing species places some constraints upon the design of the surface. To determine the impact of the structure it is important that the barrier be constructed so that it will only behave as a physical barrier, rather than producing a more complex interaction based on statics or some strong nonpolar interaction. A simple solution is to use a barrier made of the very molecule that is diffusing. By tethering PEG to a substrate a barrier can be constructed, with the PEG forming a polymer brush. To ensure that this will be a dense barrier that will act to hinder diffusion, the brush can be made slightly more complex by using poly([ethylene glycol] methyl ether methacrylate) (POEGMA). This polymer can be roughly treated as a methacrylate backbone surrounded by very dense PEG chains.

The substrate that this patterned brush is grown upon must meet two requirements. The first demand of the substrate being that it is compatible with the observation techniques used for measuring diffusion, while the second is that it be hydrophobic so as to encourage the diffusing PEG to be on the surface. A glass substrate with a self-assembled monolayer (SAM) is suitable in both regards, as the glass and SAM will be optically transparent while the SAM can be selected to be hydrophobic. In this work the SAM is of (3-Aminopropyl)triethoxysilane (APTES) were used which act as the initiator for the polymer brush. This SAM of APTES had a nitrophenylpropyloxycarbonyl (NPPOC) protection group that was used to select which initiators were used (to allow fabrication of a pattern) while also being hydrophobic.

Once a surface is patterned topographically to produce the analogous systems of compartments, the PEG will be allowed to diffuse upon the surface to examine the diffusion behaviour. The diffusion of PEG on the patterned surface is measured using fluorescence correlation spectroscopy (FCS). FCS allows single molecules to be observed as they move through a volume of typically one femtolitre. This technique has been used extensively to observe the diffusion of biomolecules within the cell membrane and so it seems appropriate

to use this method when examining an analogue of the cell membrane. This thesis will present data showing PEG diffusing on the patterned surface so that a comparison can be made with the equivalent biological system. The FCS diffusion laws put forward by Wawrezinieck *et al* (2005) will be used to look at similiraties and differences between the two regimes [52]. The aim is to present an explanation for the behaviour observed in the polymeric system.

1.6.3 Diffusion in the Bulk - Cytoplasmic Response

It appears that there must be some mechanism for the control of bulk diffusion in *R. Sphaeroides*. Even if this is not the case in *R. Sphaeroides*, it would be very desirable to control the diffusion of species in the bulk in a device to some degree. During the discussion of the photosynthetic pathway, it was identified that the cytochrome bc_1 pumped protons across the cell membrane to produce a gradient. This excess of protons would then drive an ATP synthase protein to produce the energy unit ATP. Three protons are required to drive the protein in order to produce ATP while a fourth is required to actually produce the ATP, so there is understandably a drop in power efficiency at this point in the photosynthetic pathway. This is the portion of the photosynthetic pathway where the *R. Sphaeroides* bacterium is at its least efficient, with the drop from 90% power efficiency reaching the cytochrome bc_1 to 3% power efficiency after ATP has been produced. While this is clearly not a problem for the bacterium, it must produce enough ATP or it would die, it would be ideal from a artificial perspective to improve upon this.

It would be desirable to have some control over the diffusion of the protons once they have been pumped across the membrane. This diffusion will be in the bulk, the protons will experience no confinement and consequently will be able to diffuse randomly in all three dimensions. Therefore it seems reasonable that the cell might have some method of controlling this motion, or if not, that it would be beneficial from an artificial perspective to be able to control diffusion in three dimensions at some level.

If we consider the fundamental description of diffusion, a one dimensional stepping process where a diffusant will go one unit of distance for each time step. We will now extend this for the case where there is some directionality, for example in viscosity. Consider the Stokes-Einstein Relation (eq. 1.7.5), if the viscosity (or some other parameter) were to vary based upon location within the medium, then the diffusion would be conceivably faster in one position than at some other point. At higher viscosities the diffusant will diffuse slower than at lower viscosities, all other parameters being equal. In the case of our thought experiment let the high viscosity reside to the left and the lower viscosity to the right. Diffusion is purely random, so there will be as many steps to the left as to the right. However, by using the logic presented above, the diffusant would step further right than it would to the left. Effectively this means that over time, the diffusant will move to the right. Could a similar phenomenon be used in the case of diffusion of protons in the cytosol?

The cytosol is composed of water, salts and organic molecules [12]. This description is very similar to that of a gel and as such it is possible to examine how diffusion in the cytosol might be controlled by examining diffusion in a gel. Ideally the gel, and by extension the cytosol, would undergo some change that would impact the diffusion of the protons. The most obvious and the simplest change that would be applicable, and that could occur, is that of a viscosity change in the gel in response to a stimulus.

Gels as a cytosol analogue

In his book 'Cells, Gels and the Engines of Life', Gerald Pollack made a number of comparisons between the cytosol and polymer gels [53]. He made the point that cells perform a number of tasks in their interior. Cells produce substances that must be moved about and they also need to react to stimuli. All cells divide so as to multiply and specialized cells perfom a diverse range of tasks. He posits that polymer gels offer a paradigm that could explain, or at least allow for a unified description of, the cytosol.

The cytosol and polymer gels have a number of similarities, and by recognising these similarities it is possible to treat the cytosol as a gel. Such a treatment can then be examined to find whether it aids in explaining the behaviours observed in cells.

A gel is a polymer network where individual polymer molecules typically cross-link to one another, doing so either chemically or physically. The 'pores' of the polymer network contain solvent and, for the purposes of this work, water will be considered. The amount of solvent, and consequently the size of the pores, is defined primarily by the polymer surface. If the surface is hydrophobic, water will self-associate to form a moderately well ordered three-dimensional hydrogen bonded network [54]. In the case of hydrophilic surfaces (the case with the majority of biological polymers), water will be attracted to the surface. The surface-adhered water will in turn attract more water so that layers of water are formed.

The water content of the gel will therefore be highly dependent on the nature of the polymer and particularly the surface that the polymer has in contact with the water. The work of Osada and Gong (1993) stated that gels of uncharged polymers had a water-to-polymer volume ratio typically between 5:1 and 10:1 while gels made of charged polymers can have a ratio up to 3000:1 [55]. It should be noted that the layering behaviour of water may not be the only factor involved in this water retention. For example, osmotic forces will draw water when a counter-ion is present about a surface bound charge. However, the fact that such a high ratio is present in the uncharged case and is easily achievable suggests that other factors might be secondary.

Swelling in polymer gels is the process by which the gel increases in size as it draws solvent into the pores in the polymer network. In 1968 the swelling of polymer gels was predicted, by Dusek and Patterson, in response to changes in the composition of the solvent [56].

This was shown experimentally by Tanaka (1978) [57], when a polyacrylamide gel was shown to swell and contract with changes in temperature and solvent content, specifically the change in concentration of acetone. The change in gel volume was enormous (two orders of magnitude) when a threshold temperature was passed. This can be treated as a form of phase transition, much as the change between water and ice, the two states bear little resemblence. Crucially, the transition is bought about here by nothing but a minor change in the environment.

Gels act in a number of ways; in his review article Hoffman (1991) picked out a number of both stimuli and responses that had been observed in polymer hydrogels [58]. Changes to any part of the environment, or any input of energy, can act as stimuli. For example, changes in pH, temperature and solvents as well as fields and input of light, have all been observed to produce an action. The action itself can again vary greatly depending upon the gel in question. Hoffman draws attention to not only swelling and shrinking of the gel; but also the phase separation of components within the gel, mechanical responses (hardening or softening) as well as chemical responses. As an aside, it should be noted that gels that chemically cross-link are generally stable with changes in their environment and so will only rarely exhibit transitions. A physical cross-link is one formed by intermolecular interactions such as van der Waals forces. As such these bonds are more susceptible to their environment and can be disrupted, potentially leading to the transitions discussed as their structure changes to accomodate the disruption.

When considered in terms of the cell, certain parallels can be drawn. Cells of various types will use pH change, temperature change, chemical agents and mechanical forces as triggers to initiate various processes or tasks. The response to these triggers will usually take the form of changes in shape and volume as well as changes in permeability and electrical potential. If the step in logic is taken that there is a common denominator in function within these cells, then the phase transition of the gel seems a suitable candidate.

Using a Diblock Copolymer Gel for Studying Diffusion

It is the aim of this study to observe the change in conformation by using FCS to measure the diffusion coefficient of the diffusing polymers in the gel. A block copolymer of poly(glycerol monomethacrylate) (PGMA) extended with poly (hydroxypropyl methacrylate) (PHPMA) forms a gel which is made of cylindrical micelles, or worms, but changes to an aqueous solution of spherical micelles, or spheres, when temperature is lowered or the pH is raised beyond a critical value [59, 60]. The transition between worms and spheres, from a gel to an aqueous solution, leads to a significant change in the viscosity of the system. The reduction in viscosity produced by the change will lead to an increase in diffusion coefficient. In this study it will be the block copolymer that is tracked, while in the case of the *R. Sphaeroides* it is protons that diffuse within the cytosol. The proton is obviously much smaller than the copolymer, which is more analogous to the medium of the cytosol than the diffusing species, but intuitively it can be taken that a change in how the medium diffuses will have a profound impact on the motion of the molecules that diffuse within it. Not least because the transition itself is accompanied by a stark change in viscosity.

By observing the change in diffusion coefficient of the PGMA-PHPMA with changes in temperature and pH, it will be argued that the cytoplasm of a cell may be treated as a gel. In consequence the results of this study will also be used to discuss the impact this has upon the description the photosynthetic pathway of *R. Sphaeroides* and by extension devices that could be constructed using design principles in the model of biological systems.

1.6.4 Research Questions

The overarching theme examined in this thesis concerns the diffusion of biological analogues in polymeric systems based upon the photosynthetic pathway of *R. Sphaeroides.* A research question could therefore be formulated that addressed this theme. This question must

address the fabrication of analogous systems in addition to the examination of diffusion:

> Can a polymeric system be produced that acts as an analogue for specific regions of the photosynthetic pathway of *R. Sphaeroides* and that can be used to examine diffusion in these regions as well as inform designs for use in devices?

This overarching theme can be broken down into three distinct areas, that can themselves be used to generate more questions. The three main groups of questions that will be examined in this thesis with respect to the diffusion of polymers in biologically analogous systems are:

1. Can a topographically patterned POEGMA brush surface (based upon the schemes in figure 1.9) be produced that can be used as an analogue of the structure of the cell membrane, particularly as described by the membrane skeleton fence model and the transmembrane protein picket model, in relation to the diffusion of membrane molecules? Is the methodology used to produce this surface capable of upscaling? How good is the resolution and how repeatable is it?

2. What is the diffusion behaviour of PEG on this surface? Is it faster or slower than diffusion on either homogeneous surface? Does the behaviour have any similarities with that observed in biological membrane systems? Is it possible to attribute a cause to this behaviour in the polymeric case?

3. Can the rate of diffusion of molecules in a gel be significantly modified with changes in pH and temperature? Does this have any value when considering the control of diffusion in the cytosol with respect to the photosynthetic pathway of *R. Sphaeroides*?

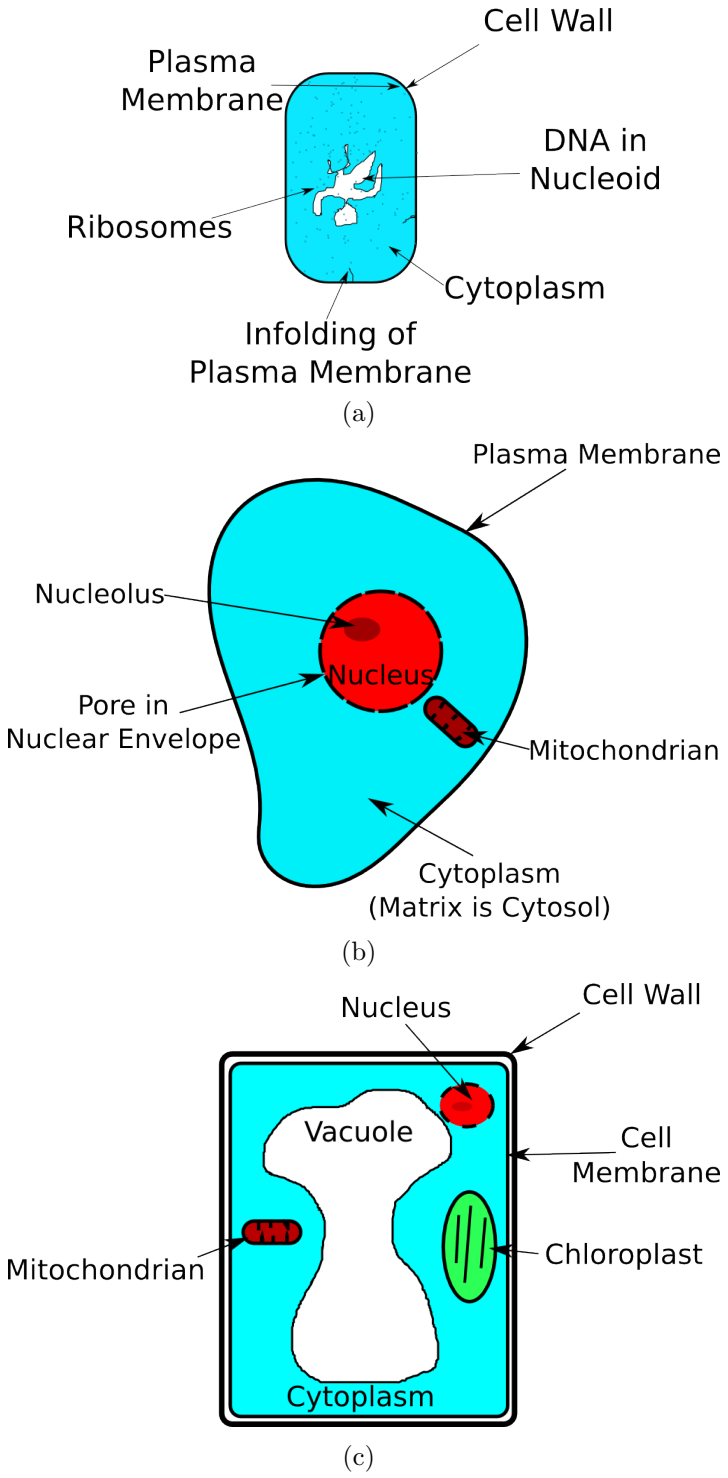

Figure 1.8: Diagrams of the structure of different cells. A cell membrane surrounding a matrix, known as the cytosol, in all types of cell. (a) a generalised bacterium, demonstrating the structure of a prokaryotic cell. (b) demonstrates the structure of a generalised animal cell, however much of the fine structure has not been displayed for ease of viewing (e.g. the absense of ribsomes and organelles such as the endoplasmic reticulum). (c) illustrates the structure of a generalised plant cell, and as in the case of (b), much of the fine structure is not shown.

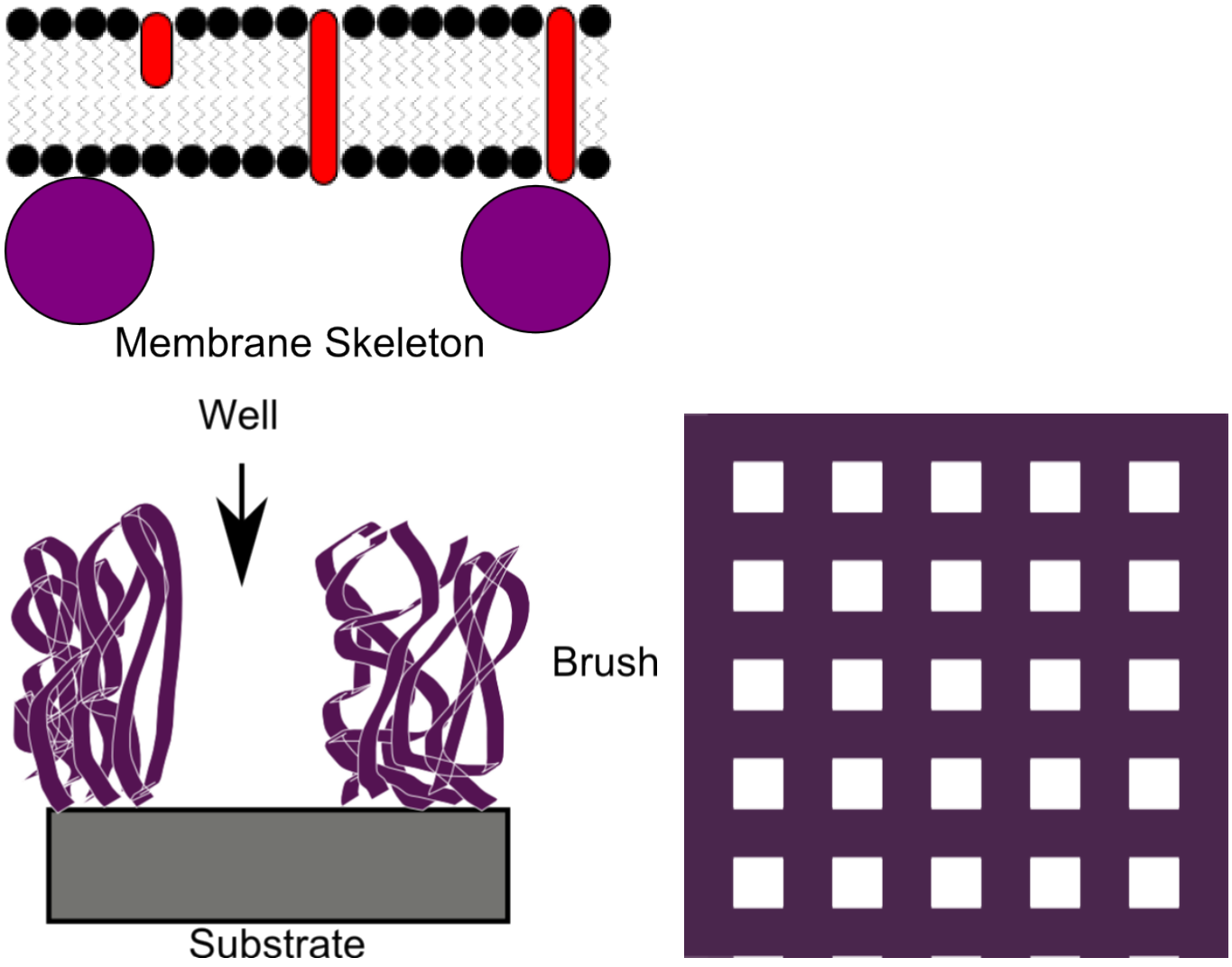

(a) (b)

Figure 1.9: Schematic diagrams demonstrating the design of the patterned POEGMA surfaces. (a) the profile of the surface as seen in the z-plane and shows the brush grown from the substrate so as to form wells with a comparison to the structure of the cell membrane. The Purple represents the part of the structure that relates to the barrier (the membrane skeleton and the brush respectively). (b) a top down scheme showing the square well nature of the surface with the polymer brush again shown in purple.

1.7 Theory

1.7.1 Diffusion

Simple diffusion is defined as the process by which different substances mix as a result of the random motions of their component atoms, molecules and ions [61]. Diffusion on the molecular level is propelled by thermal energy while larger particles move via collisions with the molecules of the solvent (Brownian motion). In simple cases the rate of diffusion (diffusion coefficient) is directly related to the temperature of the system, and the net motion is down the concentration gradient of the system. This simple example is described by Fick's Laws of Diffusion. Fick's First Law (derived in appendix A.2) described the mass flux, J, as:

$$J = -D\frac{\partial \rho}{\partial x}, \tag{1.7.1}$$

where ρ is the concentration and x is position and D is the diffusion coefficient. The diffusion coefficient itself is defined as:

$$D = \frac{\langle x \rangle^2}{(d \cdot t)}, \tag{1.7.2}$$

where $\langle x \rangle^2$ is the mean-squared displacement, t is the time interval and d refers to the dimensionality of the system ($d = 2, 4, 6$ for 1-, 2-, 3-dimensions). $\langle x \rangle^2$ can be thought of as the space explored by the diffusing particle.

Bulk Diffusion

Diffusion in three dimensions has been examined extensively, with the earliest analysis of the process revolving around Brownian motion. Brownian motion is the random motion of a particle that is suspended in a fluid of some description (a liquid or a gas) caused by the collision of the particle with atoms or molecules within the fluid.

The first written description of Brownian motion is in the poem 'On The Nature of Things' by the Roman philosopher Lucretius, circa 60 AD. Lucretius was an ardent follower of atom theory and discussed the motion of dust particles in air as a proof of the existance of atoms. Although presented in the style of a poem the underlying science is correct, yet the work was largely ignored for centuries. The next mention of Brownian motion was in 1785 by Jan Ingenhousz (coincidently credited as the discoverer of photosynthesis) when he observed the motion of coal dust on the surface of alcohol [62]. Despite this earlier finding, the discovery of Brownian motion is credited to Robert Brown in 1827. Brown, looking at pollen grains suspended in water, observed particles ejected by the pollen execute stuttering motion. He repeated the experiment with particles of inorganic matter to rule out the possibility of the phenomena being due to biological origins but was unable to establish the origins of the motion [63].

A mathematical description of the behaviour was first made by Thorvald Thiele in 1880 [64] and subsequently followed up by Louis Bachelier in 1900 [65]. In both cases the problem was treated purely mathematically with no desire to examine a root cause. The next step in the development of Brownian motion came from Albert Einstein [66] and Marian Smoluchowski [67], who independently presented their descriptions. The descriptions presented by both relied heavily on the existance of atoms, a concept that was at the time seen as useful but that scientists still debated whether they were real entities. The work of Einstein and Smoluchowski gave a statistical description of atomic behaviour that would allow experimentalists to count atoms with ordinary optical microscopes. In relatively short order the equations presented by the pair were verified experimentally by Jean Baptiste Perrin in 1908 [68].

In Einstein's theory there were two distinct parts; the first involving the formulation of a diffusion equation for Brownian particles, where the diffusion coefficient was related to the mean squared displacement (as in Fick's Law), with the second part relating

the diffusion coefficient to measurable physical quantities [66]. The first part effectively provides equation 1.7.2 (see appendix A.4), but presents it such that both systems of an ensemble of Brownian particles and a system containing a single Brownian particle are well defined. This allows the for the discussion of the relative number of particles at an instant as well as the time required for a particle to reach a given point.

The second part of Einstein's theory is perhaps more interesting in that it relates diffusion to physically measurable quantities. Einstein made his formulation by considering a dynamic equilibrium between opposing forces, a key facet being the unimportance of the particular forces involved in producing the equilibrium itself. The derivation of this equation is presented in appendix A.5 but the final result is

$$\mu = \frac{D}{k_B T}, \tag{1.7.3}$$

where μ is the mobility of the diffusing particle, D is the diffusion coefficient and T is the temperature.

The general case presented by Einstien can be modified to deal with the various plausible scenarios where it is desirable to calculate the diffusion coefficient of a particular species. For the work described here a specific relationship known as the Stokes-Einstein equation is particularly relevant. The Stokes-Einstein equation deals with a spherical particle, of radius r, diffusing in a medium in the limit of a low Reynolds number and uses the Stokes Force as the 'driving force'. In the case of low Reynolds number the mobility of the particle is simply the inverse of the drag coefficient ζ, Stoke's law gives

$$\zeta = 6\pi\eta r, \tag{1.7.4}$$

where η is the viscosity of the medium. This can be used to find the Stokes-Einstein relation:

$$D = \frac{k_B T}{6\pi\eta r}. \tag{1.7.5}$$

Thus far the diffusion of spheres in three dimensions has been considered and this broadly works across a variety of systems that are not explicitly spheres but can be taken as such, including that of polymers diffusing in a medium. A point of particular relevence with polymers is the degree of polymerisation (molar mass): as this increases, the diffusion coefficient is reduced. In fact early work by Debye and Bueche found that in the dilute limit (individual chains in a solvent) the radius of gyration of the polymer chain could be effectively treated as the hydrodynamic radius required in the Stokes-Einstein relation [69]. As already stated the degree of polymerisation, N, plays a key part in the diffusion of the polymer and can be used to calculate the radius of gyration. Depending on the conditions the radius of gyration is proportional to $N^{3/5}$ in a good solvent (one where the polymer chain stretches), and to $N^{1/2}$ in theta conditions (where the polymer conforms to a idealised random walk).

Bulk diffusion differs from surface diffusion in that it is not constrained; when on a surface the diffusant in question is limited to where it can move. One of its degrees of freedom has been removed, namely the motion out of the plane of the surface. As a consequence, diffusion coefficients are faster in the bulk than upon surfaces [50], often by as much as two orders of magnitude.

Surface Diffusion

Surface diffusion is a process specifically concerned with particles moving along solid interfaces. A general picture of surface diffusion is that of particles jumping between adjacent adsorption sites on the surface. Like simple bulk diffusion, an important parameter

describing the diffusion coefficient is temperature. In addition to this, the interactions between the adsorbed particle and the surface play an important role.

Mathematically, a very simple description can be produced to describe the kinetics of surface diffusion [70]. Consider a system where adatoms (defined as an atom on a crystal surface that should be thought of as the opposite of a surface vacancy) reside on a surface constructed as a 2D lattice of adsorption sites. The adatoms can move between adjacent (nearest neighbour) sites by some 'jumping' process. The rate of the jump process (Γ) will be described by an Arrhenius equation that includes an attempt frequency and a thermodynamic factor that deals with the probability of a sucessful jump. The attempt frequency is simply the vibrational frequency of the adatom (ν), while the thermodynamic factor is a Boltzmann factor that depends on the temperature (T) and the potential energy barrier to diffusion (E_{diff}) that holds the adatom in place. Putting this together gives the relationship

$$\Gamma = \nu \mathrm{e}^{-\frac{E_{\text{diff}}}{k_{\text{B}}T}}. \tag{1.7.6}$$

Clearly E_{diff} must be lower than the energy required for desorption, or desorption processes would dominate over those of surface diffusion. A crucial factor to consider is the importance of temperature shown in equation 1.7.6. The relationship between E_{diff} and temperature suggests a number of scenerios, firstly that where $E_{\text{diff}} < k_{\text{B}}T$ the barrier effectively does not exist. This leads to a regime known as mobile diffusion and is relatively uncommon [70]. Fickian diffusion is much more common and comes about when $E_{\text{diff}} \gg k_{\text{B}}T$ meaning that $\Gamma \ll \nu$.

The surface diffusion of polymers, and indeed of macromolecules in general, is similar in theory to this description with a single caveat. Polymers are intrinsically large molecules, made up of several units (or monomers). Each of these units can effectively

behave as a adatom and as a consequence each unit has limited options as to where it can 'hop'. This means that a polymer is not treated as a single entity but rather as an ensemble of adatoms. The length of the polymer chain clearly matters from this logic, while the adsorption energy of a single segment is small ($\sim k_{\mathrm{B}}T$) it is significant over numerous segments.

Theoretical considerations predict that diffusion of a polymer on a homogeneous solid surface scales as $D \sim M^{-1}$, where M is the molar mass of the polymer [71, 72]. This dependence comes about as friction scales linearly with the molecular weight. The relation has been examined in depth via simulations and has been found to be a good description of polymers on homogeneous surfaces [73, 74, 75]. However, experimentally the levels of homogeneity required have not been achieved. Indeed it is not known precisely the limit at which the surface would be considered 'homogeneous enough' to apply this relation for the diffusion coefficient. As way of an example, single crystal surfaces have a regular homogeneous crystalline structure but there are also defects present, and the effect the presence of these defects would have on diffusion is not known.

In relation to the idea of disorder having an impact on diffusion, it is known that theoretically a chain can be guided between surface obstacles produced by surface disorder [76, 77]. This behaviour is characterised as reptation-style diffusion and the diffusion scales as $D \sim M^{-3/2}$ [78, 79, 80]. Reptation-style diffusion is known to hold in situations where the chain is adsorbed to the surface in a pancake structure but the limit to which this applies to chains not so well 'held' (polymers with train and loop conformations) is again not entirely known.

The diffusion coefficient of a polymer upon different surfaces is known to vary. This has been attributed to a number of factors, yet perhaps the most consistent is that of the polymer conformation upon the surface, and this links very easily to the arguments

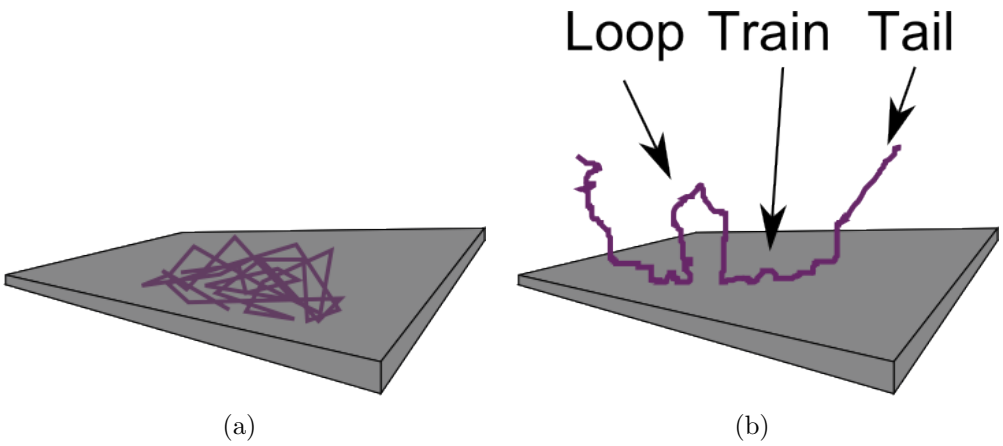

Figure 1.10: Conformation of polymers at an interface. (a) shows the pancake conformation where the polymer is strongly attracted to the interface and is in complete contact with it. (b) demonstrates the case where the polymer is less strongly attracted and as a consequence loops, trains and tails form.

previously discussed. The three way interaction between the polymer chain, the surface and the solvent is the defining relationship leading to specific conformations. As a general rule more hydrophobic surfaces force water-soluble polymers to assume a more compact, pancake structure [51, 81]. This in turn leads to a slower diffusion coefficient than the same polymer on a hydrophilic surface, where the water in the solvent will compete with the polymer for a binding site on the surface [81]. Simulations have also shown that monomer friction coefficients (directly related to the surface energy of the system) have a strong influence on surface diffusion, with smaller friction coefficients leading to larger diffusion coefficients [82].

A key facet of this thesis is to observe how modifying a surface can lead to a control of diffusion upon said surface. It has been demonstrated that the diffusion of a species on a surface can be directed. Chaudhury and Whitesides (1992) demonstrated that a water droplet could be moved 'uphill' [13]. The water droplet was placed on a surface with a gradient of hydrophobicity, causing the droplet to steadily move towards the more hydrophilic region. This was even the case when the hydrophilic region was raised so that the droplet needed to work against gravity. Suzuki (1994) demonstrated that droplets

of oil could be made to behave in a similar way, moving along a hydrophobicity gradient [14]

A further example of directed motion, relating to polymers specifically, is Burgos *et al.* (2009). Here it was shown that single molecules of PEG could be sent down a surface energy gradient [15]. The surface gradient produced went from stongly hydrophobic to strongly hydrophillic over the space of a few microns, with motion driven to the hydrophilic region. The observations were made using fluorescence correlation spectroscopy and showed that surface diffusion was elevated by more than an order of magnitude with respect to surfaces without the gradient. Diffusion along the gradient was increased greatly, with diffusion coefficients $\sim$100 times larger than the diffusion coefficient in the orthogonol direction.

Diffusion and Barriers

The traditional description of diffusion needs to be extended for certain conditions. One such condition of interest is the addition of partially permeable barriers. If we consider a two-dimensional system partitioned by permeable one-dimensional barriers we find that on short time scales the diffusing particle will be confined to a single compartment. In contrast working at longer time scales shows that the particle will escape to an adjacent compartment. This anomalous diffusion process, known as hop diffusion, causes a reduction in the macroscopic diffusion coefficient, as the diffusing particle cannot explore the same size region of space as an unconfined particle.

A number of theoretical studies have looked at how the behaviour of diffusing particles would change with the addition of permeable barriers. In his 1966 paper for the Mathematical Association of America, Mark Kac showed that certain information about the geometry of a drum could be collected based upon the sound it produces [83]. Kac suggested that the area and perimeter of the drum can be 'heard', and the main example provided in support of this was the diffusion of particles on a plane bounded by an

absorbing interface. He demonstrated that the volume to surface area ratio could be deduced from the information in the limit of long times.

A more recent example by Novikov *et al.* (2011) presented a treatment of free diffusion impeded by randomly placed and orientated barriers ($d-1$ dimensional planes in a d dimensional system) [84]. This study established that the barriers introduced distinct features to the transport of particles. One such feature was described as how the diffusing species gained a long-term memory of the system, induced by the spatially extended disorder introduced by the diffusion barriers. This memory is seen as a characteristically slow decrease of the diffusion coefficient

$$D(t) = D_\infty + const \cdot t^{-\frac{1}{2}}. \tag{1.7.7}$$

The barrier is treated as an idealised thin slice of a poorly diffusive material, with a thickness that is negligible when compared to the shortest observable diffusion length. In this limit the diffusion coefficient D_m and the thickness l_m of the membrane vanish, the ratio $\kappa = \frac{D_\mathrm{m}}{l_\mathrm{m}}$ is the definition of the membrane permeability. The diffusing particles are treated as idealised random walkers in a macroscopic sample with randomly placed barriers. The study proposed that the diffusion behaviour of the random walkers would vary significantly between characteristic time scales. The first such result is in the extreme case of $t \to \infty$. In this limit, the diffusion was Gaussian with a diffusion coefficient greatly reduced from that of diffusion within the space between barriers (D_0)

$$D_\infty = \frac{D_0}{1+\zeta}, \tag{1.7.8}$$

where $\zeta = \frac{Sl}{Vd}$ is defined as the ability of the barriers to hinder diffusion (S is the surface area of the barriers, $l = \frac{D_0}{\kappa}$ is the effective thickness of the barrier, V is the volume of the sample and d is the dimensionality of the system). This result is exact in the case $d = 1$ and is a good approximation in the case $d > 1$. A strong restriction on diffusion

is characterised by $\zeta > 1$ and primarily means that the effective thickness of multiple barriers overlaps so that the diffusion across a single barrier is strongly affected by the diffusion across its neighbours.

In finite time periods there is different behaviour dependent on how much the barrier hinders diffusion. The first case, where a barrier strongly hinders diffusion ($\zeta > 1$), has three distinct timescales with corresponding behaviour. The first such regime describes the diffusion coefficient in the period where only a very small fraction of the random walkers have encountered the barriers ($t \ll \tau_{\mathrm{D}}$ where $\tau_{\mathrm{D}} = \frac{a^2}{2D_0}$ is the diffusion time across the average compartment of size a). This regime is described by:

$$D(t) \simeq D_0 \left[1 - \frac{S}{Vd}\left(\frac{4\sqrt{D_0 t}}{3\sqrt{\pi}} - \kappa t\right)\right]. \tag{1.7.9}$$

and is in perfect agreement with theory and simulation for all ζ.

The second regime describes the impermeability of the barriers at times shorter than the residency time of the compartment ($t \ll \tau_{\mathrm{r}} = \frac{\zeta}{d}\tau_{\mathrm{D}}$ where τ_{r} is the residency time of the compartment). The behaviour in this regime is described as

$$\frac{D(t)}{D_0} \approx \frac{2\tau_{\mathrm{D}}}{t}. \tag{1.7.10}$$

The final regime deals with the behaviour of the random walkers for times longer than τ_{r}. The leakage through the barriers is now significant enough for the system to be 'aware' of it. $D(t)$ now approaches the D_∞ limit and can be described as:

$$D(t) \simeq D_\infty \left(1 + \sqrt{\frac{8\zeta d}{\pi}}\frac{(\sqrt{1+\zeta} - 1)}{(\sqrt{1+\zeta})}\sqrt{\frac{\tau_{\mathrm{r}}}{t}}\right). \tag{1.7.11}$$

The second case treated in this study was the case of highly permeable barriers ($\zeta \ll 1$). In this case, τ_{r} and τ_{D} become comparible and only two regimes are observed, the intermediate

$^1/_t$ regime is not observed. The behaviour of diffusion is now described by:

$$D(t) \simeq D_\infty \left(1 + \frac{2\zeta}{\sqrt{\pi}}\sqrt{\frac{\tau}{t}}\right), \tag{1.7.12}$$

where $\tau = \zeta \frac{d}{2} \tau_{\mathrm{r}}$.

The study by Novikov *et al.* is primarily concerned with describing the motion of diffusing particles in a system, it is regularly demonstrated that by recording the diffusion coefficient as a function of time it is possible to extrapolate information concerning the system.

Wawrezinieck *et al.* (2005) proposed a set of FCS diffusion laws to define the structure of the cell membrane [52]. It was shown that by making FCS measurements at different spatial scales that different models of confinement could be distinguished. The importance of taking measurements at different waist widths (the width of the focal point) is demonstrated by considering the experimental diffusion data presented by Wawrezinieck and her colleagues. The observations were on COS-7 cells (American type culture Collection No CRL-1657) with a fluorescent probe attached to the lipids, BODIPY-ganlioside GM1 (FL-GM1), within the plasma membrane. Molecules undergoing anomalous diffusion exhibit a non-linear exploration (or $\langle x \rangle^2$) with respect to time. As such their $\langle x \rangle^2$ can be defined as $\langle x \rangle^2 \sim Dt^\alpha$, where α is 1 for simple Brownian motion, $\alpha < 1$ for systems with some level of confinement and $\alpha > 1$ where there is active transport. In the system discussed by Wawrezinieck and her colleagues, the data extracted exhibited an $\alpha \approx 1$ suggesting free diffusion despite the diffusion clearly being constrained (the diffusion time was $\sim$10 times longer than that of FL-GM1 in an artificial membrane). They point to this as a reason why multiple measurements over several waist sizes provides an interesting and necessary measure of confinement.

For free diffusion it would be expected that the diffusion time would be directly proportional to the square of the waist size (w^2). As the waist size is extrapolated back to zero, the diffusion time should intersect the origin. It can be shown that for systems experiencing anomalous diffusion, the diffusion is not directly proportional to w^2, but is described more accurately by

$$\tau_{\mathrm{d}}^{\mathrm{app}} = t_0 + bw^2, \tag{1.7.13}$$

where $\tau_{\mathrm{d}}^{\mathrm{app}}$ is the observed diffusion time and t_0 is the extrapolated diffusion time to a zero beam waist. Although the real value for the diffusion time at zero beam waist will be itself zero, the extrapolated value can provide information about the structure of the system.

After many simulations of various structures, Wawrezinieck *et al.* defined how diffusing molecules would behave in three scenarios [52], in a simple free diffusion case (figure 1.11(a)), in a system containing isolated microdomains (figure 1.11(b)) and in a system with a meshwork-style barrier (figure 1.11(c)). A confinement parameter was introduced for ease of analysis ($X_c^2 = \left(\frac{w}{L}\right)^2$ where L is the domain radius). It was demonstrated that simple free diffusion would, as expected, show that diffusion time was directly proportional to the square of waist size (figure 1.11(d)).

The second scenario of permeable isolated micro-domains was defined as microdomains surrounded by an energy barrier, designed to simulate raft behaviour as well as other phase-separated domains that might be present. Static circular domains were inserted into a large square membrane with the inside and outside of the domains containing different phases of material. The beam was focussed on the centre of a single domain. Three distinct diffusion time regimes were observed as the waist size increased. The first regime is seen when the waist is much smaller than the domain size ($X_c^2 \leq 0.1$) and diffusion is seen to behave as in free diffusion. A second transient regime is observed when the

waist and domain sizes are comparable ($X_c^2 \approx 1$) and complex diffusion due to barrier effects is observed. The last regime is seen when the waist size is much larger than the domain size ($X_c^2 \geq 10$) and a linear scaling of diffusion time with beam waist returns. The linear scaling in the third regime is different to that of the first, with the value of b, from equation 1.7.13, increasing (equivalent to a decrease in diffusion coefficient) and a strictly positive t_0 (figure 1.11(d)).

The third scenario relates to the idea of the cytoskeleton acting as a hindrance to diffusion through the introduction of a meshwork geometry. In simulations this system was described as a set of multiple domains separated by barriers. The beam is focussed on a knot of the meshwork (the point between four domains). A slight redefinition of the confinement parameter is required for the meshwork as now, rather than circles with radius L, the domains are squares of side 2L. The confinement parameter should now be defined as $X_c^2 = \frac{\pi}{4}(\frac{w}{L})^2$. The meshwork geometry also exhibits three regimes, the first and second of which are very similar to that of the isolated microdomain geometry, but with different confinement parameter values ($X_c^2 < 2$ for the first regime and $X_c^2 \approx 2$ for the second regime). When the probed area becomes much larger than the domain size ($X_c^2 > 2$) a linear relation is recovered as seen in the isolated microdomain case, but the value of t_0 is strictly negative (figure 1.11(d)).

An experimental study by Lenne *et al.* (2006) demonstrated these scenarios in live cells, confirming the validity of these FCS diffusion laws [85]. As the systems of microdomains and meshwork exhibit much of the same diffusion behaviour, it is the value of t_0 that is required to differentiate the geometries.

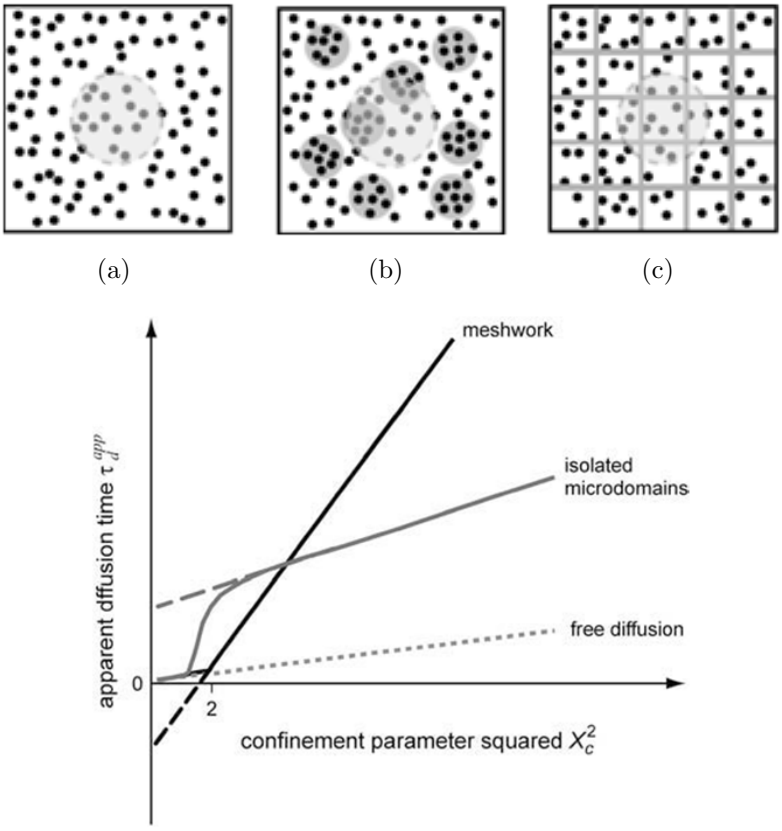

Figure 1.11: The structures simulated for the FCS diffusion laws: free diffusion (a), isolated microdomains (b) and a meshwork (c). (d) shows the expected changes in diffusion time as the confinement parameter increases or conversely the size of structure decreases. Modified from source [85] and presented with permission

1.7.2 Polymer Brushes

Polymer brushes are polymers that are tethered to a surface or an interface [86]. The tethering must be sufficiently dense so that the polymer chains are crowded, and are therefore forced to stretch away from the surface or interface. This stretching is sometimes farther than the typical unstretched unconfined length of the polymer chain. The stretching behaviour occurs under equilibrium conditions with no need for external processes such as an applied field and no confining geometry is required.

The derivations of brush thickness in good and theta solvents are presented in appendix

A.6. The critical result in these situations is that brush thickness is directly proportional to the degree of polymerisation in a polymer brush in both good solvents and theta solvents. This can be contrasted to a free polymer chain, demonstrating that the confining interface causes the polymers to stretch from the surface (summarised in table 1.2).

	Tethered Polymer Brush Chains	Free Polymer Chain
Good Solvent	${}^{L}/_{a} \approx N\left({}^{a}/_{d}\right)^{2/3}$	$R_g \sim N^{3/5}$
Theta Solvent	${}^{L}/_{a} \approx N\left({}^{a}/_{d}\right)$	$R_g \sim N^{1/2}$
Bulk state	$L \sim N^{2/3}$	$R_g \sim N^{1/2}$

Table 1.2: The relationship between the dimensions of a polymer and the degree of polymerisation based upon the Alexander Model.

In general there are two paths to fabricating polymer brushes on solid surfaces, polymer physisorption and covalent attachment [87]. In polymer physisorption, block copolymers adsorb onto a suitable surface where one of the blocks strongly interacts with the surface and the other interacts very weakly. This methodology will not be considered in this thesis.

Covalent attachment looks to firmly fix the polymer to the substrate by means of a covalent bond [87]. This can be achieved in two ways, referred to as the grafting-to and the grafting-from approaches. In the grafting-to approach, a preformed end-functionalised polymer molecule is reacted with the substrate to form polymer brushes. The approach relevant to the work described in this thesis is the grafting-from approach. This method leads to the synthesis of polymer brushes with a higher grafting density as the polymer chain is 'grown' *in situ* from a suitable initiator.

This thesis will focus on the grafting-from approach where the initiator is within a well defined self-assembled monolayer (SAM) on the substrate. There are a wide range of

polymer synthesis methods that can be used to produce brushes. The methodology of interest in this thesis is atom transfer radical polymerisation (ATRP).

ATRP is termed a controlled radical polymerisation and as such gives great control over the molecular weight distribution of the brush produced [88]. The precursor for ATRP was a form of organic synthesis known as atom transfer radical addition (ATRA) [89]. In this synthesis, atom transfer from organic halides to transition metal complexes acts to produce an organic radical. This radical is then deactivated by the transfer of the atom from the transition metal back to the organic radical.

The low dispersity of ATRP arises due to the transition metal based catalyst [88]. The catalyst provides the system with an equilibrium between the active polymer, when the polymer can propagate, and an inactive (dormant) form of the polymer. The equilibrium between these two states is heavily skewed to the dormant state of the polymer, which limits the rate of active propagation.. This leads to the low dispersity as all chains are equally likely to propagate. It also leads to the fact that termination of the radicals is avoided until almost 100% of the monomers has been converted.

There are five important components that are varied between ATRP reactions but there are consistent factors throughout. The factors that can be changed are the monomer itself, the initiator, the catalyst, the solvent and the temperature. Each factor will be discussed as a contribution to the polymerisation reaction.

The monomers that are typically used in ATRP are molecules that can stabilise the propagating radicals [88]. Examples of this are styrenes and acrylates. If polymers with a high average molecular weight and low dispersity are desired, the concentration of the propagating radicals must balance the rate of termination of radicals. It is important that the concentration of the dormant polymer be greater than the concentration of the radicals

so that termination can be prevented. Despite this it is crucial that the concentration of the dormant polymer not be not so great that the reaction is slowed or halted [88, 90]. Each monomer species has a unique propagation rate, which can be combined with the other components of ATRP to optimise the reaction.

The number of polymer chains that are growing is determined by the initiator present [88]. The faster the initiation process is, the more consistent the number of growing chains are, which leads to the low dispersity. This stems from the fact that the faster the initiation process, the fewer terminations of radicals occur and the fewer atom transfers can occur between the growing polymer chains and the catalyst. Organic halides are a popular choice of initiator [91], with most initiators being alkyl halides, specifically alkyl bromides which are more reactive than alkyl chlorides [88]. The structure and shape of the initiator will determine the architecture of the polymer. In the case of polymer brushes, the initiator is immobilised onto a surface such that the brush will grow away from the substrate.

The catalyst is arguably the most important component of the ATRP process. It determines the equilibrium between the active and dormant species and this equilibrium determines the polymerisation rate [88]. If the equilibrium is too skewed to the dormant species the reaction proceeds too slowly, while if it is skewed to the active species then the low dispersity is lost and a high distribution of chain lengths is produced. As already stated, there are a number of requirements for the metal catalyst:

- The catalyst needs two oxidation states (separated by one electron) that are accessible during the reaction,
- The metal centre needs to have an affinity for halogens,
- The coordination sphere of the metal needs to be expandable. This allows the halogen to be accommodated when the metal is oxidised,

- The catalyst needs to strongly form a complex with a ligand. This allows greater control over the reactivity of the metal centre.

The most popular, and from the view of this work, most useful catalysts, are those that include copper [88].

The temperature and solvent used in the ATRP reaction are important and are chosen so as to allow the other components to exist in solution and to easily reach the activation energy of the reaction [88]. As such these are perhaps of the least concern and are the easiest to optimise once the specific monomer is decided upon.

The first step in forming a polymer brush strucutre by ATRP is to modify the substrate such that the polymer will be grafted. This can be accomplished by the use of self-assembled monolayers (SAMs), which are highly ordered films of molecules on the surface [92, 93]. SAMs form spontaneously after the substrate has been immersed in a solution of a suitable adsorbate with the resulting film being a single molecule thick. For a SAM to form, the adsorbate requires three key components; a head group that will attach to the surface, an alkyl chain, and a terminal group that can be used to effectively functionalise the surface [92]. In the case of this work, the SAM will be placed on glass as this allows for the use of fluorescence as a characterisation technique. As such this limits the family of SAMs that can be used. Alkylsilanes are appropriate for using on oxide surfaces such as glass [94, 95].

The exact mechanism that allows the formation of SAMs of alkylsilanes on oxide surfaces is not completely understood but it is believed that in solution the alkylsilanes form siloxane groups which condense with both the hydroxyl groups of the surface and water to form a cross-linked network.[96]. This cross-linked network gives alkylsilane SAMs excellent thermal and oxidative stability.

The formation of defect free alkylsilane monolayers is a major challenge and at the time of writing there is no consensus in the community for the optimum conditions for their formation. This is because there are a large number of parameters that influence the quality of the monolayer that is formed. One example is the water content of the solvent, which needs close control as it is believed to have an extremely strong influence on the properties of the film produced. Water acts as a catalyst for the formation of alkylsilane monolayers, which makes the inclusion of water in the solvent crucial or else an incomplete monolayer would form [97]. However, if there is too much water present then there will be polymerisation between the alkylsilane molecules while in solution which leads to the formation of globular deposits on the substrate of the resulting polymer. This in turn greatly increases the surface roughness [97]. Other important parameters to consider are the temperature and the concentration of alkylsilanes introduced. To read further discussions on the paramters involved in the formation of alkylsilane SAMs and their impact of film quality, see the works of Rozlosnik *et al.* (2003) [97] and Schwartz (2001) [98] where more complete treatments are presented.

1.7.3 Diblock Copolymers

Diblock Copolymers and Self-Assembly

So far, discussion has revolved around polymers made of a single species of monomer, referred to as homopolymers. It is of course possible to construct more complicated polymers formed from many species of monomer. Molecules of this variety are known as copolymers. If the species are mixed randomly and allowed to form a random sequence then the random (or statistical) copolymer that is formed will generally have properties in between those of polymers made of the two species yet, due to the inherent disorder in their make up, these copolymers struggle to crystallise and form ordered arrangements [99]. Sequenced copolymers are a step up from this, being made of a strictly defined, yet non-repeating, sequence. These varieties of copolymer are critical to life, proteins can

be viewed as existing within this family and the crucial property of this variety is the ability to self-organise into larger structures. The block copolymer is an even more rigidly organised member of the copolymer family and is the member of interest to this work.

As the name block copolymer suggests the species are arranged so that they are in blocks. If the species of monomer are chemically very different the two species will attempt to seperate. However as the blocks are covalently attached this is not possible. Instead the blocks 'microphase separate' into a variety of complex (possibly ordered) morphologies [99]. Considering only a block copolymer of two species, with only two blocks, a number of self-assembled structures are possible. These types of copolymers are known as AB diblock copolymers. If the two species of polymer are correctly selected, molecules will arrange themselves supramolecularly. These assemblies will then pack together in structures that may be highly ordered over dimensions much larger than the individual copolymers, crucially inspite of the fact that the copolymers are not crystalline.

Appendix A.7 deals with the mixing and phase separation of homopolymers of different species. Much of the theory surrounding block copolymers is similar to that of homopolymers with one significant difference, the covalent bond between the species in the block copolymer. While in mixtures of homopolymers the phase separated domains have a tendency to grow to macroscopic sizes, which reduces interfacial energies between the species, this is not possible in the block copolymer case [100]. There is a clear constraint on domain size due to the covalent bond between blocks. This leads to a tendency of block copolymers to microphase separate when the energetics of mixing are unfavourable.

To illustrate this consider the case of a simple diblock copolymer consisting of two chemically different blocks of equal length bonded covalently. This symmetric copolymer will segregate into regions of each polymer but due to the constraint of the covalent bond between the blocks, bulk separation does not occur. Instead, lamellar morphology is

achieved where layers of each block are formed that regularly alternate. Using simple arguments, in the same vein as those used to produce equation A.7.7, it is possible to produce an equation decribing the layer thickness (d):

$$d \sim a\chi^{\frac{1}{6}} N^{2/3} \tag{1.7.14}$$

where a is the monomer thickness and χ is the interaction parameter between the two monomers. This is in rough agreement with expressions derived using more rigourous proofs with the only difference in result being the numerical prefactors [100].

In the idealised case of symmetric block copolymers, layers of each block are formed. Block copolymers are however not always of this nature and therefore this morphology will not always be the produced. Most obviously the length of each block might vary; but other contributions can come from the size of monomer and the way the monomers pack in the random coil, all of which can have a significant effect on the size and shape of the blocks formed and the subsequent morphology [100]. To simplify the argument concerning the different situations we shall consider this only in terms of volume fractions. This can be taken to be roughly equivalent to all of the above contributions, as greater polymerisation leads to a larger volume fraction and the other parameters will also have an impact on the volume fraction. When it is said that there is more of a polymer this should be taken as it has a larger volume fraction. It should also be noted that all the morphologies described only occur when a critical concentration of block copoylmer is surpassed. If there is more polymer A than polymer B, it is observed that A forms a matrix that B forms structures within. When A greatly 'outnumbers' B, B forms spheres. As the volume fraction of B increases the structure changes to cylinders of B in a hexagonal lattice through to more complicated gyroid structures. The same is observed in the reverse where B has a larger volume fraction than A. These miceller structures are examples of ordered morphologies that can span several length scales.

By careful selection of polymers and by manipulating the length of the blocks, it is possible to produce a range of possible morphologies. Thus far the polymers have been treated as being in the melt, where there is little or no solvent. For the rest of this chapter this is not the case and the block copolymer will be in water. Much of the behaviour of block copolymers in water is similar to the basic theory described to this point. There will still be microphase separation and the morphologies observed are similar. However there is also the matter of interactions between the polymer and the water (or other solvent), which must be considered.

If the constituent polymers are properly selected for the solvent it is again possible to produce well ordered morphologies. In the case of water a block copolymer where polymer A is hydrophobic and polymer B is hydrophilic, will behave as an amphiphile. Amphiphilic molecules can form bilayers, spheres and cylinders based upon the ratio of the size of the hydrophobic region to the hydrophilic region. It is also possible to form vesicles and tubes, again based upon the size of the two regions. Examples of this behaviour are seen in biology in lipids and other surfactants, as well as in various detergents outside of biology [101]. The key difference between these amphiphilic molecules and the block copolymer molecules is size. Lipids are small molecules that are generally smaller than 1 kDa while the copolymers can be orders of magnitude bigger.

Examples of producing amphiphilic structures with block copolymers exist. In 1995 Zhang and Eisenberg presented observations of six different (and stable) morphologies in polystyrene-poly(acrylic acid) block copolymers in solvent [102]. Four of the morphologies observed were spheres, rods, lamellae and vesicles in the solution. The other two morphologies were observed as the polymer weight fraction was increased so that micronscale structures were observed. In 2001, Förster *et al.* presented a block copolymer of poly(butadiene) extended with poly(ethylene oxide) (PB-PEO) [103]. It was observed

that as solvent conditions changed from a high polymer proportion to a lower proportion (greater solvent content) that the ordered cylinder structures broke down into sphere- and worm-like micelles. Similar behaviour was observed previously by Hajduk *et al.* (1998) with a block copolymer of poly(ethylene oxide) extended with poly(ethylethylene) (PEO-PEE) [104].

PGMA-PHPMA Gels

It is well known in polymer chemistry that AB amphiphilic diblock copolymers form ordered micellar gels at relatively high concentrations (around 20 w/w% in water) [105]. This comes about as the hydrophilic 'A' block surrounds the hydrophobic 'B' block forming micellar structures. When the concentration gets high enough the individual structures can interact with one, allowing physical cross-links to form. ABA triblock copolymers can also form micellar gels and at lower copolymer concentrations (5-10 w/w% in water). Qualitatively this can be seen to occur as the hydrophilic B block can form connections between hydrophobic A block micellar cores [106]. The use of this concept has allowed the formation of gels that are responsive to temperature [107, 108] and pH [109].

A block copolymer of poly(glycerol monomethacrylate) (PGMA) extended with poly (hydroxypropyl methacrylate) (PHPMA) will be considered, which has previously been studied [59]. The PGMA is water soluble while the PHPMA is water insoluble, with the difference producing an amphiphilic block copolymer. The PGMA-PHPMA (refered to as G_m-H_n for brevity where 'm' and 'n' refer to the degree of polymerisation) was prepared using the same methodologies as described in this thesis in the study of Blanazs *et al.*

Blanazs *et al.* produced three different well-defined, uniform, G_{53}-H_n block copolymers at a concentration of 10 w/w % [59]. With n of 90, 140 and 220, transmission electron microscopy (TEM) studies indicated three separate morphologies. Spherical micelles were observed for G_{53}-H_{90} while worm-like micelles were observed for G_{53}-H_{140}.

At G_{53}-H_{220} the block copolymer was observed as a purely vesicular phase.

G_{53}-H_{140} that is stirred at 70°C remained a fluid until cooled, when it became a soft free-standing physical gel as interworm entanglements formed [59]. This form of gelation has been previously observed in worm-like surfactants micelles [110]. In contrast the sphere and vesicular phases remained free-flowing liquids after undergoing the same processing.

Rheological studies on the worm gels of G_{53}-H_{140} demonstrated that at 10 w/w % undergoes degelation on cooling [59]. There was some hysteresis observed, with degelation occuring at 14°C on cooling from 25°C yet regelation (in terms of the storage and loss moduli) did not occur until 22°C. The hysteresis is expected if the transition is treated as being a first-order phase transition and the belief was that the hysteresis was related to the timescale of the interworm entanglements.

Blanazs *et al.* examined the degelation mechanism with dynamic light scattering (DLS) studies on a 0.50 w/w % G_{53}-H_{140} solution, where the block copolymer was in a worm-like micelle form [59]. Above 20°C a hydrodynamic diameter of around 150 nm was observed, which is consistent with the sphere-equivalent hydrodynamic radius indicitive of worm-like micelles. As the temperature was decreased below 10°C a hydrodynamic diameter of 30 nm was observed. The cause of this significant size reduction is a morphology change from the worms to spherical micelles, and this was confirmed by TEM with only spherical micelles being observed at 4°C. Since the spheres cannot form entanglements it follows that the mechanism for degelation must be a temperature-dependent reversible worm-to-sphere transition. The morphological change was further confirmed by small angle x-ray scattering (SAXS) measurements.

The PGMA-PHPMA molecule is not only responsive to temperature changes, a conformation change is also observed when the pKa of the block copolymer is surpassed [60].

The copolymer is naturally in the worm state at low pH and the addition of negative ions causes the cylinders to break down to an aqueous solution of spheres.

1.7.4 Photolithography

Scanning Near-Field Photolithography

Photolithographic methods rely on propagating electromagnetic fields and as such are subject to diffraction effects. This imposes a limit on the resolution that can be achieved, accepted to be around half the wavelength of the light as a first approximation. However it is possible to circumvent this diffraction limited restriction by taking advantage of the near field. If light is passed through an aperture that is smaller than the wavelength of the light, then very close to the aperture that light is not subject to diffraction effects. This behaviour only occurs very close to the aperture, and rapidly decays to the conventionally observed behaviour in the far field. The near field behaviour is only observed closer to the aperture than the wavelength of the light. A scanning near-field optical microscope (SNOM) coupled to a UV laser can be used for photolithography and is referred to as scanning near-field photolithography (SNP).

SNOM is recognised as a complex technique; however, SNP is straight forward in comparison. The main problems associated with the use of SNOM are connected to signal detection and the translation of the probe across the surface. The detection of a signal is clearly not an issue when lithography is the end product.

As stated, conventional photolithographic techniques have a resolution limit imposed by the diffraction of light. The resolution that can be achieved is defined by a specific expression of the Rayleigh Criterion:

$$R = \frac{0.61\lambda}{n \cdot \sin\theta}, \tag{1.7.15}$$

where R is the resolution achievable, λ is the wavelength of light and $n \cdot \sin\theta$ is the numerical aperture of the system. This leads to an estimate for the minimum feature size produced using visible light (violet light being the shortest wavelength with $\lambda = 400\,\text{nm}$) as about 200 nm.

Using a near-field approach, by scanning the aperture close to the surface (typically 5-10 nm in SNP), features of much smaller than 200 nm can be produced. Considering the same violet light source as the previous example, it is possible to create features on the scale of 45 nm; although the methods and details required to reach this value are beyond the scope of this work, they are available in standard texts [111]. By using wavelengths in the UV region of the electromagnetic spectrum it is possible to achieve even smaller structures. For example, in Sun *et al.*, using a 244 nm laser, structures as small as 20 nm were produced by photo-oxidation of an alkanethiol SAM, mecraptopropanoic acid, on gold [112].

A major limitation of the SNOM set-up is the slow throughput. Patterning via SNOM is a serial procedure and as such the time it takes to produce a pattern, is the sum of the time it takes to produce each individual component. As more and more complex patterns are designed, it takes longer and longer to actually produce the required sample. This sets a limit on the size of pattern that can be produced, as it quickly becomes unreasonable to produce larger scale patterns. The development of the 'snomipede' is one such method to combat this limitation [113]. The snomipede uses 16 parallel scanning probes which are scanned simultaneously across the surface, so that effectively many pens can write at the same time. The result is that a large number of very small structures can be produced in parallel. In principle this methodology can be scaled up to larger arrays, allowing processing of materials at nanometre resolutions over macroscopic areas.

Interferometric Lithography

Interferometric Lithography (IL) is a technique that can be used to fabricate periodic patterns over a large area efficiently without the use of a mask. Crucially the technique results in patterns that are smaller than those produced by conventional mask based lithography.

In IL, two or more coherent light waves are set up so that interference between the waves occurs. This leads to the creation of a sinusoidal pattern of intensity, that can be used for patterning a SAM or photoresist. When two coherent beams are allowed to interfere, a periodic pattern of lines is created. This pattern is well defined based on the position on the surface and the periodicity of the lines (d) can be expressed as:

$$d = \frac{\lambda}{2n \cdot \sin\theta}, \tag{1.7.16}$$

where λ is the wavelength of light used, n is the refractive index and θ is the half-angle at which the beams interfere.

To carry out simple two beam IL, the set-up most commonly used is that of a 'Lloyd's mirror'. The Lloyd's mirror approach is incredibly simple and cheap to construct with all the apparatus for patterning being common optical bench equipment. The Lloyd's mirror is an 'L' shaped construct where one arm holds the sample and the other has a mirror. A coherent laser beam is expanded and aimed so that half of the beam strikes the sample directly, while the other half must reflect off the mirror to interfere with the first half of the beam [114]. The resolution of IL is limited by the diffraction of light, but by using UV wavelength lasers very small structures, some as small as 19 nm [115], can be formed.

The use of IL forces patterns to be periodic in nature, rather than in SNP patterns where any shape is possible providing the probe can be programmed to draw the desired

pattern. It is possible to produce smaller patterns using SNP than IL. However, when producing polymer brush patterns this is largely levelled due to the requirement of having enough tethered polymers within a certain area to produce the polymer brush. The key advantage that IL has over SNP is the speed and simplicity with which patterns can be produced. Complex step-by-step paths need to be programmed and due to the linear processing involved in SNP, patterns can take a long time to produce. IL requires equipment that is common to most optics labs and is compartively simple; all that is required is a timer to aid in calculating the dose of light that the pattern receives and a protractor to measure the angle needed from equation (1.7.16). A second advantage, due to much the same reasoning, is the scale of pattern that is produced. SNP produces truly nanoscale patterns but due to the linear nature by which they are manufactured it is not feasable to produce patterns with nanoscale dimensions over square centimetres. This is not a problem with IL, as the patterning occurs across the entire region that is illuminated by the interference pattern simulataneously. To a point, any sized pattern could be produced if a large enough area could be illuminated. The process is however diffraction limited so there will be an upper limit, nevertheless the example of squared centimetres is routinely achieved.

1.7.5 Fluorescence Correlation Spectroscopy

FCS is a technique for measuring diffusion that is characterised by its high levels of temporal and spatial resolution. A defining feature of the technique is that measurements are taken with ultra low concentrations of the diffusing species. In contrast to other fluorescence techniques the parameter that is of greatest interest is not the absolute intensity of the emission, but rather the fluctuations of the intensity. FCS makes it possible to examine the parameters that are directly responsible for these fluctuations. For example, the local concentration, the mobility of coefficients and the reactions of the fluorescently tagged molecules.

FCS was developed in the 1970s and makes use of the spontaneous fluctuations in the physical parameters that affect the fluorescence emisson. At ambient conditions these changes happen continuously and are observed as noise patterns. FCS takes its name from the mathematical process of autocorrelating which allows the fluctuations to be quantified in terms of their strength and duration. Autocorrelation measures the self-similarity of a temporal signal and can be viewed as a measure of the persistance of information.

The basic operating principle in FCS is to make the number of observed molecules low enough that each molecule has a substantial contribution to the measured signal. Ideally, the molecules also need to have a high photon yield for each molecule. All of this can be achieved by integrating this idea of analysing fluctuations with a confocal detection set up (The theory of confocal microscopy is presented in appendix A.8).

In the most simplistic sense, FCS treats each peak in the noise on an intensity spectra as when a fluorescent molecule is within the detection volume (figure 1.12. Similarly, the troughs can be treated as the absense of a fluorophore. This means that the width of each peak can be treated as the time it takes for a fluorophore to move into and out of the detection volume. The process of autocorrelation formalises this logic, and provides a statistical measure of the time required to cross the detection volume. Obviously this simplistic approach does not deal with all the reasons an intensity signal might fluctuate but it provides a good starting point. This simple argument does, however, explain why it is so important that the concentration of fluorophore be optimised. With a large population of fluorophore, any one moving into or out of the volume produces a small change in intensity in comparison to the total intensity. If there is only a single fluorophore, it entering or leaving the confocal volume produces the largest change in terms of relative intensity.

In principle the autocorrelation procedure provides a measure of self-similarity of a time

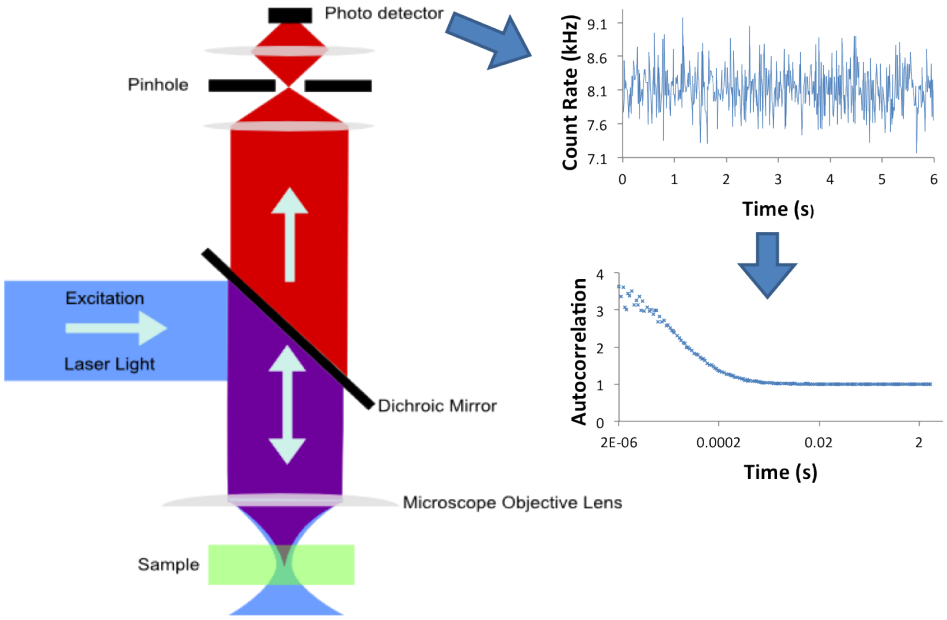

Figure 1.12: A schematic diagram illustrating the process with which an autocorrelation curve is formed. The fluorescence from the sample is collected using a confocal approach and the photons are collected at a photodetector. This produces an intensity spectrum in time that can be autocorrelated to form the correlation curve which in turn can be fitted to obtain diffusion times. The process of autocorrelation measures the persistance of light intensity and can be treated as showing the timescale of residency within the focal volume.

signal and highlights the characteristic time constrants of the underlying processes. Different modes of diffusion produce different shaped correlation curves, while non-radiative causes produce an entirely different shape, and it is possible to work out the number of diffusion modes, their relative speeds and proportions from a single curve. A correlation curve for three dimension diffusion can be described by

$$G(\tau) = 1 + \left((1-T) + Te^{\frac{-t}{\tau_T}}\right) \frac{1}{\langle N \rangle} \cdot \frac{1}{\left(1 + \left(\frac{\tau}{\tau_D}\right)^2\right)} \cdot \frac{1}{\sqrt{1 + \left(\frac{z_0}{r_0}\right)^2 \cdot \frac{\tau}{\tau_D}}}, \tag{1.7.17}$$

where $G(\tau)$ is the autocorrelation function in terms of light intensity, τ is the time delay between sampling, N is the average number of fluorophores in the detection volume, τ_D is the diffusion time of the species in motion through the confocal volume, z_0 and r_0 are the dimensions of the confocal volume, and the T and τ_T describe the non-radiative be-

haviour due to the triplet state of the fluorophore. This equation is derived in appendix A.9.

The final equation presented describes the situation where a fluorophore can diffuse either in the bulk of a solution or upon a surface. This illustrates the point about different shaped curves and how autocorrelation curves for different modes of diffusion are combined. In the case of this thesis, all samples contain the same fluorophore and as such the different contributions can simply be added to one another. The proportion of the correlation curve describing each behaviour then translates to the fraction of molecules diffusing in each mode.

$$G(\tau) = 1 + \frac{1}{\langle N \rangle}\left(\frac{1-f}{\left(1+\left(\frac{\tau}{\tau_{3D}}\right)^2\right)\left(1+\left(\frac{z_0}{r_0}\right)^2 \cdot \frac{\tau}{\tau_{3D}}\right)^{1/2}} + \frac{f}{1+\left(\frac{\tau}{\tau_{2D}}\right)}\right)\left((1-T)+Te^{\frac{-t}{\tau_T}}\right) \tag{1.7.18}$$

where in addition to the terms previously defined τ_{3D} is the three dimensional diffusion time, τ_{2D} is the two dimensional diffusion time and f is the fraction of fluorescent molecules upon the surface.

1.8 Summary

In summary, this thesis will set out to examine the diffusion of polymeric systems that are designed as analogues of the photosynthetic pathway of *R. Sphaeroides*. In doing so it will be possible to isolate behaviours that can indicate how biological systems might control diffusion as well as possible design principles for biologically inspired devices.

One strand of this thesis will examine diffusion upon a patterned surface as an analogue for the structure of cell membrane. By following the diffusion of a polymer it will be possible to examine the impact that structure has upon diffusion. The second strand will

track diffusion of a diblock copolymer in a responsive gel as an analogue of the cytosol of a cell. In doing this, it will be possible to suggest whether a responsive polymer gel is a good representation for the cytosol and whether this could be used as a model for transport in the cell.

Finally, these two strands will be brought back together to suggest that it is indeed a control of diffusion that leads to the impressive efficiency in the photosynthetic pathway of *R. Sphaeroides*. In addition to this, certain design principles will be extrapolated for use in biologically inspired devices.

For ease of access, the location of where each topic and research question is addressed, is presented in table 1.8, as well as a brief description of the arguments dealing with each topic.

Table 1.3: Brief summary of the research questions, where they are addressed and a summary of the discussion on each question.

Question	**Location addressed**	**Summary**
Can a topographically patterned polymer brush surface, matching the scheme in figure 1.9, be produced?	Chapter 3	It is possible to produce a surface of this type through a combination of surface chemistry and photolithographic methods, allowing a brush to form in only designated areas.
Is a surface produced to be like this suitable as an analogue of the structure of the cell membrane?	Section 3.4	Patterns were produced by using interferometric lithography (IL). IL produced wells that are of comparible size to those observed in cells. However the barrier is much thicker. This could be compared more favourably with a system such as that of the neuron (as described in section 1.5).
Can the patterned surface be compared favourably with the membrane skeleton (MSK) fence model and the transmembrane protein (TMP) picket model?	Section 3.4 & Section 4.1	Although the barrier width is much thicker than that commonly seen in biological cases, it is still possible to use this as an analogue for the membrane in the MSK fence model and TMP Picket model. Both models treat their respective barriers as a 'slice' of poorly diffusive material, the patterned surfaces can be seen to have a thicker slice yet one that will have a lower impact upon diffusion.

Continued on next page

Table 1.3: Brief summary of the research questions, where they are addressed and a summary of the discussion on each question.

Question	**Location addressed**	**Summary**
Is the methodology used capable of up-scaling?	Section 3.3 & Section 3.4	IL is a methodology that produces patterns on the scale of squared centimetres in the space of minutes. The limit on the patternable area is the amount that the beam can be expanded without blurring the interference pattern. This will also put a limit on the speed with which patterning will occur. Due to the parallel nature of the technique it is feasible that the patterning methodology could be expanded to industrial lengthscales. The methodologies for growing brushes are also expandable.
How good is the resolution and how repeatable is the methodology?	Section 2.3 & Chapter 3	With polymer brushes the smallest width of wells made with this methodology are on the region of 100 nm, although patterns with wells of 80 nm can be formed. Repeatability of both the brush growth and the patterning is dependent on the quality of materials, when high quality precursors are available the methodology routinely produces good quality patterned surfaces.

Continued on next page

Table 1.3: Brief summary of the research questions, where they are addressed and a summary of the discussion on each question.

Question	**Location addressed**	**Summary**
What is the behaviour of PEG on these surfaces?	Chapter 4	The presence of a periodic pattern induces a form of confinement, producing a third component in the autocorrelation curve relating to a second surface diffusion mode. This mode is two orders of magnitude slower than the normal mode (which is related to the diffusion of PEG on NPPOC). Although the diffusion coefficient stays consistent with changes in well size, the proportion of diffusion in this confined mode increases as the well is shrunk.

Continued on next page

Table 1.3: Brief summary of the research questions, where they are addressed and a summary of the discussion on each question.

Question	**Location addressed**	**Summary**
How is the diffusion different to on either homogeneous surface?	Section 4.2.1	There are three components in the autocorrelation curves for the patterned surface rather than the two on either homogeneous surface. The first component is the bulk component and matches with that present for PEG on each surface. The second and third components are the surface diffusion modes and the first of these is similar to that present in the NPPOC homogeneous surface, implying that the PEG diffuses at the bottom of the well. The third component is two orders of magnitude slower and is not observed in either case. The proportion of this component increases as the feature size is reduced, another observation not seen in the homogeneous case.

Continued on next page

Table 1.3: Brief summary of the research questions, where they are addressed and a summary of the discussion on each question.

Question	**Location addressed**	**Summary**
Does the behaviour of the polymeric system have any similarities to that observed in biological systems?	Section 4.2.4	When the surface diffusion is analysed with the FCS diffusion laws, the results suggest an appropriate design of the surface, suggesting that there are some similarities between the two cases. A major difference is that the polymeric case includes a bulk diffusion mode but if this is disregarded, allusion to a hop diffusion regime can be made. In the case of biological systems, all membrane molecules are affected to some degree by the presence of structure, while in the polymeric case the highest recorded case is 45%. The discrepency between values is believed to be due to the interactions that occur between the membrane molecules.

Continued on next page

Table 1.3: Brief summary of the research questions, where they are addressed and a summary of the discussion on each question.

Question	**Location addressed**	**Summary**
Can a cause be suggested for the behaviour observed in the polymeric case?	Section 6.2	The bulk and faster surface modes are consistent with those observed in homogeneous surfaces, with traditional explanations being used to describe the motion in these cases. The third surface mode is linked to the presence of an interface between the NPPOC well region and the POEGMA brush region, and two mechanisms are proposed to explain the behaviour. The first is that the well acts as a well and confines a proportion of the polymers within it, while the second is transient knotting and entanglements of the PEG with the brush. Both cases are discussed in detail in Section 6.2.

Continued on next page

Table 1.3: Brief summary of the research questions, where they are addressed and a summary of the discussion on each question.

Question	**Location addressed**	**Summary**
Can the rate of diffusion of molecules in a gel be significantly modified with changes in pH and temperature?	Chapter 5	By using a diblock copolymer molecules as the basis of the gel, changes in pH and temperature can be used to induce morphological changes. These morphological changes alter the size and shape of the diffusing species thereby significantly changing the diffusion behaviour of the species. As pH was increased or temperature decreased the diffusion coefficient increased by a factor of between four and eight.
Does this have any value when considering *R. Sphaeroides*?	Chapter 5	Changes in the diffusive behaviour of the gel are analogous to changes to the diffusive behaviour of the cytosol. It is proposed that the diffusion of smaller diffusants would be similarly affected by this change in morphology meaning that the bacteria could confine species of interest to a region of the cytosol, potentially increasing the likelihood that the diffusant would be used in the cell processes.

Chapter 2

Experimental Methods

A number of techniques were used in this thesis. Surface-grafted polymers were produced using atom transfer radical polymerisation (ATRP) to form barriers for the diffusion studies. Patterned surfaces were then characterised by scanning force microscopy (SFM) and confocal microscopy before the diffusion of a probe was measured using fluorescence correlation spectroscopy (FCS). In addition to these techniques, surface analysis techniques were used to characterise the produced surfaces, using both contact angle measurements and x-ray photoelectron spectroscopy.

2.1 Contact Angle Measurements

The theory of contact angle measurements is presented in appendix A.10. Advancing sessile drop contact angles were measured using a Rime-Hart model 100-00 goniometer (Netcong, NJ). Using a microlitre syringe, a 2 L drop of water was placed onto the surface of the sample and the sample stage was lowered until the water droplet separated from the tip of the syringe. The contact angle of the drop was then measured and repeated 5 times on different areas of the sample to give a mean value.

2.2 X-ray Photoelectron Spectroscopy

The theory of X-ray photoelectron spectroscopy (XPS) is presented in appendix A.11. The uncertainties associated with XPS spectra are treated as being too small to be presented. XPS was carried out using a Kratos Axis Ultra spectrometer (Kratos Analytical, Manchester, UK) with a monochromatized Al Kα X-ray source operating at a power of 150 W with an emission current of 8 mA and a pressure in the analysis chamber between 10^{-8} to 10^{-10} mbar. Electron energy analyzer pass energies of 160 eV and 20 eV were used to acquire survey (wide) scans and high resolution spectra, respectively. The samples were prepared with approximate dimensions ca. 5x5 mm^2 and then rinsed with ethanol and dried under dry N_2 before analysis. High- resolution peaks were fitted and processed using CasaXPS software (Casa, http://www.casaxps.com, U.K.).

2.3 Growth of Poly (oligo[ethylene glycol] methacrylate) brushes by ATRP

2.3.1 Materials

SAM Formation and Derivation: (3-Aminopropyl)triethoxysilane (APTES) (99%), adipoyl chloride (98%) and glutaraldehyde (25% solution in H_2O) were supplied by Sigma-Aldrich. Ethanolamine was supplied by Riedel-de Haën. Sulphuric acid (1.83 S.G. 95+%), ammonium hydroxide solution (35%), hydrogen peroxide solution (30%) and ethanol (HPLC grade 99.8+%) were supplied by Fisher Scientific. Cover slips (22 mm × 64 mm and 22 mm × 26 mm, thickness 1.5 mm) were supplied by Menzel-Gläser.

Polymer Brush Growth: Poly(ethylene glycol) methyl ether methacrylate (M_n = 475 g/mol), 2,2-bipyridyl (>99%), copper(I) bromide (99%), copper(II) bromide (99%) were purchased from Sigma-Aldrich. 2-methacryloyloxy ethyl phosphorylcholine (MPC) was purchased from Lipidure.

2.3.2 Self-assembled Monolayer Formation and Derivation

To clean the glassware and substrates prior to SAM formation, they were first sonicated in a solution of sodium dodecyl sulphate (SDS) in water for 10 minutes and then rinsed with de-ionised water. Following this the glassware and substrates were immersed in piranha solution, a mixture of 30% hydrogen peroxide and 70% sulphuric acid, for 20-30 mins before being rinsed and sonicated in de-ionised water. The substrates for SAM formation were further cleaned in a Radio Corporation of America solution (RCA), which is a 5:1:1 mixture of H_2O: NH_4OH: H_2O_2, and heated to 80°C for 20 minutes before being rinsed thoroughly with de-ionised water. To ensure the substrates and glassware were dry before use, they were placed in an oven at 120°C overnight.

Films of APTES were prepared by immersing clean silicon or glass slides into a 1% (v/v) solution of APTES in toluene for 30 minutes. After the formation of the APTES monolayers, the slides were removed from solution, washed with toluene and ethanol and annealed in a vacuum oven at 120°C for 30 minutes.

Films of APTES on glass were then placed in solution of 2.5 ml of Dichloromethane (DCM), 10 μL of triethylamine (TEA) and 3.5 μL of α-bromoisobuyryl bromide (BiBB). The slides were left to react for 20-30 min and then rinsed with ethanol and DCM before being dried under a stream of nitrogen

2.3.3 Surface initiated ATRP reaction

In a round-bottom flask a mixture of 16 mL of de-ionised water and 16.35 g of poly(ethylene glycol) methyl ether methacrylate (POEGMA) was degassed with nitrogen for 30 minutes. To this solution 248 mg (1.58 mmol) of bipyridine (bipy), 80 mg (0.559 mmol) of Cu(I)Br and 38 mg (0.17 mmol) of Cu(II) Br_2 were added. The solution was degassed for 5 more minutes and sonicated to dissolve any remaining solids. Slides of BIBB-APTES were then

placed in a Schlenk tube, degassed and put under nitrogen. The polymerisation solution was carefully added to the Schlenk tubes to begin the polymerisation process and left for 5-30 min depending on the brush height that was required. Once the polymerisation step was complete the slides were removed and rinsed with methanol and sonicated in a 1:1 mixture of acetone and water before being dried under a stream of nitrogen.

2.3.4 Characterisation of POEGMA polymer brushes

Films formed by the adsorption of APTES on silica, and then derivatised with BIBB, act as the initiator for ATRP (figure 2.1). A first method of characterisation of the samples was to make contact angle measurements before and after the derivatisation. The contact angle rose from 45° on the amine terminated surface to 69° when the BIBB group was present. This is in agreement with literature values for these surfaces [116].

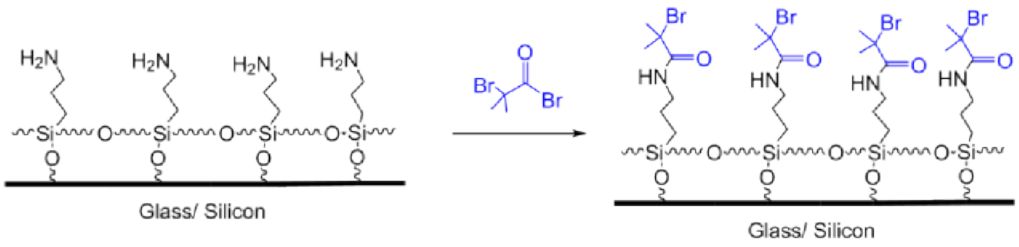

Figure 2.1: A schematic diagram showing the formation of a BIBB-APTES monolayer

It is possible to obtain samples with multiple layers of APTES rather than a single layer, however from the perspective of producing brushes this is not important as long as the top layer is smooth. The methodologies outlined should provide a monolayer of APTES which is shown experimentaly using ellipsometry and AFM (A. Ahmed, unpublished 2013).

X-ray Photoelectron Spectroscopy (XPS) was also used at this stage for characterisation of the surface. In the XPS spectrum a Br 3d peak was observed at 68.9 eV (figure 2.2(a)), while in the C 1s spectrum of the BIBB-APTES surface three components can be

fitted to the peak (figure 2.2(b)). These components suggest the prescence of C-H/C-C carbons (285.0eV), C-Br/C-NCO carbons (286.4eV) and O=CN carbons (288.0eV).

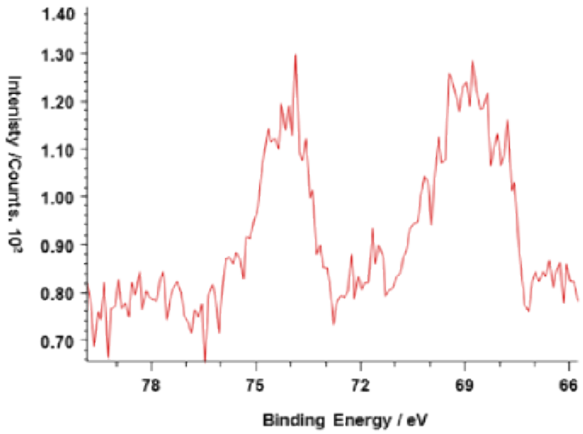

(a)

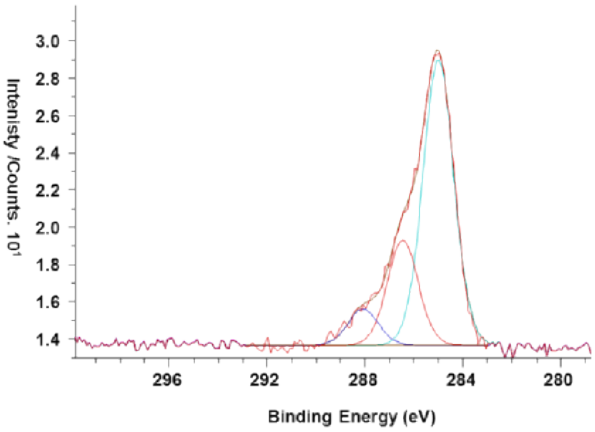

(b)

Figure 2.2: XPS spectra of BIBB-APTES on glass. (a) the Br3D region of the XPS with a peak at 68.9 eV, note that the second peak at 74.2 ev is from Al $(OH)_3$ and is related to the glass substrate. (b) the C1s region of the XPS spectrum, with the three components fitted to the peak envelope, corresponding to the C-C/C-H (285 eV), C-Br/C-NCO (286.4 eV) and O=CN (288.0 eV) carbons atoms.

Following the formation of the BIBB-APTES surfaces, POEGMA polymer brushes were grown via surface inititiated ATRP (SI-ATRP) reactions. XPS studies were completed for this new system, with focus on the C1s spectrum (figure 2.3). Again three components are observed within the peak envelope at 285.0 eV, 286.4 eV and 288.8 eV which correspond

to C-C/C-H, C-O and COOR carbons respectively. This spectrum is consistent with the structure of POEGMA brushes.

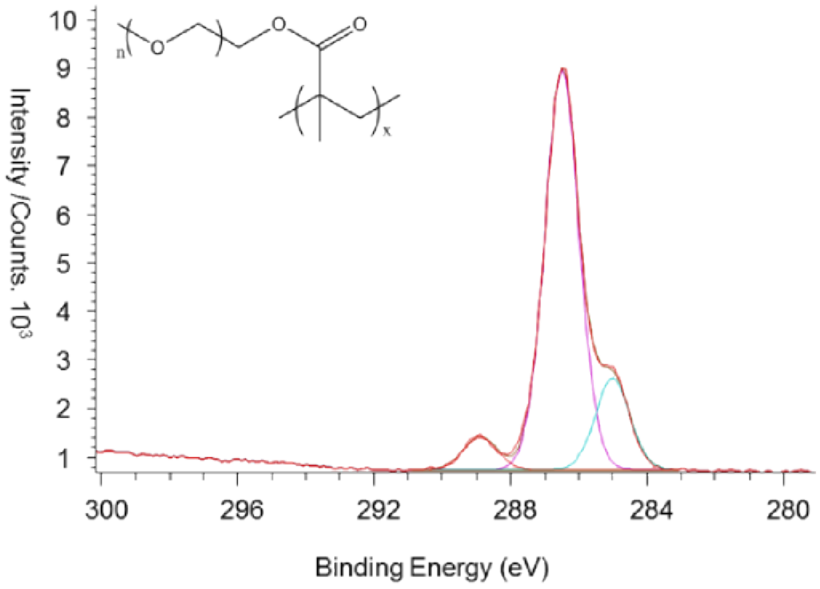

Figure 2.3: C1s XPS spectra for POEGMA contains three components in the peak envelope corresponding to the C-C/C-H (285.0 eV), C-O (286.4 eV) and COOR (288.8 eV) carbon atoms. The structure of POEGMA is shown as an insert.

2.4 Synthesis of N-[2-(2-Nitrophenyl)propan-1-oxycarbonyl]-3-aminopropyl-triethoxysilane

2.4.1 Materials

2-Ethylnitrobenzene (98% GC), hydrochloric acid (> 30%), paraformaldehyde (> 95%), 3-(triethoxysilyl)propyl isocyanate (95%) and benzyltrimethylammonium hydroxide (Triton B) (40 wt % in methanol), triethylamine (> 99%), potassium dihydrogen phosphate (> 99%) were supplied by Sigma-Aldrich (Poole, UK). Magnesium sulfate, dichloromethane

(HPLC grade), petroleum ether (40-60), ethyl acetate (HPLC grade) and diethyl ether (anhydrous grade) were supplied by Fisher Scientific.

2.4.2 Synthesis of 2-(2-Nitrophenyl)propan-1-ol

2-ethylnitrobenzene (first species in figure 2.4) (8.1 ml, 60.0 mmol) was added to a 40% benzyltrimethylammonium hydroxide (Triton B) solution in MeOH (27.7 ml of solution, 61 mmol), followed by the addition of paraformaldehyde (1830 mg, 61 mmol). The mixture was refluxed at 80 °C for 20 h, evaporated under reduced pressure to a small volume, and adjusted to pH 7 with 1 M aq HCl (∼40 mL). The mixture was extracted three times with EtOAc (60 mL each), and the organic layers were combined, dried with $MgSO_4$, and evaporated under reduced pressure to give a dark brown oil. This was purified by flash column chromatography (hexanes/EtOAc, 4:1 2:1) to yield the desired product (Second species in figure 2.4) as a deep orange oil (3912 mg, 21.6 mmol, 36%); Rf 0.1 (hexanes/EtOAc, 4:1); δH (400 MHz, CDC13) 1.34 (3H, d, *J7*, C*H3*CH), 1.70 (1H, s(br), O*H*), 3.52 (1H, m, CH3C*H*), 3.81 (2H, m, CHC*H2*O) 7.39 (1H, dd, *J*8 and 8, 5-Ph), 7.50 (1H, d, *J*8, 3-Ph), 7.59 (1H, dd, *J* 8 and 8, 4-Ph), 7.76 (1H, d, *J*8, 6-Ph).

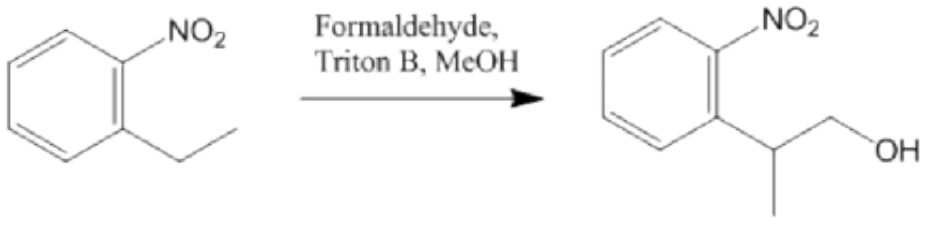

Figure 2.4: The reaction by which 2-(2-Nitrophenyl)propan-1-ol is produced.

2.4.3 Synthesis of N-[2-(2-Nitrophenyl)propan-1-oxycarbonyl]-3-aminopropyl-triethoxysilane

2-(2-Nitrophenyl)propan-1-ol (3518 mg, 19.42 mmol) was dissolved in dichloromethane (DCM) (18 mL), after which 3-isocyanatopropyltriethoxysilane (5.5 mL, 22.2 mmol) was added, followed by triethylamine (250 μL, 1.8 mmol), and the mixture was then refluxed at 60 °C for 24 h. Et2O (25 mL) was added, and the mixture extracted with 0.1 M potassium phosphate buffer pH 7 (50 mL thrice). The organic layer was dried with $MgSO_4$ and evaporated under reduced pressure, and the residual yellow oil was purified by flash column chromatography to yield the desired product as a yellow oil (6020 mg, 14.05 mmol, 72%); Rf 0.50 (hexanes/EtOAc, 4:1); δH (400 MHz, CDC13) 0.59 (2H, t, *J*8, C*H2*Si), 1.21 (9H, t, *J*7, OCH2C*H3*),1.34 (3H, d, *J* 7, C*H3*CH), 1.58 (2H, tt, *J* 7 and 8, CH2C*H2*CH2), 3.12 (2H, td, *J* 7 and 6, NHC*H2*), 3.70 (1H, m, CH3C*H*), 3.81 (6H, q, J 7, SiOC*H2*), 4.10 (1H, m, CHC*H2*O), 4.23 (1H, m, CHC*H2*O), 4.85 (1H, s(br), CON*H*CH2), 7.36 (1H, dd, *J* 8 and 8, 5-Ph), 7.47 (1H, d, *J* 8, 3- Ph), 7.56 (1H, dd, *J* 8 and 8, 4-Ph), 7.73 (1H, d, *J* 8, 6-Ph).

2.5 Fabrication of PGMA-PHPMA gels

The production and characterisation (for purity purposes) of PGMA-PHPMA gels was completed by Joseph Lovett.

2.5.1 Material

Glycerol monomethacrylate (GMA; 99.8%) was donated by GEO Specialty Chemicals (Hythe, UK) and used without further purification. 2-Hydroxypropyl methacrylate (HPMA) was purchased from Alfa Aesar and used as received. Glycidyl methacrylate (GlyMA), 4,4-azobis(4-cyanopentanoic acid) (ACVA; V-501; 99%), ethanol (99%, anhydrous grade), rhodamine B, thionyl chloride, piperazine, sodium chloride, sodium sulfate,

diethyl ether, isopropanol, methanol and dichloromethane were purchased from Sigma-Aldrich UK and were used as received. All solvents were of HPLC quality and were purchased from Fisher Scientific (Loughborough, UK). 4 - Cyano - 4 - (2 - phenylethanesulfanylthiocarbonyl) sulfanyl pentanoic acid (PETTC) was prepared and purified as reported elsewhere (see E.R. Jones *et al.* [117]).

2.5.2 Preparation of Fluorescently-tagged Gels

The production of samples was completed by Joseph Lovett, following the protocols laid out in Blanazs *et al.* (2012) and Lovett *et al.* (2015) [59, 60]. The only difference between the samples produced in these studies and those presented in this thesis is the addition of a fluorophore so that the system could be studied with FCS. The methodologies for this can be found in Clarkson *et al* (2015) [118].

2.5.3 Gel Characterisation

Gels were characterised by NMR spectroscopy and gel permeation chromatography, and the morphologies formed were examined through dynamic light scattering and transmission electron microscopy [59, 60, 118]. This was performed by Joseph Lovett.

2.6 Scanning Force Microscopy

The theory of scanning force microscopy, more commonly refered to as atomic force microscopy (AFM), is presented in appendix A.12. AFM images were captured with a Digital Instruments Multimode Nanoscope IIIa (Digital Instruments, Cambridge, U.K.), equipped with a 'J' scanner for large scale images.

Samples were washed with ethanol and dried under flowing nitrogen before use. The samples were mounted on adhesive carbon tabs on magnetic discs, which were placed on the scanner head. The scan position on the sample was monitored using the optical

video on the microscope and the cantilever holder was then mounted over the sample. The atomic force microscope was used in tapping mode, using a silicon tip with a spring constants of between 20 and 80 Nm^{-1}. The tip was mounted in the tip holder and placed over the scanner and sample. Then, the feedback laser was aligned on the end of the back of the cantilever. The horizontal and vertical position of the photodetector was aligned. The tip was then manually moved to be almost in contact with the surface. The tip was then tuned to find the resonant frequency of the cantilever. The tip was driven by the software to be in interaction with the surface and then image can be acquired. The height images were acquired with a scan angle of 0 and gain setting was monitored by the software.

2.7 Confocal Microscopy

Confocal fluorescence microscopy images with a LSM 510 meta laser scanning confocal microscope (Carl Zeiss, Welwyn Garden City, UK). POEGMA brush patterns with Green Fluorescent Protein were imaged with the upright LSM510 microscope while all others were obtained with an inverted model LSM510 microscope.

For imaging the POEGMA brush patterns with green fluorescent protein, the sample was placed between two microscope glass slides. A drop of Citifluor as an antifade reagent (glycerol-PBS solution, AF1) (Citifluor Ltd, London, United Kingdom) was placed between the sample surface and the top glass slide. 40 x magnification oil dipping lens with numerical aperture of 1.30 was used for imaging. A drop of immersion oil (Immersol 518 F, Zeiss) was placed between the slide and the lens. An Ar laser at 488 nm was used to excite the Green Flourescent Protein and the fluorescence was collected at wavelengths above 505 nm. All fluorescence images were analysed using Zeiss LSM image browser software.

2.8 Interferometric Lithography

IL was carried out using a Coherent Innova 300 C frequency doubled argon ion laser emitting at 244 nm. A Lloyds mirror interferometer was used in conjuction with the laser for lithography. The angle between the mirror and the sample in the interferometer, and the degree of exposure, were varied depending on the periodicity of pattern that was required, calculated from equation (1.7.16). A single exposure with IL gives a periodic pattern of lines; to form a grid a second exposure is required that is orthogonal to the first

2.9 Fluorescence Correlation Spectroscopy

A Carl Zeiss Axiovert 200M microscope with an inverted stage connected to a FCS (ConfoCor2) module is used for all FCS measurements. The microscope is connected to its own class 3B laser module which contains a number of excitation wavelengths:

- Argon/2 - 458, 477, 488, 514 nm
- HeNe1 - 543 nm
- HeNe2 - 633nm

For the purposes of this thesis, it is the HeNe1 laser that is used in all experiments. A wide range of dichroic mirrors and emission filters are available on this microscope, as well as a number of objective lenses. All experiments were completed using the same set-up of these factors. Firstly, the objective used is a C-Apochromat water immersion lens with a magnification of 40× and a numerical aperture of 1.2. A schematic diagram showing the filters and dichroic mirrors is presented in figure 2.5. As shown in figure 2.5, the HeNe1 laser is used to excite the sample at 543 nm. The HFT 543 is the main dichroic beam splitter that works by reflecting light of 543 nm wavelength and transmitting all others. After the light has been absorbed by the sample and emitted at the emission wavelength of the dye the photons are transmitted through this filter. The band pass filter, the filter

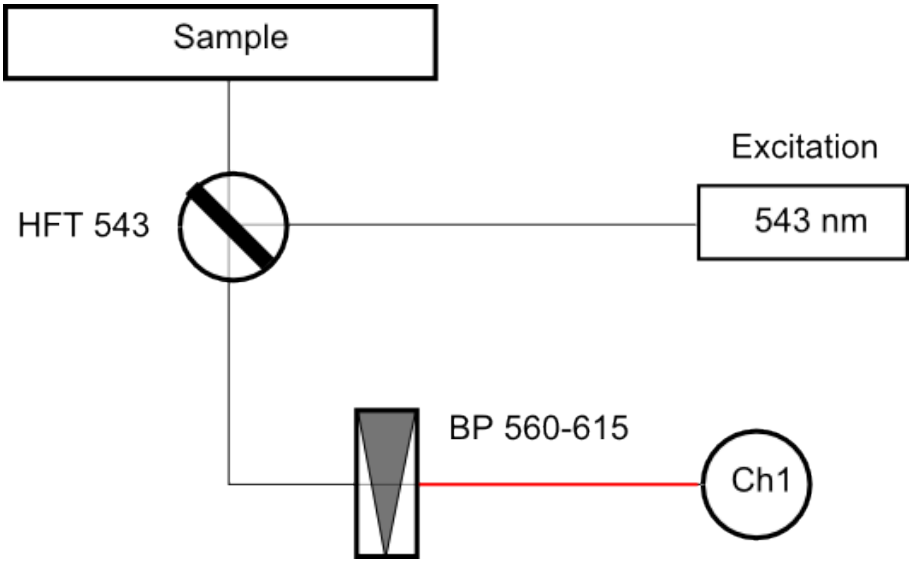

Figure 2.5: A schematic diagram illustrating the path the excitation light must take. Photons with a wavelength of 543 nm are reflected off of the HFT 543 into the sample where the sample becomes excited and emits light of a second, longer wavelength. This passes through the HFT 543 filter before reaching the BP 560-615 filter where only photons with a wavelength between 560 nm and 615 nm are allowed through to be counted by the detector.

that controls which wavelength of photons pass into the photomultiplier tube, used in this thesis was the BP 560-615. This means that only photons with wavelengths between 560 nm and 615 nm were counted.

The fluorescent tag used in this thesis is Rhodamine B (RhB), which has an absorption peak at 540 nm and an emission peak at 565 nm. The RhB was preattached to poly(ethylene glycol) (Mw of 1, 5, 20 and 40 kDa) and purchased from Nanocs. RhB was purchased from Sigma-Aldrich for calibration purposes. Coverslips were obtained from Fisher-Scientific.li

2.9.1 Calibration

Before samples were analysed using FCS, the set-up was calibrated using a solution of free RhB. A solution of RhB in milliQ water was diluted to 10^{-6} mol L^{-1} and 1 mL was placed on a coverslip within a silicone isolator. A second coverslip is then mounted onto the isolator. 100 μL of milliQ water was then placed on the objective lens and the coverslip

was placed into the standard microscope mounting. The objective lens was brought up so that the focal volume passed through the coverslip and into the bulk, using the reflection of light off the glass as a guide. Pinhole adjustments were then made with the focus in this position, the focal volume in the bulk. These adjustments were to allow the maximum amount of photons into the detector while maintaining as small a confocal volume as possible.

Once adjustments had been made to the pinhole the objective was moved away and the coverslip removed. A second solution of RhB solution in milliQ water was produced with a concentration of 10^{-8} mol L^{-1}, with 1 mL of this solution placed on another coverslip with silicone isolator and is then topped with another coverslip. Again 100 μL of milliQ water was placed upon the objective lens, the coverslip was mounted and the objective lens raised so that the focal volume passed into the bulk solution. At this point a diffusion measurement was taken for 6 s and repeated 100 times. The resulting autocorrelation data were averaged and then fitted (using equation 1.7.18) to obtain a diffusion time for RhB through the focal volume. The diffusion coefficient of RhB in water is well known and can be taken to be (427 ± 4) $\mu m^2 s^{-1}$ at 298.15 K [119, 120]. Using the literature value for the diffusion coefficient and the diffusion time fitted, it is possible to calculate the dimensions of the focal volume, as is standard in the field.

2.9.2 Diffusion measurements in the bulk

Once the system is optimised and calibrated, the samples to be examined in the bulk can be prepared. The concentration of dye molecules is tuned to 10^{-8} mol L^{-1} before being placed in a suitable carrier for measurement. In general the set-up described in calibration involving two coverslips and a silicone isolator was sufficient but other carriers were used. Where an alternative carrier was used, the carrier will be described and the implications to the methodology will be discussed where appropriate.

Once the sample was prepared and placed in the carrier, 100 μL of milliQ water was placed upon the objective lens and the carrier was mounted into the microscope using the standard microscope mounting. The objective was then raised so that the focal volume could pass through the bottom of the carrier and into the bulk solution. Diffusion measurements were made in this position, with the focal plane in the bulk solution so that interfaces were in the focal volume of the microscope. The measurement time and number of repetitions vary from experiment to experiment and, as such, will be described where relevant. Data collected from measurements in the bulk were analysed as described below.

A Linkam FTIR600 stage with a T20 system controller was used to control temperature during FCS measurements when required. The sample was placed in an Ibidi μ-Dish$^{35mm,\ High}$ imaging dish. The temperature was cycled from 298 K down to the desired temperature for observation. The system was allowed to rest at this temperature for 5 min, the measurement was taken and then the system was returned to room temperature. For studies of the pH dependence, 400 μL of each solution was placed in a seperate well of a Nunc Lab-Tek II 8 chamber slide.

Each measurement was made for 6 s and repeated 150 times and measurements with average count rates less than 1 kHz were discarded.

2.9.3 Diffusion measurements at a surface

Once the system is optimised and calibrated, the samples that will be examined at the surface can be prepared. The concentration of dye molecules is tuned to 10^{-8} mol L^{-1} and 100 μL of the solution is placed upon the objective lens. The surface of the sample is then placed in the microscope mounting and the objective raised. To find the surface a two step process was followed. The first part involved making use of the reflection of the laser from the surface with the objective set so that the first reflection pattern was made as small as possible. Using this method it is possible to get the

focal volume to within 5 μm of the surface. To get closer to the surface, a z-scan was made. During the z-scan, the objective steps over a range of positions and measures the intensity of light at each position. A sharp peak is formed during this measurement, with the peak maximum being the surface itself. Using this second step the surface is known to be within 10 nm of the focal plane, and as a consequence within the focal volume.

Patterns upon the surface were located through the use of 'methanol patterns'. When the surface was cleaned prior to use, the methanol would 'highlight' the location of the patterned region, as the methanol would not form droplets in that region. The location of the pattern could then be marked so that it was possible to quickly and easily find the pattern for future measurements.

When the focal volume is on the pattern there is no way to know what particular region of the pattern is being observed. It was not possible to grow the polymer brush in such a way that it could be imaged directly in the confocal microscope. Due to this, the patterned region was focussed upon, and then measurements were taken across the whole region, stepping 5 μm in a random direction between each measurement.

Once the surface, and pattern, has been 'found', diffusion measurements are made. It is necessary to repeatedly check the position of the surface, as it can drift over time. The measurement times and number of repetitions vary between experiments and will be described in further detail when relevent. Data collected from meaurements at the surface were analysed as described below.

For each surface, measurements of each polymer (RhB-tagged PEG with molar masses of 1 kDa, 5kDa, 20 kDa and 40 kDa) were taken consecutively so that the same pinhole dimensions were used in each case. The surface and objective lens were cleaned thoroughly between each measurement with a different polymer to avoid contamination.

Measurements of three seconds were repeated 100 times for a total acquisition time of five minutes. After the acquisition of this data set, the process for finding the surface was repeated to ensure that the pattern was still centred within the focal volume. If it was found that the surface had shifted more than 100 nm then the data set was discarded. Data were acquired until each data set had the equivalent of 1500 repeats. The raw data were then averaged to form a single autocorrelation curve that was fitted to extract the data presented. Only data sets with an average intensity of over 1 kHz were used, any below this threshold were discarded.

Fitting data collected during diffusion measurements

The LSM-FCS program provided by Carl Zeiss outputs the autocorrelation data as a plain text file. The data within theses file are analysed using the software pro-Fit from QuantumSoft. Before analysis it is necessary to transform the time sequence from microseconds to seconds. The data are fitted to equation 1.7.18 using the Levenberg-Marquardt algorithm. The key parameter obtained from the fitting process is the diffusion time, τ, which can be used in conjuction with the focal volume dimensions to obtain the diffusion coefficient.

Chapter 3

Using Photolithography to Produce Patterned Polymer Brush Surfaces

One of the main aims of this work is to produce a surface patterned in such a way that it is analogous to the partitioning of the cell membrane. By selecting polymer brushes (synthesised via ATRP) as the barrier between corrals there will be a bottom-up approach to the nanofabrication of the system. The nanofabrication will also involve lithographic methods to include a top-down approach. Modern molecular nanoscience has endevoured for some time to integrate these two approaches yet there is a length scale, between 100nm and the size of a single molecule, where there are very few methodologies that can produce specific transformations.

Photolithography was used to produce the surfaces being examined. In semiconductor industries, photolithography involves focussing a beam of light onto a responsive surface (a resist) to modify the surface somehow. The simplest examples of photolithography being used for patterning specific areas involves the use of a mask of some material resistant to the high intensity light. The mask can be thought of as being analogous to a mask used when spraypainting and acts as a guide; only allowing light to reach certain regions of the surface while blocking its passage to others.

In synthetic chemistry it is accepted that methodologies are bottom-up approaches and the processes work by forming specific covalent bonds so as to modify the structure or function of the targeted molecule. The combination of synthetic chemistry, where single molecules are manipulated, with photolithography seems to be a powerful combination with which to pattern the surfaces of interest. However, typically mask-based photolithography forms structures on the scale of 100 μm while the systems that are of interest to this work are on the scale of 100 nm.

Firstly a means of modifying the surface so that bringing light on to it will produce surface chemistries conducive to the selective growth of brushes will be discussed. Subsequently, two methodologies will be discussed which bring the light to the surface in a more controlled fashion and can consequently reach the size of structure that is required. Lithography can be undertaken using a Scanning Near-field Optical Microscopy (SNOM) set-up, which allows a narrow beam of photons to be brought incident to the surface. A second methodology refered to as Interferometric Lithography (IL) uses the wave-like nature of light to produce variations in the intensity of light based upon position on the surface. The use of NPPOC-protected silane films (to address the selective growth of brushes) and photolithographic techniques have been used to produce a series of periodic POEGMA polymer brush patterns that can be used to examine diffusion in a biologically inspired and analogous system.

3.1 Using Photocleavable Protection Groups as a Guide for Brush Growth

In light directed chemical synthesis, functional groups that are photo-removable are incredibly useful to protect key groups of a molecule. Selective removal of the photo-removable group enable the protected group to be accessed and it is possible to take advantage of

this idea and use it to pattern surfaces on the nanoscale.

Nitrophenyl protecting groups are very attractive in this respect and show high photodeprotection efficiencies. One such group is nitrophenylpropyloxycarbonyl (NPPOC) protecting group which has been shown to be removed with high efficiencies when exposed to light with $\lambda > 320$ nm [121].

NPPOC-protected aminopropyltriethoxysilane (NPPOC-APTES) can be synthesised and forms films on silicon dioxide as a self-assembled monolayer. This allows polymer brushes to be grown using the same methodology as described in 2.3 where the NPPOC has been removed while no brush can be grown elsewhere. The methodologies for producing NPPOC-APTES are described in section 2.4

3.1.1 Characterisation and Patterning of NPPOC-APTES films

NPPOC-silane films were formed on silicon substrate and characterised by water contact angle measurements, AFM roughness measurements and XPS. The water contact angle was measured to be 70° and the surface roughness (R_q/R_a) obtained by AFM is 0.54/0.42 nm; both of these values are consistent with those found in the literature [122].

An XPS survey scan (not shown) for the NPPOC-silane films showed peaks at 285 eV, 400 eV, 532 eV and 99 eV. These peaks correspond to the C1s, N1s, O1s and Si2p orbitals respectively. High resolution spectra for the C1s region (figure 3.1) shows that the spectrum can be fitted with three components at 285.0 eV, 286.3 eV and 289.4 eV which relate to the C-C/C-H, C-O/C-N and the NCOOR carbons respectively. The percentage contibution of each component in the C1s band was measured to be 68.2%, 22.0% and 7.7% respectively (calculated values for NPPOC-silane adsorbate molecules are 69.2%, 23.1% and 7.7%).

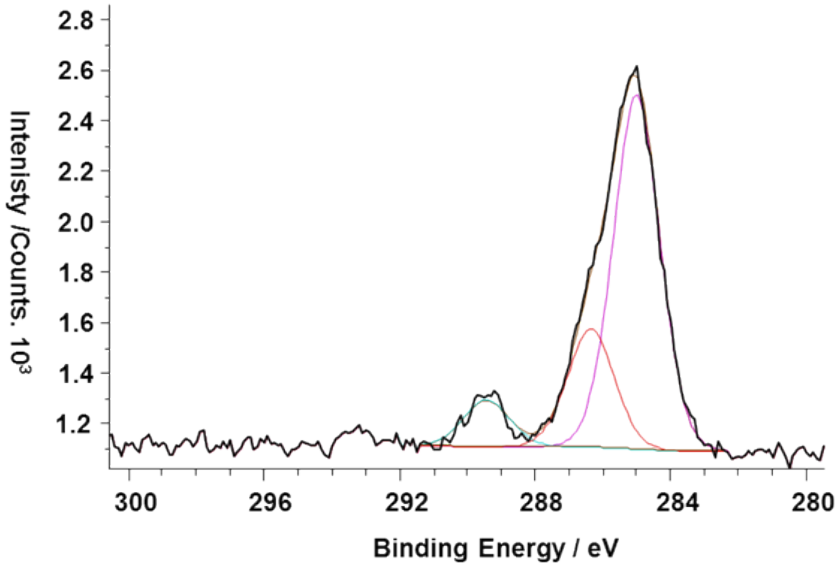

Figure 3.1: A high resolution XPS scan of the C1s region of NPPOC-silane film on Silicon, showing three components beneath the peak envelope corresponding to C-C/C-H (285.0 eV), C-O/C-N (286.3 eV) and the NCOOR (289.4 eV) carbons. The proportions of these components (68.2%, 22.0% and 7.7% for C-C/C-H, C-O/C-N and the NCOOR carbons respectively) is in reasonable agreement for calculated values (69.2%, 23.1% and 7.7% for C-C/C-H, C-O/C-N and the NCOOR carbons respectively) for NPPOC-silane adsorbate molecules.

The high resolution XPS spectrum of the N1s region has two bands, one at 400.0 eV and another 406.1 eV (figure 3.2), which correspond to the nitrogen atoms in the carbamate (NH_2COOH) group and the nitro (NH_2) group respectively. The ratio between the amplitude of the two peaks should be 1:1 due to an equal number of carbamate nitrogen atoms and nitro nitrogen atoms; however the ratio is in fact measured to be 1:0.35. The reduction in the intensity of the nitro peak in the spectrum is most likely to be due to deprotection of the NPPOC-silane film by the X-rays used in the XPS measurements, cleaving away a portion of the NPPOC group

To determine the dose used for the photo-deprotection of the NPPOC-silane film by a 244 nm laser (a frequency doubled argon ion laser), XPS was used to monitor the change in the N1s spectrum with increasing laser exposure time. As the exposure time increases, the intensity of the nitro peak is observed to decrease as the NPPOC-silane protecting

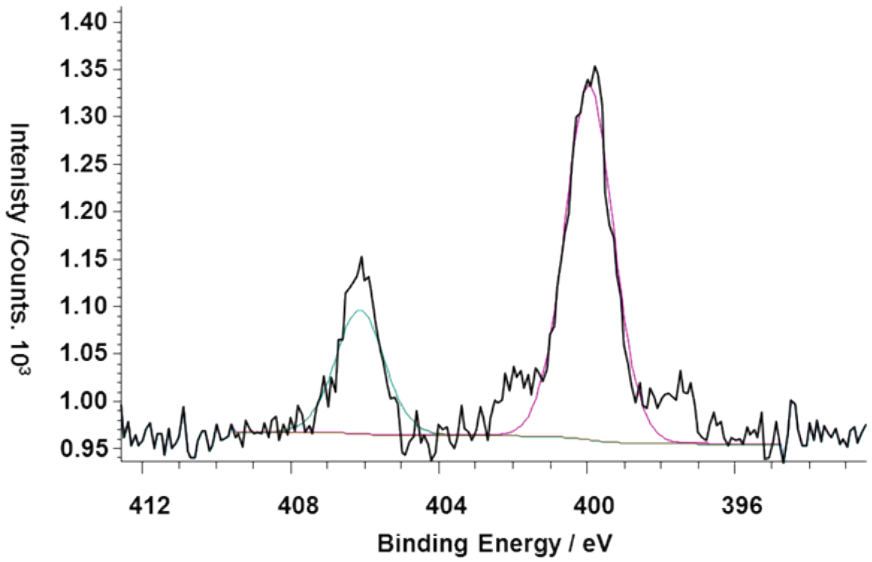

Figure 3.2: A high resolution XPS scan of the N1s region of NPPOC-silane film on Silicon showing two components beneath the peak envelope corresponding to NH_2COOH (400 eV) and NH_2 (406.1 eV) nitrogens. The proportion of these groups is 1:0.35 (NH_2COOH:NH_2) which is different to the expected proportion of 1:1. This difference is due to deprotection of the NPPOC-silane film by the X-rays used in the XPS measurements.

group is cleaved off (figure 3.3). At a dose of 1.52 J cm^{-2} the intensity of the nitro peak becomes undetectable, leading to the conclusion that a dose of $\geq$ 1.52 J cm^{-2} will ensure complete deprotection of the adsorbate.

To prove the concept of using NPPOC-silane films for patterning via photolithography, micron scale patterns were formed by exposing the films to a 244 nm laser while using a 2000 mesh copper TEM grid as a mask. The exposure time was such that the film received a dose of 1.52 J cm^{-2}. Using AFM, clear differences in contrast can be seen between the masked areas and the exposed areas. Figure 3.4(a) shows a friction force microscopy image of a micron patterned NPPOC silane film. The masked areas are the bars while the exposed areas are the squares, the bright contrast in the exposed regions being due to high frictional forces between the tip and the surface. This is consistent with the idea that an amine terminated surface is formed in the exposed area, which will interact stongly

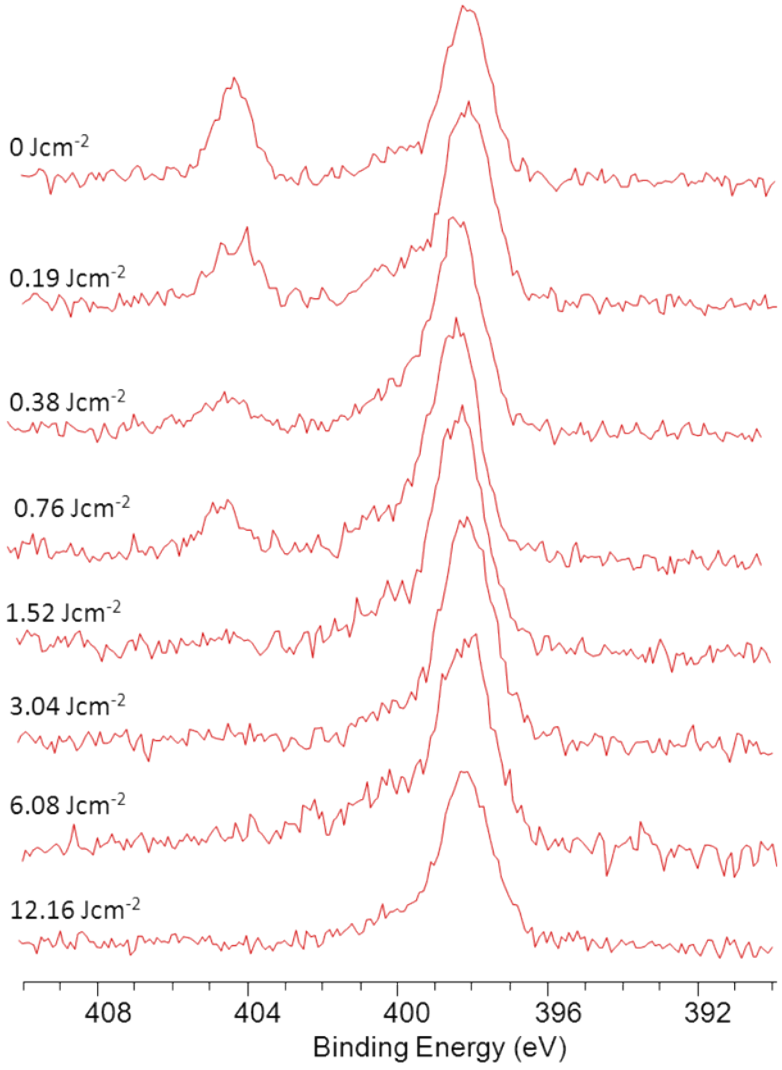

Figure 3.3: The variation in the XPS N1s region of the NPPOC-silane films with increasing exposure time from a 244 nm UV laser. The nitro peak intensity decreases as the exposure time (and consequently dose) increases. At a dose of 1.52 J cm^{-2} the intensity of the nitro peak becomes undetectable, indicating that this dose provides complete deprotection of the NPPOC-silane film.

with the polar silicon nitride tip. Conversly the weaker interaction between the non-polar NPPOC terminal group leads to a darker contrast. In the AFM height image presented in figure 3.4(b), a slight reduction in height is observed, in the region of 2 nm. Previous ellipsometry studies have suggested that the NPPOC-silane film consists of multilayers of the adsorbate with a thickness of about 5 nm [122]. This leads to the conclusion that the exposure has led to the removal of the topmost layer of siloxane.

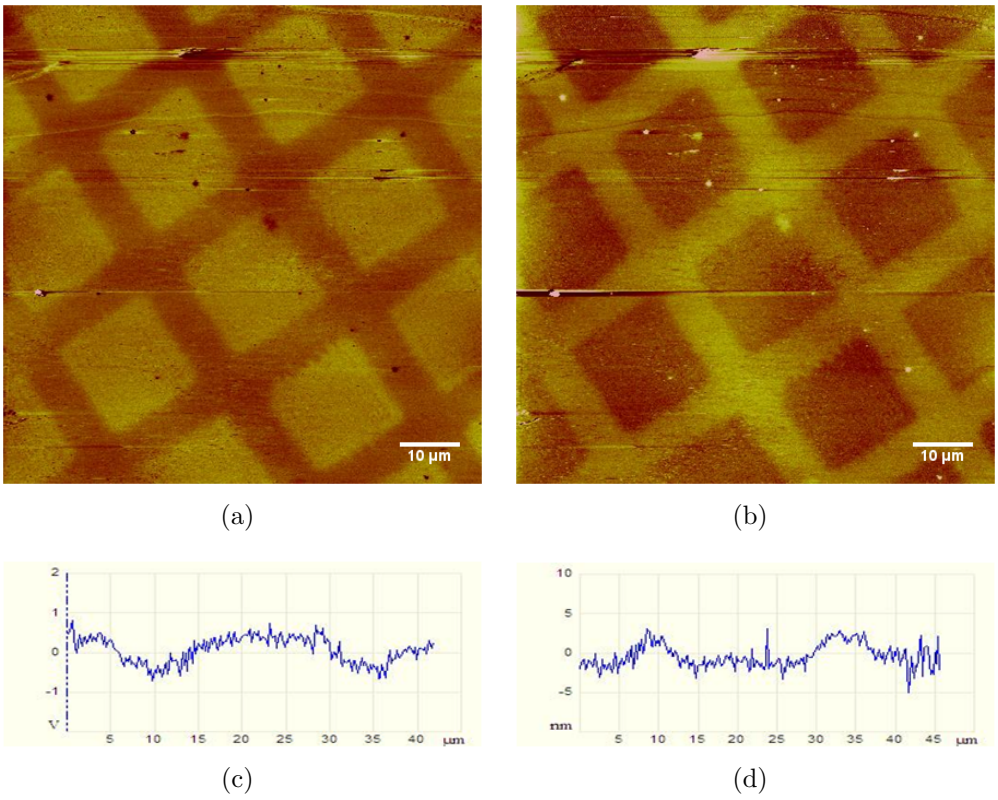

Figure 3.4: 80 μm $\times$ 80 μm friction force (a) and height (b) images of micron patterened NPPOC films. Line sections of the friction (c) and height (d) are also shown. The clear contrast between regions suggests that the NPPOC-silane films have been deprotected in the regions where the mask does not block.

To form POEGMA polymer brushes using the micron-patterned NPPOC-silane films, the exposed areas are functionlised so that the exposed amine is coupled to BIBB. This allows for the initiation of the Si-ATRP reaction with squares of POEGMA polymer brush. A good way to visualise this is by taking advantage of the protein-resistant properties of POEGMA. The brush systems were incubated overnight with Green Fluorescent Protein (GFP) and then imaged using confocal microscopy. The images (figure 3.5) show a clear difference in fluorescence between the polymer brush region, where the protein cannot adhere, and the non-brush region. There are some regions where the fluorescence is observed where there should be brush. These speckles are where the GFP has accumulated in sufficient levels to be observable. This is suggested to be due to the POEGMA brush

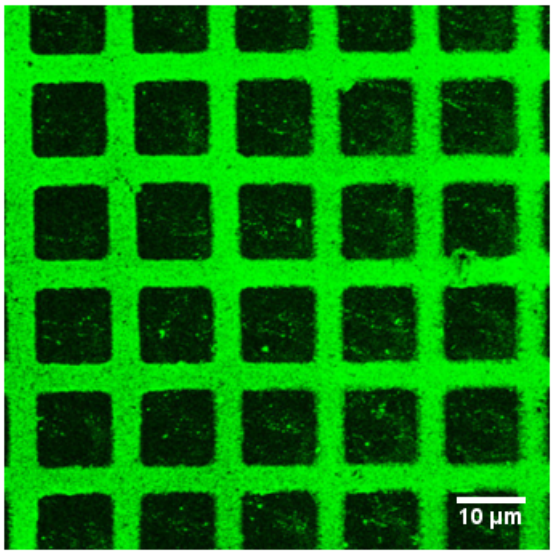

Figure 3.5: A confocal image of POEGMA polymer brush patterns with GFP. The GFP adheres to regions where there is no brush. The speckles of fluorescence in the brush region is due to GFP adhering to the regions were the brush is not dense enough allowing the GFP to reach the underlying substrate. Once one GFP molecule has adhered a form of nucleation occurs so that an observable level of fluorescence if produced.

not being sufficiently dense to prevent the GFP molecule from reaching the underlying substrate. When this is the case a GFP molecule can adhere which in turn allows a form of nucleation producing the observable speckle. The reduced brush density can be attributed to the photolithography removing the initiator molecules in the NPPOC-APTES film preventing the growth of brush.

3.2 Scanning Nearfield Photolithography

Initial experiments using SNP to produce patterns were sucessful (figure 3.6). Patterns of arbitary lines could be formed with ease and square grids of various sizes could be routinely formed. POEGMA brushes grown from these patterns were well defined.

The slow throughput of SNP was the major issue with using this technique to produce suitable patterns. The programming of the probe path was a time consuming process

that had to be repeated for producing samples of different sizes. In addition, the serial nature of SNP with respect to the probe path meant in the time it took to produce one sample by SNP, in excess of ten samples were produced by Interferometric lithography. With little difference in the quality of the pattern and the much larger patterned area from Interferometric lithography, SNP was rejected as the methodology for patterning the polymer grid structures.

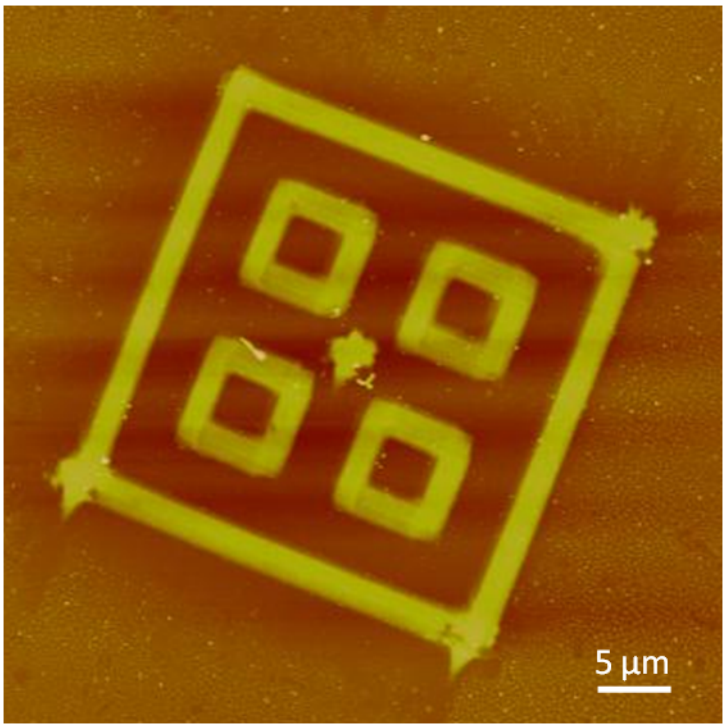

Figure 3.6: A POEGMA brush box structure produced with Scanning Near-field Lithography imaged with AFM. Brighter regions indicate higher regions and therefore brush. The brush thickness is 30 nm in this micrograph. The pattern is well defined with very few stray brush formation.

3.3 Interferometric Lithography

Interferometric lithography was used to produce square grids, with walls of POEGMA brushes and pores showing the NPPOC-protection group.

To determine the correct exposure for forming patterns with IL, single exposure lines were formed and polymer brushes were grown. The result was then imaged with AFM (figure 3.7). The shortest exposure time (providing a dose of 1.37 Jcm^{-2}) produced poorly defined patterns as the NPPOC-silane films were not fully deprotected. As the exposure time increases, the brush lines become more defined and increasingly wide as more NPPOC-silane is deprotected.

A dose of 2.74 Jcm^{-2} upon the NPPOC-protected SAM produced patterns with well defined polymer brush lines. Consequently this same dose was used for forming polymer brush grids by IL. The pitting on the patterns formed after doses of 4.11 Jcm^{-2} and 6.85 Jcm^{-2} are attributed to uneven deprotection of the NPPOC-silane films. In the extreme case of the 6.85 Jcm^{-2} dose the pitting can be attributed to some ablation of the NPPOC-silane film. It can also be observed that the lines of brush get thicker with an increased dose of radiation. This is due to the nature of the intensity profile of the IL spectrum. The $\sin^2 x$ function has a non-zero intensity across the majority of the surface. This leads to a process known as whittling as the increased exposure time leads to deprotection over a wider region.

Sixteen surfaces were selected for use in the diffusion studies from those produced, which equated to roughly 25% of all of those surfaces produced. This is not a sufficiently high conversion rate of plane surfaces to patterned grids to be useful for industrial purposes but it should be stressed that this is currently a small scale production methodology and is highly dependent on the quality and 'freshness' of the precursor materials. Roughly a quarter of those surfaces that were deemed failures were entire batches where the NPPOC-protection hydrolised from the surface leading to a homogeneous brush, a phenomenon associated with NPPOC when it is old. When new NPPOC was produced this problem ceased. Another quarter of failures were due to problems with the growth of the polymer brush linked with the age of the initiator or catalyst to the reaction. The remaining half of all failures came from a number of smaller issues and acounted for a number of patterns

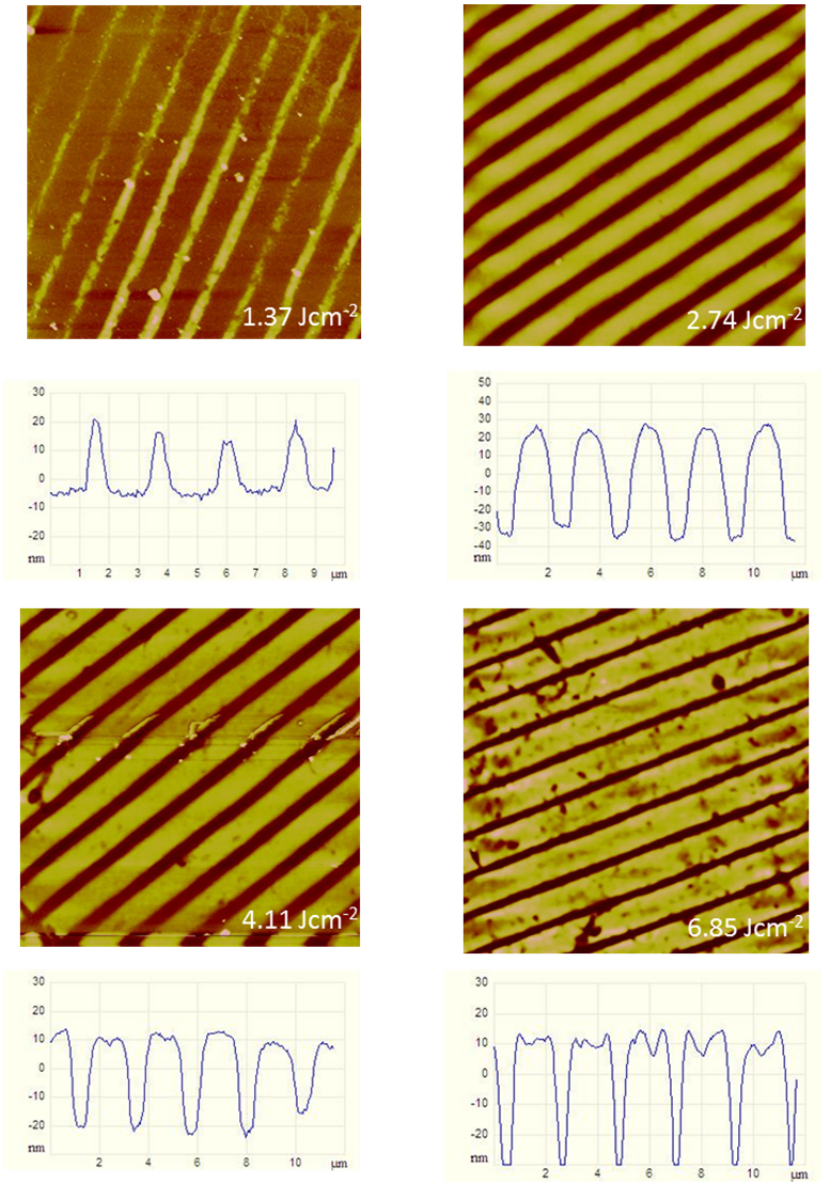

Figure 3.7: 20 μm x20 μm AFM height images, and corresponding line sections, for POEGMA polymer brush lines formed by IL at different exposures. The globular nature of the lines formed at a dose of 1.37 Jcm^{-2} is due to incomplete deprotecton of the NPPOC-silane film. The wider features observed at doses of 4.11 Jcm^{-2} and 6.85 Jcm^{-2} can be attributed to a whittling effect of the non-zero intensity profile of the incident light. The pitting observed at these doses is due to uneven deprotection of the NPPOC-silane films as the initiator is also removed from the film. The lines produced at a dose of were well defined and therefore this dose was selected for producing patterns by IL.

within each sucessful batch.

Failures not due to the quality of the precursor materials could be linked to poor definition in the patterns. This was often caused by patchiness in the brush induced by the ATRP not proceeding as quickly as predicted, meaning that very short brushes were formed. In sucessful patterns there was a dry brush thickness of at least 7 nm, patchy patterns were observed in cases where thicknesses were in the region of 2 nm. A further source of failure was in the IL patterning stage where the dose was not at the optimal value for the production of patterns or the second exposure was not precisely perpendicular to the first.

A selection of AFM height images of sucessful patterns is shown in figure 3.8 with corresponding line sections. Table 3.1 contains a breakdown of each pattern with the width of the well and the thickness of brush barrier given.

Sample	**Repeat Length (nm)**	**Well Width (nm)**	**Barrier Width (nm)**
05.09.13s10	182	90	92
05.09.13s02	400	200	200
05.09.13s04	487	240	247
09.11.13s02	400	193	207
09.11.13s03	400	200	200
09.11.13s04	460	230	230
09.11.13s05	380	190	190
30.07.14s03	426	238	188
30.07.14s06	431	225	206
30.09.14s02	236	118	118
30.09.14s11	182	81	101
21.10.14s01	329	144	185
21.10.14s03	350	142	208
14.11.14s03	218	103	115
14.11.14s04	293	110	183
14.11.14s05	269	121	148

Table 3.1: Patterned surfaces used in diffusion experiments in Chapter 4. The repeat length, well width and barrier width is shown for each surface.

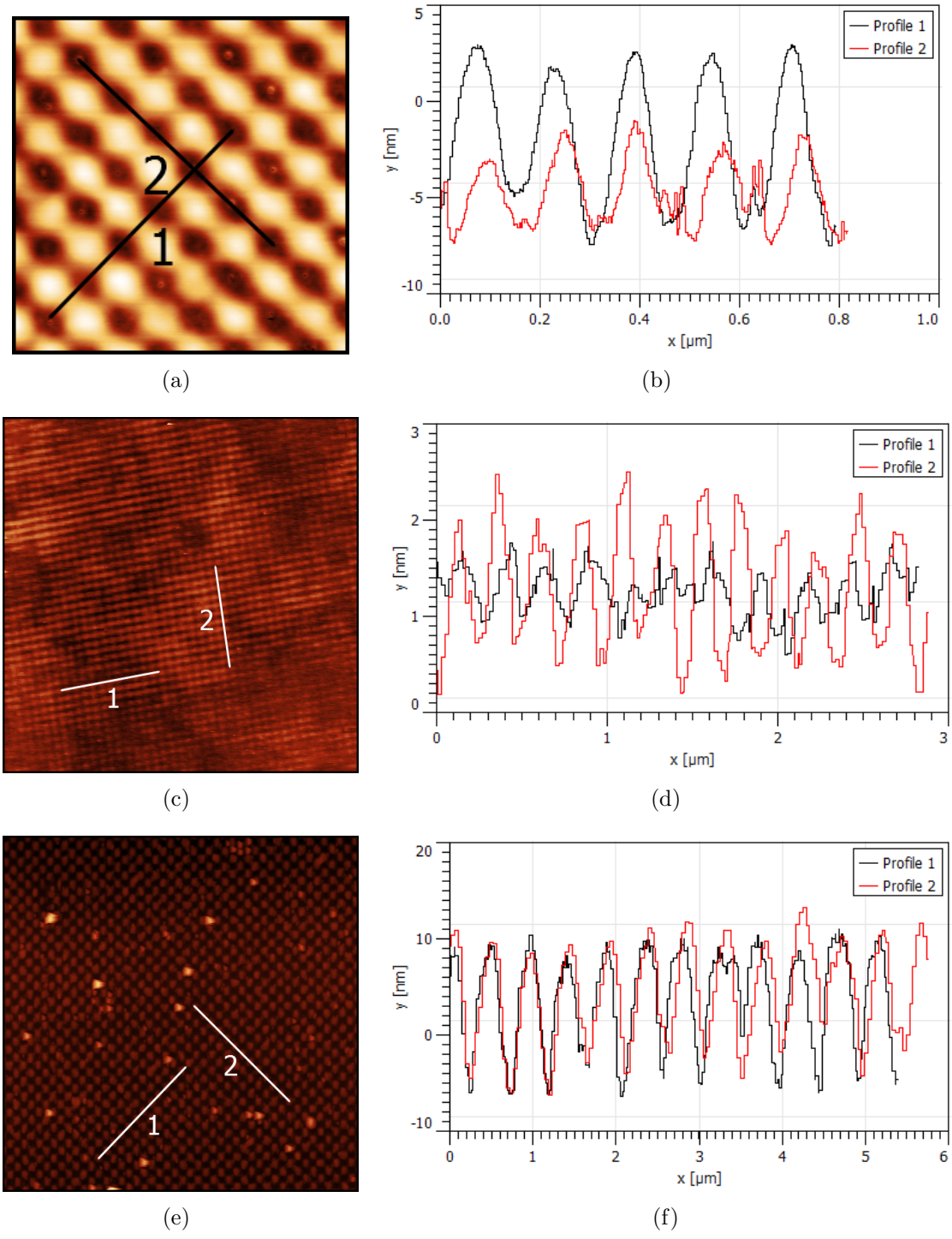

Figure 3.8: AFM height images and line sections of polymer brush patterned surfaces. (a) and (b) show the surface 14.11.14s03, the height image is a 1 μm by 1 μm scan. (c) and (d) show the surface 30.09.14s02, the height image is a 10 μm by 10 μm scan. (e) and (f) show the surface 09.11.13s04, the height image is a 15 μm by 15 μm scan.

3.4 Patterned Polymer Surfaces in relation to Cell Membrane Structure

The surfaces produced by IL are well defined squared grids and are highly reproducible. The patterns formed once the polymer brush is grown from the surface mostly retain this structure, with some issues arising due to the nature of a brush structure. The brush conformation is induced by the proximity of other tethered polymers, at the boundary of the brush region some polymers will not have the confining effect of neighbours to force the upright stance familiar in a polymer brush. This is not as noticeable on structures with larger repeat lengths yet on the surfaces with well widths in the region of 100 nm the effect can be quite noticable. As a consequence this puts a lower limit on the size of patterns that can be produced using this methodology. Obviously smaller structures could be produced, and be well defined, if brushes were not necessary.

The minimum limit on the size of polymeric grid structure is not an issue in the context of an analogue for the cell membrane. Based upon the works cited in section 1.5, the dimensions of the compartments in the cell membrane are of the order of 100 nm and, with regards to the specific case of *R. Sphaeroides*, the chromatophore vesicle itself would have a surface area equating to a well size of 100 nm [1, 2]. The smallest pattern formed for this work had a well width of around 80 nm so is already smaller than the biological equivalent. It would not be feasible, using the current methodology, to explore smaller dimensions than this.

The major difference between the polymeric grid system and the structure of the cell membrane is the relative thickness of the brush barrier to the compartment formed between the brushes. In the case of the polymeric grids there is roughly a 1:1 ratio. The barrier is the same width as the well which comes about due to the sinusoidal nature of the intensity of light used for patterning with regards to position on the surface. This can

be compared with a typical biological case, that of normal rat kidney (NRK) epithelial cells which have compartments with a width of 230 nm and an effective barrier of between 5 and 10 nm [6].

The comparison with NRK epithelial cells is especially poignant as many measurements on NRK cells show compartments have a reasonable approximation to a square grid structure [6]. The compartments in NRK cells are arranged such that a double compartment structure is observed. Four square grid compartments are arranged with an extra thick barrier (10 to 20 nm) surrounding the set to form an even larger square grid. This suggests that the choice of a square grid for the polymeric systems is appropriate not only from the mathematic and practical perspective but because it is also observed in some biological systems.

The barrier thickness of the polymeric system is much larger than would be appropriate in a comparison with a NRK cell, or many other eukaryotic cells, but could be treated as more analogous to more specialised cell membrane structures such as the initial segment of the neuron cell. As argued in section 1.6.2 a similar structure might be used to keep the photosynthetic pathway of *R. Sphaeroides*.

3.5 Summary

Periodic patterns of POEGMA polymer brushes have been formed using a combination of photolithography and synthetic chemistry. The use of NPPOC-protection groups on the APTES SAM allow selective deprotection of the film where brush will be grown. This methodology is a success, allowing the growth of polymer in selected regions when the films are patterned to form micron patterns (using traditional mask-based photolithography) and nanoscale patterns (using SNP and IL).

The use of SNP to form patterns was successful but was not efficient with regards to the time required to produced samples. Patterning through the use of IL was also sucessful and could produce patterned surfaces quickly and efficiently. Periodic squared grids of POEGMA brush were produced, with wells that had comparable sizes to the compartments of a cell membrane. The major difference between the biological and polymeric systems (excluding the obvious difference in the materials used) is primarily in the width of the barrier thickness which are comparable to the size of the well. This is not the case in NRK cells or in most eukaryotic cells, yet could be compared favourably with the structure of the initial segment of the neuron. It is also a possible structure for the region surrounding the chromatophore vesicle in *R. Sphaeroides*, which makes it a very interesting system to examine the diffusion upon.

Chapter 4

Surface Diffusion on Polymeric Grids

The diffusion of membrane molecules is a topic of great interest and as such there has been much work in this area. The key observation discussed in section 1.5 is that of the large reduction in the diffusion coefficient of the molecules in the cell membrane. The explanation of this behaviour is attributed to the structure of the membrane, leading to interactions between the membrane molecules and the cytoskeleton. A major question is how much of the behaviour is related to the physical structure imposed by the cytoskeleton and how much is related to the molecules themselves. This debate has lead to two thought processes among biologists observing diffusion in the cell membrane; those who believe that interactions with the cytoskeleton is the major 'driving' force and those believing that the behaviour can be attributed to 'rafts' and the formation of regions with markedly different compositions. It should be stressed that there are of course biologists who take a middle ground and propose there is an interaction between the two.

From the perspective of this thesis, there are similarities between these two approaches, which are that they both advocate the prescence of distinct regions subtly different from each other, whether due to the proximity of the cytoskeleton or due to different compositions of membrane molecules. A logical leap can be made that this difference will lead to a different diffusion coefficient, a leap that is in keeping with the barrier described by

Novikov *et al.* (2011) [84].

The surfaces manufactured in Chapter 3 can be seen to mimic this approach in two dimensions. The diffusion of PEG upon POEGMA brushes is faster than diffusion of the same polymer upon an NPPOC-protected SAM. However, the diffusion of probes within a brush has been observed to be much slower, often two orders of magnitude slower [123]. Although there are differences between the polymeric system and an idealised cell membrane in terms of structure (for example the width of the brush region is much larger than the corresponding width of a barrier produced by the cytoskeleton), the polymeric surface can be treated as a reasonable analogue. Polymers inside a well will be relatively unhindered as will any polymer on top of the brush or in the bulk solution. However, in the same vein as the hop diffusion model, polymers can get between wells and the mechanism for this could be in the form of a 'hop' via a transitionary phase in the bulk solution or possibly by moving through the brush itself. It is plausible that observation of the diffusion of PEG will suggest which methods are in fact used.

Another plausible result obtained from the diffusion of PEG upon the polymeric grid is the impact that topography alone has on diffusion. Using biological molecules it is virtually impossible to do this and as a result demonstrating considerable difference from either homogeneous surface (be that pure brush or pure SAM) will lead to a possible conclusion that the structure has a considerable role in the diffusion of membrane molecules.

4.1 Comparing Polymeric Grids to the Cell Membrane

The polymeric grids produced in Chapter 3 are considered analogues of the structure observed in the cell membrane that is induced by the membrane skeleton fence model and the transmembrane protein picket model. In section 3.3, the relevance of these grids

from a structural perspective is briefly addressed. The size of the structures, varying between well sizes of about 250 nm down to around 80 nm, are of similar dimensions to the compartments in the cell membrane. It was also established that the size of the well was congruent with the surface area of a chromatophore vesicle in *R. Sphaeroides*. The break in comparison of the polymeric system and the cell membrane, comes when the size of the barrier is considered. The barrier in the cell membrane is the lengthscale over which the proteins responsible for hindering diffusion act. This is observed to be in the region of 5 to 10 nm in the case of Normal Rat Kidney Epithelial (NRK) cells [6]. Taken at face value this is not a good fit for the 1:1 ratio of well to barrier in the polymeric system.

The ratio of 1:1 between barrier and compartment is not a perfect fit for the case of NRK cells, as well as the general structure in the cell membrane, but the case of the neuron, as described in section 1.5, could be seen as being in agreement with this approach (polarisation of the proteins in a membrane due to very thick barriers). It can also be recognised that the thickness of the barrier itself is not necessarily the defining factor on how constrained the diffusion will be. Using the theoretical work of Novikov *et al.* (2011) as a starting point, it can be recognised that while the barrier thickness is a contributing factor, the diffusion of the species within the barrier is also key. If the diffusing species can move relatively freely then a very wide barrier is required to have the same impact as a thin but highly confining barrier. Equation (1.7.8) describes this logic mathematically.

In addition to the structural concerns, there is also the matter of the materials used in the construction. By the very nature of the aims set out, specifically to isolate the impact of structure, the polymeric grid is chemically very different to the cell membrane. The polymer grid is designed so that there is minimal interaction between the diffusing species and the barrier. With PEG as the diffusing species, and POEGMA the barrier, there will be no interactions, bar those of physical contacts and entanglements. The substrate used, an NPPOC-protected silane SAM on glass, is hydrophobic and will consequently lead to

PEG molecules spending longer on the surface than on some hydrophilic surface, such as the brush. This is ideal, because a major problem with using polymers is the fact that the polymer is in solution and must come down to the surface. It will periodically adsorb and desorb from the surface, potentially jumping over the barrier. While the diffusion in the cell membrane is refered to as 'hop diffusion' this does not imply the proteins or lipids undergo a similar jump. The membrane molecules are confined to the plane of the membrane while the polymer being observed is not. As such there will be a bulk diffusion component that will be observed which would obviously not be observed in the biological case.

4.2 Results and Discussion

Two approaches to presenting the results were made, the first was the confinement parameter, X_c^2, described by Wawrezinieck *et al.* [52]. The second was in terms of the perimeter of well that is within the observation area. An estimate for the number of wells was reached by using the Gauss circle problem, treating the wells as lattice points (the Gauss circle problem treats the wells as lattice points and attempts to estimate the number of wells that would be under the focal volume if it were randomly placed on the surface). The first approach allowed for a more direct comparison with the cell membrane as this was the way that diffusion experiments are often presented. It is also worth noting that X_c^2 is a ratio of areas, so a comparison with the perimeter of the wells observed is also of interest from a physical perspective. Table 4.1 shows the confinement parameters and perimeters for each surface. Both of these measures required the knowledge of the size of the observation area, which was collected prior to the use of each surface using the methodology for calibration in section 2.9.1.

To better understand how the patterning of a surface impacts the diffusion upon it, it is necesssary to have knowledge of diffusion on an unpatterned surface. As control

Sample	Confinement Parameter, X_c^2	Well Perimeter in Focal Volume (μm)
05.09.13s10	26.1±1.4	2.30±0.22
05.09.13s02	4.4±0.4	0.88±0.08
13.09.13s04	2.90±0.26	0.68±0.07
09.11.13s02	2.79±0.25	0.0.70±0.07
09.11.13s03	4.0±0.4	0.81±0.08
09.11.13s04	2.98±0.27	0.69±0.07
09.11.13s05	4.3±0.4	0.82±0.08
30.07.14s03	3.16±0.29	0.94±0.09
30.07.14s06	3.4±0.3	0.84±0.08
30.09.14s02	12.1±1.1	1.4±0.14
30.09.14s11	23.3±2.1	1.5±0.14
21.10.14s01	8.3±0.8	0.92±0.09
21.10.14s03	8.6±0.8	0.81±0.08
14.11.14s03	17.6±1.6	1.62±0.15
14.11.14s04	14.5±1.3	0.90±0.09
14.11.14s05	11.3±1.0	1.11±0.11

Table 4.1: A table showing the confinement parameters and observed well perimeters of the produced patterned surfaces.

experiments, a number of measurements were made on surfaces of homogeneous POEGMA brush grown as decribed in section 2.3, as well as unpatterned NPPOC-protected SAMs on glass. Example correlation curves for the diffusion of 20 kDa PEG in both cases, are presented in figure 4.1. Extended measurements show that the PEG diffuses on the NPPOC-protected SAM at between 6 and 8 $\mu m^2 s^{-1}$, depending upon the molar mass of the polymer used. By contrast, the diffusion of PEG on the POEGMA brush is seen to proceed at a diffusion coefficient of between 15 and 20 $\mu m^2 s^{-1}$, again dependent upon the molar mass of the polymer in question. The diffusion coefficient of PEG on a POEGMA brush is consistent with the idea that the polymer diffuses on top of the brush layer rather than within it, as suggested by the magnitude of the diffusion coefficient and TIRF microscopy studies conducted by Z. Zhang (unpublised 2012). Both of these results are consistent with previous results from the research group (Z. Zhang unpublished 2012). Diffusion on the surface of the POEGMA brush is quicker than on the NPPOC-protected SAM which is in agreement with the notion that the POEGMA brush interacts with the PEG more weakly than with the SAM, which allows faster diffusion. However, the

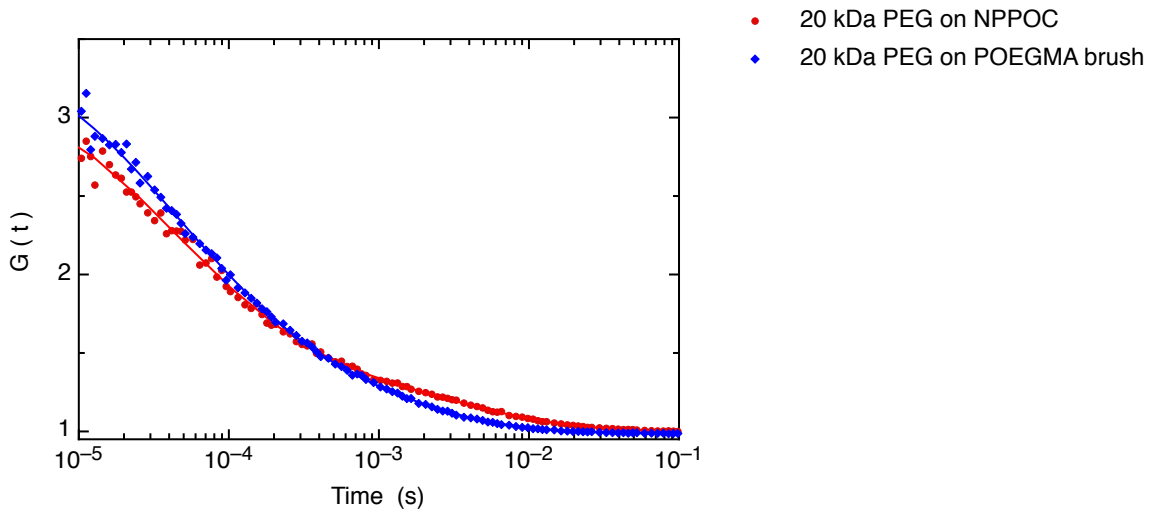

Figure 4.1: Correlation curves showing the diffusion of 20 kDa PEG chains on homogeneous surfaces of NPPOC-protected SAM and POEGMA brush. The curves show both the diffusion of PEG in the water above the surface and a separate component upon it. The diffusion on the NPPOC is slightly slower than that upon the POEGMA brush but there is a slightly higher concentration of PEG chains on the NPPOC surface than the POEGMA brush.

proportion of PEG upon the surface is slightly increased on the NPPOC-protected SAM in comparison to the POEGMA brush, which can be explained by the more hydrophobic nature of the NPPOC.

X_c^2 will be defined as

$$X_c^2 = \frac{\pi W^2}{4 \cdot L^2} \tag{4.2.1}$$

where W is the diameter of the focal point, or beam waist, used to make the measurements, and L is the width of the well being observed. Using this definition, it is possible to place the homogeneous surfaces at opposite ends of the scale. The homogeneous NPPOC-protected SAM can be seen to be a well with an infinite width, and consequently $X_c^2 = 0$. At the opposite end, the homogeneous POEGMA brush surface can be thought of as consisting of wells with a width of zero. This would equate to $X_c^2 = \infty$.

The diffusion coefficient of PEG is therefore expected to have two extreme behaviours based upon the value X_c^2; allowing for predictions of the behaviour that will be observed. At large well sizes, it would be expected that the PEG chains will diffuse as though they were on a homogeneous NPPOC surface. As the wells shrink in size, some intermediate behaviour will be observed, as in the biological case, where the size of the well is similar to the size of the observation spot. At some point the PEG will cease to diffuse on the bottom of the well and instead diffuse on the top of the POEGMA brush. It is hypothesised that this change in behaviour will occur when the feature size is comparable to the size of the PEG chain.

4.2.1 Correlation Curves

The correlation data acquired were initially treated as described in section 2.9.1, with the curves from individual measurements averaged, and then fitted using equation A.9.31 using the Levenberg-Marquardt algorithm. In the homogeneous cases two diffusion modes were extracted, a mode that was related to the diffusion of PEG in three dimensions in water and a mode that was related to the diffusion of PEG on the respective surface. In the case of the patterned surfaces, a third independent component was observed. The identity of the third component was a very slow surface diffusion mode and was observed in all samples and across all molar masses of PEG. Figure 4.2 shows the normalised correlation curves obtained from observing 1 kDa PEG on the patterned surfaces.

Figure 4.2 demonstrates that as the confinement parameter increases there is a larger proportion of molecules present in the third, very slow mode of diffusion. This is made clearer in figure 4.3 with only three normalised correlation curves. It can be seen that the bulk diffusion is unaffected by the increase in confinement parameter, primarily with the same proportion of molecules diffusing in the bulk across all of the confinement parameters observed. The first, faster surface diffusion mode, appears to relate to a consistent diffusion time across the range of confinement parameters. The slower surface mode becomes more

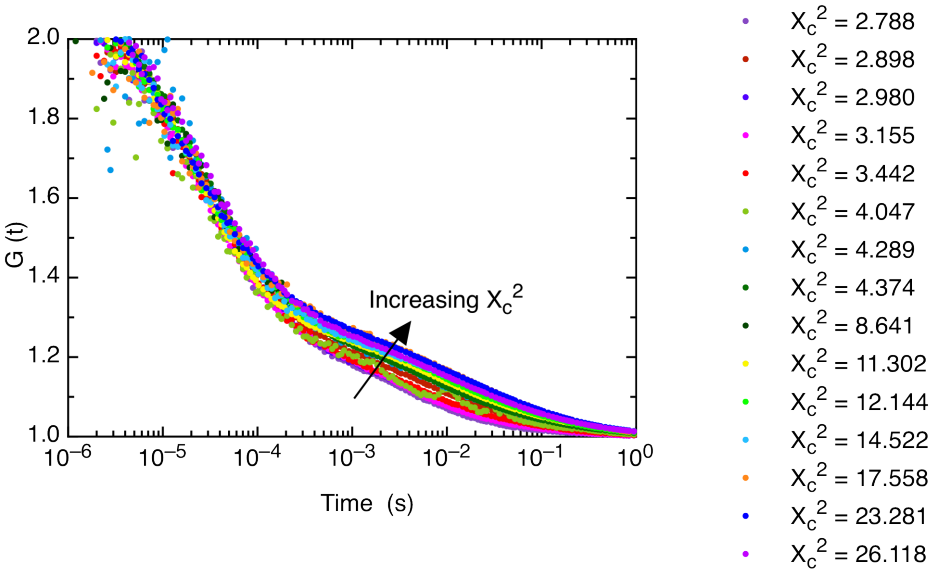

Figure 4.2: Normalised correlation curves showing the diffusion of 1 kDa PEG chains on the patterned polymeric grid surfaces, with respect to the confinement parameter that defines each surface. The curves show both the diffusion of PEG in the water above the surface and diffusion upon it. The bulk component is unaffected by the differing patterns upon the surface, with the introduction of a second mode of diffusion, whose proportion increases as the confinement parameter increases. This can be seen as an overall slowing of diffusion as the well size decreases.

prominent with an increase in the confinement parameter, yet the diffusion times also appear to remain constant across the range observed. The parameter that changes with the increase in confinement parameter is the ratio between the proportions of these modes, with the slower mode becoming more prominent with increasing confinement.

The fitting of the correlation curves collected was achieved with the use of a modified version of equation 1.7.18. With the inclusion of a second surface diffusion component, the behaviour was only slightly more complex. This was due to having the same probe in all behaviours and therefore the components were simply cumulative. The modified

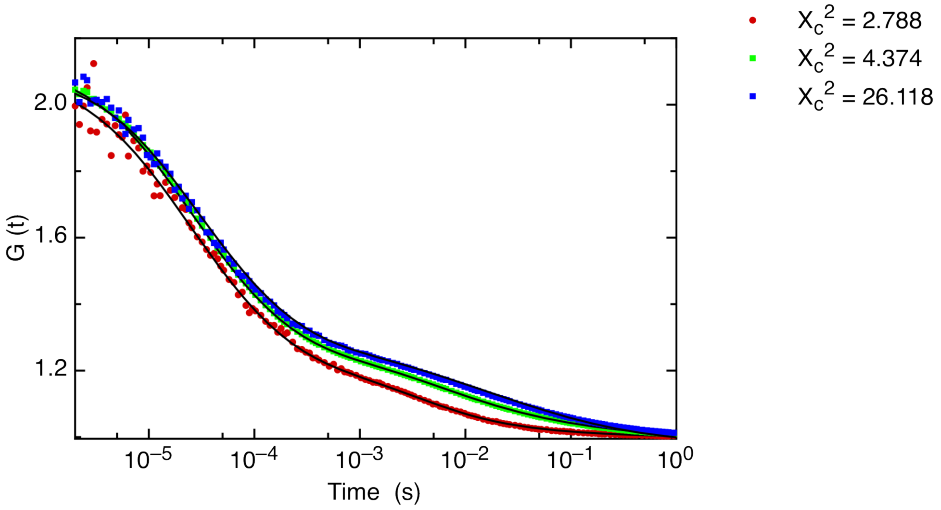

Figure 4.3: Normalised Correlation curves showing the diffusion of 1 kDa PEG chains on the patterned polymeric grid surfaces, with respect to the confinement parameter that defines each surface. The curves show both the diffusion of PEG in the water above the surface and diffusion upon it. The lines plotted through each curve are the fits of the correlation curve with respect to equation 4.2.2. As in figure 4.2 the increase in confinement parameter is seen to lead to a slowing of diffusion upon the surface, which is manifested as an increase in the proportion of molecules diffusing in the slow surface diffusion mode.

equation describing the behaviour can be taken as

$$G(\tau) = 1 + \frac{G_{triplet}(\tau)}{\langle N \rangle} \left(\frac{1 - f_2 - f_3}{\left(1 + \left(\frac{\tau}{\tau_{D1}}\right)^2\right)\left(1 + \left(\frac{r_0}{z_0}\right)^2 \cdot \frac{\tau}{\tau_{D1}}\right)^{1/2}} + \frac{f_2}{1 + \left(\frac{\tau}{\tau_{D2}}\right)} + \frac{f_3}{1 + \left(\frac{\tau}{\tau_{D3}}\right)} \right) \tag{4.2.2}$$

where τ_{D1}, τ_{D2} and τ_{D3} refers to the bulk diffusion time, the first surface diffusion time and the second surface diffusion time respectively, and f_2 and f_3 refer to the proportion of molecules that are diffusing with the diffusion times τ_{D2} and τ_{D3} respectively. The validity of adding this third diffusion mode (second surface mode) was confirmed through the use of a statisical F-test.

4.2.2 Diffusion Coefficients and Confinement

Once the raw curves are fitted it is possible to extract information like the diffusion times of each mode of diffusion and the proportion of molecules that are diffusing in this mode. It should be stressed that this is not in the strictest sense the absolute proportion of molecules in each regime. Rather it is the proportion of photons that have been collected that came from molecules in each mode. Due to the fact that the fluorescent probe is the same in each regime, it can be suggested that the proportion of photons *is* the proportion of molecules, but it should be stressed that in systems involving multiple probes this may not be the case. A further point to be considered is that this proportion is not fixed in such a way that all molecules observed within the bulk regime are fixed there permenantly. The proportions are dynamic in nature; molecules from each regime will interchange regularly. Specifically, molecules in the bulk will come to the surface and spend some time in either of the two surface modes, perhaps even transforming between the two before returning to the bulk.

The errors associated with the confinement parameter are a combination of the uncertainty in the measurement of the size of the polymeric grids and the standard error obtained when determining the size of the FCS beam waist. Similarly, the error associated with each diffusion time is related to the standard error from the fitting of the correlation curves and the uncertainty from the determination of the FCS beam size. The error associated with the proportion of each component is the standard error from the fitting of the raw correlation curves. It is possible to minimise the standard errors obtained from fitting FCS correlation curves by taking longer measurements during the acquisition of data, to produce correlation curves with better signal-to-noise. It is difficult to reduce the uncertainty involved in the dimension of the patterned surfaces, the methodology described in chapter 3 minimises this as much as possible.

Figure 4.4 shows fitted values for the diffusion times and their proportions. Three

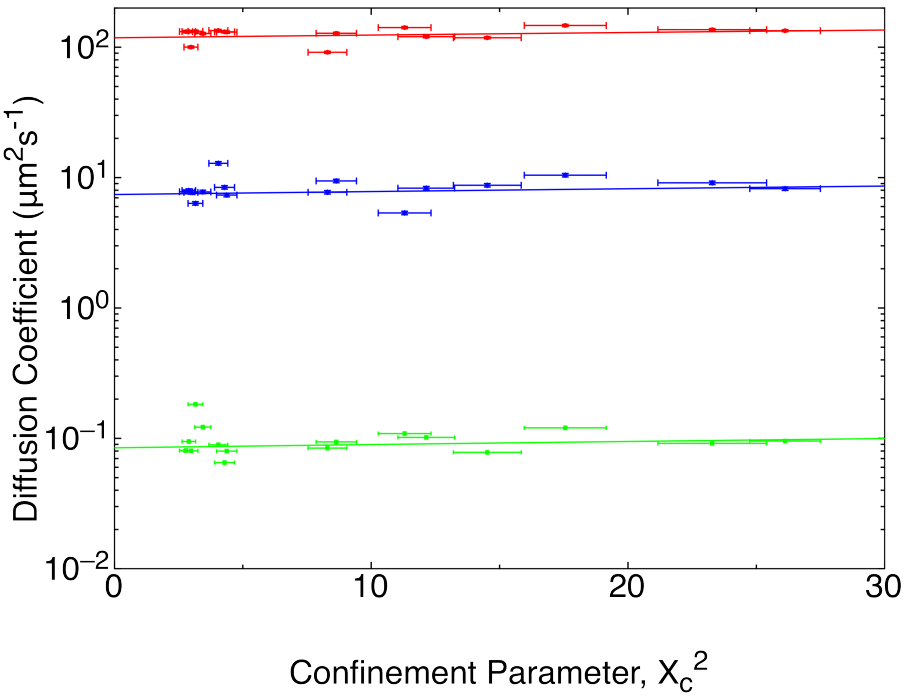

Figure 4.4: Diffusion Coefficients of 1 kDa PEG molecules on a patterned polymeric grid surface plotted with respect to the confinement parameter X_c^2. Three separate diffusion coefficients are observed, corresponding to three modes of diffusion. Errors in diffusion coefficient are plotted yet are very small in comparison to the size of their marker. Red relates to bulk diffusion mode, blue to the fast surface diffusion mode and green relates to the slow surface diffusion mode.

seperate diffusion coefficients were obtained for each polymer on each surface. Each diffusion coefficient remained consistent across the range of confinement parameters examined. While this is expected in the case of bulk diffusion, it initially appears that confinement seems to only induce a third mode of diffusion and that the diffusion coefficient is not impacted by the change in confinement.

Figure 4.5 demonstrates that the larger polymer chains diffuse slower than shorter chains, with the longer chains slower in each mode of diffusion. This is in agreement with basic theory. The diffusion coefficient values obtained from diffusion in the three dimensions are consistent with PEG chains diffusing in water. The first surface diffusion mode is consistent with a PEG chain diffusing on a homogeneous NPPOC surface, implying that

the polymer diffuses primarily at the bottom of the wells in the grid. The second surface diffusion mode is two orders of magnitude slower than this (henceforth referred to as the slow surface component). This slow surface component is therefore of the order of the diffusion of single tracer molecules through a polymer brush [123].

The proportions of moleules exhibiting each mode of diffusion does change with changes in X_c^2 within the range observed (figure 4.6). As X_c^2 increases the proportion of molecules in the slow surface diffusion mode increase until a threshold is met, whereupon the proportion of molecules in this mode levels off to a constant. It was inferred that at zero confinement there would be a proportion of slow surface diffusion of 0%, based upon the preliminary experiments. This allowed the results to be fitted with a form of the error function of the form

$$y = (0.5 \cdot A) \cdot (1 + \mathrm{erf}((B \cdot x) - C), \tag{4.2.3}$$

where A, B and C are fitting parameters. y is the proportion of molecules in the slow surface diffusion mode and x is the confinement parameter. Although physical parameters have not been linked to the fitting values, it can be seen that A relates to the maximum proportion of molecules in the slow surface mode while B and C describe how sharp the transition between the unimpeded and the confined states is. Theoretically the modified error function does not reach zero at a confinement parameter of zero, this will only happen at $X_c^2 = -\infty$ (which has no physical meaning), however the amplitude of the function will still be small in this region.

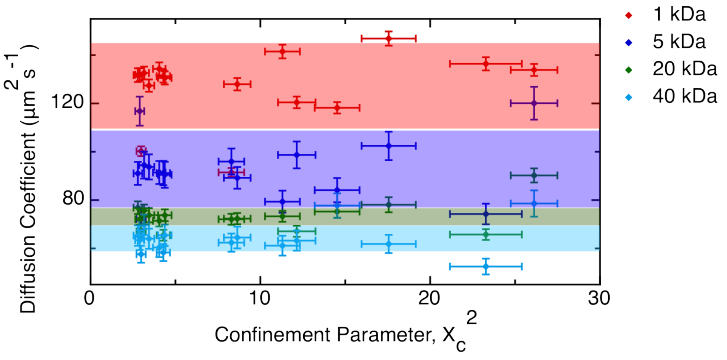

(a)

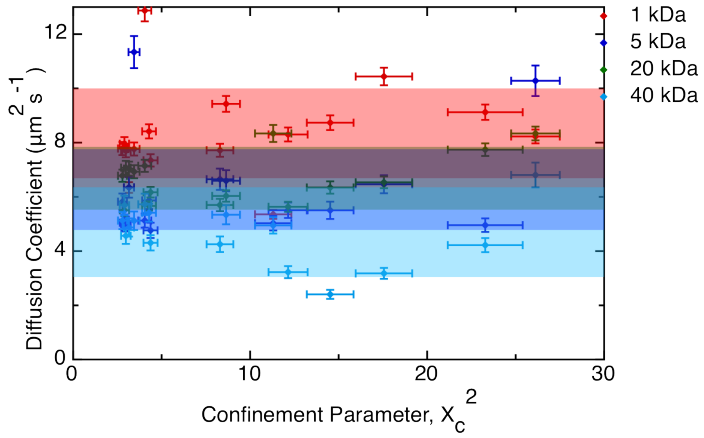

(b)

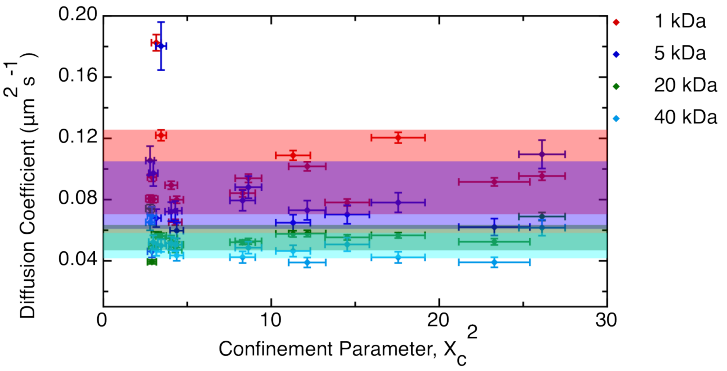

(c)

Figure 4.5: The diffusion coefficient of each mode of diffusion with respect to the confinement parameter. (a) the bulk diffusion mode. (b) the fast surface diffusion mode. (c) the slow surface diffusion mode. Longer molecules diffuse slower than smaller molecules and the line shows the mean diffusion coefficient of each molecular weight of PEG in each mode with a thickness relating to the standard deviation from the mean. Lines of best fit had been plotted yet these showed no correlation between confinement parameter and diffusion coefficient.

The fitted values for the parameters A, B and C, in equation 4.2.3, are presented in table 4.2. In conjunction with the graphs in figure 4.6, it can be seen that the amount of confinement increases (height of plateau in the graphs and the value of A in the table) as the molar mass of the diffusing polymer increases. The gradient of the curve leading up to the plateau is also much steeper in the larger molar mass polymers.

Polymer Molar Mass (kDa)	**A**	**B**	**C**
1	29.2 (±1.3)	0.190 (±0.05)	0.72 (±0.17)
5	33.8 (±2.2)	0.25 (±0.12)	0.9 (±0.4)
20	40.9 (±1.4)	0.45 (±0.11)	1.4 (±0.4)
40	40.9 (±1.6)	2.3 (±1.0)	7 (±3)

Table 4.2: The fitted values of the parameters in equation 4.2.3 as taken from the data presented in figure 4.6.

The fits are generally very good. There are isues with the region surrounding low values of X_c^2, where the fitted parameters suggest there will be a significant non-zero fraction of molecules undergoing diffusion in the slow surface mode upon unpatterned, homogeneous NPPOC-protected SAM surfaces. This is not observed experimentally. This behaviour is also not observed in the fitted values obtained for 40 kDa PEG. If the fitting parameters are constrained to produce a value of zero (or very close to zero due to the nature of the error function) the fitted value for A is heavily reduced in all polymer molar masses examined, producing a consistent value of 10% of molecules in the slow surface mode. This is also clearly incorrect as the data themselves clearly demonstrate an increase in the fraction that are in this confined motion. This suggest the model does not perfectly fit the observed data, however no other model fits the transition between states (unperturbed to confined modes) effectively. What can also be obtaind from this data and model is the idea that the polymer molar mass has a significant impact on the sharpness of the transition. In terms of relative area, molar mass is a very strong factor.

Attempts were made to produce a model, with fitted values, that would also include the

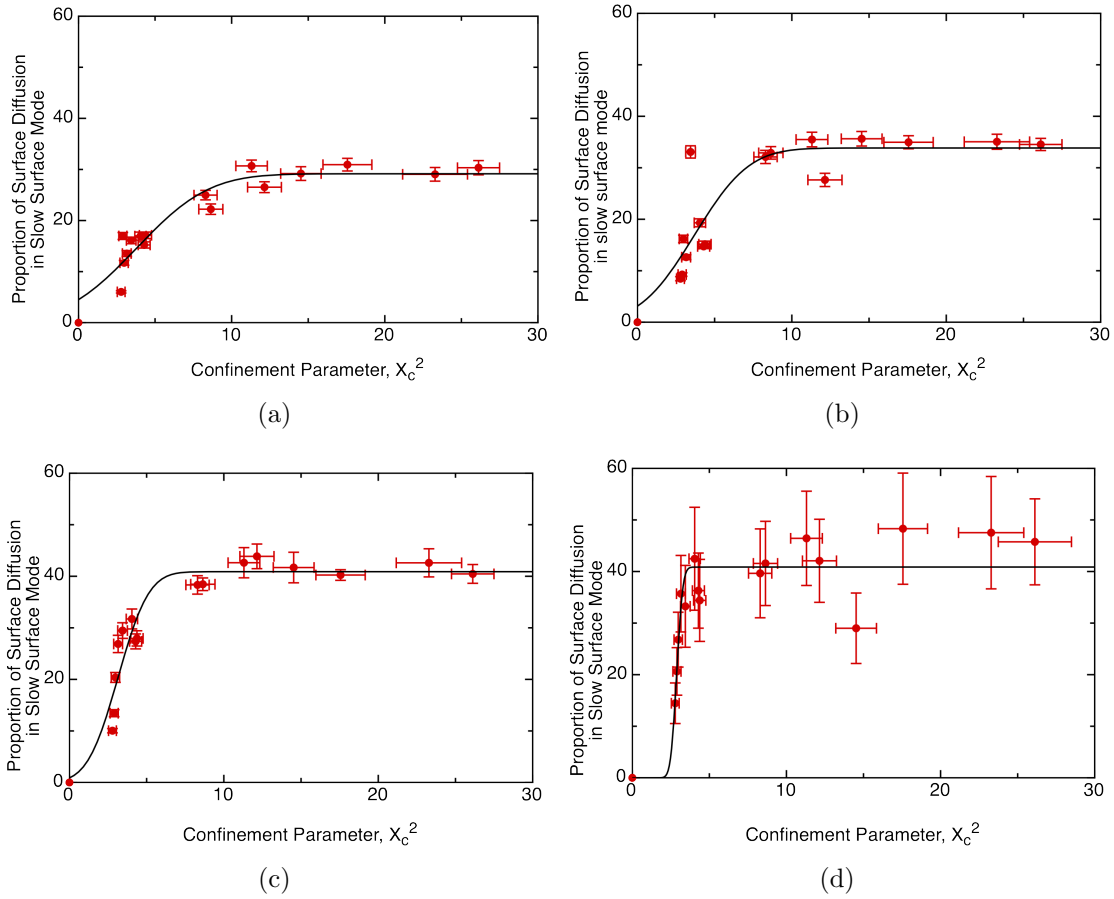

Figure 4.6: The percentage of surface diffusion of PEG that is in the slow surface diffusion mode presented in terms of the confinement parameter. (a) is 1 kDa PEG, (b) is 5 kDa PEG, (c) is 20 kDa PEG and (d) is 40 kDa PEG.

preliminary experiment suggesting $X_c^2 = \infty$. This was deemed impossible due to a lack of knowledge of the decrease from the plateau back to a proportion of slow surface diffusion of zero. Although it could be argued that this transition occurred when the size of the well was approximately the size of the polymer molecule, without a precise knowledge of the transition it was impossible to produce a suitable function. By assuming that the shape of the decrease was the same as that of the increase, it was possible to use a rational expression for a rectangular function. It was not possible to fit this using an algorithm as there were not sufficient data points across the entire range, and specifically the far edge of the function, relating to very large confinement parameters. Other models that did not produce satisfactory results included hyperbolic tangent functions and exponential

functions.

A further means of approaching the confinement of the polymer within the wells is to examine the relationship between the amount of interface between the two distinct regions of surface (NPPOC and brush) to the amount of slow surface diffusion observed. This approach is a logical step from that of the confinement parameter, as the presence of an interface between regions is the main difference between the patterned polymeric surface and the homogeneous surface. The amount of interface is presented as the well perimeter observable within the FCS observation area. The value for this parameter is reached by treating each well as a discrete point on a square lattice, and then applying the logic used in the solution to the Gauss circle problem to get an average number of wells and an associated uncertainty. Strictly the Gauss circle problem is best used when there are a large number of lattice points but the solution provided in valid and gives a good estimate for the amount of interface that will be present. The graphs illustrating data treated in this way are presented in figure 4.7 along with a fitted line based upon equation 4.2.3. The values for parameters fitted to equation 4.2.3 are presented in table 4.3.

Polymer Molar Mass (kDa)	**A**	**B**	**C**
1	29.7 (±0.5)	10 (±3)	7.6 (±2.4)
5	31.7 (±0.6)	9 (±4)	7.9 (±3.7)
20	41.3 (±2.4)	4.5 (±1.2)	3.3 (±0.9)
40	45.6 (±2.6)	3.2 (±1.0)	2.2 (±0.8)

Table 4.3: The fitted values of the parameters in equation 4.2.3 as taken from the data presented in figure 4.7.

Data takes on a subtly different appearance when treated in terms of well perimeter rather than the confinement parameter. The first difference is that the curves produced are generally sharper. This implies that the transition from normal diffusion to confined motion can be primarily treated as a being caused by the amount of interface. This leads

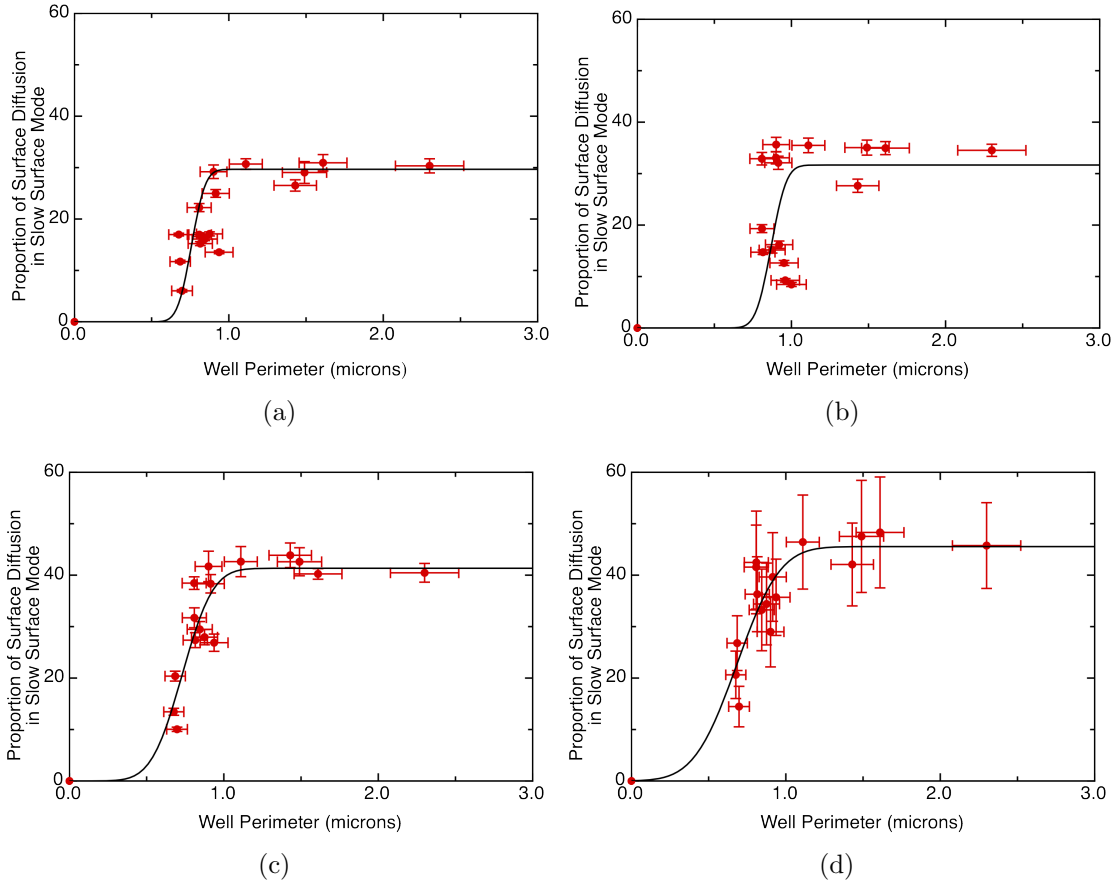

Figure 4.7: The percentage of surface diffusion of PEG that is in the slow surface diffusion mode in terms of the well perimeter in the FCS observation area: (a) 1 kDa PEG, (b) 5 kDa PEG, (c) 20 kDa PEG and (d) 40 kDa PEG.

to the second difference, which is that the four curves produced by the data have more similarities in shape, all of the curves having a sharp transition at the same point. The only major difference between the four curves in figure 4.7 is the height at which they level off into a plateau, which increases with the molar mass of the polymers.

As previously stated, the value that the transition between diffusive modes occurs appears to be consistent between all four polymer molar masses. This suggests that there is some importance to a value of 0.7 μm of interface within the observation volume. The significance of this is not clear, it is suggested that this amount of interface provides the optimal amount of brush for the diffusing PEG to interact with.

Attempts were made to produce a function that would be in keeping with the preliminary experiments, specifically that the slow surface diffusion mode would disappear at some suitably large value for the amount of interface within the observation area. This fails for the same reasons that the attempt using confinement parameters failed, the range of values is too large and there are too few known data points at the far edge.

4.2.3 FCS diffusion laws

The FCS diffusion laws aim to use the variations in the diffusion time of a diffusing species to work out the structure of the medium in which it is moving. Originally designed to deal with the strucutre of the plasma membrane, it seems more than reasonable to use this approach to analyse the diffusion on the analogous polymeric system. The FCS diffusion laws are discussed in more detail in section 1.7.1.

The first requirement to use the FCS diffusion laws is to have a single 'macroscopic' diffusion time. This is achieved by taking the weighted average diffusion time based upon the correlation curves previously presented. The average diffusion time can then be plotted against the confinement parameter and a straight line fitted through the points at a sufficiently high X_c^2. This follows the arguments presented by Wawrezinieck *et al.* (2005) [52]. The straight line will be fitted to data with a confinement parameter that is greater than 10 (as is the case in Wawrezinieck *et al.* (2005)) and the structure will then be evaluated.

Figure 4.8 shows the graphs plotted using the FCS diffusion laws with an accompanying straight line fitted appropriately. It can be seen that all four polymers produce straight lines with a positive intercept, which suggests an 'isolated microdomain' structure based on the FCS diffusion laws. At first this may not seem correct, due to the similarities of the polymer brush grid to that of the 'meshwork' structure, but it should be noted that

a meshwork structure would have a well that was much larger than the barrier between neighbouring wells. Crucially, the meshwork structure implies that the lengthscale that each barrier effects is larger than the average seperation between barriers. In the polymer brush grid, a 1:1 barrier to well structure is seen, which would be much closer to the isolated microdomains in that the lengthscale impacted by the presence of the brush is quite small in comparison to their seperation. Although the isolated microdomain structure is supposed to be random, it is unlikely that the periodic nature of the grid will have an impact upon this lengthscale (or the y-intersept), rather for conceptual purposes it will suggest the use of the term corrals to avoid confusion between a random and ordered orientation.

The positive y-intercept, and therefore the corral structure, is reproduced if the line of best fit is drawn through points with a X_c^2 above 15 and 20. Although there are too few points to draw large conclusions it is a good control suggesting that the same behaviour is observed at larger X_c^2.

4.2.4 Comparison to the Biological Case

The introduction of wells into a polymer brush surface has a significant impact on the diffusion of polymers diffusing upon it. This is not entirely dissimilar from the biological case, where the behaviour of membrane molecules is markedly different between artificial membranes and those of a cell. The introduction of structure has changed the behaviour of molecules diffusing within the system. As previously recognised, the polymeric system is not a true analogue of the cell membrane, yet will function as one for the purposes of observing the impact of the structure upon the diffusion of molecules.

The first point of comparison is the observation of three, distinct, modes of polymer diffusion. The bulk diffusion mode is of no importance to the physics beng discussed, but is useful for the purpose of comparison. The two surface modes are therefore compared with

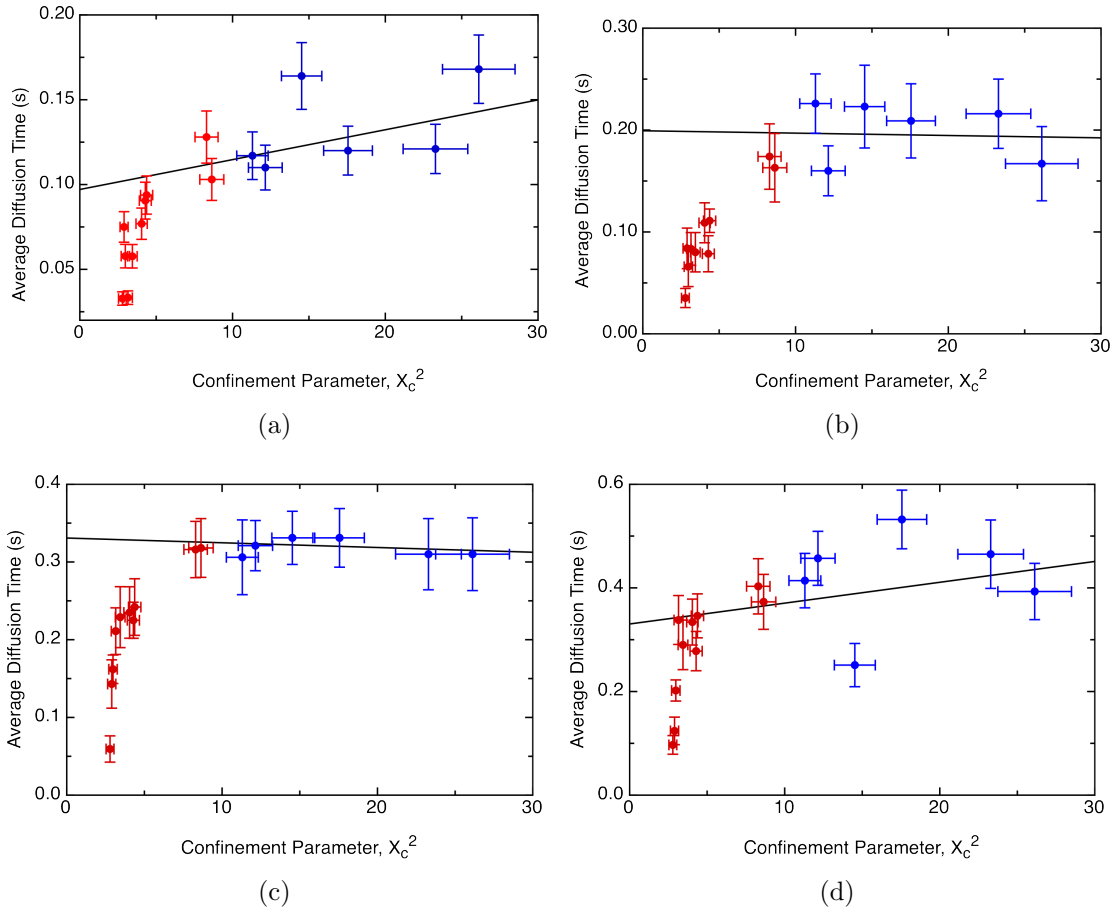

Figure 4.8: Average diffusion time plotted with respect to the confinement parameter. A straight line fitted through the points above a confinement parameter of 10 (shown in blue) gives a positive y-intercept in all cases, which suggests a system of isolated microdomains. This is largely in agreement with the known structure being examined.

the single mode observed in the cell membrane. It is known that the diffusion coefficient of the single mode observed in cell membranes is related to the size of the observation area with respect to the size of the compartment in the membrane. The first point to make is that within the membrane, all molecules are confined. More specifically they cannot leave the bilayer. In the polymeric case, the PEG can leave the surface so as to escape the wells. This is the culprit behind the fast surface mode of diffusion and is the normal behaviour of PEG upon an NPPOC surface. The slow surface mode is bought about by some interaction with the brush and is perhaps more closely linked with the mechanism that causes hop diffusion in the cell membrane. It is suggested that this is

what is occuring on a cruder level within the polymeric system. The PEG 'hops' from well to well with some interaction confining polymers to a well for a certain period.

The second point of comparison is the amount of surface diffusion observed that is within the slow surface mode. In the cell membrane, almost all membrane molecules are confined by the partitioned behaviour. Larger molecules are impacted more strongly, but even the lipids are greatly affected with the vast majority of lipids exhibiting noticably slower diffusion coefficients than in artificial membranes. In the polymeric case, a maximum of 45% of surface diffusion is in the slower mode (as taken from fitted values of 40 kDa PEG treated in terms of perimeter). This is a significant proportion of surface diffusion but not as much as in the biological case. This result suggests that if the system is treated as being a suitable analogue, the structure of the membrane plays a significant role in the sucessful partitioning of the cell membrane but that other factors are important. It has been strongly suggested in literature that it is the protein-protein and protein-lipid interactions that primarily lead to the observed partitioning behaviour. It is in no way suggested that these processes are not involved, however this work strongly implies that the confined behaviour can be reproduced without the need for these interactions. Simply having structure, regardless of the nature of that structure, will induce anomalous diffusion behaviour. It is the various interactions between membrane molecules (combined with the fact that they are trapped within the membrane) that allow such a relatively thin barrier to surpass the confinement observed in this work.

4.3 Conclusions

The work presented here shows that the introduction of structure to a surface has a major impact on the motion of molecules upon it. Although this statement in itself is not surprising, the introduction of a third diffusion mode is very significant. The combination of the two surface diffusion modes can be treated as the single diffusion

time that is usually observed in biological systems. The fact that these two modes can be combined into an average diffusion time that allows for analysis using the FCS diffusion laws, adds to the suggestion that this is a good analogue for the plasma membrane.

The most important implication of the data obtained is the suggestion that it is the interface itself that is responisble for the observed behaviour, with the change in well perimeter leading to a sharper transition than a change in confinement parameter (relative area). This is again unsurprising. However what is surprising is the level of 'confinement' achieved by PEG chains in the dilute limit in a POEGMA walled well. Although below the level of confinement that is observed in the cell membrane, a proportion of molecules in the slow surface mode of 45%, is none the less large for a system of this construction. The system is intentionally designed so that there were not strong interactions between the various species of the system.

The results presented here suggest that a system of similar design could be used in the design of man-made devices. A design of this variety could also explain the behaviour observed in the chromatophore vesicle of *R. Sphaeroides*, in particular the high efficiencies observed. If the complex interactions of the membrane molecules were to be included into the system, it would not be unreasonable to believe that a greater level of confinement would be reached. If the level of confinement were high enough, the membrane molecules of the photosynthetic pathway could be completely confined into the vesicle. This in itself is not unknown, with the polarisation of the cell membrane of the neuron being a good example.

The most fundamental and important observation is that the nature of the confining system appears to be relatively unimportant. PEG diffusing with a (for all intents and purposes) PEG barrier exhibits similar behaviour to that observed in cell membranes, despite not being able to interact in a complex fashion. It could be argued that having a

structure of any sort has a profound impact upon diffusion on a surface. The inclusion of the strong, and often complex, interactions of biological molecules are responsible for the increased confinement observed, but this could be seen as a similar situation to diffusing a charged polymer between oppositely charged brushes. This would be an interesting and important avenue for future research.

Chapter 5

Diffusion of a Stimulus Responsive Block Copolymer

The ability of the cytosol to respond to stimuli is a possible mechanism leading to relative high efficiencies in biological processes. It is the intention of this work to examin a possible mechanism that would facilitate this behaviour. The use of a polymeric system can allow the examination of how potential mechanisms would impact the diffusion of species in a controlled fashion. Section 1.6.3 describes why the use of polymer gels appears to be a good approximation of the cytosol.

The chapter examines how a PGMA-PHPMA gel responds to changes in temperature and pH, and in doing so undergoes an order-order morphology transition. This in turn leads to observable changes in the nature of the system as well as measurable differences to the diffusion of fluorophore-tagged diblock copolymers. This system has been examined previously but without the use of fluoresence and without examining the diffusive behaviour extensively [59, 60].

The observation of a significant change in diffusion coefficient as the temperature and pH are changed is shown to be due to the order-order transition between cylindrical micelles

(worms) and spherical micelles (spheres). This transition causes a change in the size of the diffusing species which, from the Stokes-Einstein relation (eq. 1.7.5), leads to a change in the diffusion coefficient. The change in size, caused by a morphology change, is much larger (and consequently the change in diffusion coefficient) than that expected in the cytosol. The change does however demonstrate how small changes in system can have a major impact upon the transport of species which could in turn be used by the cell to increase the efficiency of processes.

It is argued that mechanisms of a similar kind take place in the cytosol, where even subtle changes in viscosity will aid the transport of protons (in the photosynthetic pathway of *R. Sphaeroides*) to their destination. The nature of the macromolecules within the cytosol, as proteins and polysaccharides, suggest that conformation changes would be possible. Although this change will not be of the same scale as the change in morphology in a polymeric gel, an observable effect could be observed.

5.1 Results and Discussion

The first study involved the variation of temperature, with an aim to make a direct comparison with the dynamic light scattering experiments that had been previously attained [59, 60]. Previous results suggested a hydrodynamic radius for the spheres of 15 nm, while the equivalent radius for the worms was 75 nm. A second study with variations of pH was then completed, using the results from the thermal response for ease of comparison as well as the work of Lovett *et al* (2015) [60].

5.1.1 Thermal Response of Worm Gels

The thermal response was analysed through the use of FCS and the autocorrelation curves were analysed to obtain diffusion times, and consequently the diffusion coefficient. The diffusion coefficients were then transformed into a particle size using the Stokes-Einstein

equation. Normalised autocorrelation curves are presented in figure 5.1a, while two curves with associated fits are presented in figure 5.1b. Only one component was observed in each curve, that of a single species diffusing in three dimensions. This is reassuring for two reasons; firstly it suggests that the fluorophore Rhodamine B (RhB) is well attached to the polymer and secondly that it is indeed the bulk motion of the polymer that is being observed. Figure 5.1a shows a clear change in diffusion time as the temperature is decreased (which the inset, the value for the autocorrelation at a time of 10^{-3} s, makes clearer), with a shift of the curve to the left indicating an increase in the diffusion coefficient.

Fitting of the curves in 5.1a gave high values for the proportion of molecules that enter the dark triplet state. This would ordinarily result in the data set being discarded yet it became apparent that the proportion could not be lowered significantly through the normal methods (longer measurement times with a lower excitation intensity). Comparison of the modified RhB with stock RhB that was purchased from Sigma-Aldrich showed that there was some significant differences in this regard (figure 5.2). The diffusion time (and subsequently diffusion coefficient) was largely in agreement with one another; with the stock RhB having a diffusion coefficient of (450 $\pm$ 40) $\mu m^2 s^{-1}$, while the modified form of RhB had a diffusion coefficient of (500 $\pm$ 80) $\mu m^2 s^{-1}$.

The triplet fraction in the unmodified RhB was observed to be (7.00 $\pm$ 0.10)%, while in the modified case this was observed to be (34.2 $\pm$ 0.4)%. While this value is much higher than would ordinarily be acceptable it should be noted that the diffusion times collected in both the temperature study and the pH study are several orders of magnitude slower than the lifetime of the triplet state and as a consequence, this effect can be largely ignored and treated as an interesting curiosity rather than a factor that has a severe impact. It must be considered when fitting to correlation curves but otherwise should not impact the obtained values themselves.

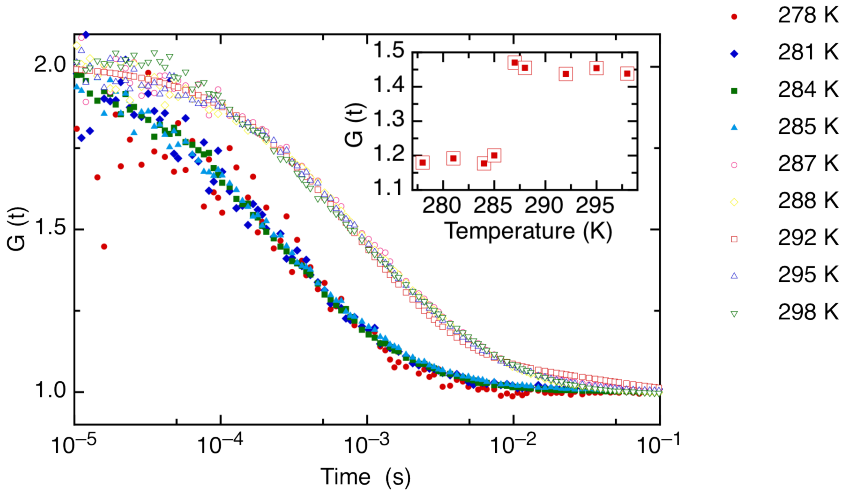

(a)

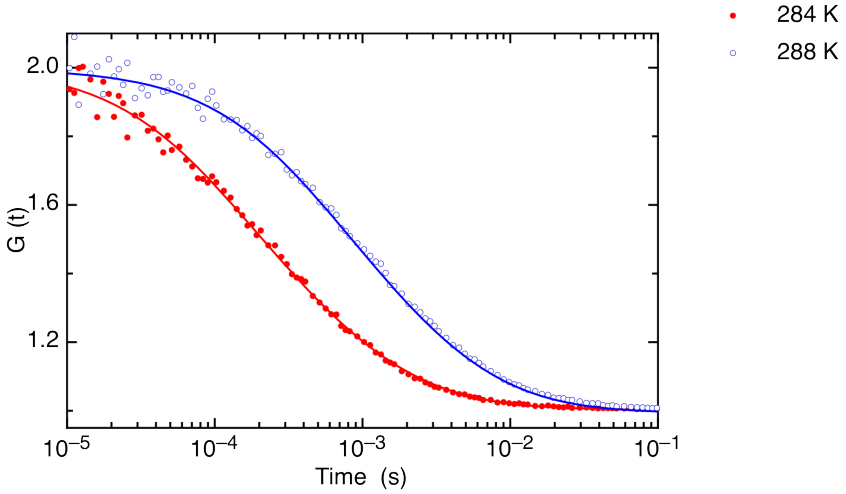

(b)

Figure 5.1: Autocorrelation curves showing the diffusion of tagged block copolymers of PGMA-PHPMA. (a) shows all the autocorrelation curves while (b) shows two with their associated fits. The inset in (a) shows the value for the autocorrelation at a time of 10^{-3} s The discontinuity shows that there is a difference in diffusion time as the temperature changes, a higher value of autocorrelation suggesting slower diffusion. In (a) and (b) solid points represent temperatures below the degelation temperature while hollow points represent those above, or sphere and worm morphologies respectively. The shift of the autocorrelation curves with an increase in temperature illustrates a slowing of diffusion associated with the increased size of the diffusing species.

Another point of interest from the comparison of the two forms of RhB, was that of the

observed number of the molecules in the the confocal volume. Both solutions were diluted to a concentration of 10 nML^{-1} in milliQ water, which equates to a local concentration of 5 molecules within the cofocal volume of 1 fL. The local concentration of RhB in the stock solution was observed to be (5.74 $\pm$ 0.06) molecules while the modified RhB solution has a local concentration of (1.38 $\pm$ 0.03) molecules. The experimental set-up of the FCS is identical between the two measurements, implying that there is a subtle difference in the fluorescent behaviour of the fluorophore after modification. Although it seems to absorb and emit within the same range as the unmodified RhB, it seems that the modified RhB is either more prone to bleaching or has a smaller fluorescent cross-section. It is suggested that it is a combination of both factors that leads to the reduction in apparent local concentration (both factors are equally likely and it does not seem sensible to suggest one would have a notably larger impact than the other), pointing to the heightened proportion of molecules that enter a triplet state as evidence for altered fluorescent behaviour.

Figure 5.3 shows the diffusion coefficient of the polymer with respect to the temperature. The diffusion coefficient increases by a factor of around four, with the increase

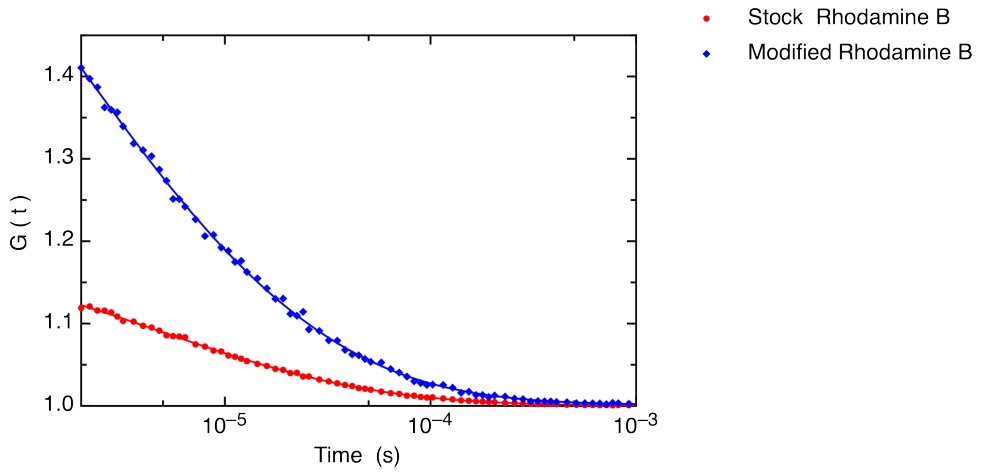

Figure 5.2: Autocorrelation curves of the stock RhB solution purchased from Sigma-Aldrich and the modified RhB solution produced for this work. Although the diffusion time is reasonably similar between the two solutions, the number of molecules and the portion of molecules entering the triplet state is different, illustrated by the differing amplitudes of the curves.

corresponding to a temperature between 12°C and 14°C. This is in rough agreement with the transition of a worm morphology to a sphere morphology as observed in the study of Blanazs *et al.* with the same polymer gel, where the transition was observed at 14°C [59].

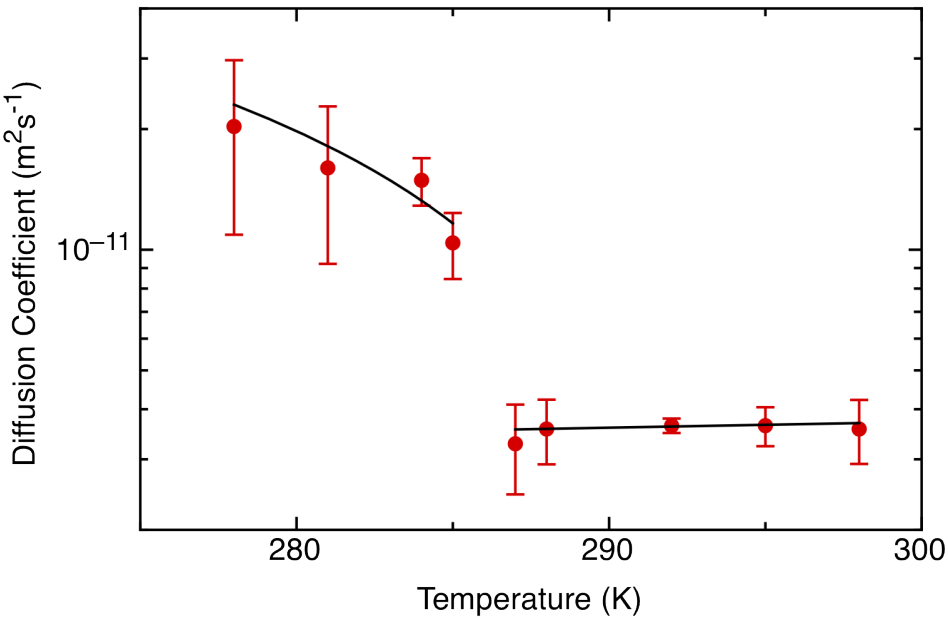

Figure 5.3: Change in diffusion coefficient with respect to temperature. Above 286 K the polymer is in a 'worm' morphology and consequently diffuses slower than the sphere morphology that is observed below this temperature. The increase in diffusion coefficient as temperature is decreased is consistent with the idea of the spheres breaking down.

An interesting observation not made by Blanazs *et al.* (2012), is the increase in diffusion coefficient of the polymer in the sphere morphology as the temperature decreases. This equates to a decrease in the size of the spheres, which could be explained by the spheres breaking into smaller portions. In principle, if cooled enough the spheres would conceivably break up into the unimers (single polymer) yet this is not seen in the range explored in this study.

When calculating the radius of the spheres the Stokes-Einstein relation was used, with the viscosity taken to be that of water. Although the viscosity of the solution, and then the

gel at higher temperature, will differ from that of water it made sense to use the viscosity of water since the polymer is in water and experiences an aqueous local environment. There were also concerns about using the Stokes' force when treating the data as it was not clear that it would be applicable. Stokes' law is used in systems where it can be assumed that there is laminar flow of spherical, homogeneous particles that are surrounded by smooth surfaces. These factors are not a problem as the worms can be treated as 'sphere-equivalent'. The final assumption is that the particles do not interfere with one another. While an argument can be made for this in the case of spheres, it cannot be true for the worms since a gel is formed.

Results in this study were found to be in reasonable agreement with that of Blanazs *et al.* (2012), where particle sizes were calculated using a mix of transmission electron microscopy (TEM) and DLS, when analysed using the Stokes-Einstein relation. Due to this it was not deemed necessary to formulate a new force (as the term is meant in the initial derivation of the Einstein relation, appendix A.5) to explain the interaction, however it is recognised that there is worth in doing this in the future.

The hydrodynamic radius of the spheres is around 10 nm which is comparable to the sphere size observed with DLS. The largest sphere was observed to have a radius of (16. 3± 0.3) nm while the smallest is (6 ± 4) nm. The unimer itself was observed to have a hydrodynamic radius of (1.01 ± 0.04) nm meaning that a complete break up of the spheres could not explain the decrease in the radius.

The sphere equivalent hydrodynamic radius of the worms was observed to be (58 ± 18) nm which although smaller than observed in the paper of Blanazs *et al.* (2012), is still in reasonable agreement.

As stated previously, this change in size is much larger than would be expected in

a system of proteins and polysaccharides yet it demonstrates clearly the potential that a morphological change has for manipulation of diffusive behaviour. The behaviour in the thermal response is very well defined and in agreement with previous work, but in the context of biological systems is not the best analogue. Proteins in particular only function properly in a very narrow range of conditions (one factor that can be improved significantly in artificial devices). A system that was reliant on temperature shifts of several kelvin would not be appropriate for a biological system. This demonstrates why the response of pH is very relevant. Firstly it is a condition that could be changed locally so as to only induce changes in a fixed region of the cytosol. Secondly, although biological macromolecules will denature with large changes in pH, it is potentially reversible when the pH change is reversed [124, 125, 126]. The denaturing process itself might even include the desired change in conformation that would facilitate the change in diffusive behaviour.

5.1.2 pH Response of Worm gels

Figure 5.4 shows how the autocorrelation curves produced by the motion of the tagged polymers changes as the pH is changed. As the pH increases the autocorrelation curves take a jump to the right, demonstrating a transition between a pH of 3.9 and 4.5. This is in agreement with rheological experiments completed on the same polymer gel [60].

All experiements were completed at 22 °C and the pH of the solutions used in the thermal response study was a pH of 3.9. As a test for consistency the diffusion coefficient from the thermal response study at 22 °C can be compared with the diffusion coefficient from the pH response study at pH 3.9. The values for the diffusion coefficient are in agreement between both cases.

Figure 5.5 shows the diffusion coefficient of the PGMA-PHPMA block copolymer gel. An increase of diffusion coefficient of a similar size was observed when the pH increases above a critical value, that lies between pH 3.9 and pH 4.5. This is consistent with the

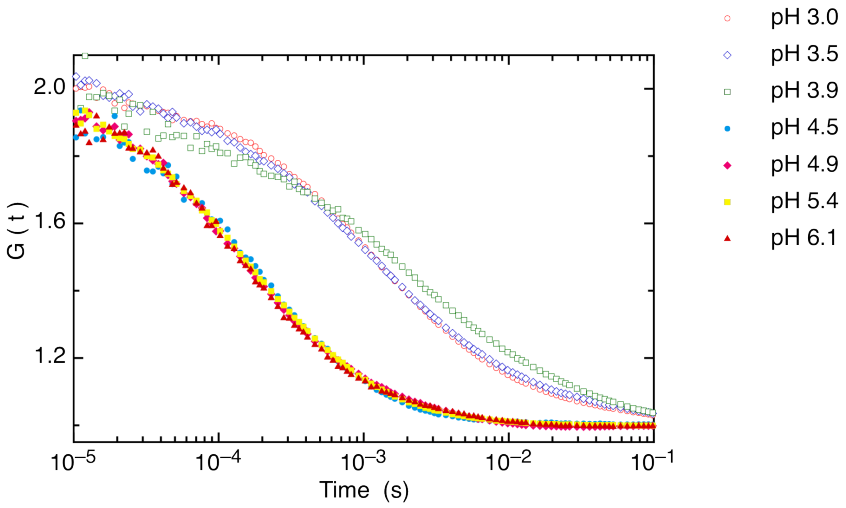

(a)

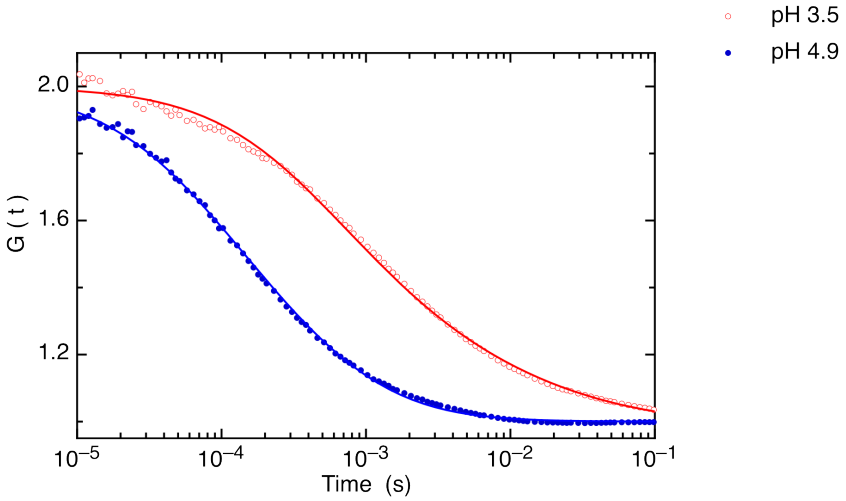

(b)

Figure 5.4: Autocorrelation curves showing the diffusion of tagged block copolymers of PGMA-PHPMA. (a) shows all the autocorrelation curves while (b) shows two with their associated fits. Solid points represent pH where the sphere morphology occurs while the hollow points represent the pH where the worm morphology occurs. The shift of the autocorrelation curves with an increase in pH illustrates an increase in the speed of diffusion associated with the decreased size of the diffusing species.

behaviour observed by rheological methods in the study of Lovett *et al.* (2015) [60].

There is no clear way to evaluate the size of the polymer morphologies as the act of changing the pH makes it difficult to quantify the parameters required to use a relation such as the Stokes-Einstein relation. The factor that impacts the viscosity is the buffer

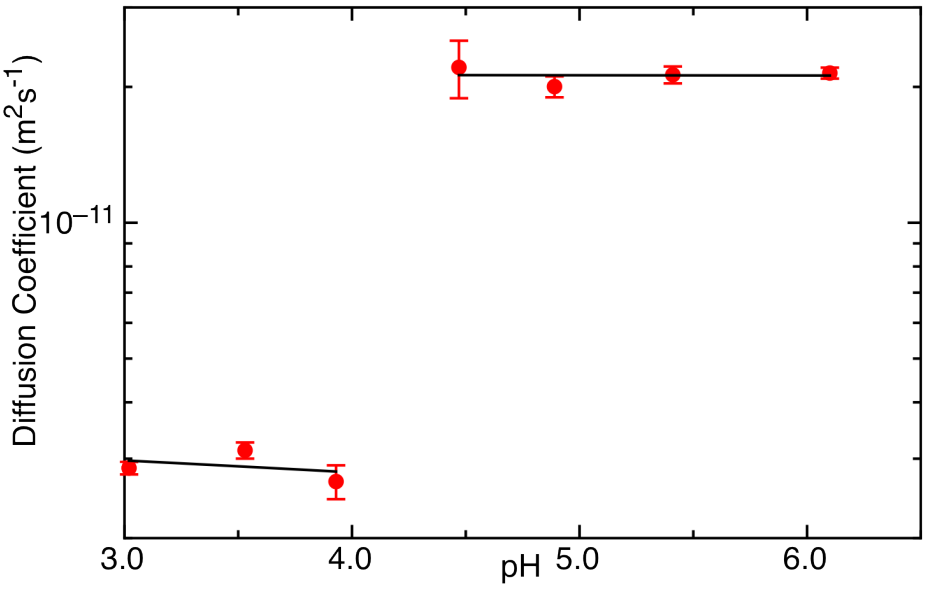

Figure 5.5: Change in diffusion coefficient with respect to pH. Above pH 4 the polymer is in a 'sphere' morphology and is consequently diffuses faster than the worm morphology that is observed below this pH.

used to change the pH, as the temperature is kept constant. The increase in diffusion coefficient is of a similar amount to that shown in the temperature dependence study, suggesting a leap in logic can be made that the larger the diffusion coefficient the smaller the particle in question. This can be used to suggest that the morphological change from spheres to worms has occurred with the change in pH.

In terms of biological processes this result is significant. The change in morphology occurs at a pH between 4 and 4.5 which are biologically appropriate values, while it is also a very sharp transition. This implies that a system can exist entirely as worms or spheres and a small input of acid or base will instigate the transition. This is of critical importance for a biological system attempting to have local changes in response to a proton gradient, as in the photosynthetic pathway of *R. Sphaeroides*. It is also extremely relevant in artificial devices, as the small change in pH required (which is also reversible [60]) means that there is a much smaller build up of buffer as the system cycles between states. This has been demonstrated to have a significant effect in polyelectrolyte systems

which are often used in systems that cycle between acidic and basic conditions [127].

5.2 Conclusions

The aim of this study was to show that the diffusion of a species can be significantly impacted by a change in a factor that is biologically appropriate. This was shown through observing the change in diffusion coefficient of a PGMA-PHPMA as the temperature and pH of the system it is diffusing in. By observing the change in diffusion coefficient it was possible to determine that the block copolymers were changing the morphology with which they were together, thereby impacting the diffusion of the diffusing particles. Biologically, and in terms of the *R. Sphaeroides* photosynthetic pathway, the impact of pH is of the most interest.

The sharp change in diffusion coefficient, so fast that it became impossible to measure the diffusion while the change occurred, is indicative of the morphological change from a sphere to a worm. The PGMA-PHPMA block copolymer changes between these states very swiftly and with only a very small change in the temperature or pH. This is unusual behaviour, particularly in terms of pH driven change, and is very useful. The two states were also not observed to coexist, suggesting that in these samples the transition was complete throughout the entire sample. In terms of the biological context, the swift nature of the transition would suggest that relatively few protons would need to be moved across the membrane to induce a change in the morphology in the macromolecules of the cytosol. Although it is the motion of the proton that is of importance in the photosynthetic pathway, the medium in which they move is important to how the protons will be transported. A more viscous medium will lead to slower motion and vice versa; the work of this study indicating that the medium of motion itself will be impacted in this way.

From the perspective of making devices, the sharp transistion between morphologies

has importance that extends beyond simply not needing many protons to effect the change but also to the way that such small changes can be used as an advantage. In the biological case, it is expected that protons that cause the morphological change will be removed by the ATP synthase, thereby reducing the level of protons and perhaps inducing the reverse transition. In a device it is conceivable that this may not be quite so straight forward (although the author stresses that this would be the ideal scenerio). Using current technologies it would be difficult, to the point of being impractical, to physically remove protons to change the pH of a system. Rather the most commonly used method to change the pH of a system is to use buffers and introduce H^+ and OH^- ions externally. Only minimal amounts of acid or base are required to change the pH enough to induce the order-to-order transition observed in the PGMA-PHPMA block copolymers. In most situations were it is deemed important to cycle between different morphological states, weak polyelectrolytes are used. With polyelectrolytes it has been noted that repeated cycling causes a build-up of salt in the solution, which can become an issue if it reaches a high level [127]. In using a block copolymer like PGMA-PHPMA, the build-up is minimised allowing for a longer usage at a higher efficiency.

In summary, it has been shown through the use of PGMA-PHPMA, a block copolymer that can be treated as an analogue for the cytosol, that it is possible to change the diffusion properties of a system significantly through changes in the temperature and pH of that system. The pH response is of particular interest and illustrates that it would be possible to control the diffusion properties of molecules of interest if such a solution was used as the medium through which the molecule of interest was moving.

Chapter 6

Conclusions and Future Work

It is the aim of this thesis to examine some of the methods that biological systems may use to control the diffusion of molecules so as to achieve highly efficient processes. With the focus on the photosynthetic pathway of *R. sphaeroides*, it is possible to investigate control of diffusion of molecules of interest in the case of both three-dimensional diffusion and at a surface. In three-dimensions, the control of diffusion was tested through changes in temperature and pH, inputs that would be likely used in both biological cases and in artificial devices. To examine the control of diffusion at a surface, a pattern analogous to that seen in the cell membrane was formed and the motion of polymers was observed upon it. In both cases it was shown that diffusion was affected, with either a large increase or decrease observed in the three-dimensional system or a form of confinement observed in the surface case.

6.1 Three-dimensional diffusion

The ability of the cytosol to regulate diffusion was examined by treating a block copolymer gel as an analogue for this system. It was demonstrated that the morphology of the block copolymer could be modified by changing the temperature or pH and in doing so the diffusion characteristics were affected. The cytosol is known to contain macromolecules

such as proteins and polysaccharides, molecules that are known to react to their environment. Proteins particularly take up totally different conformations depending upon their local environment. It was shown that changes in the conformation of a block copolymer lead to large differences in the diffusion of molecules within the solution. Changes in the conformation of proteins and other biological macromolecules will have a similar impact upon diffusion.

It is unclear whether a conformation-driven mechanism actually occurs within the cytosol to drive the various processes within the cell. In itself it is not of the utmost importance that such a conformation-driven mechanism does in fact occur, as the idea that this could be of use in artificial systems is both important and relevant. It would make sense that biology will act in some way to control diffusion in the bulk of the cell and the comparison between the cytosol and a polymer gel seems to be sound. Whether or not such a mechanism occurs does not change the fact that there will be devices that require molecules of interest to be moved or contained. Responsive block copolymer gels appear to produce the desired effect.

Observing the change in conformation of proteins and polymers with FCS is not new [128]. The methods used to induce conformational changes were generally laser heating or a denaturant. FCS was used to observe the diffusion of proteins in a number of studies, from which it was possible to calculate the size of the macromolecule. This is in keeping with the methodologies set out and described in chapter 5. The major difference between the works described by Serrano *et al.* (2012) and that presented in chapter 5, other than the difference in polymers and proteins, is the scale of the transformation. The change in size of a protein that unfolds is minimal in comparison to that observed with the morphology transition (spheres to worms) in chapter 5. This means that the impact on diffusion of the conformation change is not as great. However it should be stressed that in the FCS measurements described in the review article, the protein is not within its

native environment but is in solution at the dilute limit. This suggests that the impact on the medium may be larger if it were a more complex gel such as the cytosol.

An example of the unfolding of proteins is the work of Chattopadhyay *et al.* (2005), where the unfolding of Intestinal-type fatty acid-binding proteins (IFABP) was measured as a function of the concentration of urea (Gdn) [129]. IFABP is a small protein around 15 kDa in size, that can form complexes with other proteins to produce larger structures. The protein contains two β-sheets consisting of five β-strands, meaning there are layers of parallel strands of protein. The introduction of Gdn makes the strands separate, breaking up the sheets. By using FCS, the protein was measured to have a radius of 1.7 nm in its native state, which increased to a radius of 3.1 nm with the introduction of Gdn, a value consistent with that expected for a random coil. Similar values were obtained by Sherman *et al.* (2008) for different proteins and denaturants, with protein L changing from 1.5 nm to 2.3 nm and Adenylate kinase from 3.0 nm to 4.3 nm [130]. These values are reasonably consistent with the size of the single block copolymer chains observed in chapter 5, giving some comparison between the relative size of structures. The proteins presented are much smaller than the morphologies that were examined and although the relative size of the protein almost doubles, the change is still quite small requiring careful data acquisition and detailed analysis.

Although the comparison with proteins is quite interesting, the medium used is not directly comparable with the work of chapter 5 which aimed to analyse an analogue of a biological system. In chapter 5, it is established that a polymer gel would be a good description of the cytosol. The work related to the conformation of proteins does not occur in this sort of medium, so while relevant in demonstrating the ability of proteins to change their shape and diffusion properties, this does not give any clues as to how diffusion of other species will be impacted. Due to this shortcoming in the literature it becomes necessary to examine polymeric systems.

The work of Wang *et al.* (2012), examined the conformational transition of poly (N-isopropylacrylamide) (PNIPAM) chains with FCS . The radius of single chains of PNIPAM were measured as the composition of the solution was changed. The solution was a mixture of water and ethanol, and as the composition changed, the hydrodynamic radius was altered as the solution went from a good solvent to a poor one (larger radius in a good solvent and a smaller radius in a poor one). This work shows that simple changes such as composition of the medium will have a profound impact on the size, and hence diffusion, of a polymer. Again it should be noted that these are single polymer chains in solution so this study cannot be used for direct comparison with the work presented in chapter 5, rather the work of Wang *et al.* (2012) demonstrates possible 'triggers' for a conformational transition and the applicability of polymers as a comparison to biological macromolecules.

The works of Adelsberger *et al.* (2010) and Laschewsky *et al.* (2013) examine the thermal response of block copolymers [131, 132]. Adelsberger *et al.* looked at a triblock copolymer of polystyrene (PS) and PNIPAM, in the form PS-PNIPAM-PS forming a symmetric amphiphillic block copolymer [131]. In aqueous conditions, the PS-PNIPAM-PS forms spherical micelles with a core of PS, the radius of which is dependent on the size of the blocks. PS_{11}-$PNIPAM_{280}$-PS_{11} formed micelles with hydrodynamic radius of 20.8 $\pm$ 0.7 nm while PS_{11}-$PNIPAM_{370}$-PS_{11} formed micelles with a radius of 25.8 $\pm$ 0.9 nm. Both of these have larger blocks than the PGMA-PHPMA block copolymer used in chapter 5, and consequently it is reasuring to observe that they have a larger radius than the PGMA-PHPMA spherical micelles. However, it is notable to see that they are of a similar size (i.e. 10 nm scale rather than 100 nm scale), suggesting that the results obtained in chapter 5 are consistent with other block copolymer systems. As the temperature is increased the micelles congregate and form a gel before eventually collapsing.

Laschewsky *et al.* (2013) discuss the thermal response of block copolymer systems

involving two small hydrophobic blocks made of vinyl polymers sandwiching a long block of PNIPAM or poly(methoxy diethylene glycol acrylate) (PMDEGA) [132]. These polymers behave in a similar fashion to the PS-PNIPAM-PS of Adelsberger *et al.* (2010), forming spherical micelles that cluster as the temperature increases. The clustered micelles eventually form a gel before undergoing a collapse transition at even higher termperatures. Laschewsky *et al.* (2013) conclude that it is a combination of the polymer architecture and the chemical nature of the blocks that leads to this series of behaviours.

The works of Adelsberger *et al.* (2010) and Laschewsky *et al.* (2013) have some similarities with the work presented in chapter 5. The use of block copolymers is the first and most obvious similarity. By using these more structured molecules it is possible to form the micelle morphology that is observed in both the publications and in chapter 5. While the number of blocks is different (triblock and diblock respectively) the way the block copolymer orientates itself is similar, having a hydrophobic core surrounded by a hydrophillic shell. The thermal response is also similar, as in all three cases the micellar solution becomes a gel as temperature increases. However, in the case of both Adelsberger *et al.* (2010) and Laschewsky *et al.* (2013), the micelles congregate together forming a globular network as temperature increases. The PGMA-PHPMA block copolymers behave slightly differently in that they form a completely different morphology before physical contacts between the worms form a gel. This change between morphologies is an order-to-order transition that is not seen in any literature involving diffusion measured by FCS. The response to pH is also rare in an uncharged polymer and the ability to undergo a transition with only minimal changes in pH make PGMA-PHPMA a relevant block copolymer for use in a system where cyclic pH response is required.

In the comparison between the cytosol and polymer gels, the motion of polymers that form the medium itself has been discussed. The change in conformation or morphology of the polymer has a profound impact on the diffusion of the polymer, and in the case

of the latter examples the form that the medium takes. It has been shown that as the temperature is increased (or the pH is decreased in the case of the PGMA-PHPMA block copolymer) the system undergoes a transition that leads to a gel forming. Thus far, the motion of other molecules has been ignored, yet it is likely that one of these molecules will be of greater interest. Taking the PGMA-PHPMA block copolymer as an example, it is expected that the change in morphology that leads to a gel forming will reduce the diffusion coefficient of every diffusant in the gel. This comes about by simple arguments concerning the viscosity of the medium. Future studies with the aim of improving upon the analogue between cytosol and polymer would therefore require a second species which would act in the role of the diffusant of interest in biological systems, be that protons or some molecule. The diffusion of molecular and macromolecular tracers in a PGMA-PHPMA system would therefore be the next step.

Molecular and macromolecular tracers have been studied extensively in undiluted polymer systems [133, 134, 135]. It is known that the diffusion of these tracers does not follow the standard paradigm of Stokes-Einstein behaviour with anomalous behaviour being observed [134, 135]. It is also known that the size, shape and flexibility of the tracer has a significant impact upon the diffusion, both the value of the diffusion coefficient and its temperature dependence [133, 134, 135]. It would therefore be appropriate to examine a variety of tracers, ranging from unattached dyes such as RhB up to larger molecules such as small chains of PEG with an appropriate fluorophore. There would undoubtedly be issues with integrating a larger molecule such as PEG into such a system. However it might be possible to add the polymer when the responsive block copolymer is cooled and in the aqueous sphere state. It is expected that similar results would be observed, with diffusion being much slower when the PGMA-PHPMA system was in the worm gel phase. The diffusion of these tracers could then be treated as that of the protons or other species of interest for a more complete description.

Further research that could follow from the study of diffusion in the PGMA-PHPMA system would involve the introduction of more biological features. For instance, the PGMA-PHPMA system is by volume a good representation of the water and macromolecule content of the cytosol. However, there are also mM concentrations of ions and small molecules with a molar mass below 300 Da [12]. The involvement of ions would be tested by the change in pH, but the introduction of small molecules would be of interest in addition to whatever tracer was used. This would potentially lead to a better understanding of the 'crowding' of molecules in the cytosol and could add another feature to the 'toolbox' for the design of devices.

6.2 Surface Diffusion

It was the aim of this branch of the thesis to design, construct and examine diffusion upon a surface that was an analogue for a particular model of the cell membrane. This was largely successful.

A repeating grid of polymer brush was designed and produced to be in keeping with the membrane skeleton (MSK) model and the transmembrane protein picket model (TPP) model of cell membrane structure. This design was then produced using a combination of surface chemistry, photolithography and ATRP to produce a polymer brush. The diffusion of PEG was investigated diffusing on the patterned surface and as a result a third diffusion mode was observed. This third mode was linked to the presence of the interface between the polymer brush and the brush-free region, as it was not related to the motion of PEG on either unpatterned surface (that of the POEGMA brush or the NPPOC-protected SAM).

The surfaces were designed to minimize interactions with the free species so as to examine the impact that surface structure would have upon diffusion. As such, there were some

obvious differences in terms of the make-up between the cell membrane and the patterned surfaces. There was also the issue that the 'well'-to'barrier' ratio was very different between the two cases, becoming more comparable to specialised cases such as the neuron cell (see section 1.5). This meant that the system was not a perfect analogue of a more general, less specialised, cell but it was still more than relevant to examine the effect of structure upon diffusion.

By following the methods of analysis that are applied by membrane scientists using FCS, it was shown that the diffusion behaviour observed in cells was broadly carried over to the patterned polymeric systems. Three modes of diffusion were observed in the polymeric system, one bulk component and two surface components. The fast surface mode relates to diffusion wihin the wells, while the slow surface mode of diffusion could be treated as polymers 'confined' to the wells in the same manner. There are two diffusion modes observed in biological systems, one relating to confinement and one relating to unhindered diffusion (hop diffusion with short term confinement and long term jumps between adjoining compartments). The use of FCS diffusion laws, proposed by membrane scientists to illicit membrane structure from diffusion data, was successful in suggesting an appropriate structure for the polymeric surfaces. The critical difference between the polymeric system and the cell membrane comes from the proportion of molecules that experience this confined behaviour. In the cell membrane it is accepted that all membrane molecules are confined and jump rarely between compartments. In the polymeric case the maximum confined proportion is in the region of 45%, which is significant but shows that the structure is not completely responsible for the observation of confinement in the cell membrane.

The difference in confinement between the biological and the synthetic situations is most likely due to the interactions between the membrane molecules and the barrier. Membrane molecules are likely to interact in a vast number of ways excluding physical

contact and are inherently complex molecules. By contrast the PEG, POEGMA and NPPOC are all very simple; the PEG will primarily respond to the physical presence of the barrier and anything not explained by this is due to the hydrophobic properties of the NPPOC. 45% of polymers confined is significant when the 'stickiness' of proteins (see section 1.6.1) is considered, leading to one interpretation that the physical form of the barrier matters just as much as the interactions it has with other molecules.

The diffusion coefficients obtained for PEG diffusing in the systems were roughly consistent regardless of the size of structure with the proportion of the diffusion modes varying in relation to the structure size. The bulk diffusion coefficients were in agreement with literature values for PEG in water, ranging from about 100 $\mu m^2 s^{-1}$ to about 60 $\mu m^2 s^{-1}$ for 1 kDa PEG to 40 kDa PEG respectively. The values for the diffusion of PEG on homogeneous POEGMA brushes and for NPPOC surfaces were similarly consistent with previous results by Z. Zhang (unpublished 2012). This leads to the conclusion that the first two modes of diffusion observed, that of the bulk mode and the fast surface mode were correctly identified and supports the existence of a third mode. The values for the homogeneous NPPOC surface and the fast surface diffusion mode are also in agreement which suggests that the PEG diffuses at the bottom of the wells. This is not surprising given that NPPOC is hydrophobic and will 'attract' the polymer to minimise contact with the water of the solution.

The identity of the third component, the slow surface mode, is not clear. However previous research gives some suggestions as to possible mechanisms that can produce this result. The first is that there is no third component, that in fact the motion seen is instability of the detection volume over the period of the measurement [136]. It is argued that this is not the case. The first argument is that the methodologies used involved checking the location of the focal volume on a regular basis. Anomalous detections are known to come about when the volume shifts by more than 100 nm during the measurement time, and it can be categorically stated that this did not occur. A further point is that the

apparent order of the third component. The fact that the diffusion times and coefficients were so consistent and that the proportion of the component seems to have a relationship with the structure size, demonstrates that there is in fact some diffusion process occuring. Add to this the consistency of the fast surface mode, which would itself be affected by instabilities, and it seems clear that this can not be the origin of this slow diffusion mode. It would appear that any instabilities were too small to be a problem but it is accepted that any instability will be a contributing factor in the uncertainties revolving around the mode, just as they are with any surface diffusion measurement.

The primary difference between the patterned surface and the control surface is the fact that there is an interface between the 'well' and brush. As the fast surface mode is linked to the diffusion of PEG upon an NPPOC surface, or the well, it is worth considering that the behaviour originates in some way due to the interface or possibly the brush itself. Experience from this study and from previous research shows that the diffusion of PEG in polymer brush systems occurs on top of the brush rather than within it. This is corroborated by the work of collegues, including a TIRF microscopy study that showed no tagged polymer within the brush (unpublished work of Z. Zhang, 2012). This suggestion can only be deduced from the diffusion coefficients collected, which are faster than that on a 'hard' surface such as silicon, the brush does not confine the polymer to the surface in the same way as a traditional surface and as a consequence the polymers diffuse more rapidly. It is therefore unlikely, and probably impossible, that the polymer could 'burrow' its way into the brush region. This view must however be tempered by the recognition that in the grafting-to method of producing polymer brushes, free chains must reach the underlying surface to be attached and form the brush. There are in fact a number of studies that show that free polymer chains of a similar size to those that form the brush can penetrate the brush layer to reach the substrate [137, 138]. However, these are grafted-to brushes and it is unlikely the same behaviour would be seen in a grafted-from brush formed by surface initiated ATRP, as they are much denser.

There has been work on tracer molecules within polymer networks as stated in the discussion of bulk diffusion, and similar studies have been completed with polymer brushes. The work of Reznik *et al.* (2008) examined the diffusion of rhodamine-6G (Rh6G) within a poly(styrene sulfonate) brush [139]. The diffusion coefficient obtained in this study for the motion of the Rh6G is remarkably similar to the slow surface diffusion mode obtained in this thesis. However the differences between the two situations are too great to attribute motion within the brush as the mechanism responsible. The vastly differing size of diffusing species (small molecule compared to a macromolecule), as well as the chemical nature of the system used by Reznik *et al.* (coulombic attraction is recognised as the factor that draws the tracer into the brush), make such a conclusion a major problem. Discounting the chemical factors, the simple argument that a macromolecule should diffuse much slower than the tracer clearly demonstrates the flaw in this model. Similar studies have demonstrated that polyelectrolyte brushes will have a even greater effect on the diffusion of a charged molecule on top of the brush [140]. Nevertheless the simple chemical nature of the materials used in this study prevents this from being a good explanation for the observed behaviour.

A study using a patterned surface of a similar design illustrated some control of diffusion, yet on much larger length scales. Dunderdale *et al.* (2011) [141] used 1000 mesh TEM grids as a photolithography mask to create a pattern of 6 μm polymer brush barriers and 19 μm wells. Gold (3-5 μm) and iron (2-3 μm) particles were then introduced and tracked using an optical microscope. The basis of the study was that the metal particles were sufficiently large for gravity to pull them to the bottom of the well and that the height of the brush acted as an energy barrier that the particle had to overcome. The energy that a particle has will be $\frac{3}{2}k_{\mathrm{B}}T$, which can be used to calculate a height (known as a gravitational length) which will be practically insurmountable to the particle. In the case of the gold particles this is 0.7 nm, whereas a PS particle of the same size would

have a gravitational length of 250 nm. The gold particles did not undergo diffusion upon adhering to the surface, presumed to be due to chemical attachment. The iron particles had a gravitational length of 4-15 nm and while some of the particles adhered to the surface, a significant fraction underwent diffusion on the surface. The diffusing metal particle diffused freely upon the surface in the wells, but could not escape from the wells due to the brush barrier. The brush thickness was only required to be 2-5% of the particle diameter.

The work of Dunderdale *et al.* (2011) showed similar behaviour to the observations of this thesis. Clearly the gravitational length of a 1 kDa PEG chain will be many times larger than the brush thickness (a back of the envelope calculation suggests the brush would need a thickness of around 2.5 mm to be a barrier with gravity alone), but there are many more influences than gravity on the polymer chain. One interpretation of the results is that the polymer brush does indeed behave as an energy barrier to the PEG chain. The peg chain cannot enter the brush and consequently it must detach from the surface and 'jump' over the barrier. This opens an interesting avenue for future work, by potentially utilising a technique such as total internal reflection FCS (TIRF-FCS) to observe PEG chains upon the surface and therefore investigate this hopping process.

A simple interpretation of the surface diffusion results, is that the PEG becomes entangled in the interface and must 'unknot' to escape. The PEG is actually quite a short chain, so is not likely to form lasting entanglements, but the work of various theorists suggests that short-lived physical knots can spontaneuously form and then dissipate in chains of a range of sizes [142, 143, 144]. Some finite time is required for this to occur, so it is plausible that a knot betwee the PEG chain and the POEGMA brush could occur and then unknot spontaneously. To examine this interpretation, modelling of the chain length dependence of both the brush and the diffusing polymer could suggest the time scales over which the knotting and unknotting would occur as well as the proportion of

molecules that would knot.

Another extension of this study could involve the introduction of greater complexity of the molecules involved. This could take place through either changing the chemistry of the involved participants (charged diffusing species with polyelectrolyte brushes as one example) or introducing biological aspects. An example of how this could be developed down the biological route is by supporting a lipid bilayer on top of the patterned brush. The brush and well regions would lead to subtly different diffusion behaviour in each region, potentialy leading to hop-like diffusion. By changing the polymer brush, different behaviours could be explored, particularly if further extensions were made to include proteins and other membrane molecules. By layering the complexity on top of the relatively simple basis of this study, a more complete understanding of diffusion in the membrane could be achieved.

6.3 Integration to describe the photosynthetic pathway

By integrating the work of both studies it is possible to make an intepretation of the photosynthetic pathway of *R. sphaeroides*. The prevailing belief is that there is no underlying architecture to the cell membrane in the chromatophore vesicle. This would indeed be consistent with current knowlegde of how the cytoskeleton is arranged, meaning that the cyctoskeletal structure will at most be acting to isolate the vesicle from the rest of the membrane. It is strongly suggested that this is the case as the absence of the photosynthetic pathway proteins in regions outside of the vesicle acts as support for this statement. A further suggestion is that the presence of a cytoskeletal border would aid in the formation of a vesicle; lipids added to a fixed region where they could not escape would presumably form a protrusion that could form a vesicle. As this has not been explored in the literature this is an important avenue for further research.

Using the currently proposed structure, the contents of the vesicle are of a similar size to that of the wells used in the studies concerning surface diffusion. Since this was shown to produce a significant level of confinement before the introduction of proteins and lipids, it follows that a similar structure would be in effect. This would effectively keep all of the relevant parts of the photosynthetic pathway within a tight compartment, on the order of 0.01 μm^2. It should also be recognised that structure is not just the presence of the cytoskeleton, as stated in previous arguments a barrier to diffusion need only be a region which produces a lower diffusion coefficient in the vein of Novikov *et al.* (2011) [84]. The proteins involved in the process of photosynthesis often cluster together, this presumably has an impact on the diffusion of molecules in the membrane in these regions.

The impact of the clustered proteins may aid the photosynthetic pathway by not only making the source and destination of the processes close spatialy, but potentially introducing a secondary structure that effectively blocks different regions making diffusion in certain directions preferable to others. It is suggested that this is a further way that *R. sphaeroides* achieves high efficiencies throughout the photosynthetic pathway. It is suggested that the first level of structure (forming the vesicle) forces the proteins together into a compact space, which facilitates the secondary structure with the clusters. This would in itself be analogous to the structures of proteins, which are known to have a primary structure (the order of amino acids) that informs the secondary structure (local structures stabilised by hydrogen bonding) how to form, which is in turn used to form a tertiary structure (the final shape of the protein molecule which uses nonlocal interactions to stabilise).

It is suggested that the primary and secondary structures of the chromatophore vesicle effectively confine the ubiquinols to specific, small regions of the cell membrane. This means that the random nature of diffusion is reduced in terms of direction, it will still

trace a random walk but the area that can be explored by the molecule is reduced significantly, compensating for one of the original observations that processes that are driven by diffusion should struggle to be efficient.

Once the ubiquinol reaches the cytochrome bc_1 and is oxidised to ubiquinone, a proton is pumped across the membrane, which can be intuitively thought of as lowering the pH of the cytosol. These protons are required to drive the ATP synthase protein but are not constrained by the structure that held the uqbiquinones into specific regions. If it can be taken that the macromolecules have acidic groups as part of their structure then there is a possibility for a similar behaviour to that observed in the worm gels. In the case of the worm gels, there are surface -COOH groups that interact with the solution. A similar structure to this would facilitate a quick transition between conformations (or morphologies if there are a number of macromolecules responding co-operatively) that would affect the diffusion of the protons. It is in no way suggested a conformation change as large as that seen in the worm gel study actually occurs in the cytosol and as a consequence such a large change in the diffusion behaviour. However, it is significant that even small changes to the system will perturb the diffusion of the protons, and it is suspected that there will be a significant number of macromolecules with -COOH groups to react to changes in local pH (proteins contain a great number of these groups simply due to the nature of containing amino acids). This cannot be the entire story, proteins are zwitterionic and as a consequence there will be complex behaviours as a result of the influx of protons. Nevertheless it is proposed that the presence of free ions and small molecules may go some way to producing the desired effect, keeping protons from escaping the area containing a ATP synthase protein.

A combination of the principles examined in this thesis would aid in the functioning of the photosynthetic pathway. Firstly by confining all relevant molecules to a specific area and then directing the motion of the ubiquinols, whether through some secondary

structure or otherwise. Finally the pumping of protons is expected to induce some changes in conformation of the macromolecules, whether this change is sufficient to produce a significant impact is not completely clear but any changes that slow the protons, thereby increasing their local concentration, will aid in improving the efficiency of the process.

6.4 Device construction

As technology progresses it is becoming more difficult to achieve the accepted targets: faster, lighter and smaller. As discussed in section 1.2, modern technologies based upon inorganic semiconductors reach physical limits, and devices based upon single atoms and spintronics are required to keep the progression of performance at pace with Moore's Law. Biological systems use single molecules to achieve their aims, with these molecules being stunningly well adapted to perform their task. The comparison made in section 1.1 of the entire chromatophore vesicle of *R. sphaeroides* fitting within the channel length of a commercial transistor is astounding. It is unarguable that there is something to be gained from an inspection of a biomimetic approach, or perhaps even a 'biokleptic' approach.

It should be noted that what remains of this section is predominantly conjecture on how the observations in this thesis might be applied. The actual implementation of the ideas here (which would be very difficult) is secondary to the idea itself. In attempting to produce a device of the sort suggested it is expected that fundamental understanding of Brownian engineering would be improved.

From the comparison between photosynthesis and photovoltaics, in section 1.3, it is clear that the organic solar cells are limited by the diffusion of the excited states. Similar arguments can be made about the inorganic devices. Theoretically the maximum efficiency of a silicon solar cell is 29% using the Shockley-Queisser limit applied to a single junction cell and a commercial mono-crystalline silicon cell can reach an efficiency of 22%. Losses

in commercial cells are due to factors such as reflection at the top interface and blockage due to thin wires, but can also be attributed to the escape of the excited state from the active region. To make an active region large enough to capture all relevant light in any solar cell risks potentially making it too large for the states to escape; not a massive issue in inorganc cells, due to the excited state being an electron, but still a factor that exists.

Consider now a solar cell where the active region is not an extended region of space as in inorganic solar cells but a collection of molecules within the pores of a grid, of a similar shape to those produced in chapter 3. The boundaries of the grid would be such that they can strip the collected charge or excited state of the energy acquired by illumination. The barrier would be some hard barrier rather than a brush so as to facilitate this. If the absorbing molecule were confined to the surface in some fashion, the diffusion would be hemmed into a specific pore of the grid, and with a sufficient number of these molecules, the excited state or charge could be transferred efficiently to a boundary to be collected. In this way it might be possible to ensure that all charge produced was siphoned off for use, in a similar way to the photosynthetic pathway. Using chlorophyll as a model molecule, different pores could contain different 'colours' of the molecules allowing for collection across a range of wavelengths. It is appreciated that this design is difficult to reproduce, but it gives an idea of how biological systems might be replicated in an articial fashion, particularly in relation to functions that will occur entirely upon a surface.

Integrating both control in the bulk of a fluid and upon a surface, now a catalytic system becomes of interest. Consider a system where a catalyst is bonded in some fashion to a surface, with the raw materials required in the bulk of the fluid. The catalyst in question is some biological analogue, in that it is highly efficient at a particular task but is very sensitive to its environment. A ribosome can be considered as the sort of catalyst in question as it has the ability to produce incredibly complex macromolecules precisely yet

being a protein-based machine needs a specific environment. Particularly if it were simply attached to the surface it could deform to become useless, so might require being placed in a membrane (not necessarily a lipid membrane) that was raised above the surface on a support of some kind (for example a polymer brush). It would be important that the catalyst is held to the surface in some fashion for ease of use, raw materials could be pumped into the fluid and the finished product removed leaving the catalyst in place for further use.

If only the ribosome catalyst is required it might be enough to simply allow it to diffuse randomly upon the surface. In a system with multiple different catalytic machines that transfer the reacting product between them it would be important to keep the component in close proximity. In another system it may be of use to keep the catalysts reasonably separate to make it easier to know when to replace them. In both cases a partitioned surface such as those in chapter 3 would be of great use.

The ribosome-like catalyst could produce macromolecules through condensation polymerisation reactions like actual ribosomes do. These reactions often produce byproducts that would be of use when considering the work involving responsive gels, in the case of biological systems with amino acids, water is produced (hence condensation reaction). However in the case of a product such as Kevlar it is hydrochloric acid that is produced. In the case of Kevlar, if produced in this system the introduction of the acid would lead to an increase in local concentration of protons which might allow for faster diffusion in the local environment facilitating an increase of raw material to the catalyst. The response would not need to be as strong as that observed in the worm gel case, as this would make it difficult to undergo continuous production. Nevertheless, it might be considered helpful in at a batch production level to have a strong response to give an indication that the maximum amount of reaction possible has been achieved, so that new raw materials could be provided.

There are a variety of ways these processes could be used, to allow for a degree of

control over diffusion, with these two cases just being simple and novel examples. It is clear that this form of 'Brownian engineering' offers a possible way of designing biomimetic systems that will have a major impact on the technologies of the future.

6.5 Future Work

The work presented in this thesis is valuable starting point for a number of other studies that would build upon and extend understanding of the motion of polymers in biologically important systems. There are also a number of questions raised in this thesis, for the wider scope of polymer physics and biological physics, that should examined. This section collects together the suggested work from across the body of this thesis and presents some additional questions and research topics that are of importance to extend and develop this research area.

For the work concerning diffusion in the bulk, future studies should examine:

- The work of Blanazs *et al* (2012) and Lovett *et al* (2015) used DLS to observe diffusion and infer particle size, in addition to TEM. DLS requires a dilute system to be effective, while FCS only requires the portion of fluorophore-tagged molecules to be dilute. FCS could therefore be used to examine the system across a much wider range of diblock copolymer concentrations. Although beyond the scope of a biological analogue it is conceivable that the concentration could be increased above 30% w/w diblock copolymer, and the FCS data could be compared with TEM. This would allow better understanding of the transition across a wider range of conditions.

- The addition of a second species to observe diffusion of this diffusant as the PGMA-PHPMA gel transitions to a solution. The identity of the new species should be varied to observe the impact of size and how the species interacts with the diblock

copolymer. A suggestion would be to start with free tracers like RhB and move up to macromolecules such as various molar masses of PEG.

- The introduction of small molecules (molar mass below 300 Da) to examine an analogue of the crowding in the cytosol.

- The inclusion of mM concentrations of ions would be appropriate in a comparison with the cytosol. This is partly examined through the experiments on pH dependence but it would be required when extended beyond the PGMA-PHPMA system to investigate the impact of ions on the system.

Future work to extend the studies of diffusion upon a surface should include:

- A change in brush layer thickness or barrier width. These parameters were kept as consistent as possible throughout the studies presented (10-15 nm brush thickness and a 1:1 ratio of well to barrier width) yet these are possible sources of confinement. Thicker brushes might lead to more confinement as might smaller wells in relation to the barrier width.

- An extension of the methods used to pattern the surfaces. A Lloyd's mirror interferometer was used to undertake twin beam IL, yet there are many other way IL could be used. There is no reason why many more beams could not be used, a simple example would be the use of a Fabry-Pérot interferometer to produce a more complex pattern. The observation of confinement in patterns of different geometries would be useful in suggesting there was a physical effect behind the behaviour and not some peculiarity of the specific pattern produced for this work.

- A direct extension to the methods used in this work through the use of FCS in a more dimensionally confined manner. The system examined could be described as low dimensional as there is a form of confinement. It follows that the method of examining the diffusion should also include such low dimensionality. The use of total internal reflection FCS (TIRF-FCS) or stimulate emission depletion FCS

(STED-FCS) are examples of this. TIRF-FCS has an axial resolution of 100 nm which would allow the diffusion very close to the surface to be examined without measuring diffusion in the bulk. This method could also probe the brush layer to investigate whether any PEG was diffusing within the brush. Traditional FCS does not have the resolution to do this. STED-FCS allows the resolution of the confocal volume to shrink to a spot size of 60 nm, which is on the order of the diamter of the chromatophore vesicle in *R. Sphaeroides*. Smaller volumes being examined could make the behaviour of single molecules clearer allowing better descriptions to be produced. Unfortunately, both of these techniques required either a new microscope or a highly specialised arrangement of equipment that it is not possible to do with the confocal microscope available in this work so must wait until these techniques are available.

- The use of different brushes and diffusing polymer species. It was recognised that this system minimised the impact of interactions between the diffusing polymer and the brush. If the constituent polymers were selected so that there would be interactions between them a more confining system could be produced.

- The use of lipids in the place of PEG. These lipids can be used as a bilayer in the current surface designs where a bilayer could form at the base of the well (if the well were very large) or across the top of the brush layer (lipid bilayers are quite rigid and can span the wells if it is narrow enough). It is known that POEGMA brushes will allow the formation of a lipid bilayer yet that it will not be particularly mobile (mobile fraction of lipids $\ll 5\%$, A. Blakeston, unpublished 2012) but regions where there is no brush could potentially be much more mobile. This means that the brush will act in a similar way to a series of pickets in the transmembrane protein picket model. By varying the brush thickness and barrier width of the POEGMA, various scenarios could be examined that would be close to the biological membrane.

- An extension of the previous future work would involve different brushes, or even

systems with multiple brushes located in spatially distinct regions. There is much work going into the formation of mobile lipid bilayers supported upon polymer brushes and as such there are many possible ways to design a surface to produce certain local behaviours. This could be used to simulate specific types of membranes, for different processes as well as across different types of cell.

- A further extension of the two previous future studies. The membrane does not just include lipids but also proteins and other complex species. The complexity of the supported membrane could be increased incrementaly until a cell membrane analogue was for all purposes a cell membrane upon a surface. If it were an accurate representation in terms of the diffusion behaviour as well as the composition of the membrane then there are a number of important points. Firstly, a major step forward in understanding the diffusion on a membrane could occur. Furthermore, medical research could be affected very strongly. With ethical considerations being a major part of any biologically relevant research, having a model system that is virtually a membrane to examine as a first step would be critical. In the context of drug development, possible drugs could be tested on a totally artifical, but still accurate, representation of a cell membrane before being administered to anything that was alive. Ethically this would be a great stride forward but it would also be a helpful first step showing whether a certain drug or process will work before undergoing the expense and effort of testing on organisms.

- An integration of biological features with the previous work involving responsive gels. If the polymer brush system were again similar in structure to that presented in this work, the well region could be filled with a gel. A membrane with bacteriorhodopsin included could then pump protons into the gel and the diffusion of the gel could then be observed. If the gel is selected to be a good analogue of the cytosol and it responds to this pumping by causing a change in diffusive behaviour then a further step in understanding biological systems can be made, with particular emphasis of

the interplay between the membrane and the cytosol.

A future study not focussed upon diffusion should examine vesicle formation, and in particular the nature of the architecture of the cell membrane and MSK before and after a vesicle forms. There is a wealth of literature discussing the way that certain receptors are used to form vesicles for transporting material but there is nothing on the structure of the membrane in these cases. The nature of the MSK around the chromatophore vesicle is also not described. These appear to be important gaps in knowledge that should be addressed so that understanding of the cell membrane and its processes can develop.

Future work in the realm of polymer diffusion, that would aid in the understanding of this thesis, should involve the examination of macromolecules within a brush structure. There are many publications detailing diffusion of polymers on brushes. There are some works claiming diffusion of tracers within a brush layer and while this is the most likely explanation of the results they obtain there is not sufficient axial resolution in these cases to say definitively where the tracer is diffusing. A system involving a polymer brush between two surfaces would be the perfect solution to this gap in research. If a system could be designed so that a diffusing polymer could be trapped within this region, a diffusion coefficient for a polymer within a dense brush could be obtained. This would be incredibly high impact work, as there is no current literature that can claim to have examined such a system.

Attempts to produce a system such as this have been attempted but there are major obstacles to the development of such a design and the introduction of the polymer that will diffuse. Poly(2-dimethylamino)ethyl methacrylate) (PDMA) brushes have been grown by ATRP with PEG chains in the polymerisation solution (Z. Zhang, unpublished 2012). This system was then chemically cross-linked at the top of the brush to form a psuedo-surface at the top of the brush. Ultimately this approach proved unsucessful as the PEG chain either did not grow into the brush or could not produce a fluorescent signal

strong enough to be detected. As a consequence it is known that this methodology does not work. A motivation to attempt to produce this system, despite its inherent difficulties, is that the publication based upon the study would most certainly be a guarenteed *Science* article!

6.6 Closing Remarks

Biological systems are often very efficient and part of the reason for this appears to be the level of control that can be exerted on the diffusion of important biological molecules. This has been shown to be the case in the cell membrane and it can be argued that the control must also occur in the cytosol. The photosynthetic pathway of *R. Sphaeroides* is an example of a highly efficient process and occurs across both of these locations, both in the membrane on the chromatophore vesicle and in the cytosol surrounding the vesicle.

The overarching aim of this thesis was to produce polymeric systems that were analogous to parts of the photosynthetic pathway of *R. Sphaeroides*, and then use FCS to observe diffusion within these systems. This has been an unqualified success, with two suitable systems being fabricated and examined, one to investigate diffusion in the cell membrane and another to look at diffusion in the cytosol.

Diffusion of PEG upon a patterned surface was used to simulate the confinement that is apparent in the cell membrane. The square grid structure mimicked the underlying architecture of the cell membrane, and although the proportions were not an ideal match for a general eukaryotic cell, the design was similar to many specialised cells such as neurons. The introduction of surface structure, in the form of topography, introduced a slow mode of surface diffusion that corresponded to PEG molecules trapped within the grid. Analysis through the use of the FCS diffusion laws showed that the wells in the square grid could be treated as isolated microdomains, implying that the distance

between the wells was greater than the length scale the barriers affected. Although the level of confinement was not comparable to the level observed in cell membranes ((45.6±2.6)% rather than almost 100% in the cell membrane) the difference can be put down to the nature of the structures. While the proteins and the lipids are confined to a two-dimensional fluid of the cell membrane, and are much more interactive, the PEG chains interact very weakly with the structure. This suggests that while the identity of the chemistry of a system is important, merely having a structure has a profound impact upon the diffusion of a species regardless of the materials used.

The use of a PGMA-PHPMA diblock copolymer gel simulated the potential responsive nature of the cytosol with respect to the diffusion of molecules within it. The PGMA-PHPMA gel undergoes a reversible transition, with a change in temperature (lower than 14 °C) or pH (above pH 4), between a cylindrical vesicle and a spherical vesicle which in turn leads to a change in the nature of the gel to an aqueous solution. This transition is accompanied by a change in diffusion coefficient of a factor of between 4 (temperature dependence) and 8 (pH dependence). The change in diffusion coefficient can be put down to a change in the size of the diffusing species with the cylindrical vesicle having a sphere equivalent radius of (58±18) nm and the radius of the spherical vesicles reduced from (16.3±0.3) nm to (6±4) nm as the temperature was lowered. This change in radius can be attributed to the breakup of the spheres. Although the transitions are larger than would be applicable in a biological system the nature of the transition is important and demonstrates that this is a possible method for the control of diffusion.

In the context of the photosynthetic pathway, the mechanisms observed in the polymeric system do seem applicable to the biological process. This suggests that the control of diffusion is a crucial part of the way biological systems deal with processes. The mechanisms can also be used in artificial devices to produce biologically inspired designs that can lead to more efficient processes than are currently available. It is clear that future

technologies will move to using some of the methodologies that are used in biological systems to deal with specific processes. In doing so, these technologies will need an understanding of the diffusion of the constituent parts of the devices produced, as these will be the centres where the vital work is done. Brownian engineering will become a buzzword in this state of technology, and it will be work such as that presented in this thesis that makes the basis of the designs in a toolbox used to control the diffusion of these important components.

Bibliography

[1] T Geyer and V Helms. Reconstruction of a Kinetic Model of the Chromatophore Vesicles from *Rhodobacter sphaeroides*. *Biophysical Journal*, 91(3):927–937, 2006.

[2] T Geyer and V Helms. A Spatial Model of the Chromatophore Vesicles of *Rhodobacter sphaeroides* and the Position of the Cytochrome bc_1 Complex. *Biophysical Journal*, 91(3):921–926, 2006.

[3] M Sener, J Strumpfer, JA Timney, A Freiberg, CN Hunter, and K Schulten. Photosynthetic Vesicle Architecture and Constraints on Efficient Energy Harvesting. *Biophysical Journal*, 99(1):67–75, 2010.

[4] MK Sener, JD Olsen, CN Hunter, and K Schulten. Atomic-level structural and functional model of a bacterial photosynthetic membrane vesicle. *PNAS*, 104(40):15723–15728, 2007.

[5] CA Smith and EJ Wood. *Cell Biology*. Chapman & Hall, 2nd edition, 1997.

[6] T Fujiwara, K Ritchie, H Murakoshi, K Jacobson, and A Kusumi. Phospholipids undergo hop diffusion in compartmentalized cell membrane. *Journal of Cell Biology*, 157(6):1071–1081, 2002.

[7] R Lino, I Koyama, and A Kusumi. Single molecule imaging of green fluorescent protein in living cells: E-cadherin forms oligomers on the free cell surface. *Biophysical Journal*, 80(6):2667–2677, 2001.

[8] K Murase, T Fujiwara, Y Umemura, K Suzuki, R Lino, H Yamashita, M Saito, H Murakoshi, K Ritchie, and A Kusumi. Ultrafine membrane compartments for molecular diffusion as revealed by single molecule techniques. *Biophysical Journal*, 86(6):4075–4093, 2004.

[9] KG Suzuki, TK Fujiwara, F Sanematsu, R Lino, M Eddin, and A Kusumi. Gpi-anchored receptor clusters transiently recruit lyn and g alpha for temporary cluster immobilization and lyn activation: single-molecule tracking study 1. *Journal of Cell Biology*, 177(4):717–730, 2007.

[10] H Noji, R Yasuda, M Yoshida, and K Kinosita Jr. Direct observation of the rotation of F1-ATPase. *Nature*, 386:299–302, 1997.

[11] A Blair, L Ngo, J Park, IT Paulsen, and MH Saier Jr. Phylogenetic analyses of the homologous transmembrane channel-forming proteins of the F_0F_1-ATPases of bacteria, chloroplasts and mitochondria. *Microbiology*, 142:17–32, 1996.

[12] K Luby-Phelps. Cytoarchitecture and physical properties of cytoplasm: Volume, viscosity, diffusion, intracellular surface area. *International Review of Cytology - A survey of Cell Biology*, 192:189–221, 2000.

[13] MK Chaudhury and GM Whitesides. How to make water run uphill. *Nature*, 256:1539–1541, 1992.

[14] M Suzuki. A new concept of a hydrophobicity transition of functional polymer substrate for micro/nano machines. *Polymer gels and Networks*, 2:279–287, 1994.

[15] P Burgos, ZY Zhang, R Golestanian, GJ Leggett, and M Geoghegan. Directed single molecule diffusion triggered by surface energy gradients. *ACS Nano*, 3(10):3235–3243, 2009.

[16] W Shockley and HJ Queisser. Detailed Balance Limit of Efficiency of *p-n* Junction Solar Cells. *Journal of Applied Physics*, 32:510–519, 1961.

[17] A De Vos. Detailed balance limit of the efficiency of tandem solar cell. *Journal of Physics D*, 13(5):839, 1980.

[18] R Kebede. Australia develops world's most efficient solar panels. http://rt.com/business/212383-australia-record-solar-energy/, December 2014. Valid URL as of March 2015.

[19] D Kearns and M Calvin. Photovoltaic Effect and Photoconductivity in Laminated Organic Systems. *Journal of Chemical Physics*, 29(4):950–951, 1958.

[20] AK Ghosh, DL Morel, T Feng, RF Shaw, and CA Rowe Jr. Photovoltaic and rectification properties of Al/Mg phthalocyanine/Ag Schottky-barrier cells. *Journal of Applied Physics*, 45:230, 1974.

[21] G Yu, J Gao, JC Hummelen, F Wudl, and AJ Heeger. Polymer Photovoltaic Cells: Enhanced Efficiencies via a Network of Internal Donor-Acceptor Heterojunctions. *Science*, 270(5243):1789–1791, 1995.

[22] E Gorter and F Grendel. On Bimolecular Layers of Lipids on the Chromocytes of the Blood. *Journal of Experimental Medicine*, 41(4):439–443, 1925.

[23] JF Danielli and H Davson. A Contribution to the Theory of Permeability of Thin Films. *Journal of Cellular and Comparative Physiology*, 5(4):495–508, 1935.

[24] SJ Singer and GL Nicholson. The fluid mosaic model of the structure of cell membranes. *Science*, 175(4023):720–731, 1972.

[25] PG Saffman and M Delbrück. Brownian Motion in Biological Membranes. *PNAS*, 72(8):3111–3113, 1975.

[26] BD Hughes, A Pailthorpe, and LR White. The Translational and Rotational Drag on a Cylinder moving in a Membrane. *Journal of Fluid Mechanics*, 110:349–372, 1981.

[27] O Hegener, L Prenner, F Runkel, SL Baader, J Kappler, and H Häberlein. Dyanmics of β2-adrenergic receptor-ligand complexes on living cells. *Biochemistry*, 43:6190–6199, 2004.

[28] S Nelson, RD Horvat, J Malvey, DA Roess, BG Barisas, and CM Clay. Characterization of an intrinsically fluorescent gonadotropin-releasing hormone receptor and effects of ligand binding on receptor lateral diffusion. *Endocrinology*, 140(2):950–957, 1999.

[29] DA Roess, RD Horvat, H Munnelly, and BG Barisas. Luteinizing hormone receptors are self-associated in the plasma membrane. *Endocrinology*, 141(12):4518–4523, 2000.

[30] EM Erb, K Tangemann, B Bohrmann, B Müller, and J Engel. Integrin αiibβ3 reconstituted into lipid bilayers is nonclustered in its activated state but clusters after fibrinogen binding. *Biochemistry*, 36(23):7395–7402, 1997.

[31] K Ahlén, P Ring, B Tomasini-Johansson, K Holmqvist, KE Magnusson, and K Rubin. Platelet-derived growth factor-BB modulates membrane mobility of β1 integrins. *Biochemical and Biophysical Research Communications*, 314(1):89–96, 2004.

[32] C Dietrich, ZN Volovyk, M Levi, NL Thompson, and K Jacobson. Partitioning of Thy-1, GM1, and cross-linked phospholipid analogs into lipid rafts reconstituted in supported model membrane monolayers. *PNAS*, 98(19):10642–10647, 2001.

[33] ED Sheets, GM Lee, R Simson, and K Jacobson. Transient Confinement of a Glycosylphosphatidylinositol-Anchored Protein in the Plasma Membrane. *Biochemistry*, 36(41):12449–12458, 1997.

[34] WLC Vaz, M Criado, VMC Madeira, G Schoellmann, and TM Jovin. Size dependence of the translational diffusion of large integral membrane proteins in liquid-crystalline phase lipid bilayers. a study using fluorescence recovery after photobleaching. *Biochemistry*, 21(22):5608–5612, 1982.

[35] D Axelrod, P Ravdin, DE Koppel, J Schlessinger, WW Webb, EL Elson, and TR Podleski. Lateral motion of fluorescently labeled acetylcholine receptors in membranes of developing muscle fibres. *PNAS*, 73(12):4594–4598, 1976.

[36] WL Vaz, HG Kapitza, J Stumpel, E Sackmann, and TM Jovin. Translational mobility of glycophorin in bilayer membranes of dimyristoylphosphatidylcholine. *Biochemistry*, 20(5):1392–1396, 1981.

[37] HG Kapitza, DA Ruppel, HJ Galla, and E Sackmann. Lateral diffusion of lipids and glycophorin in solid phosphatidylcholine bilayers. the role of structural defects. *Biophysical Journal*, 45(3):577–587, 1984.

[38] DE Golan, CS Brown, CML Cianci, ST Furlong, and JP Caulfield. Schistosomula of schistosoma mansoni use lysophosphatidylcholine to lyse adherent human red blood cells and immobilize red cell membrane components. *Journal of Cell Biology*, 103:819–828, 1986.

[39] A Kusumi, C Nakada, K Ritchie, K Murase, K Suzuki, H Murakoshi, RS Kasai, J Kondo, and T Fujiwara. Paradigm shift of the plasma membrane concept from the two-dimensional continuum fluid to the partitioned fluid: High-speed single-molecule tracking of membrane molecules. *Annual Review of Biophysics and Biomolecular Structure*, 34:351–378, 2005.

[40] Y Sako, A Nagafuchi, S Tsukita, M Takeichi, and A Kusumi. Cytoplasmic regulation of the movement of E-cadherin on the free cell surface as studied by optical tweezers and single particle tracking: Corralling and tethering by the membrane skeleton. *Journal of Cell Biology*, 140(5):1227–1240, 1998.

[41] Y Sako and A Kusumi. Compartmentalised structure of the plasma membrane for receptor movements as revealed by a nanometer-level motion analysis. *Journal of Cell Biology*, 125(6):1251–1264, 1994.

[42] M Tomishige, Y Sako, and A Kusumi. Regulation mechanism of the lateral diffusion of the band 3 in erythrocyte membranes by the membrane skeleton. *Journal of Cell Biology*, 142(4):989–1000, 1998.

[43] C Nakada, K Ritchie, Y Oba, M Nakamura, Y Hotta, R Lino, RS Kasai, K Yamaguchi, T Fujiwara, and A Kusumi. Accumulation of anchored proteins forms membrane diffusion barriers during neuronal polarization. *Nature Cell Biology*, 5(7):626–632, 2003.

[44] D Pavithra and M Doble. Biofilm formation, bacterial adhesion and host response on polymeric implants - issues and prevention. *Biomedical Materials*, 3(3), 2008.

[45] N Wisniewski and M Reichert. Methods for reducing biosensor membrane biofouling. *Colloids and Surfaces B - Biointerfaces*, 18(3-4):197–219, 2000.

[46] P Asuri, SS Karajanagi, RS Kane, and JS Dordick. Polymer-nanotube-enzyme composites as active antifouling films. *Small*, 3(1):50–53, 2007.

[47] RS Kane, P Deschatelets, and GM Whitesides. Kosmotropes form the basis of protein-resistant surfaces. *Langmuir*, 19(6):2388–2391, 2003.

[48] A Roosjen, HC van der Mei, HJ Busscher, and W Norde. Microbial adhesion to poly(ethylene oxide) brushes: Influence of polymer chain length and temperature. *Langmuir*, 20(25):10949–10955, 2004.

[49] D Cunliffe, CA Smart, C Alexander, and EN Vulfson. Bacterial adhesion at synthetic surfaces. *Applied and Environmental Microbiology*, 65(11):4995–5002, 1999.

[50] SA Sukhisvili, Y Chen, JD Muller, E Gratton, KS Schweizer, and S Granick. Diffusion of a polymer 'pancake'. *nature*, 406:146, 2000.

[51] SA Sukhishvili, Y Chen, JD Müeller, E Gratton, KS Schweizer, and S Granick. Surface diffusion of poly(ethylene glycol). *Macromolecules*, 35(5):1776–1784, 2002.

[52] L Wawrezinieck, H Rigneault, D Marguet, and PF Lenne. Fluorescence correlation spectroscopy diffusion laws to probe the submicron cell membrane organization. *Biophysical Journal*, 89(6):4029–4042, 2005.

[53] GH Pollack. *Cells, Gels and the Engines of Life*. Ebner & Sons Publishers, 2001.

[54] EA Vogler. Structure and reactivity of water at biomaterial surfaces. *Advances in colloid and interface science*, 74:69–117, 1998.

[55] Y Osada and J Gong. Stimuli-responsive polymer gels and their application to chemomechanical systems. *Progress in Polymer Science*, 18:187–226, 1993.

[56] K Dusek and D Patterson. Transition in swollen polymer networks induced by intramolecular condensation. *Journal of Polymer Science B*, 6(7):1209–1216, 1968.

[57] T Tanaka. Collapse of gels and the critical endpoint. *Physical Review Letters*, 40:820, 1978.

[58] AS Hoffman. Conventional and environmentally-sensitive hydrogels for medical and industrial uses: a review paper. *Polymer Gels*, 268(5):82–87, 1991.

[59] A Blanazs, R Verber, OM Oleksandr, AJ Ryan, Heathm JZ, CWI Douglas, and SP Armes. Sterilizable gels from thermoresponsive block copolymer worms. *Journal of the American Chemical Soceity*, 134:9741–9748, 2012.

[60] JR Lovett, NJ Warren, LPD Ratcliffe, MK Kocik, and SP Armes. ph-responsive non-ionic diblock copolymers: Ionization of carboxylic acid end-groups induces an order-order morphological transition. *Angewandte Chemie*, 54(4):1279–1283, 2015.

[61] *A Dictionary of Physics*. Oxford University Press, 2005. Diffusion.

[62] HS Van Klooster. Jan Ingenhousz. *Journal of Chemical Education*, 29(7):353–355, 1952.

[63] R Brown. A brief account of microscopical observation made on the particles contained in the pollen of plants. *Philosophical Magazine*, 4:161–173, 1828.

[64] SL Lauritzen. *Thiele: Pioneer in Statistics*. Oxford, 2002.

[65] L Bachelier. Théorie de la spéculation. *Annales Scientifiques de l'École Normale Supérieure*, 3(17):21–86, 1900.

[66] A Einstein. Über die von der molekularkinetishen Theorie der Wärme geforderte Bewegung von in ruhenden Fl ussigkeiten suspendierten Teilchen. *Annalen der Physik*, 322(8):549–560, 1905.

[67] M Smoluchowski. Zur kinetischen Theorie der Brownschen Molekularbewegug und der Suspensionen. *Annalen der Physik*, 326(14):756–780, 1906.

[68] J Perrin. Brownian Motion and Molecular Reality. *Annales de Chimie et de Physique*, 18:1–114, 1909.

[69] P Debye and AM Bueche. Intrinsic Viscosity, Diffusion and Sedimentation Rate of Polymers in solution. *Journal of Chemical Physics*, 16(6):573–579, 1948.

[70] K Oura, VG Lifshits, AA Saranin, AV Zotov, and M Katayama. *Surface Science: An Introduction*. Springer-Verlag Berlin Heidelberg, 2003.

[71] I Carmesin and K Kremer. Static and dynamic properties of two-dimensional polymer melts. *Journal de Physique*, 51(10):915–932, 1990.

[72] A Milchev and K Binder. Static and Dynamic Properties of Adsorbed Chains at Surfaces: Monte Carlo Simulation of a Bead-Spring Model. *Macromolecules*, 29(1):343–354, 1996.

[73] D Mukherji, G Bartels, and MH Müser. Scaling laws of single polymer dynamics near attractive surfaces. *Physical Review Letters*, 100(6), 2008.

[74] TG Desai, P Keblinski, and SK Kumar. Polymer chain dynamics at interfaces: Role of boundary conditions at solid interface. *Journal of Chemical Physics*, 128(4), 2008.

[75] N Hoda and S Kumar. Parameters influencing diffusion dynamics of an adsorbed polymer chain. *Physical Review E*, 79(2-1), 2009.

[76] GW Slater and SY Wu. Reptation, Entropic Trapping, Percolation, and Rouse Dynamics of Polymers in Random Environments. *Physical Review Letters*, 75(1):164–167, 1999.

[77] R Azuma and T Hajime. Diffusion of single long polymers in fixed and low density matrix of obstacles confined to two dimensions. *Journal of Chemical Physics*, 11(18):8666–8671, 1999.

[78] TG Desai, P Keblinski, SK Kumar, and S Granick. Molecular-dynamics simulations of the transport properties of a single polymer chain in two dimensions. *Journal of Chemical Physics*, 124(8), 2006.

[79] TG Desai, P Keblinski, SK Kumar, and S Granick. Modeling diffusion of adsorbed polymer with explicit solvent. *Physical Review Letters*, 98(21), 2007.

[80] HJ Qian, LJ Chen, ZY Lu, and ZS Li. Surface diffusion dynamics of a single polymer chain in dilute solution. *Physical Review Letters*, 99(6), 2007.

[81] Z Zhang, MR Tomlinson, R Golestanian, and M Geoghegan. The interfacial behaviour of single poly(N,N-dimethylacrylamide) chains as a function of pH. *Nanotechnology*, 19(3), 2008.

[82] AL Ponomarev, TD Sewell, and CJ Durning. Surface diffusion and relaxation of partially adsorbed polymers. *Journal of Polymer Science*, 38(9):1146–1154, 2000.

[83] Kac M. Can one hear the shape of a drum? *The American Mathematical Monthly*, 73(4):1–23, 1966.

[84] DS Novikov, E Firemans, JH Jensen, and JA Helpern. Random walks with barriers. *Nature Physics*, 7(6):508–514, 2011.

[85] PF Lenne, L Wawrezinieck, F Conchonaud, O Wurtz, A Boned, X-J Guo, H Rigneault, H-T He, and D Marguet. Dynamic molecular confinement in the plasma membrane by microdomains and the cytoskeleton meshwork. *Embo Journal*, 25(14):3245–3256, 2006.

[86] ST Milner. Polymer brushes. *Science*, 22:905–914, 1991.

[87] B Zhao and WJ Brittain. Polymer brushes: surface-immobilized macromolecules. *Progress in polymer science*, 25(5):677–710, 2000.

[88] K Matyjaszewski and JH Xia. Atom transfer radical polymerisation. *Chemical reviews*, 101(9):2921–2990, 2001.

[89] DP Curran. The design and application of free radical chain reactions in organic synthesis. part 2. *Synthesis*, 7:489–513, 1988.

[90] J Queffelec, SG Gaynor, and K Matyjaszewski. Optimization of atom transfer radical polymerization using Cu(i)/tris(2-(dimethylamino)ethyl)amine as a catalyst. *Macromolecules*, 33(23):8629–8639, 2000.

[91] K Matyjaszewski and T Nicolay. Nanostructured functional materials prepared by atom transfer radical polymerisation. *Nature Chemistry*, 1(4):276–288, 2009.

[92] JC Love, LA Estroff, JK Kriebel, RG Nuzzo, and GM Whitesides. Self-assembled monolayers of thiolates on metals as a form of nanotechnology. *Chemical reviews*, 105(4):1103–1170, 2005.

[93] SM Barlow and R Raval. Complex organic molecules at metal surfaces: bonding organisation and chirality. *Surface Science Report*, 50(6-8):201–341, 2003.

[94] P Silberzan, L Leger, D Ausserre, and J Benattar. Silanation of silica surfaces. a new method of constructing pure or mixed monolayers. *Langmuir*, 7:1647–1651, 1991.

[95] J LeGrange, J Markham, and C Kurkjian. Effects of surface hydration on the deposition of silane monolayers on silica. *Langmuir*, 9:1749–1753, 1993.

[96] P Harder, M Grunze, R Dahint, GM Whitesides, and PE Laibinis. Molecular conformation in oligo(ethylene glycol)-terminated self-assembled monolayers on gold and silver surfaces determines their ability to resist protein adsorption. *Journal of Physical Chemistry B*, 102(2):426–436, 1998.

[97] N Rozloznik, MC Gerstenberg, and NB Larsen. Effect of solvents and concentration on the formation of a self-assembled monolayer of octadecylsiloxane on silicon. *Langmuir*, 19(4):1182–1188, 2003.

[98] DK Schwartz. Mechanisims and kinetics of self-assembled monolayer formation. *Annual Review of Physical Chemistry*, 52(1):107–137, 2001.

[99] RAL Jones. *Soft Condensed Matter*. Oxford University Press, 2013.

[100] G Strobl. *The Physics of Polymers*. Springer, 3rd edition, 2006.

[101] DE Discher and A Eisenberg. Polymer vesicles. *Science*, 297:967–973, 2002.

[102] L Zhang and A Eisenberg. Multiple morphologies of "crew-cut" aggregates of polystyrene-b-poly(acrylic acid) block copolymers. *Science*, 268:727, 1995.

[103] S Förster, B Berton, HP Hentze, E Krämer, M Antonietti, and P Linder. Lyotropic phase morphologies of amphiphilic black copolymers. *Macromolecules*, 34(13):4610–4623, 2001.

[104] DA Hajduk, MB Kossuth, MA Hillmyer, and FS Bates. Complex phase behaviour in aqueous solutions of poly(ethylene oxide)-poly(ethylethylene) block copolymers. *Journal of Physical Chemistry B*, 102(22):4269–4276, 1998.

[105] B Jeong, YH Bae, DS Lee, and SW Kim. Biodegradeable block copolymers as injectable drug-delivery systems. *Nature*, 388:860–862, 1997.

[106] C Tsitsilianis. Responsive reversible hydrogels from associative smart macromolecules. *Soft Matter*, 6:2372–2388, 2010.

[107] C Li, Y Tang, SP Armes, CJ Morris, SF Rose, AW Lloyd, and AL Lewis. Synthesis and characterisation of biocompatible thermo-responsive biocompatible ABA triblock copolymers. *Biomacromolecules*, 6:994–999, 2005.

[108] J Madsen, SP Armes, and AL Lewis. Preparation and aqueous solution properties of new thermoresponsive biocompatible ABA triblock copolymer. *Macromolecules*, 39:7455–7457, 2006.

[109] YH Ma, YQ Tang, NC Billingham, SP Armes, and AL Lewis. Synthesis of biocompatible stimuli-responsive, physical gels based on ABA triblock copolymers. *Biomacromolecules*, 4:864–868, 2003.

[110] CA Dreiss. Wormlike micelles: Where do we stand? Recent developments, linear rheology and scattering techniques. *Soft Matter*, 3:956–970, 2007.

[111] E Hecht. Fresnel diffraction. In *Optics*, chapter 10, pages 485–509. Addison Wesley, 4th edition, 2002. Specifically section concerning planar waves through a circular aperture.

[112] S Sun and GJ Leggett. Matching the resolution of electron beam lithography by scanning near-field photolithography. *Nano Letters*, 4(8):1381–1384, 2004.

[113] EU Haq, Z Liu, Y Zhang, SAA Ahmad, Wong LS, Armes SP, JK Hobbs, GJ Leggett, J Micklefield, CJ Roberts, and JMR Weaver. Parallel scanning near-field photolithography: The snomipede. *Nano Letters*, 10(11):4375–4380, 2010.

[114] SRJ Brueck. Optical and interferometric lithography - nanotechnology enablers. *Proceedings of the IEEE*, 93:1704–1721, 2005.

[115] HH Solak, D He, W Li, and F Cerrina. Nanolithography using extreme ultraviolet lithography interferometry: 19 nm lines and spaces. *Journal of Vacuum Science & Technology B: Microelectronics and Nanometer Structures*, 17:3052–3057, 1999.

[116] DM Jones, AA Brown, and WTS Huck. Surface-initiated polymerizations in aqueous media: effect of initiator density. *Langmuir*, 18(4):1265–1269, 2002.

[117] ER Jones, M Semsarilar, A Blanazs, and SP Armes. Efficient synthesis of amine-functional diblock copolymer nanoparticles via RAFT dispersion polymerization of benzyl methacrylate in alcoholic media. *Macromolecules*, 45(12):5091–5098, 2012.

[118] CG Clarkson, JR Lovett, J Madsen, SP Armes, and M Geoghegan. Characterization of diblock copolymer order-order transitions in semidilute aqueous solution using flourescence correlation spectroscopy. *Macromolecular Rapid Communications*, 36(17):1572–1577, 2015. doi: 10.1002/marc.201500208.

[119] PO Gendron, F Avaltroni, and KJ Wilkinson. Diffusion coefficients of several rhodamine derivatives as determened by pulsed field gradient - nuclear magnetic resonance and fluorescent correlation spectroscopy. *Journal of Fluorescence*, 18:1093, 2008.

[120] CT Culbertson, SC Jacobson, and JM Ramsey. Diffusion coefficient measurements in microfluidic devices. *Talanta*, 56:365, 2002.

[121] MC Pirrung, L Wang, and MP Montague-Smith. 3-‘nitrophenylpropyloxycarbonyl (NPPOC) Protecting Groups for High Fidelity Automated 5‘→ 3‘ Photochemical DNA Synthesis. *Organic Letters*, 3(8):1105–1108, 2001.

[122] SAA Ahmad, LS Wong, EU Haq, JK Hobbs, GJ Leggett, and J Micklefield. Micrometer- and nanometer-scale photopatterning using 2-nitrophenylpropyloxycarbonyl-protected aminosiloxane monolayers. *Journal of the American Chemical Society*, 131(4):1513–1522, 2009.

[123] C Reznik and CF Landes. Transport in supported polyelectrolyte brushes. *Accounts of Chemical Research*, 45(11):1927–1935, 2012.

[124] C Branden and J Tooze. *Introduction to protein structures*. Taylor and Francis, 2nd edition, 1998.

[125] TE Creighton. *Proteins*. Freeman, 1993.

[126] CO Faggain. *Protein Stability and Stabilization of Protein Function*. Landes Bioscience, 1997.

[127] AJ Morse, SP Armes, KL Thompson, D Dupin, LA Fielding, P Mills, and R Swart. Novel pickering emulsifiers based on pH-responsive poly (2-(diethylamino)ethyl methacrylate) latexes. *Langmuir*, 29(18):5466–5475, 2013.

[128] AL Serrano, MM Waegle, and F Gai. Spectroscopic studies of protein folding: Linear and nonlinear methods. *Protein Science*, 21(2):157–170, 2012.

[129] K Chattopadhyay, S Saffarian, EL Elson, and C Frieden. Measuring unfolding of proteins in the presence of denaturant using fluorescence correlation spectroscopy. *Biophysical journal*, 88(2):1413–1422, 2005.

[130] E Sherman, A Itkin, YY Kuttner, E Rhoades, D Amir, E Haas, and G Haran. Using fluorescence correlation spectroscopy to study conformational changes in denatured proteins. *Biophysical Journal*, 94(12):4819–4827, 2008.

[131] J Adelsberger, A Kulkarni, A Jain, WN Wang, AM Bivigou-Koumba, P Busch, V Pipich, O Holderer, T Hellweg, A Laschewsky, P Muller-Buschbaum, and CM Papadakis. Thermoresponsive PS-b-PNIPAM-b-PS micelles: Aggregation behaviour, segmental dynamics and thermal response. *Macromolecules*, 43(5):2490–2501, 2010.

[132] A Laschewsky, P Muller-Buschbaum, and CM Papadakis. Thermo-responsive amphiphilic di- and triblock copolymers based on poly(n-isopropylacrylamide) and

poly(methoxy diethylene glycol acrylate): Aggregation and hydrogel formation in bulk solution and in thin films. In G Sadowski and W Richtering, editors, *Intelligent Hydrogels*, volume 140 of *Progress in Colloid and Polymer Science*, pages 15–34. Springer International Publishing, 2013.

[133] D Ehlich and H Sillescu. Tracer diffusion at the glass transition. *Macromolecules*, 23(6):1600–1610, 1990.

[134] DD Deppe, RD Miller, and JM Torkelson. Small molecule diffusion in a rubbery near Tg: effects of probe size, shape and flexibility. *Journal of polymer science, Part B: Polymer Physics*, 34(17):2987–2997, 1996.

[135] DB Hall, DD Deppe, KE Hamilton, A Dhinojwala, and JM Torkelson. Probe translational and rotational diffusion in polymers near Tg: roles of probe size, shape an secondary bonding in deviations from Debye-Stokes-Einstien Scaling. *Journal of non-crystalline solids*, 235-237(235):48–56, 1998.

[136] J Ries and P Schwille. New concepts for fluorescence correlation spectroscopy on membranes. *Physical chemistry Chemical Physics*, 10(24):3487–3497, 2008.

[137] LS Penn and H Huang. Polymer brushes are not always barriers to diffusion. *Macromolecules*, 41(7):2747–2748, 2008.

[138] HS Lee and LS Penn. In situ study of polymer brushes as selective barriers to diffusion. *Macromolecules*, 41(21):8124–8129, 2008.

[139] C Reznik, Q Darugar, A Wheat, T Fulghum, RC Advincula, and CF Landes. Single ion diffusive transport within a poly(styrene sulfonate) polymer brush matrix probed by fluorescence correlation spectroscopy. *Journal of Physical Chemistry B*, 112(35):10890–10897, 2008.

[140] CF Zhang, X Chu, ZL Zheng, PX Jia, and J Zhao. Diffusion of ionic fluorescent probes atop polyelectrolyte brushes. *Journal of Physical Chemistry B*, 115(51):15167–15173, 2011.

[141] GJ Dunderdale, JR Howse, and JPA Fairclough. Controlling the motion and placement of micrometer-sized metal particles using patterned polymer brush surfaces. *Langmuir*, 27(19):11801–11805, 2011.

[142] A Likhtman and M Ponmurugan. Micrscopic definition of polymer entanglements. Preprint MPS-2014-07, 2014. URL: https://www.reading.ac.uk/web/FILES/maths/Preprint_MPS_14_07_Likhtman.pdf (valid as of March 2015).

[143] Y Zhao and F Ferrari. The study of polymer knots using a simple knot invariant written consisting of multiple contour integrals. *arXiv Soft Condensed Matter*, 2013. arXiv:1306.555[cond=mat.soft].

[144] Y Kantor. Knots in polymers. *Pramana*, 64(6):1011–1017, 2005.

[145] S Alexander. Polymer adsorption on small spheres - scaling approach. *Journal de Physics (Paris)*, 38(8):977–981, 1977.

[146] PJ Flory. *Principles of Polymer Chemistry*. Cornell University Press, 1971.

[147] M Stamm and DW Schubert. Interfaces between incompatible polymers. *Annual Reviw of Material Science*, 25:325–356, 1995.

[148] S Inoué. Foundations of confocal scanned imaging in light microscopy. In JB Pawley, editor, *Handbook of Biological Confocal Microscopy*, chapter 1, pages 1–17. Plenum Press, 2nd edition, 1995.

[149] J Widengren, U Mets, and R Rigler. Fluorescence Correlation Spectroscopy of Triplet-States in Solution - A Theoretical and Experimental-Study. *Journal of Physical Chemistry*, 99(36):13368–13379, 1995.

[150] CJ Blomfield. Spatially resolved x-ray photoelectron spectroscopy. *Journal of Electron Spectroscopy and Related Phenomena*, 143(2-3):241–249, 2005.

[151] BD Ratner and DG Castner. Electron spectroscopy for chemical analysis, 2009.

[152] G Binnig, H Rohrer, C Gerber, and E Weibel. Surface studies by scanning tunneling microscopy. *Physical Review Letters*, 49:57–61, 1982.

[153] G Binnig, CF Quate, and C Gerber. Atomic force microscopy. *Physical review letters*, 56:930–933, 1986.

[154] S Scheuring and J Sturgis. Atomic force microscopy of the bacterial photosynthetic apparatus: plain pictures of an elaborate machinary. *Photosynthesis research*, 102:197–21, 2009.

[155] N Jalili and K Laxminarayana. A review of atomic force microscopy imaging systems: application to molecular metrology and biological sciences. *Mechatronics*, 14:907–945, 2004.

[156] SN Magonov and DH Reneker. Characterization of polymer surfaces with atomic force microscopy. *Annual Review of Materials Science*, 27:175–222, 1997.

[157] TMH Wong and P Descouts. Atomic force microscopy under liquid: A comparative study of three different AC mode operations. *Journal of Microscopy*, 178:7–13, 2011.

[158] A Wawkuschewski, HJ Cantow, SN Magonov, JD Hewes, and MA Kocur. Scanning force microscopy of high modulus polyethylene fibers. *Acta Polymerica*, 46:168–177, 1995.

Appendices

Appendix A

Basic Theory and Derivations

Collected in this section are the derivations of key equations and basic theory associated with brushes, block copolymers and polymer diffusion.

A.1 Semiconductor PV Cells

When a photon is incident on a piece of silicon there are three processes that can occur. Firstly the photon can pass straight through the silicon, a process that mostly occurs with low energy photons. The second possibility is that the photon is reflected off of the surface. The third process, and the most relevant to the production of charge carriers, is the absorption of the photon by the silicon. This can only occur if the photon has more energy than the band gap, the energy difference between the valance band and the conduction band. The valance band is where the electrons are used to bond the atoms of the semiconductor together and as such the electrons are unable to move any real distance. However, when the photon excites the electron, it is possible for the electron to jump to the conduction band where it can then move throughout the semiconductor. This jump from valence to conduction band leaves a hole where the electron was bonding atoms together. This hole can also move through the semiconductor, moving between neighbouring atoms as electrons try to fill the gap where no bond is present. When a

photon with energy greater than that of the band gap is absorbed, the additional energy is simply lost as heat.

At this point there is a mobile electron-hole pair within the semiconductor lattice yet this is of no great use as if left for sufficient time the electron will recombine with the hole. The electron and hole are attracted to one another coulombically and when they recombine a photon with the energy of the band gap is emitted. When looking to generate electricity from light, this is clearly a process we do not want to occur. We must therefore separate the charge carriers and there are two modes that can lead to this separation; drift induced by an electric field will move the electron and holes in opposite directions, and diffusion, where the random thermal motion will allow the carriers to move. It is a combination of the two that allows the separation. An internal electric field within the active region draws electrons and holes in different directions. However only those carriers within a diffusion length (the length a carrier can diffuse during the 'recombination time') are able to traverse the interface between the active region and the rest of the cell. The electrons that leave the active region are then swept away so that they can not recombine with holes and vice versa.

The most commonly known solar cell is that of the large area silicon cell. This is a large p-n junction, that is a layer of n-type silicon (more electrons than holes) with a layer of p-type silicon (more holes than electrons) on top it. When placed in contact, electrons will diffuse from an area of high concentration (the n-type) to an area of low concentration (the p-type). When they diffuse across, the electrons recombine with holes. However, this process does not happen indefinitely as an electric field is generated by the build up of charge. This field acts to induce a drift current which opposes the diffusion of electrons and holes. As the charge builds up the electric field increases until there is enough charge to produce a field that entirely counters the diffusion, leaving a region with no mobile carriers. This depletion region is the active region of our solar cell.

A.2 Fick's First Law

Fick's First Law describes the flux of concentration under steady-state conditions. This is usually observed as diffusion from a high to low concentration.

Consider a collection of particles undergoing a one dimensional random walk, where the number of particles at a specific location,x, and time, t, is defined as $N(x,t)$. At a time interval Δt all particles step either left or right a length Δx. At any given time step, half of the particles will move left while half will move right. This means that half of the molecules as the point x move right to $x+\Delta x$, while half of those molecules at point $x+\Delta x$ move left to x. The net movement of particles right is therefore $-\frac{1}{2}[N(x+\Delta x,t)-N(x,t)]$. The flux ($J$) is net movement through an area (a), that is normal to random walk, during Δt, so

$$\begin{aligned} J &= \frac{1}{2}\left[\frac{N(x+\Delta x,t)}{a\Delta t} - \frac{N(x,t)}{a\Delta t}\right] \\ &= -\frac{(\Delta x)^2}{2\Delta t}\left[\frac{N(x+\Delta x,t)}{a(\Delta x)^2} - \frac{N(x,t)}{a(\Delta x)^2}\right], \end{aligned} \tag{A.2.1}$$

where the second equation is produced by multipilying the top and bottom by $(\Delta x)^2$.

Concentration can be define as the number of particles per unit volume ($\rho(x,t) = \frac{N(x,t)}{a\Delta x}$) and the one dimensional diffusion coefficient ,D, is defined as $\frac{(\Delta x)^2}{2\Delta t}$. These two definitions can be used in confunction with equation A.2.1 to produce

$$J = -D\left[\frac{\rho(x+\Delta x,t)}{\Delta x} - \frac{\rho(x,t)}{\Delta x}\right]. \tag{A.2.2}$$

Finally, it is possible to use the limit of $\Delta x \to 0$ on equation A.2.2:

$$J = -D\frac{\partial \rho}{\partial x}. \tag{A.2.3}$$

It is possible to provide Fick's First Law in any dimensionality required by changing to the appropriate space derivative.

A.3 Fick's Second Law

Fick's Second Law is derived from Fick's First Law and the conservation of mass. In the absence of chemical reactions the following statement is true in one dimension

$$\frac{\partial \rho}{\partial t} + \frac{\partial}{\partial x} J = 0, \tag{A.3.1}$$

where the first term represents the change in concentration with time and the second term is the flux of particles in relation to space. ρ represents the concentration of particles while J represents the flux of particles.

Equation A.3.1 can be simplified by substituting Fick's First Law (equation A.2.3) for the flux. This results in

$$\frac{\partial \rho}{\partial t} - \frac{\partial}{\partial x}\left(D \frac{\partial}{\partial x} \rho\right) = 0, \tag{A.3.2}$$

where D is the diffusion coefficient.

Equation A.3.2 can be simplified further if the diffusion coefficient describing the motion of the particles is location invariant. This means that

$$\frac{\partial}{\partial x}\left(D \frac{\partial}{\partial x} \rho\right) = D \frac{\partial}{\partial x} \frac{\partial}{\partial x} \rho = D \frac{\partial^2 \rho}{\partial x^2}. \tag{A.3.3}$$

Collecting equation A.3.2 and the statement A.3.3, Fick's Second Law in one dimension is found to be

$$\frac{\partial \rho}{\partial t} = D\frac{\partial^2 \rho}{\partial x^2}. \tag{A.3.4}$$

In the case of three dimensions Fick's Second Law is described as

$$\frac{\partial \rho}{\partial t} = D\nabla^2 \rho. \tag{A.3.5}$$

Finally, if the diffusion coefficient is known to not be independent of location, Fick's Second Law can be described by

$$\frac{\partial \rho}{\partial t} = \nabla \cdot (D\nabla \rho). \tag{A.3.6}$$

A.4 Einstein's First Equation on Diffusion

Einstein found that he was unable to use classical mechanics to calculate the position of a single particle due to the vast number of 'bombardments' that the Brownian particle undergoes (about 10^{21} collisions per second), instead he considered the collective motion of the particles. Consider a system of N particles that start at a specific point ($x = 0$) at an initial time ($t = 0$). The density of the particles,$\rho(x, t)$, can be calculated by considering the standard diffusion equation (Fick's Second Law):

$$\frac{\partial \rho}{\partial t} = D\frac{\partial^2 \rho}{\partial x^2}. \tag{A.4.1}$$

By solving this using the boundary conditions stated ($\rho(0, 0) = N$) it is possible to find a description for the 'spread' of Brownian particles with time:

$$\rho(x, t) = \frac{N}{\sqrt{4\pi Dt}} \exp(-\frac{x^2}{4Dt}). \tag{A.4.2}$$

If the average displacement is taken, a value of zero is returned. This follows intuitively from the fact that Brownian particles will move to the left as often as to the right. If the mean square displacement is taken then:

$$\langle x \rangle^2 = 2Dt, \tag{A.4.3}$$

which agrees with equation 1.7.2 for the case of one dimension. It is noteworthy that this result allows for a description in both the case of an 'ensemble' of Brownian particles and a 'single' Brownian particle, allowing for a discussion of the relative number of particles at an instant as well as the time it takes a particle to reach a given point.

A.5 Einstein's Second Equation on Diffusion

Einstein made his formulation by considering a dynamic equilibrium between opposing forces. As the identity of the forces is unimportant (as mention in section 1.7.1), the general case will be considered in one dimension. The proof is identical across two or three dimensions only needing use of the correct dimensionality of functions and differential operators.

A fixed, external potential energy U creates a force on our particles, $F = -\mathrm{d}U/\mathrm{d}x$. The particle will respond to this force by moving with a velocity, $v = \mu F$ where μ is the particle mobility. This can be expanded to treat a large number of particles, such that their local concentration is a function of position $\rho(x)$. After some time an equilibrium will establish, such that the particles will mainly congregate around areas with the lowest U with some spread due to random diffusion. At this point there is no net flow of particles, and the motion induced by a 'pull' towards the lower regions of U will be balanced by an equal and opposite tendency for spread by diffusion.

The net mass flux induced by a drift current alone is

$$J_{\text{drift}}(x) = \mu F(x)\rho(x) = -\rho(x)\mu\frac{\mathrm{d}U}{\mathrm{d}x}. \tag{A.5.1}$$

The net mass flux induced by diffusion current is known from Fick's First law given in equation 1.7.1. Equilibrium requires that

$$0 = J_{\text{drift}}(x) + J_{\text{diffusion}}(x) = -\rho(x)\mu\frac{\mathrm{d}U}{\mathrm{d}x} - D\frac{\mathrm{d}\rho}{\mathrm{d}x}. \tag{A.5.2}$$

In equilibrium conditions it is possible to apply thermodynamics, and particularly Boltzmann statistics, to infer that

$$\rho(x) = A\mathrm{e}^{-\frac{U}{k_{\mathrm{B}}T}}, \tag{A.5.3}$$

where A is a constant relating to the number of particles. By using the chain rule it is possible to produce:

$$\frac{\mathrm{d}\rho}{\mathrm{d}x} = -\frac{1}{k_{\mathrm{B}}T}\frac{\mathrm{d}U}{\mathrm{d}x}\rho(x). \tag{A.5.4}$$

Substituting equation A.5.4 into equation A.5.2

$$\begin{aligned} 0 = J_{\text{drift}}(x) + J_{\text{diffusion}}(x) &= -\rho(x)\mu\frac{\mathrm{d}U}{\mathrm{d}x} + \frac{D}{k_{\mathrm{B}}T}\frac{\mathrm{d}U}{\mathrm{d}x}\rho(x) \\ &= \rho(x)\frac{\mathrm{d}U}{\mathrm{d}x}\left(\mu - \frac{D}{k_{\mathrm{B}}T}\right). \end{aligned} \tag{A.5.5}$$

As the system is in a state of equilibrium, this result must be location invariant leaving a final result of:

$$\mu = \frac{D}{k_B T}. \tag{A.5.6}$$

A.6 Polymer Brushes

In polymer brushes, the way the chain can configure itself is limited by the presence of the interface. The configuration of densely populated tethered chains and their deformation from the random coil, is reflected by the balance between the elastic free energy of the chains and the interaction between individual monomers [145]. Dense tethering on an interface causes there to be a strong overlap among the coils. This increases the monomer-monomer unit contacts which in turn increases the interaction energy of the system. The stretching of the polymer chains in a direction perpendicular to the surface allows the monomer concentration to decrease while increasing the thickness or height of the brush layer. While this stretching acts to lower the interaction energy per chain (F_{int}), it produces an increase in the elastic free energy (F_{el}) as the chain becomes more ordered. The relationship between these two terms determines the equilibrium thickness of the layer.

A simple model to explain this interplay is the Alexander model in which a flat non-adsorbing surface is considered [145]. On this surface a number of uniform polymer chains are tethered, with each chain consisting of N statistical segments, each of a diameter a. The average distance between the tethering points is d, which is much smaller than the radius of gyration of a free, untethered and undeformed chain. Given this, the free energy of each chain is:

$$F = F_{\text{int}} + F_{\text{el}}. \tag{A.6.1}$$

Two assumptions are required to enable simple expressions to be made of the two terms in equation (A.6.1). The first is that the volume fraction of statistical segments is constant within the brush layer ($\phi = \frac{Na^3}{d^2L}$). The second assumption is that all of the free ends of the polymer chains can be located in a single plane at a distance L from the surface.

It is possible to use the Flory approximation to obtain an explicit expression for the free

energy [146]. This estimates the reduction in configurational entropy that is a result of stretching an ideal random walk, a distance L from the grafting surface, thus allowing the free energy to be described as:

$$\frac{F}{k_B T} \approx \frac{\nu \phi^2 d^2 L}{a^3} + \frac{L^2}{R_0^2}, \tag{A.6.2}$$

where ν is a dimensionless parameter quantifying the excluded volume of the chain, and R_0 is the radius gyration of an unperturbed ideal coil.

The first term of (A.6.2) represents the interaction energy between statistical segments while the second term represents the elasticity of the chain. The equilibrium thickness of the brush layer is easily produced by minimising the free energy with respect to the parameter L:

$$\frac{L}{a} \approx N \left(\frac{a}{d}\right)^{2/3}. \tag{A.6.3}$$

This result is notable, due to the demonstration that brush layer thickness scales linearly with the degree of polymerisation. This is perhaps the most important and distinctive property of polymer brushes and can be compared to a free polymer chain in a good solvent (a solvent where the polymer chain stretches), where the dimension of the coil varies as $R \sim N^{3/5}$. This behaviour can also be contrasted with that of a free polymer chain in a theta solvent (a solvent where the chain can be seen to act as an idealised random coil). In a theta solvent the dimensions of the chain scale as $R_0 \sim N^{1/2}$.

The central tenet of the Alexander model, the balance of interaction energy and elastic free energy, can also be applied to other situations involving polymer brushes. Namely, the brush in a theta solvent or a poor solvent.

In a theta solvent, the interaction between statistical segments disappears, allowing

the free energy per chain to be expressed as:

$$\frac{F}{k_B T} \approx \frac{w\phi^3 d^2 L}{a^3} + \frac{L^2}{Na^2}, \tag{A.6.4}$$

where w is a dimensionless third Virial coefficient. The result for the equilibrium thickness can be obtained in the same way as the previous result and is described as:

$$\frac{L}{a} \approx N\left(\frac{a}{d}\right). \tag{A.6.5}$$

Again the linearity of L and N is recovered. However, the length of the chains have shrunk in comparison with that of a good solvent. It should be stressed however that the polymer chains are still distorted with respect to that of a free polymer in a theta solvent ($R_0 \sim N^{1/2}$).

In the case of melt conditions with no solvent, the relationship between the equilibrium thickness and the degree of polymerisation can be found in the same way. In this case the relationship can be described as:

$$L \sim N^{2/3}. \tag{A.6.6}$$

This again demonstrates the deformation of the polymer brush in comparison with that of a free chain.

Table A.1 summarises the results for the length scales of both free polymer chains and tethered chains in terms of the number of statistical segments (N).

	Tethered Polymer Brush Chains	Free Polymer Chain
Good Solvent	${}^{L}/_{a} \approx N\left({}^{a}/_{d}\right)^{2/3}$	$R_g \sim N^{3/5}$
Theta Solvent	${}^{L}/_{a} \approx N\left({}^{a}/_{d}\right)$	$R_g \sim N^{1/2}$
Bulk state	$L \sim N^{2/3}$	$R_g \sim N^{1/2}$

Table A.1: The relationship between the dimensions of a polymer and the degree of polymerisation based upon the Alexander Model.

A.7 Mixing and Phase Seperation in Polymers

It is possible to consider the mixing of polymers as well as the phase separation of the mixture by extending the simple models for solution models [99]. In the regular solution model the free energy of mixing is formed by balancing an entropic contribution with an enthalpic contribution. If monomer species A and monomer species B are mixed then it is possible to produce an expression for the free energy of mixing (F_{mono}):

$$\frac{F_{\text{mono}}}{k_B T} = \phi_A \ln \phi_A + \phi_B \ln \phi_B + \chi \phi_A \phi_B, \tag{A.7.1}$$

where ϕ_A and ϕ_B are the volume fractions of the monomers and χ is the interaction parameter between the monomers A and B.

This equation can be modified to deal with polymers made of the monomers A and B [99]. The case where both polymers have a degree of polymerisation N will be considered. With reasonably simple arguments this can be achieved by noticing that the first two terms of equation A.7.1 relate to the entropy of mixing. The term arises from the fact that a site in space has a probability of ϕ_A of being occupied by monomer A and a probability of ϕ_B of being occupied by monomer B. If the number of monomer units is increased from one for the monomer solution to N for the polymer case, the probability will remain the same. However, the energy of mixing (the final term) must increase by a

factor of N to account for the increase in monomer units.

This means that the free energy of mixing per polymer molecule ($F^{\text{mol}}_{\text{poly}}$) can be written as:

$$\frac{F^{\text{mol}}_{\text{poly}}}{k_B T} = \phi_A \ln \phi_A + \phi_B \ln \phi_B + N\chi\phi_A\phi_B. \tag{A.7.2}$$

Here the interaction parameter is the interaction energy per monomer treated as being independent of the degree of polymerisation. It is however customary to provide the free energy per monomer unit (or per site when treated mathematically) rather than as the molecule as a whole. The free energy in this form (F^{site}_{poly}) is:

$$\frac{F^{\text{site}}_{\text{poly}}}{k_B T} = \frac{\phi_A}{N} \ln \phi_A + \frac{\phi_B}{N} \ln \phi_B + \chi\phi_A\phi_B. \tag{A.7.3}$$

In literature, the approximation of free energy given in equation A.7.3 is known as the Flory-Huggins free energy.

In single small molecules (i.e. the monomeric solution case) there exists a critical value for the interaction parameter which separates the case of a mixture of molecular species to that of phase separation of the two species

$$\begin{aligned} \chi > \chi_c = 2 \text{ for phase separation and} \\ \chi < \chi_c = 2 \text{ for a single phase.} \end{aligned} \tag{A.7.4}$$

However, in the case of polymers this needs to be modified to account for the degree of polymerisation and therefore the increase of monomers per molecule. Instead we find that

$\chi_c = \frac{2}{N}$, so that

$$\chi > \chi_c = \frac{2}{N} \text{ for phase separation and}$$
$$\chi < \chi_c = \frac{2}{N} \text{ for a single phase.} \tag{A.7.5}$$

Most pairs of polymers have an interaction parameter in the range of $0.01 - 0.1$ [99], so we can expect polymers to phase separate if the degree of polymerisation is high. There are two points that are critically important to consider:

- the coexisting phases are for all intents and purposes pure,
- the interface between the phase is not atomically sharp.

The first point comes from calculating the coexisting compositions from the Flory-Huggins free energy of mixing. In the case where $\chi N \gg 1$, the coexisting composition ϕ_B is well approximated by:

$$\phi_B \approx \exp(-\chi N) \tag{A.7.6}$$

For a polymer pair that is highly polymerised and has even a modestly unfavourable interaction parameter, the exponent in equation A.7.6 will be much larger than 1 and therefore meaning that the region is essentially polymer A (equation A.7.6 is only valid where $\phi_B \sim 0$).

To justify the second statement we must first consider the random walk of a polymer chain. An atomically sharp interface would minimise the number of unfavourable contacts that exist between the segments of the different polymers. However, this will reduce the number of configurations that the chain could assume, thereby reducing the entropy of the chain. Rather than being atomically sharp, the interface must be diffuse, to the point that a balance between the entropy and energy due to unfavourable contacts is reached.

It is possible to derive simple expressions from simple arguments to show that the width of the interface, w, is:

$$w \sim \frac{a}{\sqrt{\chi}}, \tag{A.7.7}$$

where a is the size of the monomer, and the value for the width is typically 1-3 nm [99]. Much more sophisticated theories (such as FHS theory [147])can be used to produce similar expressions for the interface width with only numerical factors being introduced.

A.8 Confocal Microscopy

In a traditional fluorescence microscope, light is allowed to excite the molecules being imaged. If the molecule is fluorescent, then a different colour is observed and this can be used to build up an image. The major advantage in fluorescence microscopy is that by adding specific dye molecules to the sample it possible to image only specific sections. It is also possible to use multiple dyes, each attached to different molecules of interest within the sample so as to distinguish different regions within the sample. By adding a pinhole, confocal microscopy is able to increase the resolution of the images obtained.

Consider a microscope with a set of lenses that focus light from the focal point of one lens to some other arbitary point. Light originating from another point will still be imaged by the lenses of the microscope, though the image from this second point will not be in the same location as the light from the focal point. To observe just the light from the focal point, a pinhole is introduced to the system [148]. The pinhole is placed on the other side of the lens system at the image produced by the light from the focal point. This allows all light from the focal point to be imaged while light from any other point is out of focus and gets blocked by the pinhole.

In the traditional microscope the entire sample is illuminated by the excitation light,

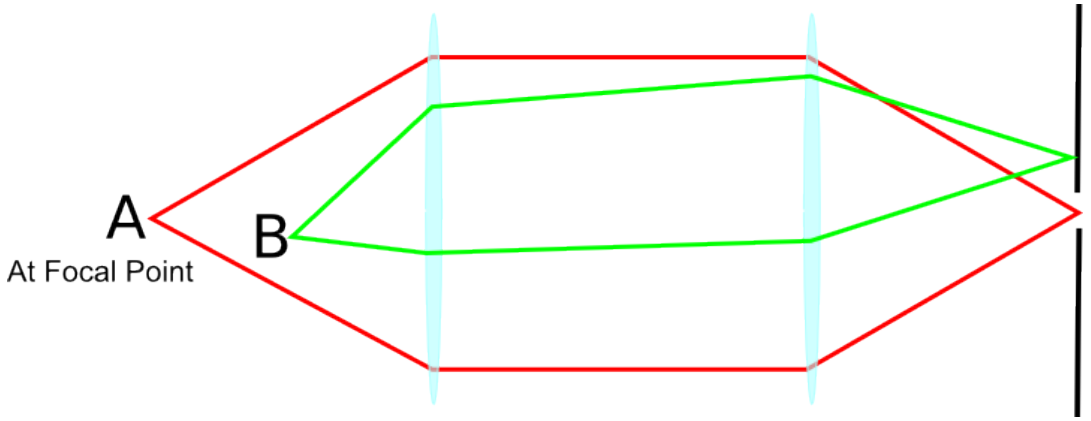

Figure A.1: A schematic diagram demonstrating the basic principle of confocal microscopy. The red trace represents light originating from the focal point of the lens, at A, and is able to pass through the pinhole, while the green light which is from some other point, B, is blocked by the screen.

meaning that the entire sample fluoresces at the same time. The highest intensity of excitation light is at the focus of the lens system but this does not prevent the rest of the sample receiving some light. This leads to a background haze in the resulting images, which is removed by the introduction of the pinhole [148].

The resolution of confocal microscopy is limited by the point-spread function, as the fluorescence can be treated as originating from a point source [148]. Specifically the size of the pinhole will have a major impact on the resolution so that the maximum of focussed light can be collected. Ideally the pinhole is large enough to allow the Airy disk of the point-spread function to be transmitted while blocking out all other fringes. The size of the Airy disk (d_{Airy}), specifically the diameter of it, can be extracted from the Rayleigh criterion

$$d_{\text{Airy}} \approx 1.22\frac{\lambda}{NA}, \tag{A.8.1}$$

where λ is the wavelength of light and NA is the numerical apperture of the lens system.

This relation needs to be modified to account for the impact of the magnification of

the lens (M), meaning that the pinhole diameter (d_{pinhole}) must be

$$d_{\text{pinhole}} = M \cdot d_{\text{Airy}} \approx 1.22 \cdot M \frac{\lambda}{NA}. \tag{A.8.2}$$

The axial resolution (d_{axial}) can also be calculated and equates to the distance from the centre of the diffraction pattern to the first axial minimum of the pattern [148]. This is given by:

$$d_{\text{axial}} \approx \frac{2\lambda \cdot n}{(NA)^2}, \tag{A.8.3}$$

where n is the refractive index of the object medium. A typical set-up used with the available equipment (514 nm laser, 40× magnification and a numerical aperture of 1.3 imaging a fluorophore in aqueous conditions) requires a pinhole diameter of 19 μm, and has a lateral and axial resolution of 480 nm and 810 nm respectively. The axial resolution can be doubled to get the thickness of the 'optical slice', that is the thickness of the region that is imaged. In the case of the set-up already considered this is of the order of 1.5 μm.

A.9 Theory of FCS

The number of molecules that are within the focal volume at any time is governed by the Poisson distribution. This means that the root mean square fluctuation of the particle number N is well defined as

$$\frac{\sqrt{\langle (\delta N)^2 \rangle}}{\langle N \rangle} = \frac{\sqrt{\langle (N - \langle N \rangle)^2 \rangle}}{\langle N \rangle} = \frac{1}{\sqrt{\langle N \rangle}}. \tag{A.9.1}$$

Since the relative fluctuations get smaller as the number of molecules increase, it is important to minimise the number of the molecules in the focal volume. Despite this it is essential that the fluorescence signal be higher than that of the background signal. If the concentration of molecules in solution is too low then there may be times when there is

no molecule in the focal point.

The molecules within the focal point emit fluorescence which is recorded photon by photon. If there is a constant excitation power, then the fluctuations of the signal are defined as deviations from the temporal average:

$$\delta F(t) = F(t) - \langle F(t) \rangle \tag{A.9.2}$$

$$\langle F(t) \rangle = \frac{1}{T} \int_0^T F(T) dt. \tag{A.9.3}$$

If all fluctuations are solely due to changes in the local concentration δC of the fluorescent molecule within the effective volume V_{eff} of the focal spot, the fluctuations can be written as:

$$\delta F(t) = \kappa \int_V I_{\text{ex}}(\vec{r}) \cdot S(\vec{r}) \cdot \delta(\sigma \cdot q \cdot C(\vec{r}, t)). \cdot dV \tag{A.9.4}$$

The majority of the parameters in equation (A.9.4) are describing the probability of exciting a fluorophore within the confocal volume and then detecting the photon that is emitted. The parameters are defined as

- κ : The overall detection efficiency.

- $I_{\text{ex}}(\vec{r})$: Spatial distribution of the excitation energy with a maximum amplitude of I_0 .

- $S(\vec{r})$: The optical transfer function of the objective-pinhole combination, which determines the spatial collection efficiency of the setup and is a dimensionless factor.

- $\delta(\sigma \cdot q \cdot C(\vec{r}, t))$: The dynamics of the fluorophore where σ relates to the molecular absorption cross-section, q is the quantum yield and $C(\vec{r}, t)$ is the local concentration of particles at time t.

Determining all of these parameters is impossible in most cases and extremely difficult in others. It is possible to define some parameters by careful combination and manipulation of the factors that lead to the parameters. To simplify equation (A.9.4), the two spatial optical factors ($\frac{I_e x(\vec{r})}{I_0} \cdot S(\vec{r})$) are combined into a single function $W(\vec{r})$, which decribes the distribution of emitted light. This is usually approximated by a three-dimensional Gaussian which decays to $\frac{1}{e^2}$ of its initial value at r_0 in the lateral direction and at $z = z_0$ in the axial direction.

$$W(\vec{r}) = \exp\left(-2\frac{x^2+y^2}{r_0^2}\right) \cdot \exp\left(-2\frac{z^2}{z_0^2}\right). \tag{A.9.5}$$

A subsequent simplification of equation (A.9.4) involves combining the parameters κ, σ and q with the excitation intensity amplitude I_0 to give a parameter that determines the photon count rate per detected molecule:

$$\eta_0 = I_0 \cdot \kappa \cdot \sigma \cdot q. \tag{A.9.6}$$

If the definitions (A.9.5) and (A.9.6) are inserted into equation (A.9.4) then:

$$\delta F(t) = \int_V W(\vec{r})\delta(\eta C(\vec{r},t)) \cdot dV. \tag{A.9.7}$$

The normalised autocorrelation function is defined as

$$g(\tau) = \frac{\langle \delta F(t) \cdot \delta F(t+\tau) \rangle}{\langle F(t) \rangle^2}, \tag{A.9.8}$$

Where the signal is analysed with respect to a lag time τ to find the measure of similarity. From (A.9.8), when the autocorrelation amplitude $g(0)$ is simply the normalised variance of the fluctuating fluorescence signal $\delta F(t)$.

If equation (A.9.7) is now substituted into equation (A.9.8) to give

$$g(\tau) = \frac{\iint W(\vec{r})W(\vec{r'})\langle(\eta \cdot C(\vec{r},t))\delta(\eta \cdot C(\vec{r'},t))dVdV'}{(\int W(\vec{r})\langle\delta(\eta \cdot C(\vec{r},t))\rangle dV)^2}. \tag{A.9.9}$$

Now it is necessary to separate the term describing the fluctuations:

$$\delta(\eta \cdot C(\vec{r},t)) = C\delta\eta + \eta\delta C. \tag{A.9.10}$$

Clearly (A.9.9) will be simplified greatly if either the concentration or η is constant in a system. If the fluorophore's fluorescent properties are assumed not to change during the observation time ($\delta\eta = 0$), then (A.9.9) can be written as

$$g(\tau) = \frac{\iint W(\vec{r})W(\vec{r'})\langle\delta C(\vec{r},0)\delta C(\vec{r'},\tau)dVdV'}{(\langle C\rangle \int W(\vec{r})dV)^2}. \tag{A.9.11}$$

The term $\langle\delta C(\vec{r},0)\delta C(\vec{r'},\tau)\rangle$ is called the number density autocorrelation term. If only particles that are freely diffusing in three dimensions, with the diffusion coefficient D, are considered then the number density autocorrelation term becomes

$$\langle\delta C(\vec{r},0)\delta C(\vec{r'},\tau)\rangle = \langle C\rangle \frac{1}{(4\pi D\tau)^{-\frac{3}{2}}} \cdot \exp\left(-\frac{(\vec{r}-\vec{r'})^2}{4D\tau}\right). \tag{A.9.12}$$

This can then be inserted into (A.9.11) to give:

$$\begin{aligned} g(\tau) &= \frac{\iint W(\vec{r})W(\vec{r'})\langle C\rangle \frac{1}{(4\pi D\tau)^{-\frac{3}{2}}} \cdot e^{-\frac{(\vec{r}-\vec{r'})^2}{4D\tau}} dVdV'}{(\langle C\rangle \int W(\vec{r})dV)^2} \\ &= \frac{1}{\langle C\rangle(4\pi D\tau)^{-\frac{3}{2}}} \frac{\iint W(\vec{r})W(\vec{r'}) \cdot e^{-\frac{(\vec{r}-\vec{r'})^2}{4D\tau}} dVdV'}{(\int W(\vec{r})dV)^2}. \end{aligned} \tag{A.9.13}$$

Two more conventions can be inserted to get to the normalised three-dimensional diffusion autocorrelation for one species of molecules. These will be discussed in turn.

The first convention for simplifying the normalised autocorrelation function, is the rela-

tionship between the lateral diffusion time, the time a molecule stays in the focal volume τ_D, and the diffusion coefficient. This is independent of the setup used:

$$\tau_D = \frac{r_0^2}{4 \cdot D}. \tag{A.9.14}$$

The second definition for the simplification of equation (A.9.13) is for the effective focal volume V_{eff}

$$V_{\text{eff}} = \frac{(\int W(\vec{r})dV)^2}{\int W^2(r)dV}. \tag{A.9.15}$$

By using equation (A.9.5) to provide the identity of $W(\vec{r})$ and solve for V_{eff} by integrating over space

$$V_{\text{eff}} = \pi^{\frac{3}{2}} \cdot r_0^2 \cdot z_0 \tag{A.9.16}$$

Therefore using (A.9.14) and (A.9.16) into (A.9.13) the autocorrelation for a species of freely diffusing molecules yields

$$g(\tau) = \frac{1}{V_{eff}\langle C\rangle} \cdot \frac{1}{\left(1 + \left(\frac{\tau}{\tau_D}\right)^2\right)} \cdot \frac{1}{\sqrt{1 + \left(\frac{z_0}{r_0}\right)^2 \cdot \frac{\tau}{\tau_D}}}. \tag{A.9.17}$$

The first term of (A.9.17) is the inverse of the average particle number within the focal volume. This means that if the dimensions of r_0 and z_0 are deduced from calibration measurements, the local concentration of the fluorscent molecules can be calculated from the amplitude of the autocorrelation curve at a lagtime of zero ($g(0)$):

$$g(0) = \frac{1}{\langle N\rangle} = \frac{1}{V_{eff} \cdot \langle C\rangle} \Rightarrow \langle C\rangle = \frac{1}{V_{eff} \cdot g(0)}. \tag{A.9.18}$$

In addition to the local concentration of fluorophores, the diffusion coefficient can be easily derived from the characteristic decay time of the correlation function (τ_D) by rearranging

(A.9.14).

To this point the fluorescent properties of the diffusing species have been treated as a constant as they traverse the focal spot ($\delta\eta = 0$). This assumption does not hold for real fluorescent dyes or at the high excitation powers provided by a laser. In real situations, the dye will sometimes appear to 'flicker' and the most common cause of this is the transition of the dye to the first excited triplet state. To understand this phenomenon it is necessary to discuss transitions between energy levels.

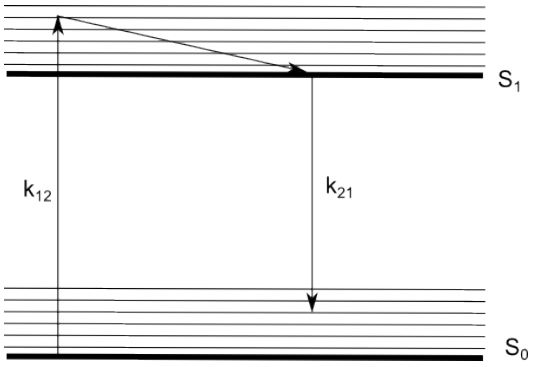

Figure A.2: A Jablonski diagram showing simple two level fluorescence with associated decay rate constants.

The ground state of the molecule will be designated as S_0 while the first excited state will be designated as S_1 (Figure (A.2)). The system will start off in the lowest vibrational energy level of the ground state. When a photon is absorbed, the molecule is elevated to one of the vibrational energy levels in the first excited state. The rate constant for this transition is k_{12}. The molecule then decays extremely quickly to the lowest vibrational level of the first excited state, so rapidly as to be treated as instantaneous. From this lowest level the system then decays to one of the vibrational energy levels of the ground state with a rate constant of k_{21}.

k_{21} is not simply the rate constant for the radiative transition where a photon is emitted,

but is rather the sum of the radiative coefficient, k_{r}, and the non-radiative coefficient, k_{nr}. A significant point is that if the radiative decay rate k_r is multiplied by the concentration of the S_1 state the fluorescence of the system is recovered.

In most fluorophores there is typically another set of parallel states referred to as triplet states. To move from a triplet state to a singlet state is forbidden in first order quantum mechanics, and requires spin-orbit coupling to proceed. Figure A.3 shows a triplet state T_1 with associated 'forbidden' transitions between S_1 and S_0. As a consequence of the nature of this transition, the rate constants κ_{23} and κ_{31} are much smaller than κ_{12} and κ_{21}.

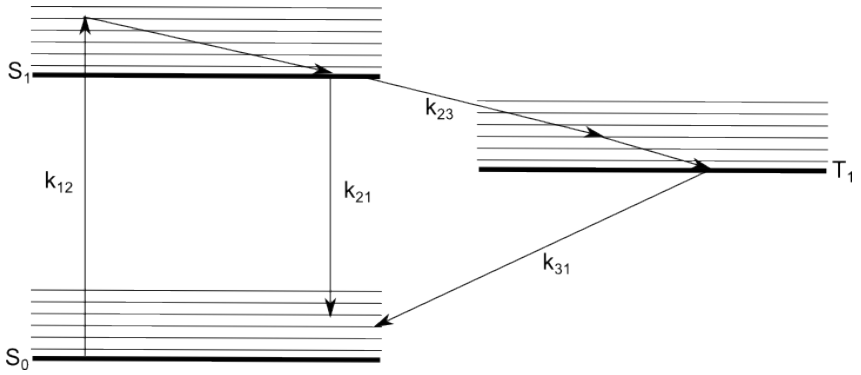

Figure A.3: A Jablonski diagram showing both singlet states and the first triplet state, with the transitions and associated decay rate constants. It should be noted that it is incredibly unlikely for an electron to jump straight into the triplet state T_1, but will rather make use of intersystem crossing to move from S_1 to some intermediary state before decaying to T_1. The rate for this entire process can be treated as κ_{23}.

So that equation (A.9.17) can be updated to include the effects of the possibility of the fluorophore using the triplet state, it is necessary to quantify the decay rate constants for the transitions. It is possible to create coupled differential equations for the three possible

states based upon figure A.3 using a matrix formula,

$$\frac{\mathrm{d}}{\mathrm{d}t}\begin{pmatrix} S_0(\vec{r},t) \\ S_1(\vec{r},t) \\ T_1(\vec{r},t) \end{pmatrix} = \begin{pmatrix} -\kappa_{12}(\vec{r}) & \kappa_{21} & \kappa_{31} \\ \kappa_{12} & -(\kappa_{23}+\kappa_{21}) & 0 \\ 0 & \kappa_{23} & -\kappa_{31} \end{pmatrix} \begin{pmatrix} S_0(\vec{r},t) \\ S_1(\vec{r},t) \\ T_1(\vec{r},t) \end{pmatrix}. \tag{A.9.19}$$

It is known from a previous definition that at $t = 0$, all molecules are in the ground state. This allows a boundary condition to be placed upon equation (A.9.19):

$$\begin{pmatrix} S_0(\vec{r},t) \\ S_1(\vec{r},t) \\ T_1(\vec{r},t) \end{pmatrix} = \begin{pmatrix} 1 \\ 0 \\ 0 \end{pmatrix}. \tag{A.9.20}$$

It is possible to solve equations (A.9.19) and (A.9.20) completely for all states but because it is just the fluorescence of the system that is of interest this is not necessary. As fluorescence is proportional to the number of molecules in S_1, it is possible to solve equations (A.9.19) and (A.9.20) for only state S_1:

$$\begin{aligned} S_1(\vec{r},t) = {} & \frac{\kappa_{12}(\vec{r})\kappa_{31}}{\kappa_{12}(\vec{r})(\kappa_{23}+\kappa_{31})+\kappa_{21}\kappa_{31}} + \frac{\kappa_{12}(\vec{r})}{\kappa_{12}(\vec{r})+\kappa_{21}} \exp\left(-(\kappa_{21}+\kappa_{12}(\vec{r}))t\right) \\ & + \frac{\kappa_{12}^2(\vec{r})\kappa_{23}}{(\kappa_{12}(\vec{r})+\kappa_{21})\kappa_{12}(\vec{r})(\kappa_{23}+\kappa_{31})+\kappa_{21}\kappa_{31}} \exp\left(-\kappa_{21} + \frac{\kappa_{12}(\vec{r})\kappa_{23}}{\kappa_{12}(\vec{r}+\kappa 21}\right)t\Bigg). \end{aligned} \tag{A.9.21}$$

If equation (A.9.21) is considered in conjunction with the notion that κ_{12} and κ_{21} are very large compared with κ_{23} and κ_{31}, the constant term can be considered to represent the equilibrium value that the system attains after infinite time. The second term is entirely dependent on the rate constants κ_{12} and κ_{21} making the value of the exponent very large. This means that the middle term will vanish at timescales much lower than that of the measurements involved in FCS. This leaves the third term, which describes the crossing between the T_1 state and the two singlet states. Upon consideration, it is possible to

rewrite equation (A.9.21) as:

$$S_1(\vec{r},t) = (1-T) + Te^{\frac{-t}{\tau_{\mathrm{T}}}}, \tag{A.9.22}$$

where

$$T = \frac{\kappa_{12}^2(\vec{r})\kappa_{23}}{(\kappa_{12}(\vec{r})+\kappa_{21})\kappa_{12}(\vec{r})(\kappa_{23}+\kappa_{31})+\kappa_{21}\kappa_{31}}$$

and

$$\tau_{\mathrm{T}} = \left(\kappa_{21} + \frac{\kappa_{12}(\vec{r})\kappa_{23}}{\kappa_{12}(\vec{r}+\kappa 21}\right)^2.$$

To integrate this into the autocorrelation function, dependence of κ_{12} on position r will be ignored, which is a very good approximation. To read further discussion and a full treatment of this proof, justifying why the dependence can be ignored, see Widengren *et al.* (1995) [149]. In the most basic sense, the triplet to singlet transition acts to alter the quantum efficiency of the system. A fraction of molecules T are non-fluorescent, while a fraction $(1-T)+Te^{-\frac{\tau}{\tau_T}}$ remain fluorescent. This fraction becomes a multiplier to the autocorrelation function, while additionally the average number of molecules $\langle N\rangle$ must be replaced with $(1-T)\langle N\rangle$, so that

$$g(\tau) = \left((1-T)+Te^{\frac{-t}{\tau_T}}\right)\frac{1}{\langle N\rangle}\cdot\frac{1}{\left(1+\left(\frac{\tau}{\tau_D}\right)^2\right)}\cdot\frac{1}{\sqrt{1+\left(\frac{z_0}{r_0}\right)^2\cdot\frac{\tau}{\tau_D}}}. \tag{A.9.23}$$

Equation (A.9.23) describes the case of a fluorophore isotropically diffusing in three dimensions but with very few changes to the derivation it is possible to produce the autocorrelation function describing two dimensional diffusion:

$$g(\tau) = \left((1-T)+Te^{\frac{-t}{\tau_T}}\right)\frac{1}{\langle N\rangle}\cdot\frac{1}{1+\left(\frac{\tau}{\tau_D}\right)}. \tag{A.9.24}$$

Finally, it is possible to integrate these two descriptions of diffusion into one expression so that it can describe both three dimensional and two dimensional motion:

$$g(\tau) = \left((1-T) + Te^{\frac{-t}{\tau_T}}\right) \frac{1}{\langle N \rangle} \left(\frac{1-f}{\left(1+\left(\frac{\tau}{\tau_D}\right)^2\right)\left(1+\left(\frac{z_0}{r_0}\right)^2 \cdot \frac{\tau}{\tau_D}\right)^{1/2}} + \frac{f}{1+\left(\frac{\tau}{\tau_D}\right)} \right). \tag{A.9.25}$$

This concludes the derivation of the autocorrelation function relating to the fluctuations in fluorescence, with equation (A.9.25) the final result. However, it should be noted that when data are collected the raw data are not presented in terms of fluctuations from a mean intensity, but as the intensity at each discrete time. This is not compatible with equation (A.9.25) but it is simple to produce the form that is.

Removing the time dependence it is straightforward to demonstrate the relationship between a correlation description in terms of an intensity I and in terms of a fluctuation in intensity δI. The correlation in terms of δI has been previously presented as an autocorrelation in terms of a time dependent term $F(\tau)$, yet in the case considered now it is much simpler:

$$g = \frac{\langle (\delta I)^2 \rangle}{\langle I \rangle^2}, \tag{A.9.26}$$

while similarly the correlation in terms of intensity is presented as

$$G = \frac{\langle I^2 \rangle}{\langle I \rangle^2}. \tag{A.9.27}$$

Upon consideration it is clear that we can integrate both the intensity and fluctuation of the intensity into a single expression:

$$I = \langle I \rangle + \delta I. \tag{A.9.28}$$

By introducing the description in equation (A.9.28) into the definition (A.9.27):

$$\begin{aligned} G &= \frac{\langle(\langle I\rangle + \delta I)^2\rangle}{\langle I\rangle^2} = \frac{\langle(\langle I\rangle^2 + 2\langle I\rangle\delta I + (\delta I)^2)\rangle}{\langle I\rangle^2} \\ &= \frac{\langle I\rangle^2 + 2\langle I\rangle\langle\delta I\rangle + \langle(\delta I)^2\rangle}{\langle I\rangle^2} \\ &= 1 + \frac{2\langle\delta I\rangle}{\langle I\rangle} + \frac{\langle(\delta I)^2\rangle}{\langle I\rangle^2}. \end{aligned} \tag{A.9.29}$$

It is possible to simplify equation (A.9.29) by recognising that random processes exhibit as many fluctuations above the mean as below it (i.e. $\langle\delta I\rangle = 0$),

$$G = 1 + \frac{\langle(\delta I)^2\rangle}{\langle I\rangle^2} = 1 + g. \tag{A.9.30}$$

The logic exhibited in this quick derivation of the link between G and g can be applied to the similar case of autocorrelation between different times. As such equation (A.9.25) can be modified to be in terms of $G(\tau)$ which is more commonly collected from raw data to give

$$G(\tau) = 1 + \frac{1}{\langle N\rangle}\left(\frac{1-f}{\left(1+\left(\frac{\tau}{\tau_D}\right)^2\right)\left(1+\left(\frac{z_0}{r_0}\right)^2\cdot\frac{\tau}{\tau_D}\right)^{1/2}} + \frac{f}{1+\left(\frac{\tau}{\tau_D}\right)}\right)\left((1-T)+Te^{\frac{-t}{\tau_T}}\right). \tag{A.9.31}$$

A.10 Contact Angle

The angle at which a liquid contacts a solid surface in the presence of a vapour is the contact angle. In equilibrium conditions, the contact angle is described by Young's equation

$$\gamma_{SL} + \gamma_{LG}\cos\theta_c = \gamma_{SG}, \tag{A.10.1}$$

where θ_c is the contact angle and γ_{SL}, γ_{SG} and γ_{LG} refers to the free energy at the solid-liquid interface, the solid-gas interface and the liquid-gas interface respectively. The geometry of this is presented in figure A.4.

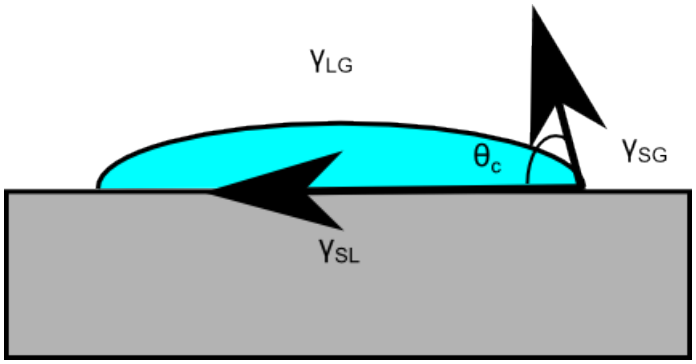

Figure A.4: A schematic diagram of a liquid drop and the free energies at each interface.

When a droplet of a liquid is placed on a solid surface it spreads. The degree of spreading is determined by the interfacial tension at the solid-liquid, solid-vapour and liquid-vapour interfaces. In the case of water, this spreading will be high for polar surfaces (leading to a small contact angle) and low for non-polar or hydrophobic surfaces (leading to a high contact angle).

A.11 X-ray Photoelectron Spectroscopy

X-ray photoelectron spectroscopy (XPS), also known as electron spectroscopy for chemical analysis (ESCA), is a surface analysis technique that can be used to provide information on the elemental composition, surface chemistry, electronic structure and morphology of a surface [150].

In XPS, the sample is bombarded with soft x-ray photons which cause the emission of electrons from the surface in process known as the photoelectric effect (figure A.5). Through the use of an electron energy analyser, the number and kinetic energy of the

photoelectrons emitted can be measured. The kinetic energy (E_k) of the photoelectrons can be used to determine the binding energy (E_B) of the orbitals from which they are emitted and from this a spectrum can be built up. The relationship between the kinetic energy and the binding energy can be expressed

$$E_k = h\nu - E_B - \phi, \tag{A.11.1}$$

where $h\nu$ is the wavelength of light used and ϕ the electron spectrometer work functions.

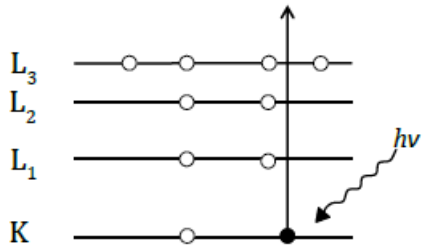

Figure A.5: A schematic diagram demonstrating the principles of XPS. An X-ray photon is absorbed which causes an electron to be emitted via the photoelectric effect.

Each element (with the exception of hydrogen and helium) has a characteristic binding energy and a corresponding set of peaks in the XPS spectra, enabling any elements present on the surface to be identified quickly [151]. The intensity for each element, as measured by the area under each peak, is directly proportional to its relative amount of each element on the surface. The stoichiometry of the sample can therefore be determined from its spectrum. XPS can also provide detailed information about the chemical states of each element present. The binding energy for each orbital is dependent on its binding environment and changes in bonding lead to small changes in binding energy. Analysis of these enables the bonding environment to be determined. For example, the XPS peak arising from photoelectrons emitted from the C1s orbital of an aliphatic carbon will occur at 285 eV [150]. When carbon is bonded to an electronegative oxygen atom, as a

consequence the XPS peak will be shifted 1.4 eV higher.

The XPS instrument is housed in thick stainless steel and is carried out under ultra-high vacuum (UHV). The use of UHV is crucial as it reduces the amount of surface contamination and prevents the scattering or adsorption of photoelectrons [150]. The X-rays are generated by the bombardment of a metal with electrons, commonly this is Mg (MgKα 1253.6 eV) or Al (AlKα 1486.6 eV) [151]. The X-rays pass through a quartz crystal, which acts as a monochromator focuser and provides a narrower excitation source, allowing a higher resolution to be obtained. Though the X-rays will penetrate far into a sample, the photoelectrons will be only detected from the top 10 nm of the surface. This is due to the short distance photoelectrons can travel without loss of energy, known as the inelastic mean free path. As a consequence XPS is a highly surface sensitive technique.

A.12 Scanning Force Microscopy

Scanning probe microscopy represents a group of techniques for surface analysis. Scanning tunnelling microscopy was the first technique invented within this family [152], yet it is the development of Scanning force microscopy (commonly known as atomic force microscopy or AFM) that sees the most use with respect to polymeric systems. The force that exists between the AFM tip and the sample can be employed in the surface analysis of practically any material. Originally, AFM was produced as the analogue of Scanning Tunneling Microscopy for profiling non-conducting surfaces in high resolution [153]. Since its inception though, AFM has developed into a multifunctional technique that can not only examine the topography of a surface but also the adhesion and mechanical properties on scales from hundreds of microns down to nanometres. As polymeric materials are important in modern technologies, and the importance of nanometre scale features becomes apparent, the significance of AFM as a technique for characterisation is enhanced.

In AFM, the surface of the sample is scanned with a probe. The probe consisted of a cantilever with a very sharp tip [154]. The point of the tip can be kept in continuous contact with the surface for imaging in contact mode, or the cantilever can be forced to oscillate causing the tip to be in intermittent contact known as tapping mode [155]. In tapping mode the oscillation is driven by a small piezoelectric element that forces the cantilever to oscillate at its resonant frequency.

The bending of the cantilever (contact mode) or the damping of its oscilation (tapping mode) in response to the forces between the microscopic tip and the sample are monitored by an optical lever [155]. A laser beam is focussed onto the cantilever where the beam is reflected onto a four quadrant photodector. These quadrants are designed to detect the bending deflection, bending oscillation and the torsion on the cantilever. The tip is scanned over the sample (or vice versa) in a raster pattern by another piezoelectric element in the horizontal plane. The motion of the tip is controlled in the vertical plane by a feedback mechanism. In contact mode, the feedback aims to keep the cantilever deflection at a set value and therefore raises or lowers the sample to achieve this. In tapping mode, the oscillation amplitude is measured. The amplitude is reduced from the amplitude of a freely oscillating probe (A_0) by repulsive interactions between the tip and the sample. The feedback attempts to keep the oscillation amplitude at a set value (A_{sp}) by again adjusting the vertical position.

The operations of contact or tapping mode are referred to as constant force measurements and is the most common form of AFM. The variations in the z-position of the sample during the scanning are plotted as a function of the position in x and y of the tip, allowing for a image of the height to be constructed.

A.12.1 Contact Mode AFM

While AFM was first introduced to obtain high resolution profiles of the surface topography, the height records are only exact when the forces applied to the sample through the tip are small enough so as not to deform the surface itself. Before a measurement it is difficult to predict whether a certain tip-to-sample force will induce such a deformation.

The impact of tip-to-sample force is perhaps best demonstrated by an example by Magonov and Reneker (1997) [156]. Height profiles on a surface of a microlayer of polyethylene (PE) were obtained in contact mode. The sample consisted of alternating layers of low density and high density polymer (layer M: $\rho = 0.92\,\mathrm{g cm^{-3}}$, layer N: $\rho = 0.86\,\mathrm{g cm^{-3}}$). The height image obtained with a tip-to-sample force on 20 nN (figure A.6a) reveals a number of surface features including traces of the ultramicrotome knife used to prepare the surface. However the image recorded with a force of 150 nN (figure A.6b) does not show this, rather it shows a microlayer pattern with alternating stripes of contrast. The bright stripes are 2-3 μm wide and are related to layers of M. The broad dark bands are related to the lower density N layers as they are depressed more by the tip than the high density layers. This example demonstrates that the magnitude of the tip-to-sample force interactions is of great interest in AFM, smaller forces allowing for the imaging of finer details such as the traces from the knife that are not visible at larger forces.

The tip-to-surface force applied can also only be classified as high or low in comparison to the stiffness of the sample being investigated. It is also intuitive that the amount of deflection for a given force will depend strongly on the tip-to-sample contact area. Measurement at different forces can not only be collected by changing the force level of the set point but it is also possible to choose cantilevers with different spring constants, or take measurements under different ambient conditions.

Estimates of the force applied during contact mode are based upon the spring con-

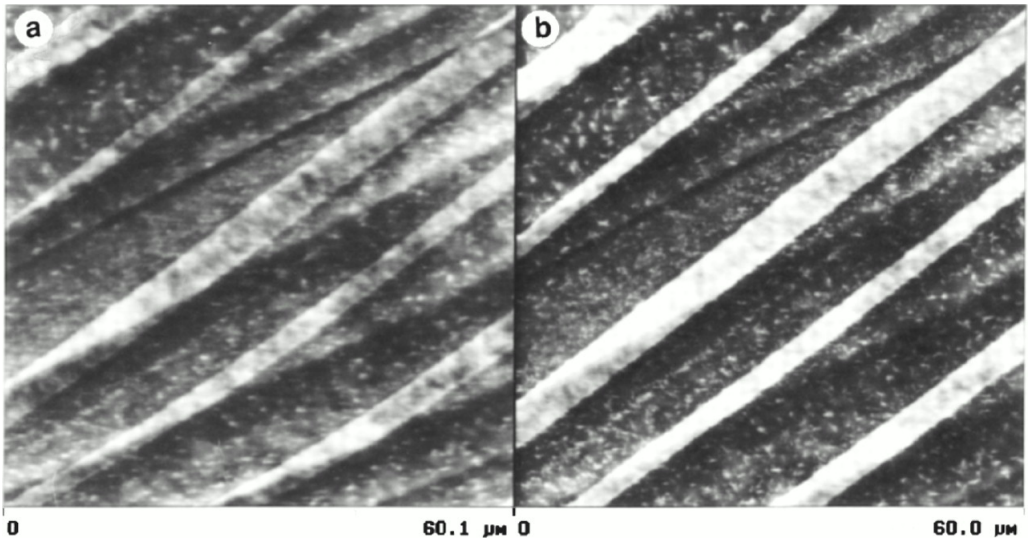

Figure A.6: An AFM height micrograph of a polyethylene surface consisting of alternating layers of low and high density polymer [156]. a) obtained at a tip-to-sample force of 20 nN. b) obtained at a force of 150 nN. Reproduced with permission.

stant of the cantilever in use. In commercially available microfabricated silicon and silicon nitride probes of different shapes it is possible to obtain cantilevers that have spring constants that vary between 0.01 and 50 Nm^{-1}. In general the soft cantilevers are used for contact mode while the more rigid ones are used for tapping mode (the extra stiffness aids the withdrawal of the tip in each oscillation cycle). At ambient conditions, the magnitude of the tip-to-sample force is between 10 and 100 nN, but this can be increased by increasing the set-point deflection.

The main function of AFM is that of mapping surface topography, yet it has several other capabilities in contact mode:

- The dependence of vertical deflection of the cantilever in terms of its position in relation to the sample position in the z-direction can be used to form a force vs distance curve (often simply referred to as a force curve). Such a curve can be used for adjusting the tip-to-sample height but it can also be used to characterise the mechanical properties of the surface or the adhesion between the sample and the tip.

- It is possible to record the lateral deflection of the probe while scanning the surface to make meausrements of 'friction' at the nanoscale. With particularly sharp probes it is possible to observe stick-slip behaviour, characteristic of macroscopic friction, on the scale of the atomic bond. This can be used when characterising surfaces as another method of characterisation of the adhesive properties as well as examining regions of a surface that might hinder diffusion.

A.12.2 Tapping mode AFM

In the case of soft materials such as polymeric surfaces, it is often the case that the tip-to-sample force in contact mode is too high, often leading to mechanical deformations of the surface. The development of tapping mode AFM was a direct response to this issue, with the main motivation of the technique being to minimise, or if possible avoid, surface damage. Tapping mode aims to achieve this by short intermittent contact between the tip and the surface, thereby minimising the deformation of the sample. There are many studies demonstrating this; that soft samples experience less damage when examined using tapping mode [157, 158].

With the introduction of tapping mode a wider range of materials can be imaged, particularly those samples with biological importance. It should be stressed that the operation of tapping mode AFM, with its lower force levels, does not remove the possibility of surface deformation entirely during measurements. The ability to make measurements at a variety of force levels is an important part of imaging in AFM and just as it is possible to alter the tip-to-sample force in contact mode it is possible to vary this force in tapping mode. In tapping mode, the variation can be achieved through the manipulation of the driving amplitude A_0 and the set-point amplitude A_{sp}. The tip-to-sample force will increase with a corresponding increase in A_0 or an increase in the difference $A_0 - A_{\mathrm{sp}}$.

In stark contrast to contact mode, the height images in tapping mode show only very

minor changes with variation of the applied force. Rather, in tapping mode the frequency and the phase of the oscillating probe is much more sensitive to the applied force. The repulsive interactions between tip and surface cause the resonant frequency to shift to higher frequencies. Attractive interaction will conversely lead to cause the resonant frequency to decrease to lower frequencies. This in turn leads to a related phase change, which is all explained by treating the probe as a harmonic oscillator. If the phase and frequency are plotted in terms of x and y, as in a height image, it is possible to access new information on the system regarding the surface topography.

Appendix B

Manuscripts

B.1 Clarkson et al (2015) - Diffusion in Responsive Gels

This Manuscript is the accepted publication sent to Macromolecular Rapid Communications. It contains the work describing the transition of PGMA-PHPMA gels with changes in pH and temperature. Supplementary information is available at the Publication website.

Characterization of Diblock Copolymer Order–Order Transitions in Semidilute Aqueous Solution Using Fluorescence Correlation Spectroscopy

Christopher G. Clarkson, Joseph R. Lovett, Jeppe Madsen, Steven P. Armes,* Mark Geoghegan*

The temperature and pH-dependent diffusion of poly(glycerol monomethacrylate)-*block*-poly(2-hydroxypropyl methacrylate) nanoparticles prepared via polymerization-induced self-assembly in water is characterized using fluorescence correlation spectroscopy (FCS). Lowering the solution temperature or raising the solution pH induces a worm-to-sphere transition and hence an increase in diffusion coefficient by a factor of between four and eight. FCS enables morphological transitions to be monitored at relatively high copolymer concentrations (10% w/w) compared to those required for dynamic light scattering (0.1% w/w). This is important because such transitions are reversible at the former concentration, whereas they are irreversible at the latter. Furthermore, the FCS data suggest that the thermal transition takes place over a very narrow temperature range (less than 2 °C). These results demonstrate the application of FCS to characterize order–order transitions, as opposed to order–disorder transitions.

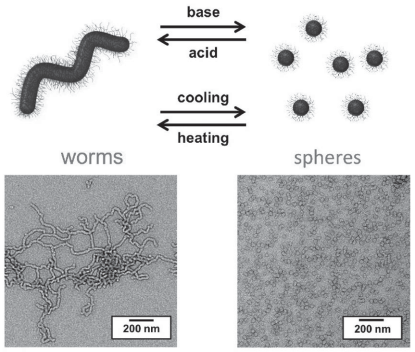

1. Introduction

It is well known that amphiphilic diblock copolymers can self-assemble in aqueous solution to form ordered micellar gels at relatively high concentrations.[1,2] Judicious choice of the copolymer allows the design of hydrogels that are responsive to temperature[3,4] or pH.[5–8] However, it is relatively unusual for such a copolymer to respond to both temperature and pH.

In principle, biocompatible block copolymer gels can be used as a long-term cell storage medium.[9] One promising candidate for such applications is a diblock copolymer comprising poly(glycerol monomethacrylate) (PGMA) and poly(2-hydroxypropyl methacrylate) (PHPMA), which are conveniently prepared via polymerization-induced self-assembly[9–13] using reversible addition-fragmentation chain transfer (RAFT) aqueous dispersion polymerization.[14–16] This versatile approach has enabled spherical, worm-like or vesicular copolymer morphologies to be generated in concentrated solution.[11,17–26] Such a nonionic PGMA-PHPMA diblock copolymer exhibits a thermoreversible

C. G. Clarkson, Prof. M. Geoghegan
Department of Physics and Astronomy
University of Sheffield
Hounsfield Road, Sheffield S3 7RH, UK
E-mail: mark.geoghegan@sheffield.ac.uk
J. R. Lovett, Dr. J. Madsen, Prof. S. P. Armes
Department of Chemistry
University of Sheffield
Brook Hill, Sheffield S3 7HF, UK
E-mail: s.p.armes@sheffield.ac.uk

DOI: 10.1002/marc.201500208

order–order transition from worms to spheres upon cooling from 20 to 4 °C, as a result of greater hydration of the core-forming PHPMA block at the lower temperature (Figure 1a,c,d).[9] However, very recently it was reported that end-group chemistry can be exploited in order to introduce pH-dependent behavior in addition to such thermoresponsive behavior (Figure 1b).[27]

More specifically, a carboxylic acid-based RAFT chain transfer agent (CTA) was utilized in the preparation of the hydrophilic PGMA block in order to confer pH-dependent behavior on the nonionic diblock copolymer chains.[27] Thus raising the solution pH above the pK_a of 4.7 causes ionization of the terminal carboxylic acid group and hence introduces anionic charge, which in turn leads to a pH-induced worm-to-sphere transition (Figure 2).[27]

Spherical diblock copolymer nanoparticles produce a low-viscosity, free-flowing solution that can be readily sterilized via ultrafiltration, which has important biomedical implications.[9] Aqueous dispersions of worms are much more viscous, with free-standing gels being formed in semidilute aqueous solution as a result of multiple inter-worm contacts. Below the critical gelation concentration, PGMA-PHPMA worms can diffuse freely in solution albeit rather more slowly than the (many) spheres from which they are formed. Thus monitoring the rate of diffusion is a potentially powerful technique for characterizing the worm-to-sphere transition. In particular, fluorescence correlation spectroscopy (FCS) is an excellent tool for measuring diffusion coefficients, because it allows access to a wide range of time scales.[28–32] FCS makes use of a confocal experimental setup to achieve high spatial and temporal resolution. Unlike confocal microscopy, FCS only requires a relatively low fluorophore concentration. This is because the latter is sensitive to fluctuations in fluorescence intensity and hence requires far fewer dye labels to diffuse through the confocal volume for analysis. In general, the concentration of fluorescently tagged molecules should be of the order of 10 μmol m^{-3}, such that there is on average only one dye label within the detection volume at any given time. It is well established that FCS is an ideal tool for measuring conformational transitions[33,34] and for studying the behavior of polymeric micelles.[35,36] In the present study, the rate of diffusion is sensitive to the copolymer morphology, which makes this technique well suited for examining the diffusion of rhodamine-labeled diblock copolymer worms/spheres as a function of both pH and temperature.

2. Experimental Section

A $PGMA_{43}$ macro-CTA containing a terminal carboxylic acid group was prepared via RAFT solution polymerization in ethanol using 4-cyano-4-(2-phenylethane sulfanylthiocarbonyl)

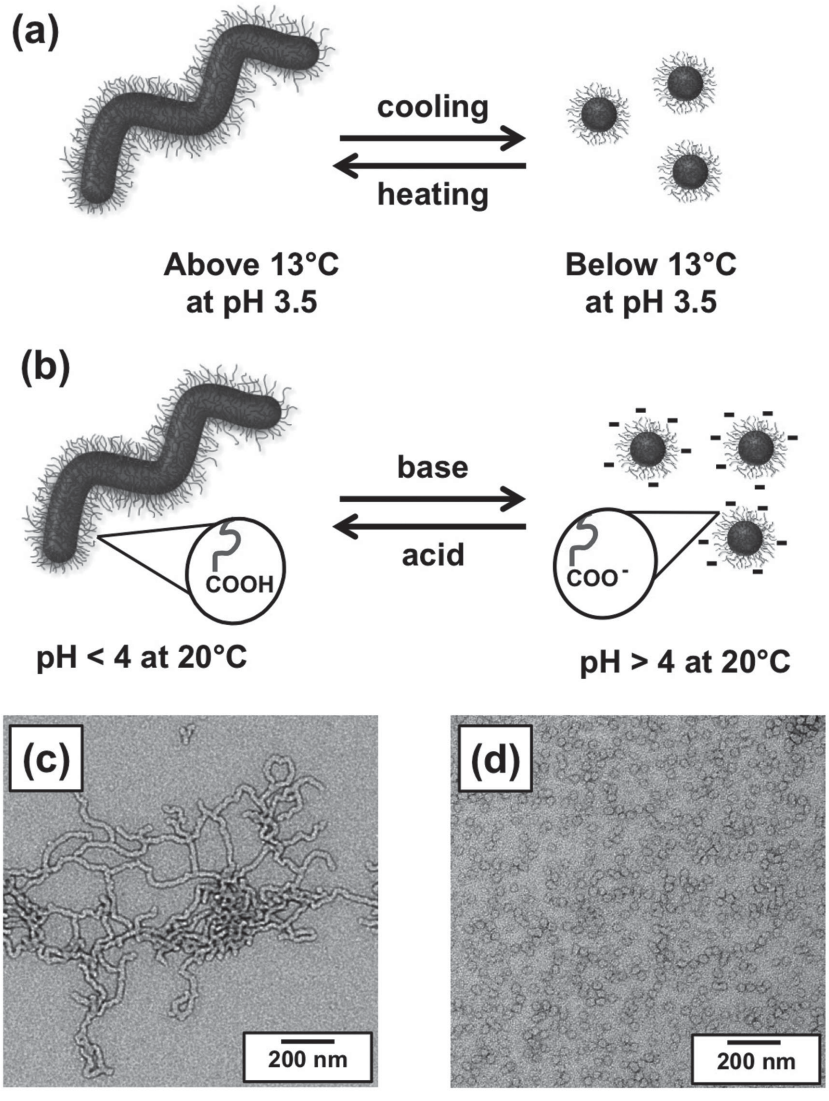

Figure 1. Top) Schematic cartoon of the reversible worm-to-sphere transition that occurs when PGMA-PHPMA diblock copolymer worms are subjected to: a) cooling below 13 °C at pH 3.5 or b) a pH switch via addition of base at 20 °C. Bottom) Transmission electron microscopy images obtained for $PGMA_{43}$-*block*-P($HPMA_{119}$-*co*-$GlyMA_1$) copolymer diluted to 0.1 w/w % in acidic aqueous solution (pH 3.5) at c) 20 °C and d) 5 °C.

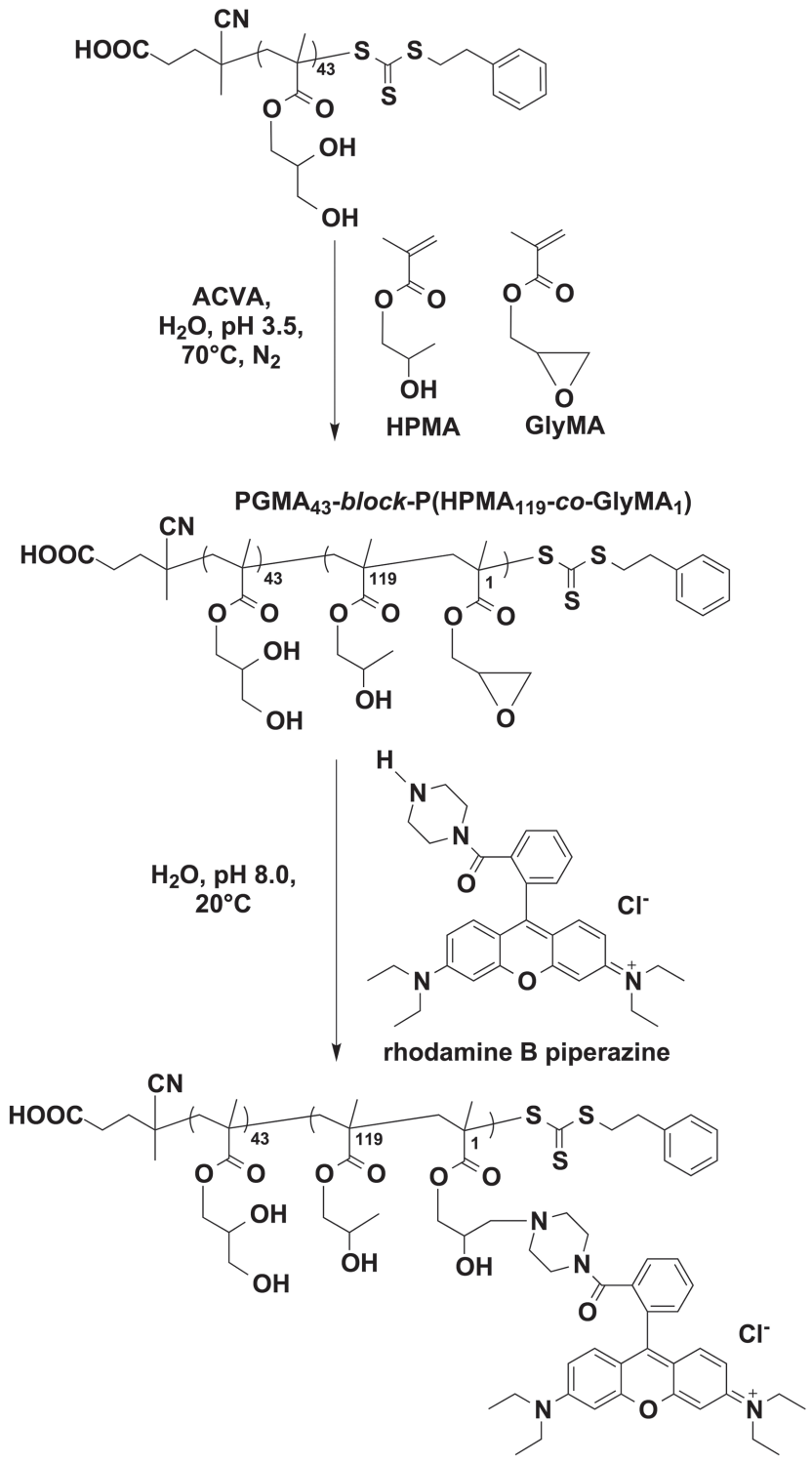

Figure 2. Chain extension of a carboxylic acid-terminated $PGMA_{43}$ macro-CTA via RAFT aqueous dispersion copolymerization of HPMA with GlyMA to form a well-defined $PGMA_{43}$-*block*-P($HPMA_{119}$-*co*-$GlyMA_1$) worm gel at pH 3.5.

sulfanylpentanoic acid (PETTC) as a CTA (Figure 2).[27] This near-uniform water-soluble macro-CTA was then chain-extended via RAFT aqueous dispersion copolymerization of HPMA and GlyMA (targeting approximately one epoxy group per copolymer chain) at 70 °C at approximately pH 3.5. ^{1}H NMR studies confirmed that a very high HPMA conversion (>99%) was achieved at 10% solids, while gel permeation chromatography analysis (*N*,*N*′-dimethylformamide eluent) indicated a relatively high blocking efficiency (>90%) and a relatively low copolymer dispersity (M_w/M_n = 1.20). The resulting HOOC-$PGMA_{43}$-*block*-P($HPMA_{119}$-*co*-$GlyMA_1$) worms formed a soft, transparent free-standing gel at 10% w/w in mildly acidic solution (pH < 4). Rhodamine B (RhB) was used as a fluorescent probe; this dye label was incorporated into the hydrophobic P($HPMA_{119}$-*co*-$GlyMA_1$) core-forming block by reacting a sub-stoichiometric amount of rhodamine B piperazine with the pendant epoxy groups (dye/epoxy molar ratio = 0.25). Using free rhodamine B piperazine dye to construct a Beer-Lambert linear calibration plot, visible absorption spectroscopy studies of the dissolved fluorescently labeled diblock copolymer in methanol prior to dilution for FCS measurements suggested that 18% (compared to a target of 20%) of the copolymer chains were fluorescently labeled (see Figure S1 in the Supporting Information). Furthermore, high-performance liquid chromatography analysis of the copolymer immediately after dye conjugation confirmed negligible contamination by the free dye (see Figure S2 in the Supporting Information). The dye content was sufficiently low that it had a negligible effect on the stimulus-responsive nature of the diblock copolymer chains. Moreover, the dye label concentration was maintained at ≈10 μmol m^{-3} during the FCS experiments by diluting the labeled copolymer with an appropriate amount of unlabeled copolymer. Experiments investigating the thermoresponsive behavior of these rhodamine-labeled PGMA-PHPMA diblock copolymer nanoparticles were performed at pH 3.9; the copolymer was freeze-dried after its synthesis and then reconstituted using ice-cold water at this initial pH.[37]

All FCS data were acquired using an inverted LSM510 Meta confocal microscope equipped with a ConFocor2 FCS module. The setup was calibrated using free RhB dye in order to allow optimization of the pinhole dimensions, placement, and filters. RhB is a widely used fluorescent probe and has a diffusion coefficient of $4.2 \pm 0.3 \times 10^{-10}$ m^2 s^{-1} at 22.5 °C in water.[38] Thus, measurement of the rate of diffusion of free RhB dye allowed the observation volume to be determined.

A Linkam FTIR600 stage equipped with a T20 system controller was used to control temperature during FCS measurements. The sample was placed in an Ibidi® μ-Dish$^{35\ mm,\ high}$) imaging dish. The temperature was lowered from 22 °C to the desired temperature for observation. After allowing 5 min for thermal equilibrium at each temperature, a series of FCS measurements were made before returning to 22 °C.

For studies of the pH-dependent behavior of PGMA-PHPMA diblock copolymer nanoparticles, addition of a buffer solution was deemed inappropriate, as this would alter the concentration of the dye label. Instead, the copolymer was freeze-dried overnight from its aqueous solution. A small quantity was placed in each well of a Nunc Lab-Tek II 8-chamber slide. The copolymer was then dispersed in an ice-cold buffer solution at a well-defined pH so that the chains adopted their equilibrium copolymer morphology (either worms or spheres) at each pH. All pH-dependent experiments were performed at 22 °C.

FCS data are acquired in the form of an autocorrelation function, $G(\tau)$, given by

$$G(t) = G_{\infty} + \frac{G_3(\tau)}{n\left(1+\frac{\tau}{\tau_D}\right)\sqrt{1+\frac{\tau}{\tau_D S^2}}} \quad (1)$$

where G_∞ describes the behavior at infinite time (for data such as these that fluctuate around a mean value, $G_\infty = 1$), $G_3(\tau)$ is the autocorrelation of the triplet state decay, n is the number of dye labels within the confocal volume, τ_D describes the characteristic diffusion time of molecules within the confocal volume, and S is a calibration parameter which depends on the width of the confocal volume (400–600 nm). The resulting curve describes the persistence of the fluorescence intensity over a given time period, and fitting is used to determine the physical parameters of the system.

Each measurement was made for 6 s and repeated 150 times. Measurements with average count rates less than 1 kHz were discarded.

To confirm conjugation of the RhB dye label to the PGMA-PHPMA copolymer chains, preliminary FCS measurements were conducted without changing either temperature or pH. If free RhB were present, its contribution to the rate of diffusion would be detected. If a contribution from free RhB was observed, the sample was removed and purification was repeated until the only contribution to the correlation curve was from covalently bound RhB labels. All data presented herein were obtained for rigorously purified samples.

3. Results and Discussion

Rheological experiments performed on the HOOC-PGMA$_{43}$-*block*-P(HPMA$_{119}$-*co*-GlyMA$_1$) diblock copolymer worm gel revealed their critical gelation temperature (CGT) to be 13 °C (see Figure S3 in the Supporting Information). For Stokes–Einstein diffusion, a higher temperature leads to a corresponding increase in the diffusion coefficient for a given molecular or colloidal species. However, in the case of the HOOC-PGMA$_{43}$-*block*-P(HPMA$_{119}$-*co*-GlyMA$_1$) nanoparticles, this relationship breaks down as the relatively massive worms are converted into much smaller spheres. The characteristic temperature at which this transition occurs is the CGT and represents the difference between the rates of diffusion of spheres and worms, respectively, in aqueous dispersion. Worms and spheres were never observed in coexistence at any temperature or pH examined in this study. This suggests a relatively rapid transition between these two copolymer morphologies (within a timescale of seconds).

The diffusion coefficient was reduced by more than a factor of four with increasing temperature; see Figure 3. Furthermore, the FCS data illustrate the sharpness of this thermal transition, with the change in diffusion coefficient occurring over less than 2 °C. The Stokes–Einstein equation was used to calculate hydrodynamic radii,

$$r_H = \frac{k_B T}{6\pi\rho D}. \quad (2)$$

The corresponding hydrodynamic radii are 15 ± 2 nm for spheres at 11 °C and 55 ± 14 nm for worms at 15 °C. Here, T is the absolute temperature, i.e., 284 and 288 K, respectively; ρ is the dynamic viscosity of water, or 1.3 mPa s at 11 °C and 1.1 mPa s at 15 °C;[39] D is the diffusion coefficient calculated from curve-fitting; and k_B is the Boltzmann constant. The worms are highly anisotropic, but the Stokes–Einstein equation is strictly only valid for spherical particles in dilute solutions of low-Reynolds number; hence sphere-equivalent diameters are reported. Using Equation (1), the dye concentration was determined to be 16 ± 2 μmol m^{-3} for the spheres and 26 ± 3 μmol m^{-3}

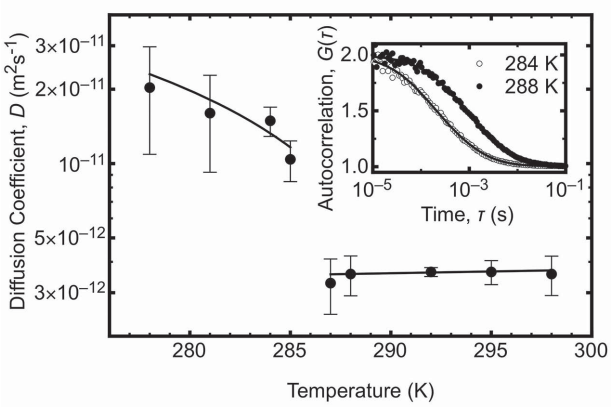

Figure 3. Diffusion coefficients determined for PGMA$_{43}$-*block*-P(HPMA$_{119}$-*co*-GlyMA$_1$) nanoparticles as a function of temperature, illustrating the worm-to-sphere transition as the temperature is lowered below 13 °C (286 K). The inset shows selected FCS data collected either side of the transition. The solid lines represent fits to Equation (1).

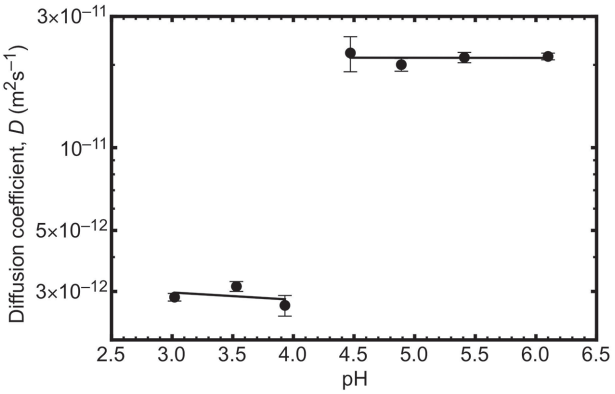

Figure 4. Diffusion coefficients determined at 22 °C for $PGMA_{43}$-*block*-P($HPMA_{119}$-*co*-$GlyMA_1$) nanoparticles as a function of pH, illustrating the worm-to-sphere transition as the solution pH is gradually increased from pH 3.0 to pH 6.2.

for the worms. The difference between the two results is likely to be because dyes located in the same micelle are correlated. Visible absorption spectroscopy analysis of the dissolved copolymer chains indicated a rhodamine dye label concentration of 7 μmol m^{-3}.

In a control experiment, the hydrodynamic radius of the HOOC-$PGMA_{43}$-*block*-P($HPMA_{119}$-*co*-$GlyMA_1$) diblock copolymer in methanol was measured to be 1.01 ± 0.04 nm, suggesting molecular dissolution of the copolymer chains under these conditions. This is consistent with small-angle X-ray scattering (SAXS) studies recently reported for closely related $PGMA_{57}$-*block*-$PHPMA_{140}$ in methanol.[37] Thus, the steady increase in diffusion coefficient that is observed in Figure 3 below the worm-to-sphere transition is consistent with the partial dissociation of the spheres to form near-molecularly dissolved copolymer chains at sufficiently low temperatures.[37] However, the temperature at which this order–disorder transition occurs is not reached in the current study, with the smallest radius observed being 8 ± 4 nm at 5 °C.

The pH-dependent behavior of the diffusion coefficient of the HOOC-$PGMA_{43}$-*block*-P($HPMA_{119}$-*co*-$GlyMA_1$) nanoparticles is shown in Figure 4. As the solution pH is increased above pH 4.0, the diffusion coefficient increases by a factor of approximately eight. Again, this indicates a worm-to-sphere transition, in this case caused by a rather subtle end-group ionization effect.[27] The critical pH observed for this worm-to-sphere transition (pH 4.2) is in good agreement with that indicated for closely related HOOC-$PGMA_{56}$-*block*-$PHPMA_{155}$ diblock copolymer nanoparticles by rheology measurements[27] and also dynamic light scattering (DLS) studies of the HOOC-$PGMA_{43}$-*block*-P($HPMA_{119}$-*co*-$GlyMA_1$) nanoparticles (see Figure S4 in the Supporting Information). When considering the self-consistency of the observed thermoresponsive behavior, it should be noted that the solution pH for the latter formulation was pH 3.9. Thus the diffusion coefficients are self-consistent when comparing identical conditions.

4. Conclusions

In summary, FCS has been used to characterize two worm-to-sphere transitions for HOOC-$PGMA_{43}$-*block*-P($HPMA_{119}$-*co*-$GlyMA_1$) nanoparticles that can be induced by varying either the solution temperature or pH. The absence of secondary components at intermediate temperatures or pH values suggests that this order–order transition is relatively fast, as the two phases do not coexist on the time scale of a single FCS measurement. It is emphasized that FCS provides additional information compared to DLS, since the former technique enables such phase transitions to be monitored over the same semidilute concentration range as that employed for rheology studies, rather than merely in highly dilute solution. This is important, because the worm-to-sphere transition is reversible when conducted at copolymer concentrations of 5%–10% solids, but becomes irreversible at 0.1%–1.0% solids (i.e., in the DLS regime).

Supporting Information

Supporting Information is available from the Wiley Online Library or from the author.

Acknowledgements: The authors gratefully acknowledge financial support from the Engineering and Physical Sciences Research Council under Programme grant EPSRC EP/I012060/1. J.R.L. thanks The University of Sheffield for a PhD studentship and S.P.A. acknowledges the ERC for a five-year *Advanced Investigator* grant (PISA: 320372). GEO Specialty Chemicals (Hythe, UK) is thanked for partial support of this work.

Received: April 8, 2015; Revised: May 15, 2015; Published online: June 22, 2015; DOI: 10.1002/marc.201500208

Keywords: fluorescence correlation spectroscopy; polymerization-induced self-assembly; RAFT polymerization; spheres; worms

[1] B. Jeong, Y. H. Bae, D. S. Lee, S. W. Kim, *Nature* **1997**, *388*, 860.
[2] C. Tsitsilianis, *Soft Matter* **2010**, *6*, 2372.
[3] C. Li, Y. Tang, S. P. Armes, C. J. Morris, S. F. Rose, A. W. Lloyd, A. L. Lewis, *Biomacromolecules* **2005**, *6*, 994.
[4] J. Madsen, S. P. Armes, A. L. Lewis, *Macromolecules* **2006**, *39*, 7455.
[5] A. P. Blum, J. K. Kammeyer, A. M. Rush, C. E. Callmann, M. E. Hahn, N. C. Gianneschi, *J. Am. Chem. Soc.* **2015**, *137*, 2140.
[6] C. de las Heras Alarcón, S. Pennadam, C. Alexander, *Chem. Soc. Rev.* **2005**, *34*, 276.
[7] Y. Ma, Y. Tang, N. C. Billingham, S. P. Armes, A. L. Lewis, *Biomacromolecules* **2003**, *4*, 864.

[8] D. Roy, J. N. Cambre, B. S. Sumerlin, *Prog. Polym. Sci.* **2010**, *35*, 278.
[9] A. Blanazs, R. Verber, O. O. Mykhaylyk, A. J. Ryan, J. Z. Heath, C. W. I. Douglas, S. P. Armes, *J. Am. Chem. Soc.* **2012**, *134*, 9741.
[10] Z. An, Q. Shi, W. Tang, C.-K. Tsung, C. J. Hawker, G. D. Stucky, *J. Am. Chem. Soc.* **2007**, *129*, 14493.
[11] A. Blanazs, J. Madsen, G. Battaglia, A. J. Ryan, S. P. Armes, *J. Am. Chem. Soc.* **2011**, *133*, 16581.
[12] Y. Li, S. P. Armes, *Angew. Chem. Int. Ed.* **2010**, *49*, 4042.
[13] J. Rieger, C. Grazon, B. Charleux, D. Alaimo, C. Jérôme, *J. Polym. Sci. A: Polym. Chem.* **2009**, *47*, 2373.
[14] J. Chiefari, Y. K. Chong, F. Ercole, J. Krstina, J. Jeffery, T. P. T. Le, R. T. A. Mayadunne, G. F. Meijs, C. L. Moad, G. Moad, E. Rizzardo, S. H. Thang, *Macromolecules* **1998**, *31*, 5559.
[15] G. Moad, E. Rizzardo, S. H. Thang, *Aust. J. Chem.* **2012**, *65*, 985.
[16] S. Perrier, P. Takolpuckdee, *J. Polym. Sci. A: Polym. Chem.* **2005**, *43*, 5347.
[17] C. A. Figg, A. Simula, K. A. Gebre, B. S. Tucker, D. M. Haddleton, B. S. Sumerlin, *Chem. Sci.* **2015**, *6*, 1230.
[18] L. Houillot, C. Bui, M. Save, B. Charleux, C. Farcet, C. Moire, J.-A. Raust, I. Rodriguez, *Macromolecules* **2007**, *40*, 6500.
[19] G. Liu, Q. Qiu, Z. An, *Polym. Chem.* **2012**, *3*, 504.
[20] G. Liu, Q. Qiu, W. Shen, Z. An, *Macromolecules* **2011**, *44*, 5237.
[21] Y. Pei, N. C. Dharsana, J. A. van Hensbergen, R. P. Burford, P. J. Roth, A. B. Lowe, *Soft Matter* **2014**, *10*, 5787.
[22] Y. Pei, A. B. Lowe, *Polym. Chem.* **2014**, *5*, 2342.
[23] Y. Pei, L. Thurairajah, O. R. Sugita, A. B. Lowe, *Macromolecules* **2015**, *48*, 236.
[24] N. Suchao-in, S. Chirachanchai, S. Perrier, *Polymer* **2009**, *50*, 4151.
[25] W.-M. Wan, C.-Y. Pan, *Macromolecules* **2010**, *43*, 2672.
[26] W. Zhao, G. Gody, S. Dong, P. B. Zetterlund, S. Perrier, *Polym. Chem.* **2014**, *5*, 6990.
[27] J. R. Lovett, N. J. Warren, L. P. D. Ratcliffe, M. K. Kocik, S. P. Armes, *Angew. Chem. Int. Ed.* **2015**, *54*, 1279.
[28] E. L. Elson, D. Magde, *Biopolymers* **1974**, *13*, 1.
[29] K. Koynov, H.-J. Butt, *Curr. Opin. Colloid Interface Sci.* **2012**, *17*, 377.
[30] O. Krichevsky, G. Bonnet, *Rep. Prog. Phys.* **2002**, *65*, 251.
[31] C. Lellig, J. Wagner, R. Hempelmann, S. Keller, D. Lumma, W. Härtl, *J. Chem. Phys.* **2004**, *121*, 7022.
[32] U. Zettl, S. T. Hoffmann, F. Koberling, G. Krausch, J. Enderlein, L. Harnau, M. Ballauff, *Macromolecules* **2009**, *42*, 9537.
[33] L. Edman, Ü. Mets, R. Rigler, *Proc. Natl Acad. Sci. USA* **1996**, *93*, 6710.
[34] F. Wang, Y. Shi, S. Luo, Y. Chen, J. Zhao, *Macromolecules* **2012**, *45*, 9196.
[35] D. Schaeffel, A. Kreyes, Y. Zhao, K. Landfester, H.-J. Butt, D. Crespy, K. Koynov, *ACS Macro Lett.* **2014**, *3*, 428.
[36] L. Yu, M. Tan, B. Ho, J. L. Ding, T. Wohland, *Anal. Chim. Acta* **2006**, *556*, 216.
[37] M. K. Kocik, O. O. Mykhaylyk, S. P. Armes, *Soft Matter* **2014**, *10*, 3984.
[38] P.-O. Gendron, F. Avaltroni, K. J. Wilkinson, *J. Fluorescence* **2008**, *18*, 1093.
[39] J. Kestin, M. Sokolov, W. A. Wakeham, *J. Phys. Chem. Ref. Data* **1978**, *7*, 941.